DRAFT
Marathon Aquifer Conceptual Model Completion Report

TWDB Contract No. 2048302454

by

T. Neil Blandford
Vincent Clause
Andrew C. A. Donnelly
Allan R. Standen
Todd Umstot
Danielle Gallo
Michelle A. Sutherland
Kenneth Calhoun

June 1, 2022

Geoscientist Seal

The following Texas-registered professionals are responsible for this report:

T. Neil Blandford, PG (Texas No. 1034)

Mr. Blandford was responsible for project and contract management, water levels and regional groundwater flow, groundwater recharge, aquifer hydraulic properties, surface water features, the conceptual groundwater flow model, and any additional portions of the report not identified below.

Seal will be added on final completion report
T. Neil Blandford

Allan R. Standen, PG (Texas No. 1227)

Mr. Standen was responsible for the geology, hydrostratigraphic framework, three-dimensional hydrostratigraphic Leapfrog model, and lineament analysis portions of this report.

Seal will be added on final completion report
Allan R. Standen

Andrew C.A. Donnelly, PG (Texas No. 737)

Mr. Donnelly was responsible for the spring flow, groundwater discharge, and water quality portions of this report.

Seal will be added on final completion report
Andrew C.A. Donnelly

Table of Contents

List of Figures

List of Tables

List of Appendices

Foreword

In 1882, Captain Albion Shephard, a former ship's captain turned railroad surveyor, bought land at a water stop along the newly constructed Galveston, Harrisburg and San Antonio line 26 miles southeast of Alpine. Captain Shephard thought the rolling grasslands ringed with hills resembled Marathon, Greece, and so when he platted the townsite, he named it Marathon. At the time, there was already a smattering of settlers around the Pena Colorada Springs, including the Halff brothers—enterprising cattlemen who established their Circle Dot brand near what would soon become a thriving little town. They would later lease the land around the springs to the United States government to establish Fort Pena Colorada, a remote outpost along the Comanche Trail. The fort was established in an effort to stem Comanche raids into Mexico; the land where the fort sat is now a county park.

Springs and surface water in Maravillas Creek provided a life-giving oasis to the nomadic peoples of the Big Bend region for millennia, and later to the cattle industry and soldiers that displaced them. When the railroad came through, Marathon was deemed an excellent water stop, and settlers soon came to supplement the sparse population of ranchers, soldiers, and adventurers.

The 2020 census indicates a population of 386 for the town of Marathon. The major industries are tourism and ranching. The median household income is $49,000, and the town has a recorded poverty rate of around 8 percent. The population is older, with a median age of 59.2 years.

Marathon has had a reputation for "strong water" since its founding. The cattle ranching industry has been a mainstay of the local economy since the 1870s. Other water-reliant industries, such as guayule rubber, found a ready home here. Since the 1940s, the Marathon region has experienced a consistent increase in tourism due to Big Bend National Park and the popularity of other Big Bend communities like Marfa. As tourism, vacation rentals, and part-time residence increase across the region, improved understanding of the Marathon Aquifer is critical to better understand the long-term availability of water.

The Big Bend area in general, and the Marathon area in particular, have long held fascination for geologists. The incredibly complex juncture of several mountain ranges creates a jumble of geologic epochs exposed at the surface, hinting at baffling complexities beneath. The terminus of the Ouachita Fold is visible in graceful arches just to the southeast of town, intersecting the tail end of the Rocky Mountains in the form of the Del Norte-Santiago range on a bias to the southwest. At Marathon, the young Rockies and the ancient Ouachita Orogeny meet, and shake hands with the vast Permian limestone deposits most Texans find familiar. Volcanic intrusions dot the landscape, and sandstone and shale formations stand vertically in roadcuts, a testament to the intense pressures in this complicated, folded landscape. Caliche, karst formations, shallow oil deposits, and the occasional report of geothermal activity add intrigue to what some geologists refer to as Marathon's "rock soup."

The sparse population means that there are a limited number of wells to test in a relatively large area, but the difficulties inherent in mapping the Marathon Aquifer are not only due to the scarcity of available data. The rugged landscape is reflected in its inhabitants, hardy descendants of desert pioneers whose reluctance to share information with outsiders is both traditional and understandable. Here water is value, in the purest sense. Many stakeholders prefer to keep information about this resource to themselves.

Despite the many challenges presented by the climate, culture, and landscape, mapping the Marathon Aquifer is vital work. As the limiting factor in a harsh and varied ecosystem, the ability to anticipate and manage changing groundwater conditions means consistency for the area residents, industries, and visitors. As Marathon grows in popularity and new residents enter the region, a deeper understanding of the mysteries of Marathon's groundwater can ensure that the town and its people will enjoy sustainable life on the edge of the Chihuahuan desert for many more generations.

—Danielle Gallo, Marathon resident

Executive Summary

The Marathon Aquifer, located in north-central Brewster County, is the most structurally complex aquifer in Texas. The Marathon Aquifer consists of two types of aquifers delineated based on the porosity and water yielding characteristics of the rocks and sediments. The first type of aquifer occurs within Quaternary alluvium that overlies consolidated rocks between prominent ridges and along the edges of the aquifer extent. The alluvium is permeable to the flow of groundwater and, where there is a significant amount of saturation, it can yield useable quantities of water to wells. The second type of aquifer consists of dipping Paleozoic formations that have been extensively deformed and faulted by structural activity. Left unaltered, the permeability of these units to the flow of groundwater is slight, but the breaking of these rocks through structural movement has created fault and fracture zones that allow for the flow of groundwater.

In the Marathon Limestone, the permeability of the rocks has also been enhanced by solutioning and enlargement of the void spaces and interconnected fractures—a process known as karstification. The Marathon Limestone is the primary aquifer where it occurs at the surface or at shallow depths. The town of Marathon obtains its water supply from wells completed in the Marathon Limestone. Where the Marathon Limestone occurs at significant depth, the younger and less productive Pennsylvanian formations (i.e., the Haymond, Dimple and Tesnus formations) are the primary aquifer units. Most wells are less than 500 feet deep, and the water quality is generally very good.

There are no perennial rivers or reservoirs within the Marathon Aquifer extent. The two major drainage systems that cross the aquifer are Maravillas Creek and San Francisco Creek. These drainages and their tributaries are ephemeral, with the exception of limited reaches fed by springs or diffuse groundwater discharge.

Previous study of the hydrogeology of the Marathon Basin has been limited because (1) the Marathon Aquifer is relatively small compared to other aquifers in Texas, (2) the water demand is limited, and (3) access to private property in the region to study the water resources is difficult or not permitted by landowners in some cases.

Groundwater pumping from the Marathon Aquifer is small, totaling only about 250 acre-feet per year. The highest value recorded was just under 450 acre-feet per year in 2010. The majority of pumping is for municipal and irrigation uses in the town of Marathon. Natural groundwater discharge occurs as spring flow, base flow to some streams along the eastern and southern margins of the aquifer extent, evapotranspiration where the water table is shallow, and as groundwater underflow.

Groundwater recharge to the aquifer based on climatic and physiographic data for the period 1981 through 2021 was developed using the Distributed Parameter Watershed Model, which is a water balance model based on a daily time step. Water budget components accounted for in the model include precipitation, bare soil evaporation, transpiration, runoff, run-on, snow accumulation, snowmelt, snow sublimation, soil water

storage, and net infiltration. Estimated average groundwater recharge to the aquifer, including the proposed expansion area, is 21,284 acre-feet per year, but the amount of simulated recharge changes significantly from year to year based on climatic conditions. The highest estimated recharge of 70,916 acre-feet occurred in 1987, and the lowest simulated recharge of 2,035 acre feet occurred in 1998. An unknown portion of groundwater recharge is lost to seepage and spring flow from perched water tables that occur at higher elevation above the regional water table.

Based on the small amount of pumping from the aquifer and the amount of estimated recharge, the Marathon Aquifer exists primarily in a quasi-steady state condition, where changes in water levels and spring flow are primarily driven by changes in climatic conditions. The exception to this appears to be the town of Marathon, where moderate effects of groundwater pumping have been observed in the form of water levels that have declined through time.

Aquifer properties have been measured only for the Marathon Limestone and only in the vicinity of the town of Marathon. The available data indicate that the hydraulic conductivity of the limestone can be high, and the permeability of other saturated formations is expected to be less than that of the Marathon Limestone. Fractures and lineaments were delineated for the Marathon region using remote sensing. Where there are greater concentrations of these features, or where these features intersect, well yield should be favorable relative to adjacent regions.

Where the Marathon Limestone occurs at greater depths, wells generally tap shallower formations for stock or domestic supply. It is possible that well yields on the order of several hundred gallons per minute may be obtained from the Marathon Limestone where it occurs at depth, but information on deeper portions of the aquifer system is virtually non-existent.

Future improvements to the Marathon Aquifer conceptual model and ultimately the groundwater availability model that will be constructed could be realized through collecting additional and more consistent water level data; through the collection of additional aquifer properties, particularly for formations other than the Marathon Limestone; and by quantifying base flow that occurs along portions of Maravillas and San Francisco creeks. If more detailed analyses or studies are performed, it would make sense for these studies to be focused on the town of Marathon area in particular, as this is the area of highest water use.

1 Introduction

The Marathon Aquifer, located in north-central Brewster County (Figure 1-1), is the most structurally complex aquifer in Texas. Figure 1-1 shows the Texas Water Development Board (TWDB) Marathon Aquifer extent, along with a proposed region where the aquifer extent may be expanded as described in Section 4.2.3. The area of the Marathon Aquifer is 576 square miles, or 636 square miles including the proposed expansion.

The Marathon Aquifer consists of two types of aquifer systems delineated based on the porosity and water yielding characteristics of the rocks and sediments. The first type of aquifer occurs within Quaternary alluvium that overlies consolidated rocks between prominent ridges and along the edges of the Marathon Aquifer extent. The alluvium is permeable to the flow of groundwater and, where there is a significant amount of saturation, it can yield useable quantities of water to wells. Porosity of the alluvial sediments is referred to as primary porosity, as it is a function of the type of sediment (or rock) as deposited.

The second type of aquifer consists of dipping Paleozoic formations that have been deformed and faulted by structural activity. Left unaltered, the permeability of these units to the flow of groundwater is slight, but the breaking of these rocks through structural movement has created fault and fracture zones through which groundwater can flow. In some units, most notably the Marathon Limestone, the permeability of the rocks has been enhanced by solutioning and enlargement of the void spaces and interconnected fractures—a process known as karstification. The creation of porosity and permeability through faulting, fracturing, and karstification is called “secondary” porosity. Both types of aquifers are addressed in this report, although the Marathon Limestone is the most significant aquifer unit based on its ability to provide relatively large quantities of water. The town of Marathon obtains its water supply from wells completed in the Marathon Limestone.

This draft completion report for the Marathon Aquifer was completed under TWDB Contract 2048302454. The format of the report follows the TWDB standard conceptual model report guidelines.

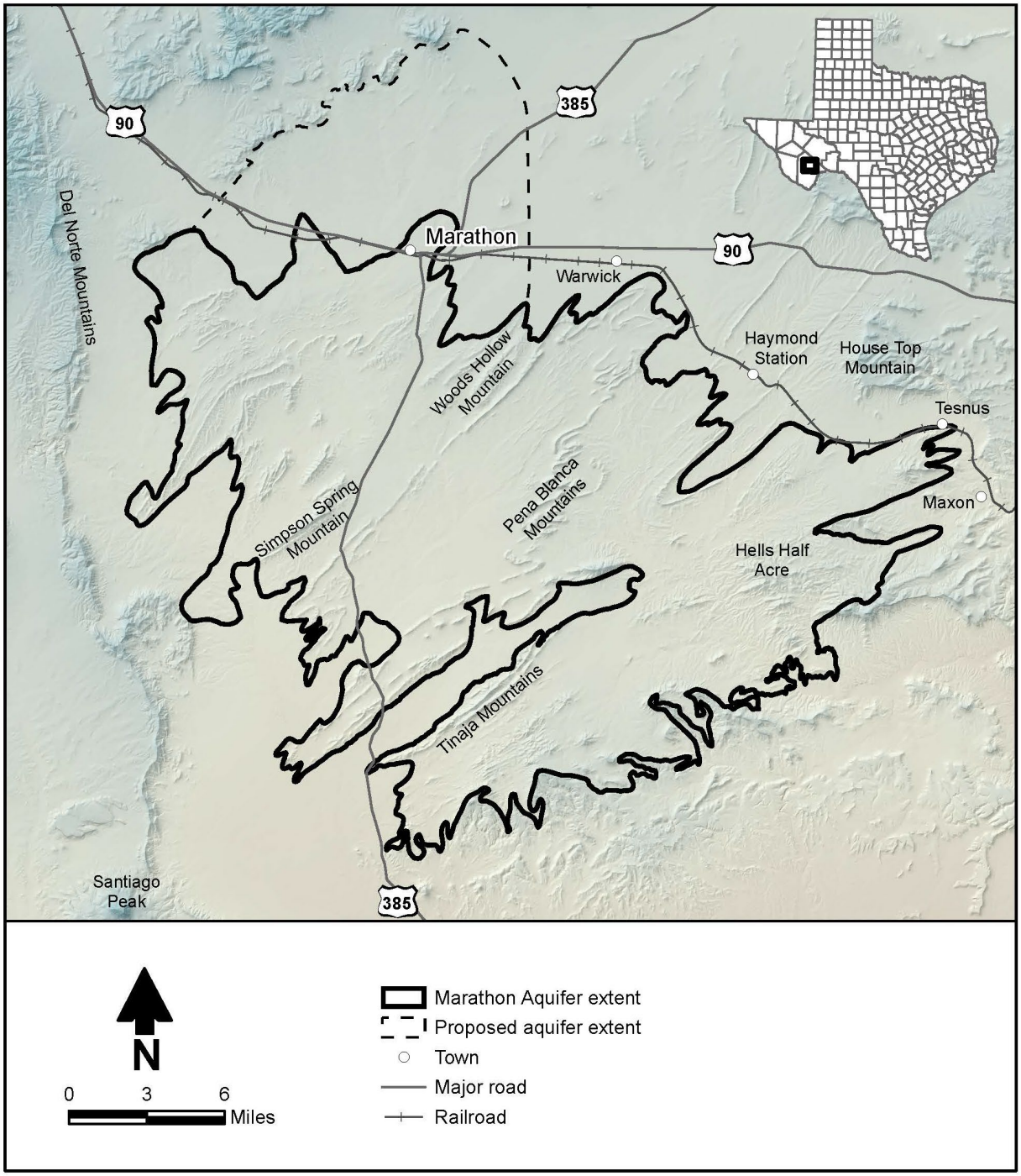

Figure 1-1. Marathon Aquifer study area.

2 Study Area

The Marathon Aquifer study area, including the proposed aquifer expansion area, is approximately 32 miles north to south and a similar distance west to east. The formal study area includes the Marathon Aquifer extent plus a 1-mile buffer beyond the aquifer extent. In addition, some aspects of the study, such as the computation of groundwater recharge, consider a larger region that includes the full upgradient areas of the Maravillas and San Francisco creek watersheds.

The Marathon Basin formed on the crest of the Marathon Dome and now consists of plains, low mountain ridges, hilly lowlands carved out from folded, highly faulted, and uplifted Paleozoic (Cambrian through the Pennsylvanian) strata. Permian formations that dip to the north outcrop in the northwestern corner of the Marathon Basin at the southern edge of the Glass Mountains. The geologic units that comprise the Marathon Aquifer are surrounded by the higher (and geologically younger) escarpments capped by Cretaceous limestone that tilt away from the uplift (King, 1937).

Native Americans, early settlers, and travelers relied on Pena Colorada Springs and other springs of the region as a consistent water source (Brune, 2002). Pena Colorada Springs also supported the first cattlemen of the region and later soldiers at Fort Pena Colorada. The cattle ranching industry has been a mainstay of the local economy since the 1870s, and the local economy was enhanced with the arrival of the railroad in the early 1880s. In addition to ranching, tourism is an important contributor to the economy. Tourism has grown over the past decades due to the proximity of Marathon to Big Bend National Park and the popularity of other Big Bend communities such as Marfa, Texas. The current use of water is limited in the region, as the population is small and there is no significant irrigated agriculture or industry that uses significant quantities of water.

There are 16 regional water planning groups in Texas that generally align with the major river systems. The Marathon Aquifer is encompassed by Region Water Planning Group E, Far West Texas (Figure 2-1). Regional Water Planning Group F is the next closest region, beginning in Pecos County to the northeast.

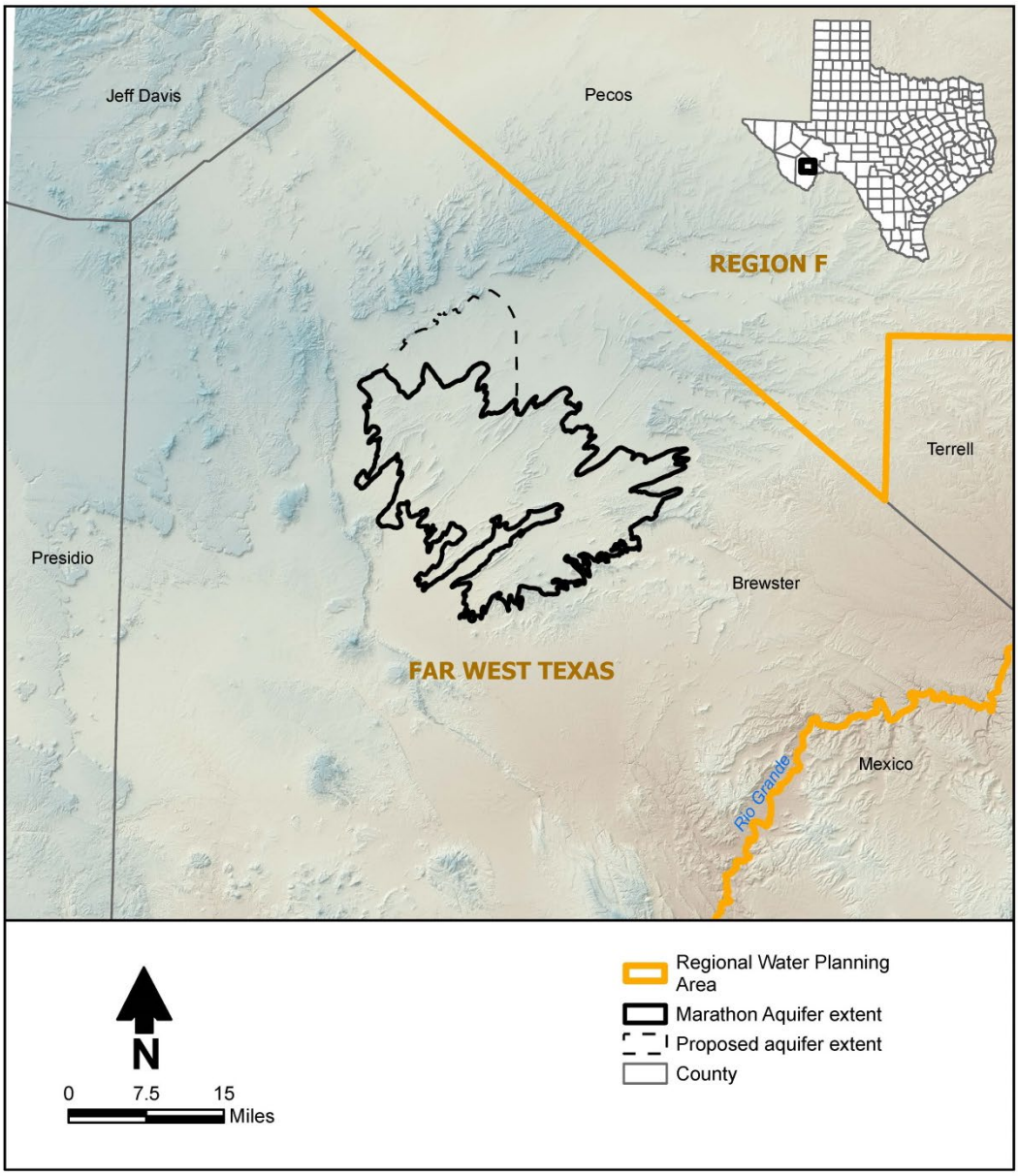

Figure 2-1. Regional water planning groups in the vicinity of the Marathon Aquifer.

The Marathon Aquifer is encompassed entirely by the Brewster County Groundwater Conservation District (Figure 2-2). Other groundwater conservation districts exist for all of the counties adjacent to Brewster County.

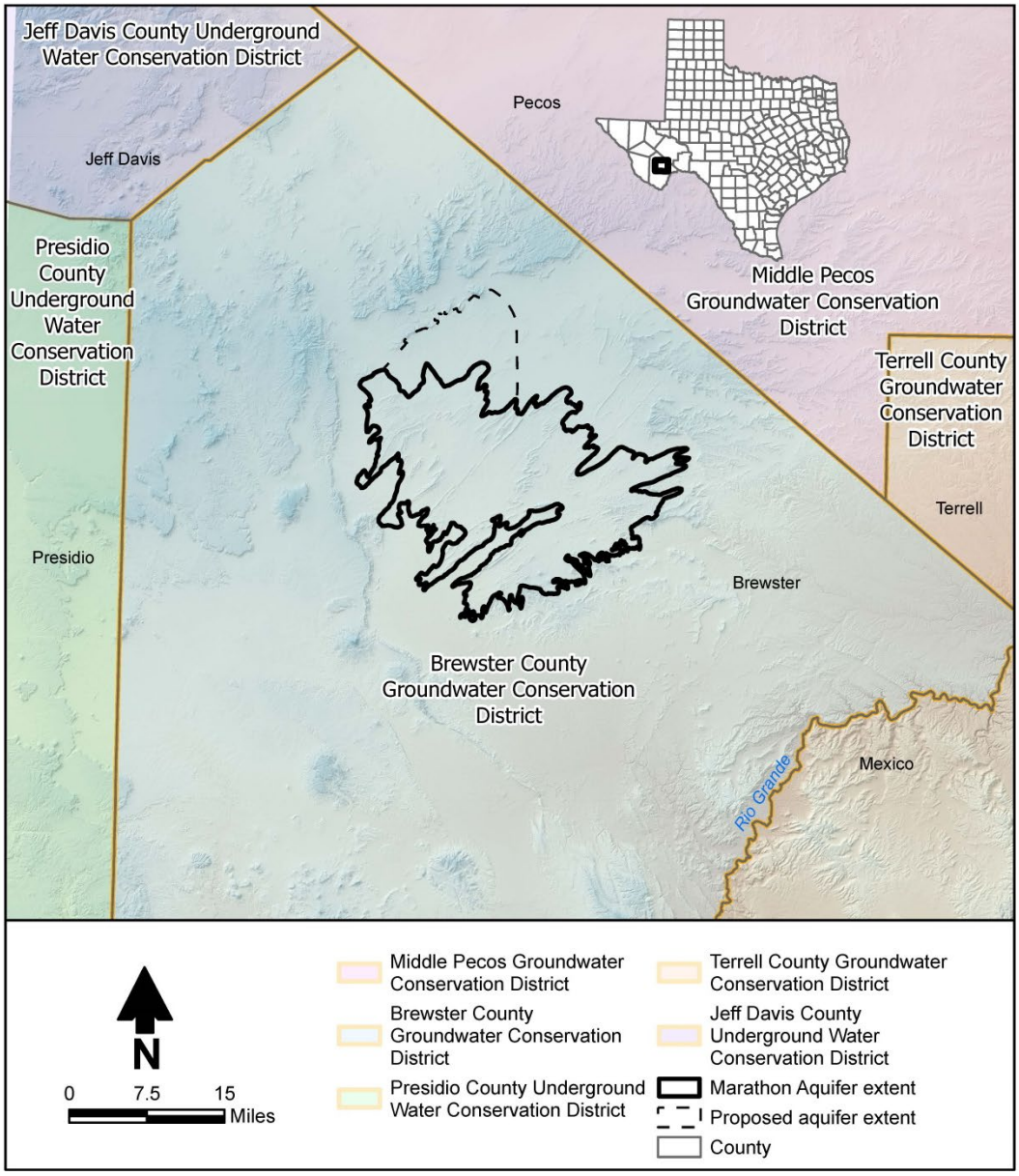

Figure 2-2. Groundwater conservation districts in the vicinity of the Marathon Aquifer.

There are 16 groundwater management areas in Texas, the extents of which approximately coincide with designated aquifers. The Marathon Aquifer is encompassed entirely by Groundwater Management Area 4 (Figure 2-3). Groundwater Management Area 7 to the northeast is the next closest groundwater management area,

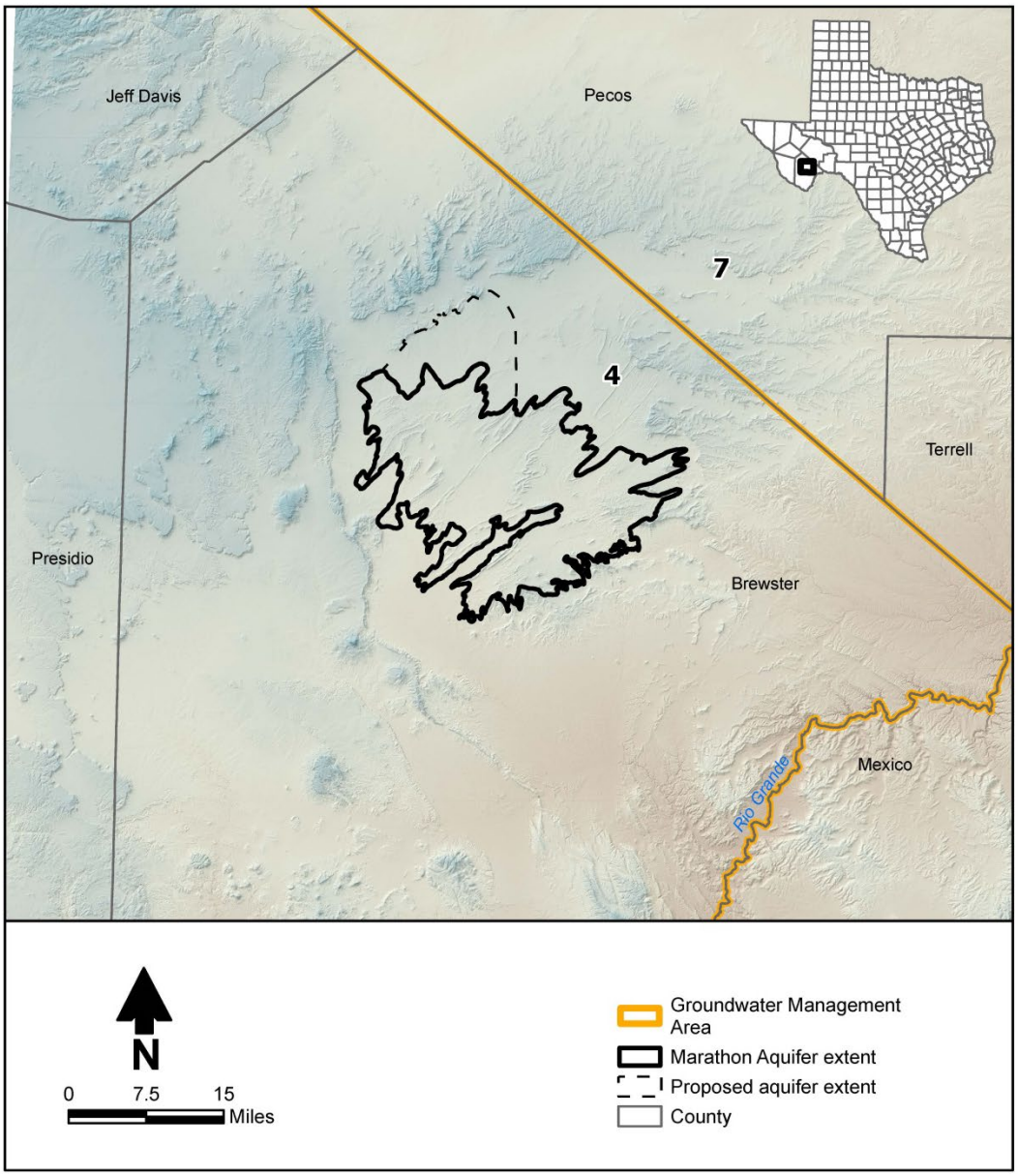

Figure 2-3. Groundwater management area that includes the Marathon Aquifer downloaded from the TWDB website (www.twdb.texas.gov/mapping/gisdata.asp).

The major surface water features within the Marathon Aquifer and adjoining areas are illustrated in Figure 2-4. The two primary watersheds are Maravillas Creek and San Francisco Creek, which extend north of the aquifer to the surface water drainage divide coincident with the Glass Mountains. The northern extent of these watersheds is included in the recharge model area as explained in Section 4.3 to allow surface water runoff generated from precipitation north of the aquifer boundary to flow into the Marathon Aquifer area in the recharge model simulations where it can potentially recharge the Marathon Aquifer. Both of these drainages are tributary to the Rio Grande.

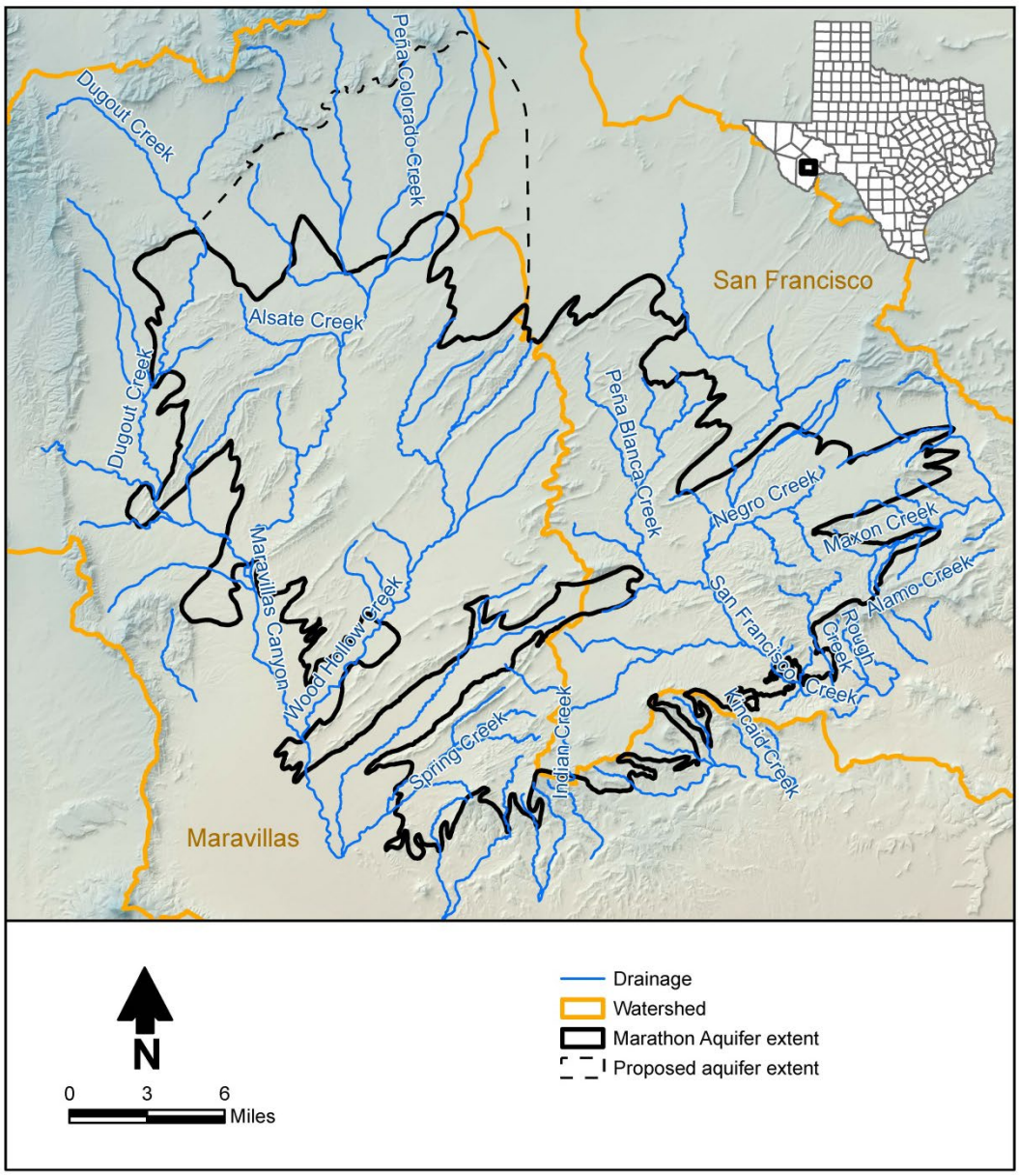

Figure 2-4. Major drainages and surface water features. Streams were downloaded from the U.S. Geological Survey National Hydrography Dataset. All streams are tributary to the Rio Grande.

2.1 Physiography and Climate

Land surface topography ranges from a maximum of about 6,521 feet above mean sea level in the Glass Mountains north of the Marathon Aquifer to a low of about 2,811 feet above mean sea level in the far southwestern portion of the study area extent (Figure 2-5).

The Marathon Aquifer occurs almost exclusively within the Basin and Range Physiographic Province (Figure 2-6) as defined by the Texas Bureau of Economic Geology (Texas Bureau of Economic Geology, 2021), and the aquifer occurs in the Trans Pecos Climate Division.

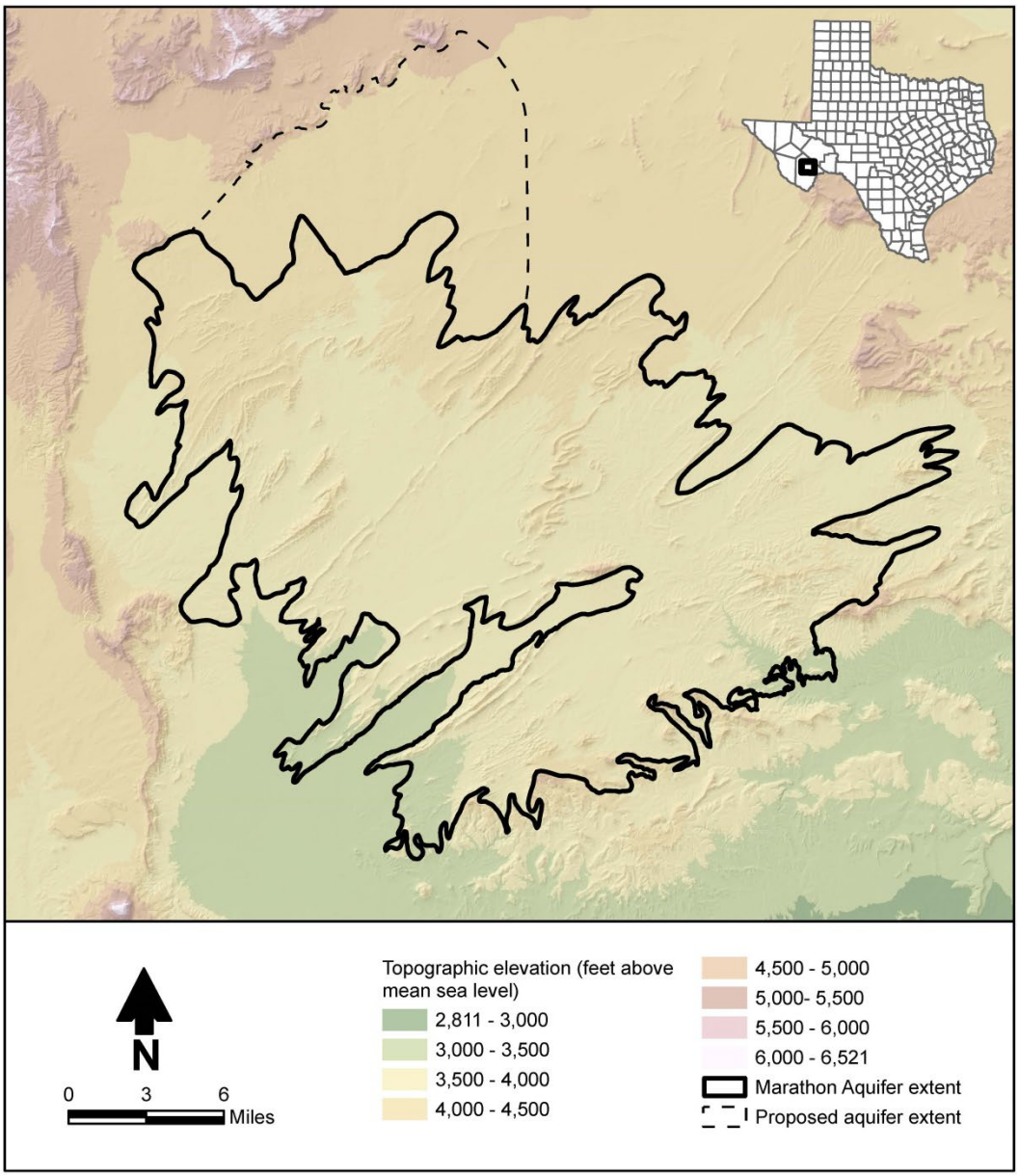

Figure 2-5. Land surface topography based on U.S. Geological Survey 1 arc-second (30-meter) digital elevation model.

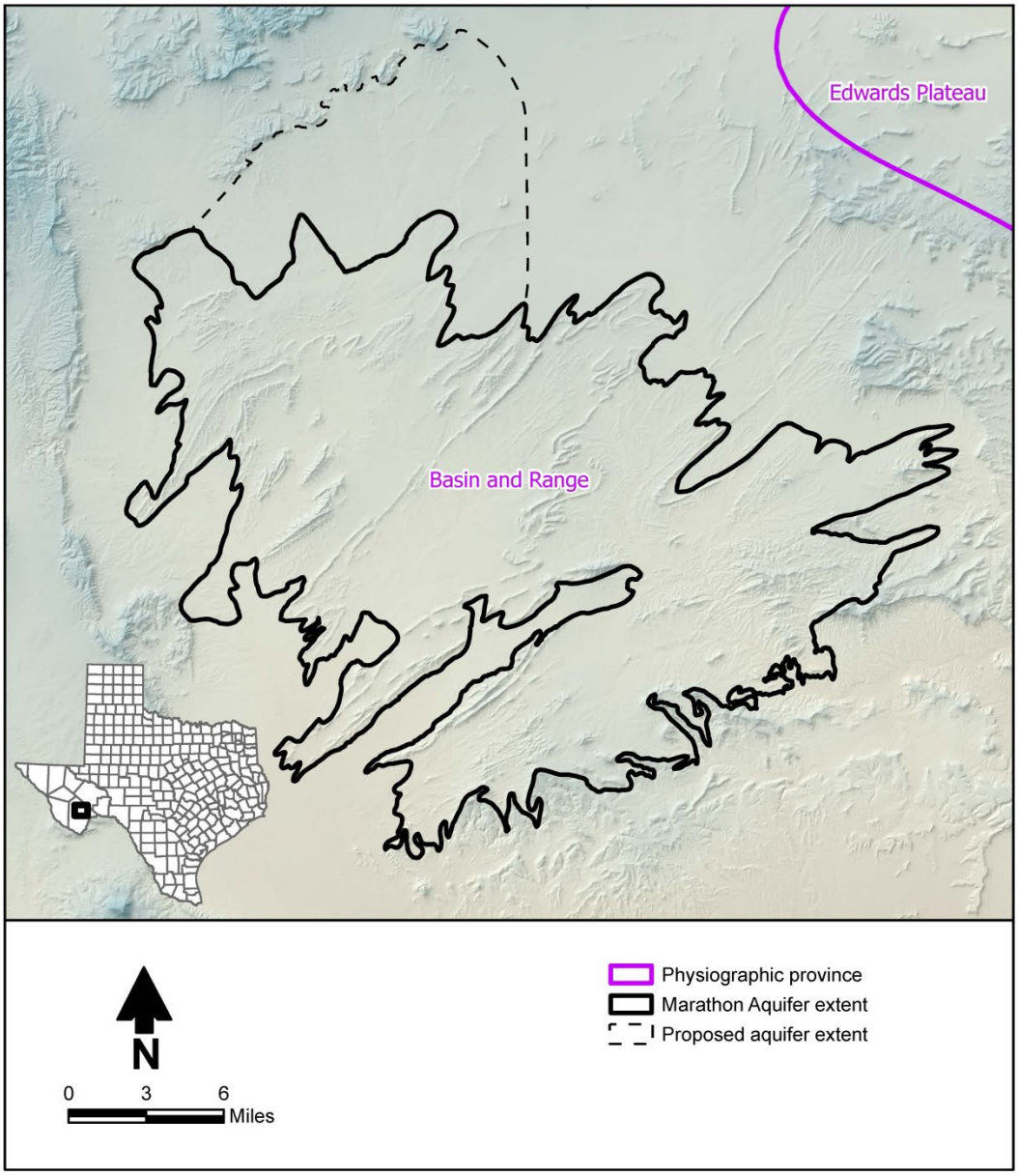

Figure 2-6. Physiographic provinces.

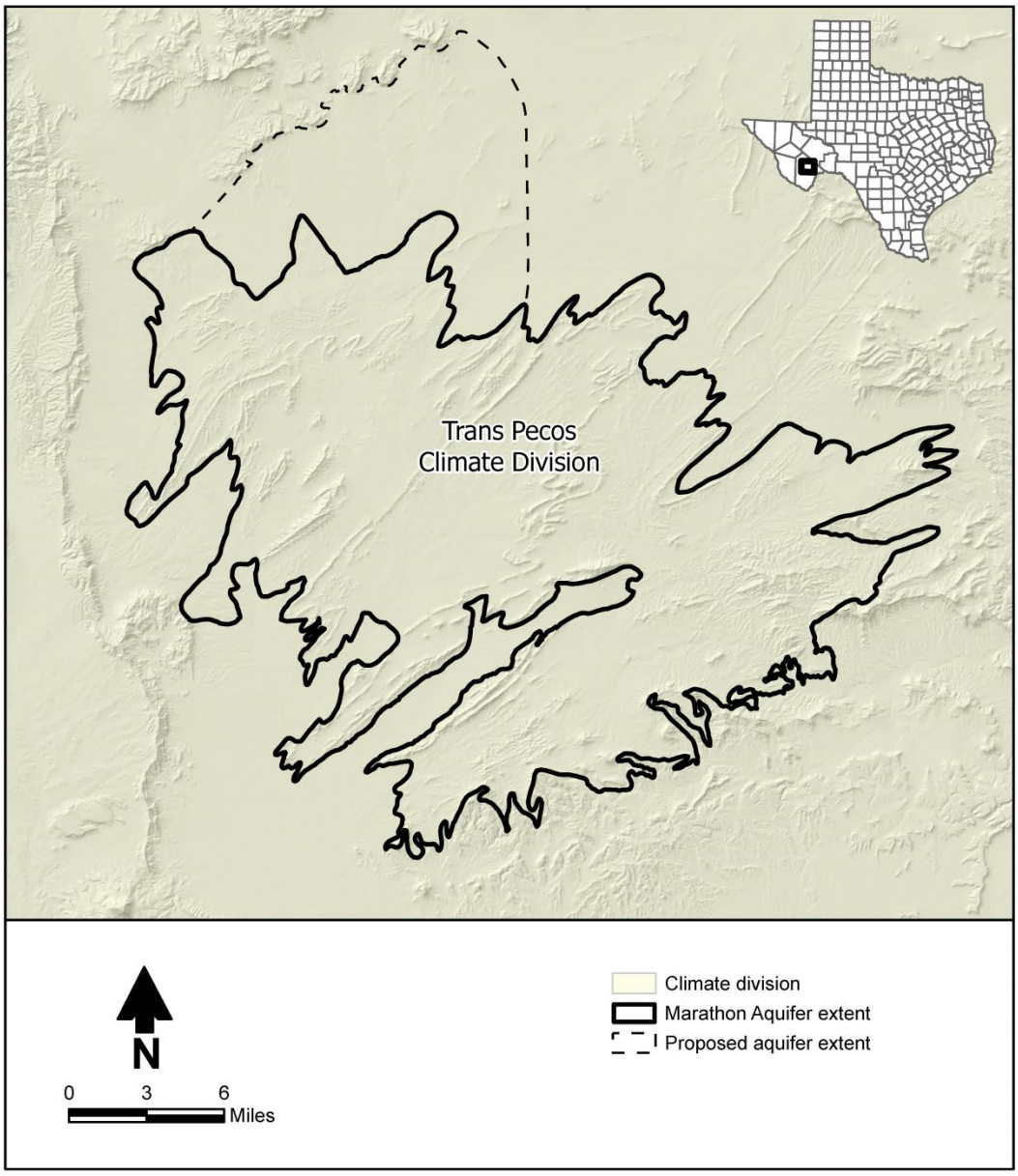

Figure 2-7. Climate divisions as delineated by the National Climatic Data Center.

The remaining portions of this section and the associated text summarizes key climatic, soil, and evapotranspiration information for the Marathon Aquifer and adjoining regions as required by TWDB guidelines. Additional details regarding the data sources and approach to developing these figures are provided in Section 4.3.

Average annual precipitation is provided in Figure 2-8. As indicated in the figure, average annual precipitation decreases from north south, generally in correspondence with changes in land surface elevation. The highest precipitation values in the region exceed 20 inches per year in the mountains north and northwest of the Marathon Aquifer. Across

the aquifer extent, precipitation ranges from about 16 inches per year in the north to 12 inches per year in the south.

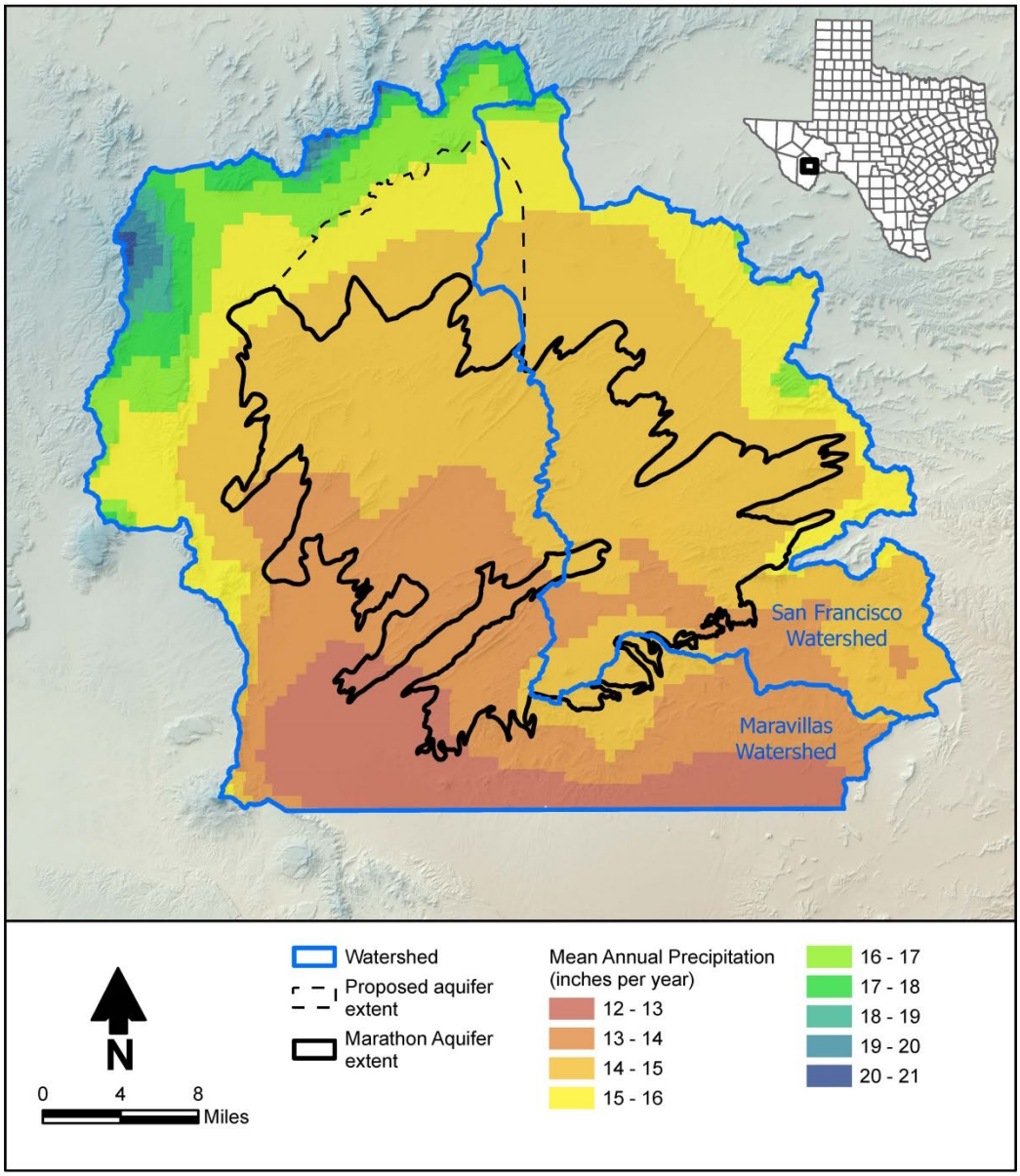

Figure 2-8. Average annual precipitation, 1981 to 2021.

Figure 2-9 shows monthly average precipitation for the Marathon weather station. The majority of annual precipitation occurs during the months of May through October, and maximum monthly precipitation occurs in July.

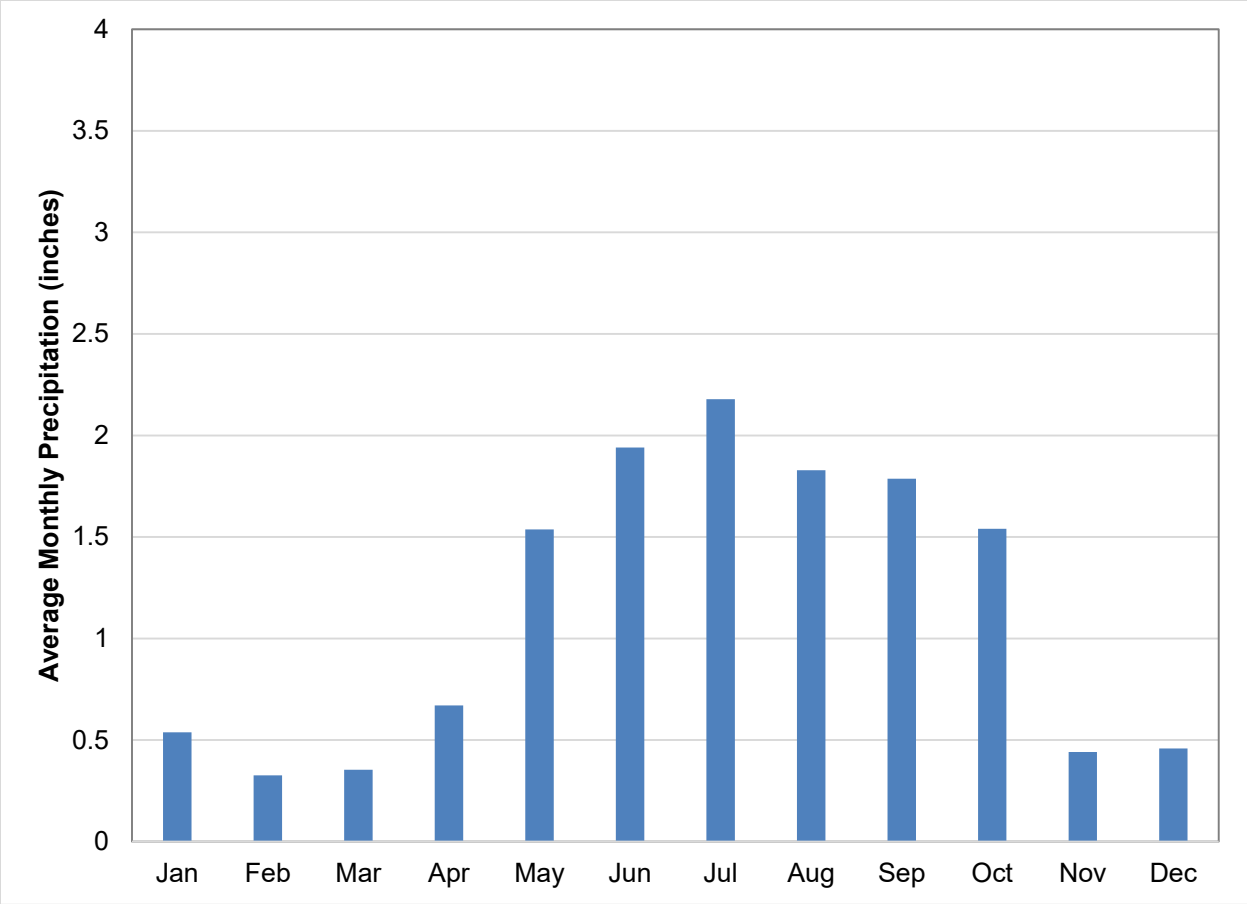

Figure 2-9. Mean monthly precipitation for the Marathon weather station for the period 1981 through 2021.

The average annual temperature (Figure 2-10) is also closely tied to elevation; it is highest in the south where it reaches 51 degrees Fahrenheit, and lowest in the northern portion of the aquifer extent where it is about 48 degrees Fahrenheit.

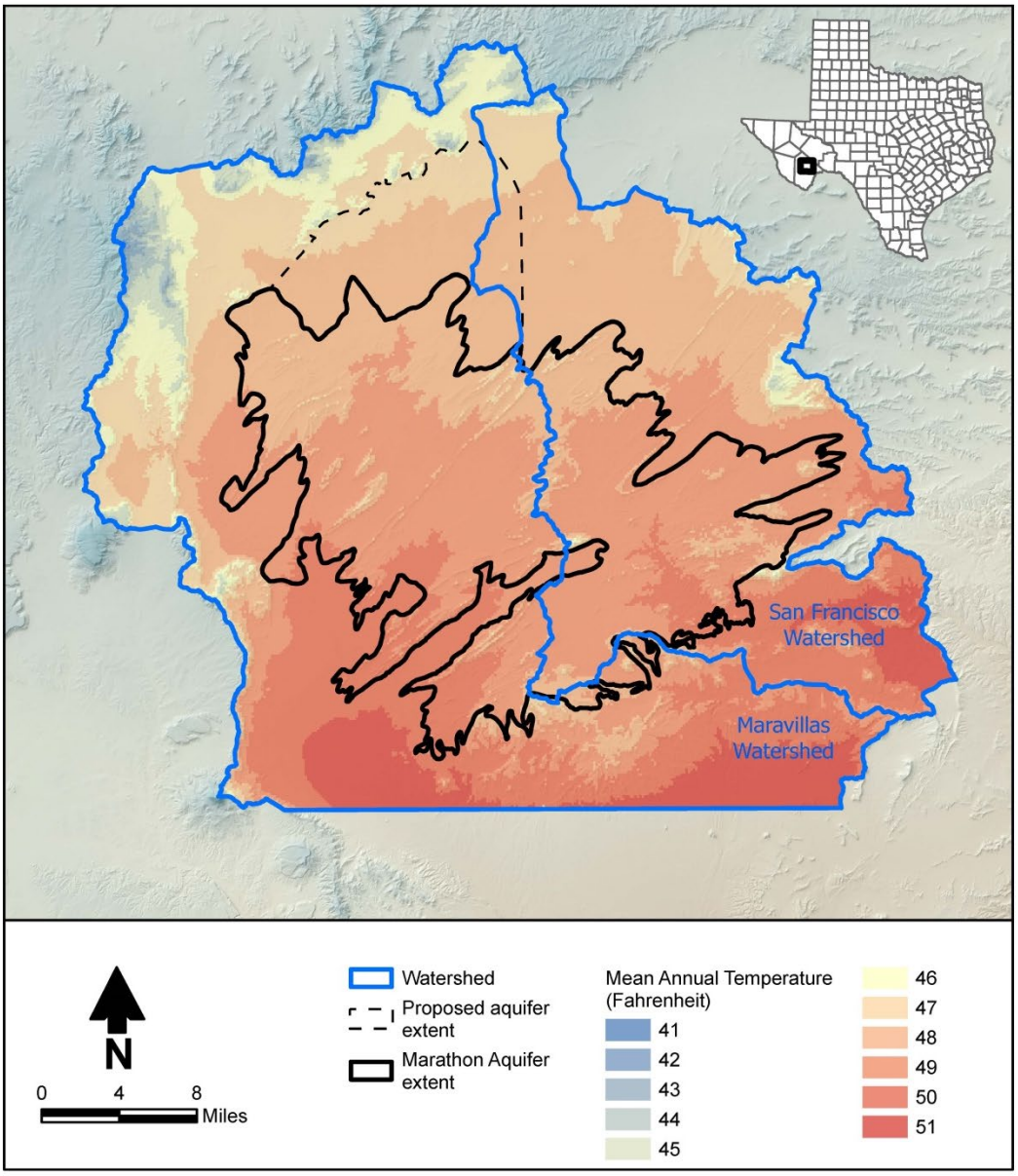

Figure 2-10. Average annual temperature, 1981 to 2021.

Net average annual lake evaporation for the period 1981 through 2021 is provided in Figure 2-11; the average annual lake evaporation was calculated from data at the Water for Texas website accessed May 25, 2022 (TWDB, 2021). Net lake evaporation ranges from 40.5 inches per year in the northwestern portion of the Marathon Aquifer study area to nearly 56 inches per year in the far southwestern extent of the aquifer area.

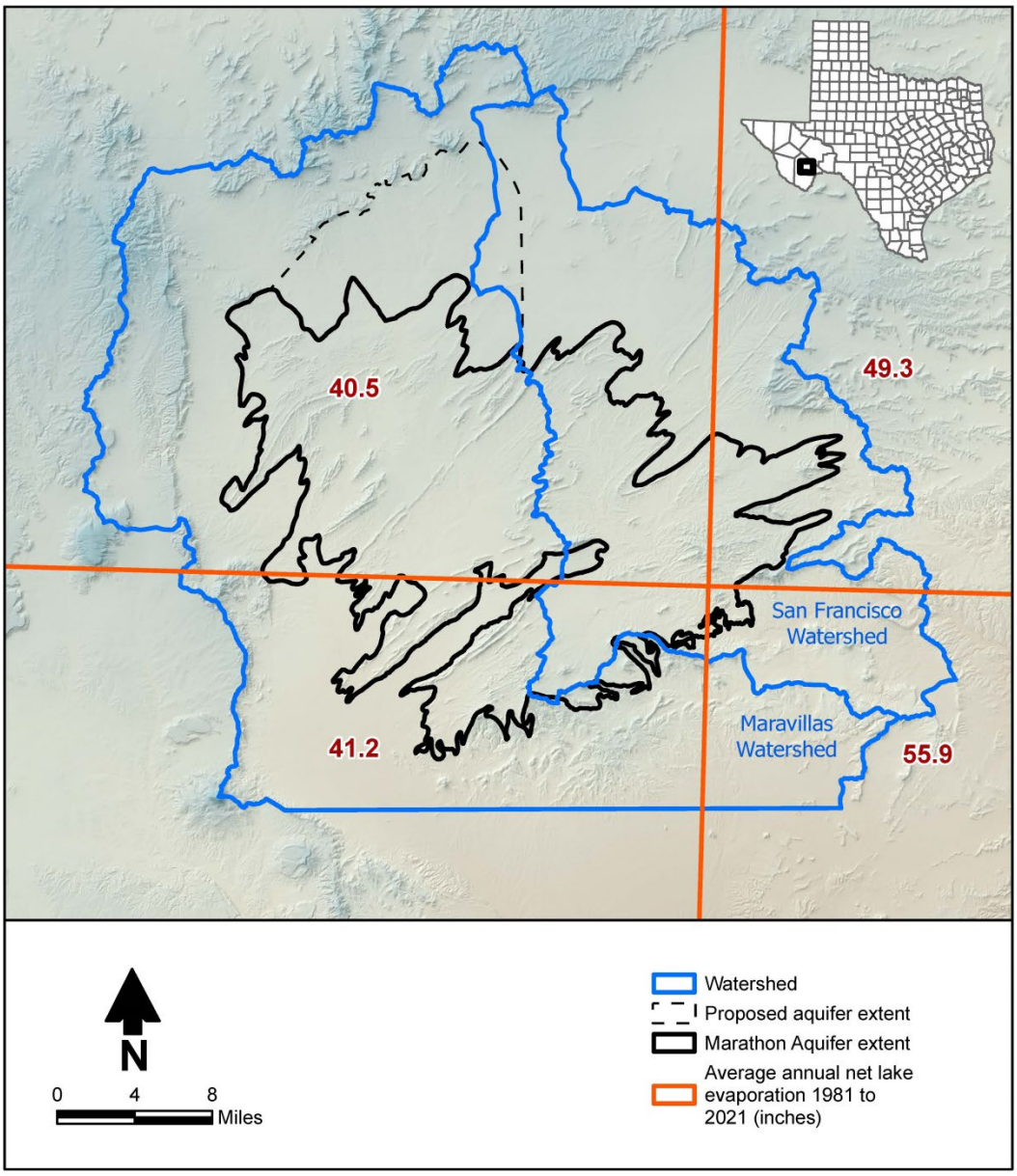

Figure 2-11. Net lake evaporation.

A map of vegetation distribution is provided in Figure 2-12. The data for this map were obtained from the 2016 National Land Cover Database, downloaded on January 13, 2020. The predominant vegetation types within the Marathon Aquifer extent are shrub/scrub (90 percent) and herbaceous (9 percent). The remaining 1 percent of land area (not visible in Figure 2-12) is covered by various categories of forest, wetlands, and developed space.

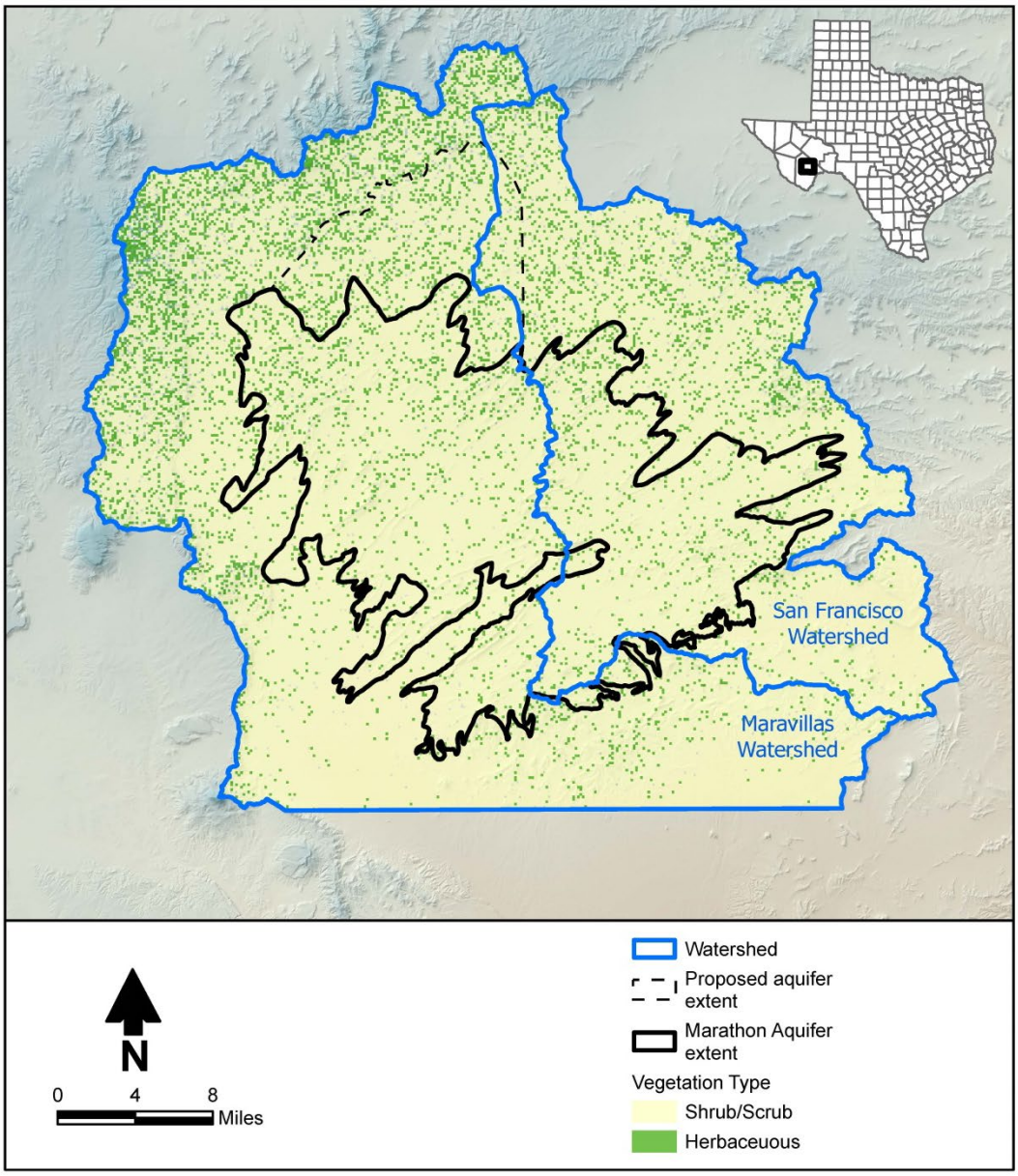

Figure 2-12. Distribution of vegetation across the study area.

Soil permeability, depth, and water-holding capacity are provided in Figures 2-13 through 2-15, respectively. Soil permeability is generally less than 3 feet per day (Figure 2-13). Soil depth is less than 0.5 meters (1.6 feet) in regions where bedrock is at or near land surface, and greater than 2 meters (6.6 feet) where alluvium occurs (Figure 2-14). Soil water holding capacity (Figure 2-15) is the maximum quantity of soil-water available to the vegetation and is based on the soil thickness, rooting depth of the vegetation, and soil texture. Soil water holding capacity is smallest for bedrock areas and highest for soils that contain a range of grain sizes.

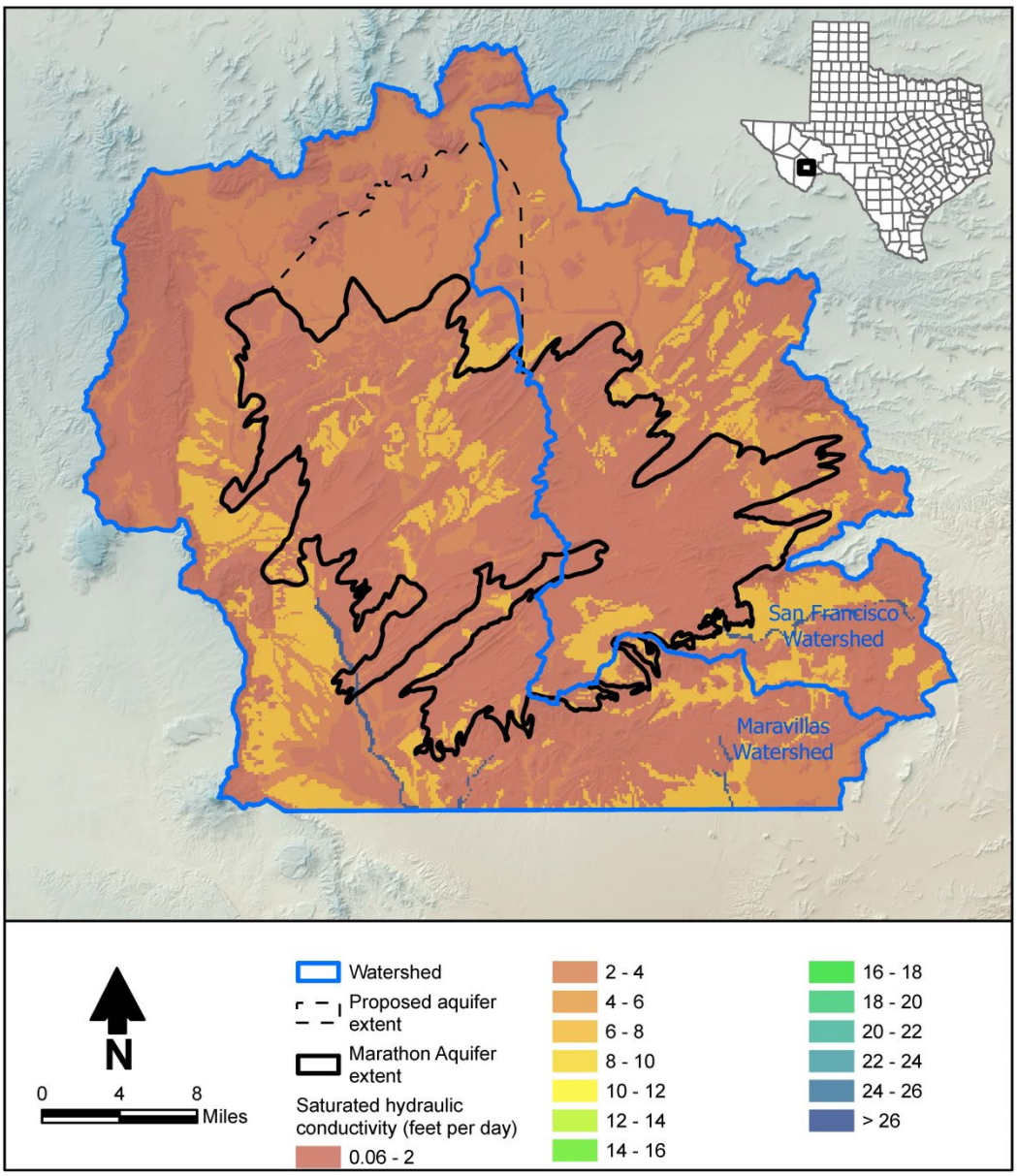

Figure 2-13. Distribution of soil permeability.

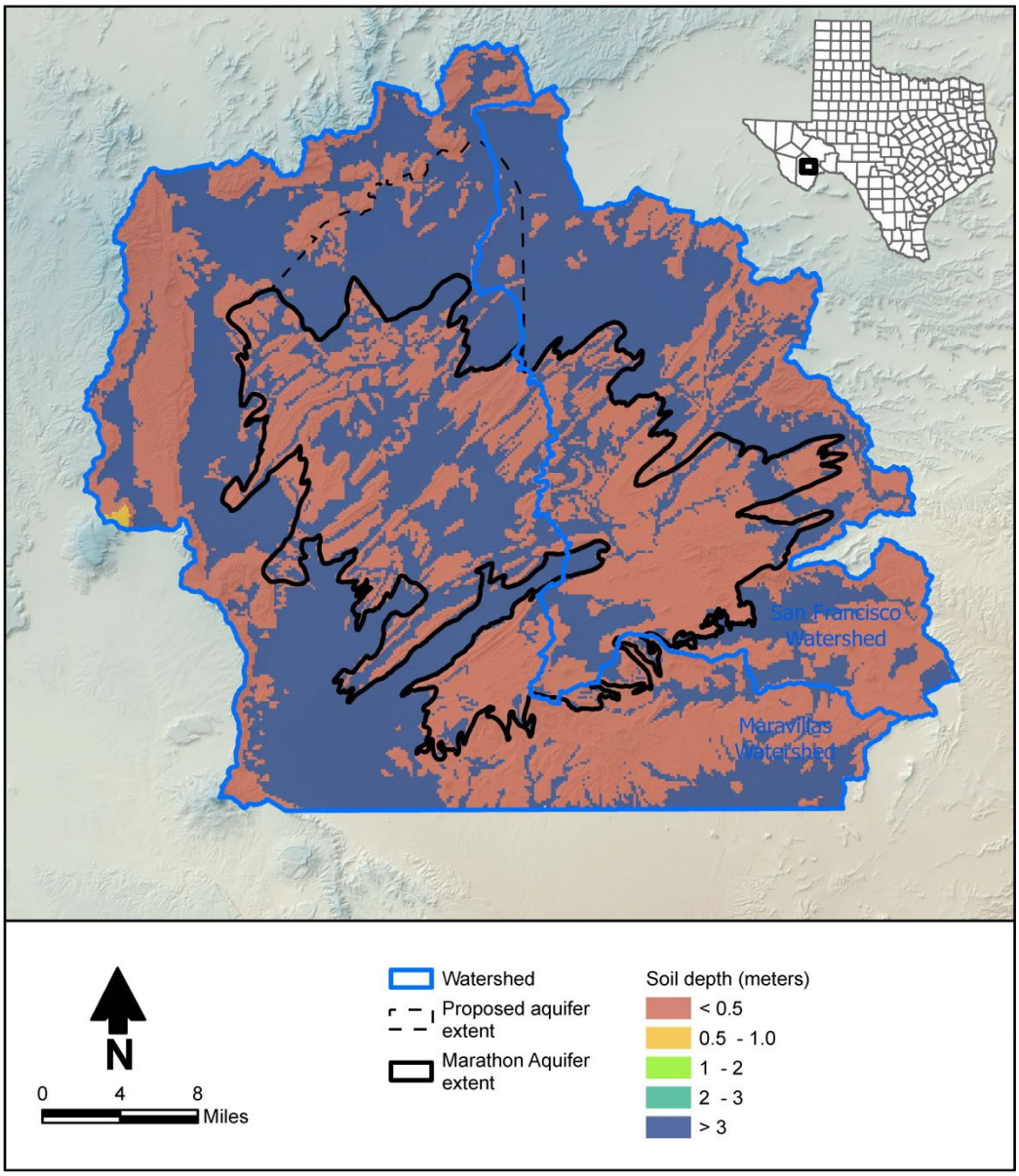

Figure 2-14. Distribution of soil depth.

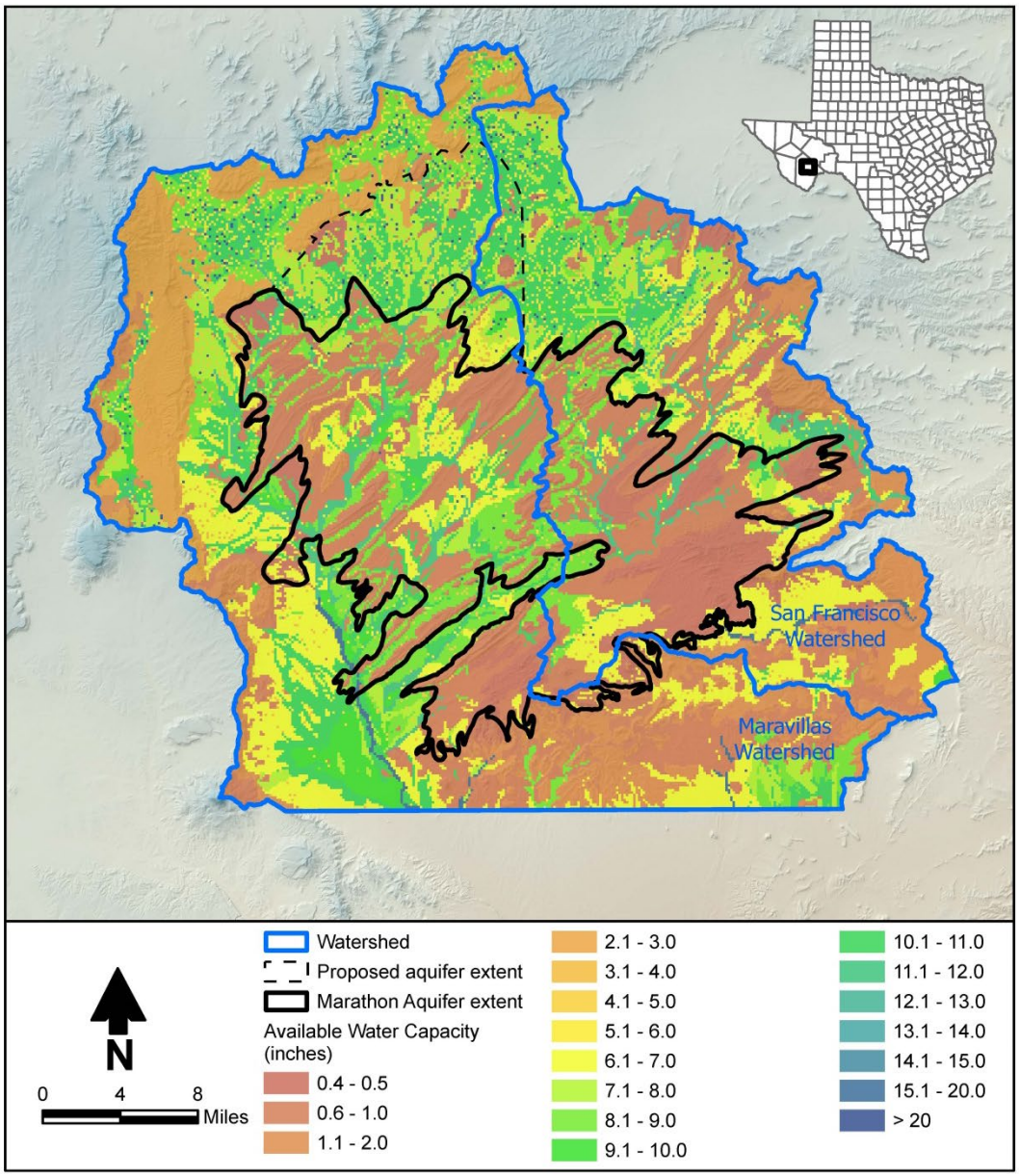

Figure 2-15. Distribution of soil water holding capacity.

Maps of mean annual potential and actual evapotranspiration are provided in Figures 2-16 and 2-17, respectively, for water years 1981 through 2021. The potential evapotranspiration is computed by the Distributed Parameter Watershed Model using the FAO-56 Penman-Monteith methodology (Section 4.3), and represents the potential evapotranspiration for a well-watered grass surface based on the climate and topography for the study area. The actual evapotranspiration is computed by the Distributed Parameter Watershed Model, and is the potential evapotranspiration modified to account for the soils and vegetation in the study area and limited by the available soil-water in the

root zone. As indicated in the figures, the actual evapotranspiration is much lower than the potential evapotranspiration.

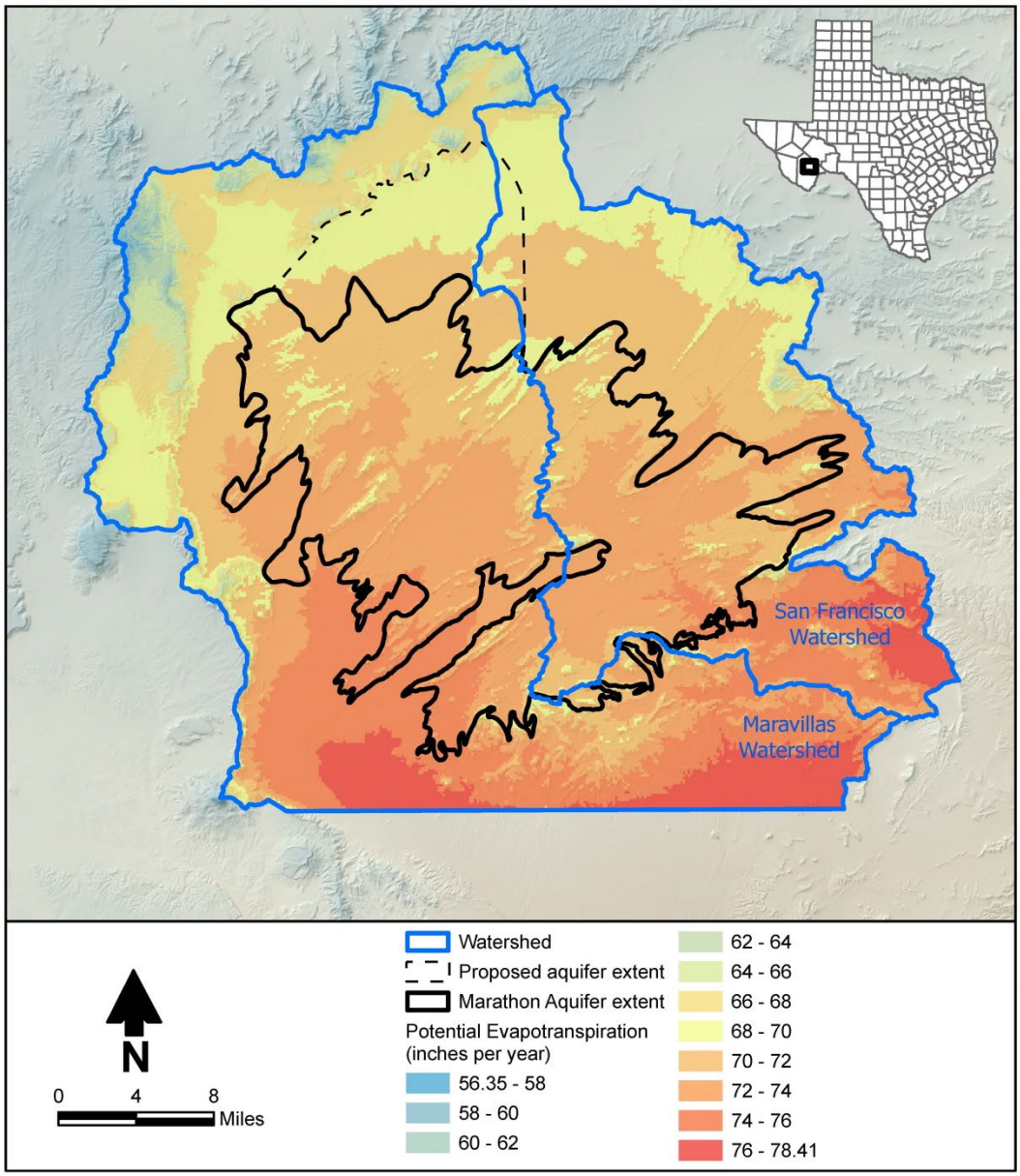

Figure 2-16. Potential evapotranspiration.

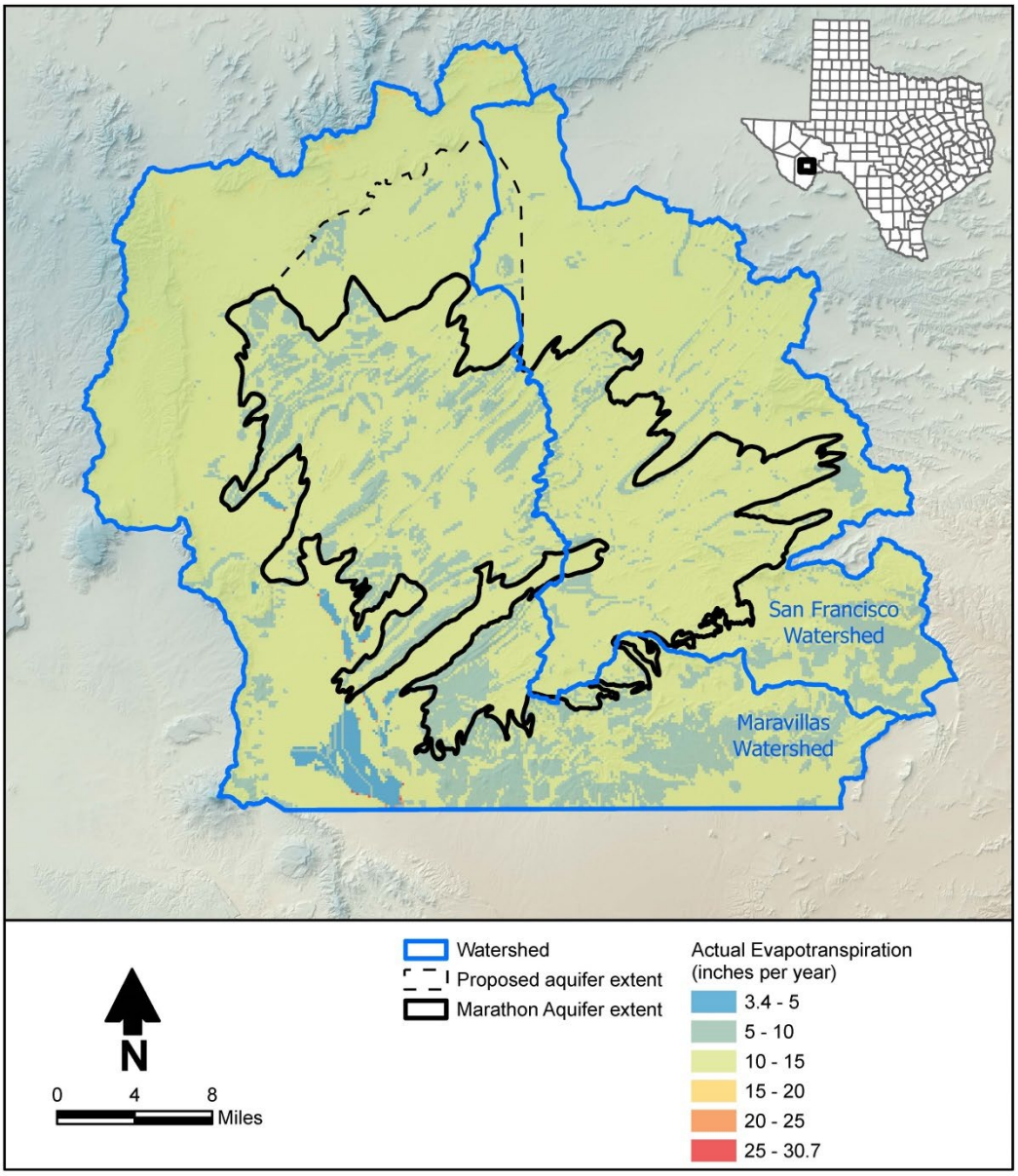

Figure 2-17. Actual evapotranspiration.

2.2 Geology

The Marathon Basin region has been shaped by major North American tectonic events over a period of more than a billion years. Major geologic periods that affected the basin include the Precambrian Grenville orogeny, late Paleozoic closure of that ocean and upthrusting of the Appalachian-Ouachita-Marathon Mountain chain, Laramide to early Tertiary block faulting (formation of Rocky Mountains) and uplift of the Marathon dome, and late Tertiary-Quaternary Rio Grande rifting (Muehlberger and Dickerson, 1989).

Precambrian rocks forming the basement of the Marathon Basin consist of metamorphic gneisses and schists; these Precambrian rocks are not exposed within the basin. During early Paleozoic—the Cambrian through the Mississippian—the Marathon Basin continued to deepen and received 3,100 feet of fossiliferous sediments during rifting about 700 to 500 million years ago (McBride, 1988). The Early Ordovician Marathon Limestone is part of this depositional sequence. This rifting episode established persistent northeast and northwest structural trends within the Marathon Basin. During Late Silurian through Early Mississippian time, hundreds of feet of fine-grained carbonates of the Caballos Novaculite were deposited (King, 1937).

During the late Paleozoic collision of North and South America (Ouachita Orogeny), the Marathon Basin continued infilling during the Upper Mississippian through Pennsylvanian, resulting in the deposition of the Tesnus Formation siliciclastics and the Dimple Limestone. Pre-Ouachita rocks were then deformed, although not metamorphosed, during late Pennsylvanian through earliest Permian. Pre-existing Ouachita northwest and northeast fault blocks were strongly influenced during deformation by the Marathon fold-thrust belt (Tauvers, 1988).

As the Pennsylvanian and Early Permian Marathon orogeny progressed, additional thrust sheets continually deformed the thick sediments and incorporated them into a series of progressively younger structural belts that formed northwestward. In the western part of the Glass Mountains, the Permian Lenox Hills Formation is part of the younger structural Dugout fold belt, and consists of clastic and cherty intervals, slope and basinal sediments, and some upper slope-margin limestones (Ross and Ross, 2003).

During Late Cretaceous to early Tertiary, the Laramide Orogeny occurred. Doming elevated and fractured the late Paleozoic structures, as well as post-Ouachita strata, all of which were subsequently eroded to create the present topographic basin. The dips of the Paleozoic formations steepen from the crest to the flanks of the Marathon Dome (King, 1937). During the Mid-Tertiary, small localized igneous plugs of basalt intruded around the perimeter of the Marathon Dome (King, 1937). Finally, from the Late Tertiary to Quaternary, the local stress regime changed from compression to extension, and the north to north-northwest trending structured were rejuvenated by the Basin and Range tectonism (Dickerson, 2013).

The following subsections provide an overview of the stratigraphy and structure of the Marathon Basin rocks.

2.2.1 Stratigraphy

The Marathon Aquifer study area stratigraphic column is presented in Table 2-1. This table is based on the integration of multiple references, including King (1937), King (1980), Tauvers (1988), Anderson and others (1982), Barnes (1979), and Reed (1990). Unconformities as described by King (1937) are noted in Table 2-1 to provide a temporal perspective of the episodes of structural activity, deposition, and erosion. General lithology descriptions along with the estimated range of formation thickness are also provided.

The Cambrian through the Permian stratigraphic nomenclature for the Marathon Basin is entirely different than that of the Delaware Basin, which lies a few tens of miles to the northwest. The two basins are separated by the Glass Mountains and a major structural offset that occurs at the southern end of the Glass Mountains.

A publication by Reed (1990) provides insight to the stratigraphic equivalents between the Marathon and Delaware basins. The major groundwater-producing formation in the Marathon Basin is the Marathon Limestone, which is stratigraphically equivalent to the Ellenburger Formation in the Delaware Basin. A summary of the stratigraphic equivalents between the two basins is provided in Table 2-1 to provide additional stratigraphic context for the reader. The stratigraphic equivalents for the Marathon Permian Cathedral Mountain and Cretaceous Del Carmen and Telephone Canyon were not determined. Surface geology of the study area based on Barnes (1979) and Anderson and others (1982) is provided as Figure 2-18.

The following subsections provide geologic and lithologic descriptions of each formation included in Barnes (1979) and Anderson and others (1982) in order of oldest to youngest geologic age. The descriptions are paraphrased from King (1937) unless otherwise noted. King's descriptions commonly reference a location, spring, mountain range, creek name, structural feature, and/or a cross section location from a King (1937) cross section to provide lithologic or structural descriptions at a given location. A series of figures are provided to assist the reader with identification of the location of these descriptions. Figure 2-19 provides towns, ranches, or historical settlements referenced by King (1937); the ranch names are not representative of current ownership. Figure 2-20 labels major geographic features, such as mountain ranges and the intervening "flats." Figure 2-21 provides the locations of major, still active, structural features. Figure 2-22 illustrates the locations of the King (1937) cross sections. Figure 2-23 is a map of the drainages that intersect the Marathon Aquifer extent and the springs identified in King (1937).

Table 2-1. Stratigraphic column for the Marathon Aquifer study area and corresponding geologic units in the Permian Basin.

Period and Series	Delaware Basin, Foreland Formations	Marathon Thrust Belt Formations	Primary Lithology of Marathon Formations	Approximate Thickness (feet)
Quaternary	Alluvial types	Alluvial types	Gravel, sand, silt, clay	50–100
Tertiary	Volcanic, intrusives	Volcanic, intrusives	Volcanic, intrusive rocks	
Cretaceous, Lower Trinity	?	***Unconformity*** Del Carmen and Telephone Canyon	Limestones, chert, and shales	400
	Maxon Sand	Maxon Sandstone	Sandstone and marl	50–160
	Glen Rose	Glen Rose	Limestone, marl, chert, conglomerate	400–550
Permian, Leonard	?	***Unconformity*** Cathedral Mountain	Shale, limestone, and pebble conglomerate	0–700
	Bone Spring	Skinner Ranch and Hess Limestone	Limestone and pebble conglomerate	2,500–3,250
Permian, Wolfcamp	Wolfcamp	Lenox Hills	Conglomerate, shale, and limestone	0–650
Upper to Lower, Pennsylvanian	Cisco, Canyon and Strawn	***Unconformity*** Gaptank	Limestone, sandstone conglomerate	1,900
	Atoka	Haymond	Sandstone, shale, boulder beds	2,000–4,000
Lower Pennsylvanian to Upper Mississippian		Dimple Limestone	Limestone and shale	0–1,000
	Morrow and Barnett	Tesnus, ***Unconformity***	Sandstone and shale	300–6,200
Devonian to Upper Ordovician	Miss. Lime, Woodford, Devonian, Upper Silurian, Fusselman	Caballos Novaculite ***Unconformity***	Novaculite and chert	125–560
	Montoya	Maravillas Chert	Chert conglomerate	125–560
	Simpson	Woods Hollow Shale	Shale	180–500
		Fort Pena	Limestone, chert and shale	125–600
		Alsate Shale	Shale, limestone, sandstone	25–145
Lower Ordovician to Upper Cambrian	Ellenburger	Marathon Limestone	Limestone, sandstone and conglomerate	0–1,100
	Cambrian Sands	Dagger Flat Sandstone ***Unconformity***	Sandstone	300–940

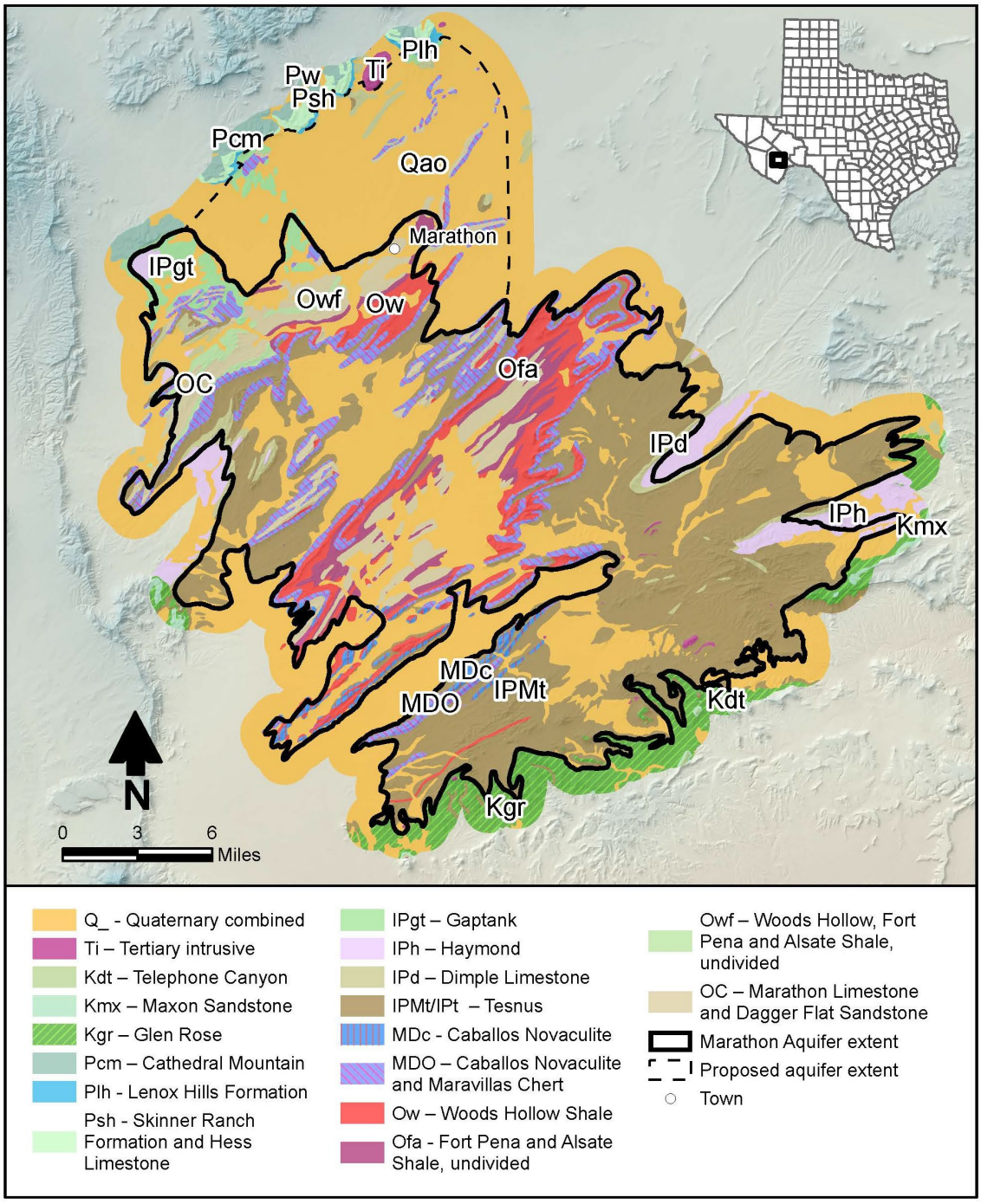

Figure 2-18. Surface geology of the Marathon Aquifer study area based on Barnes (1979) and Anderson and others (1982).

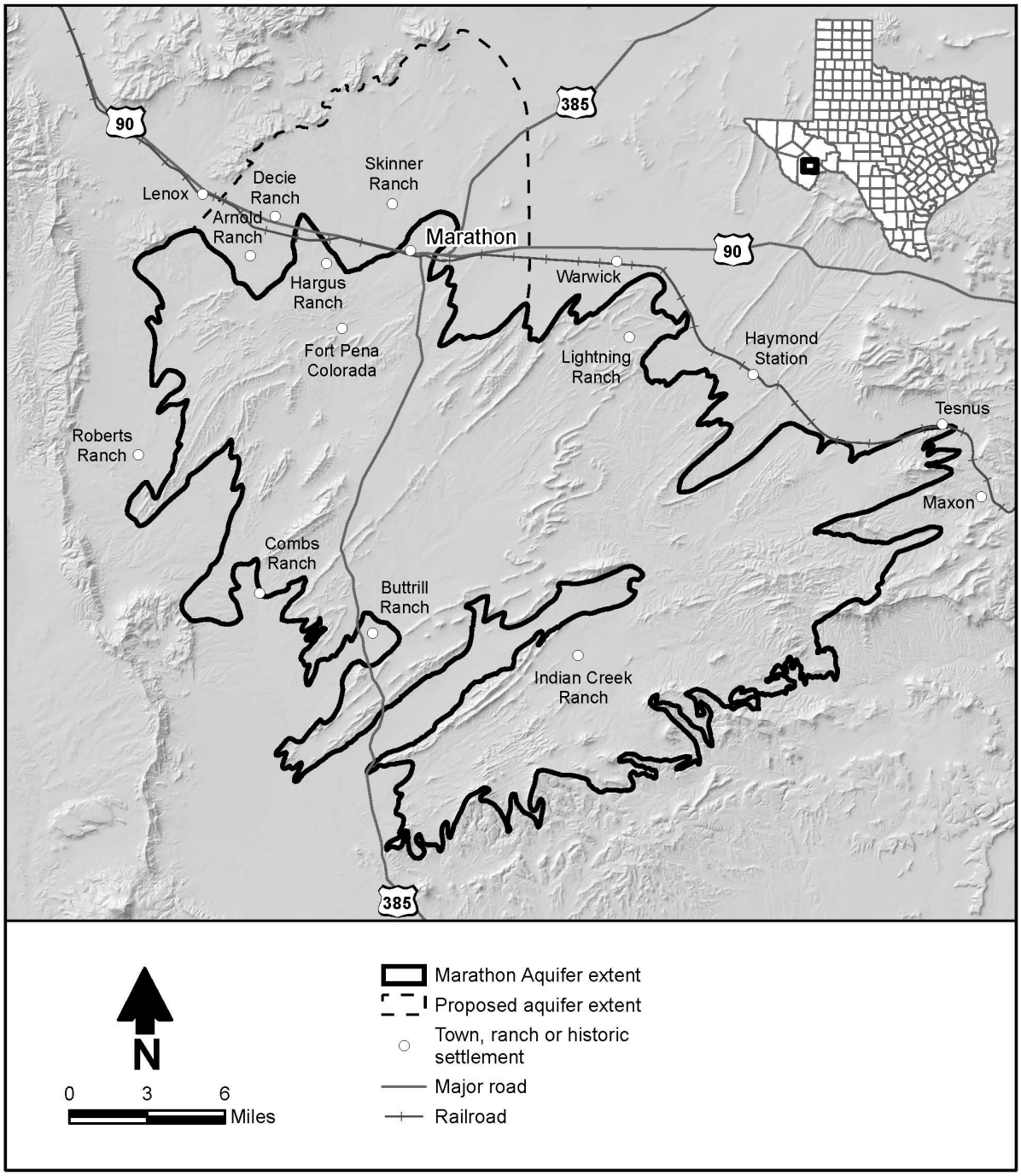

Figure 2-19. Selected towns, ranches, and settlements referenced in King (1937).

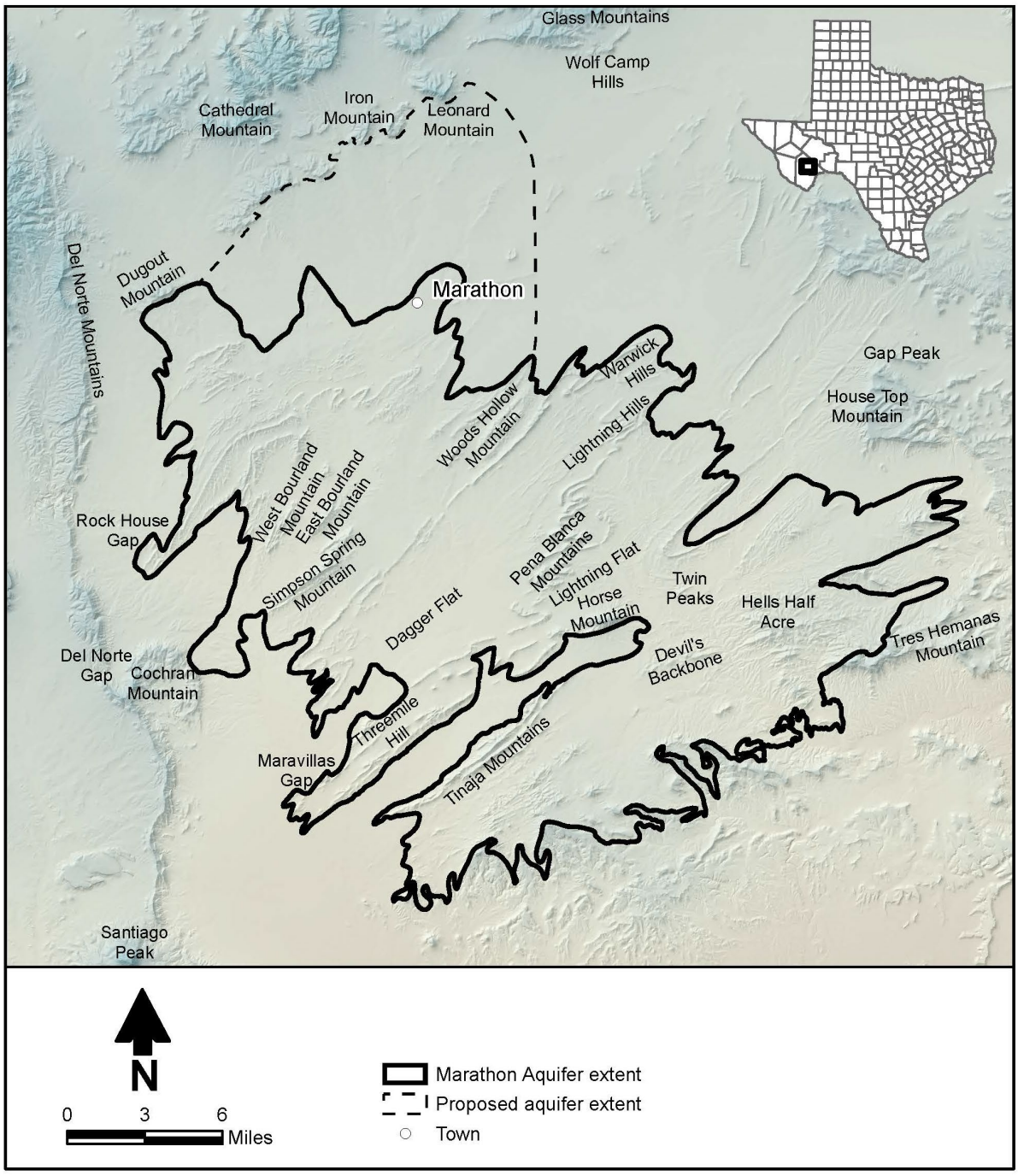

Figure 2-20. Primary geographic features of the Marathon Aquifer study area.

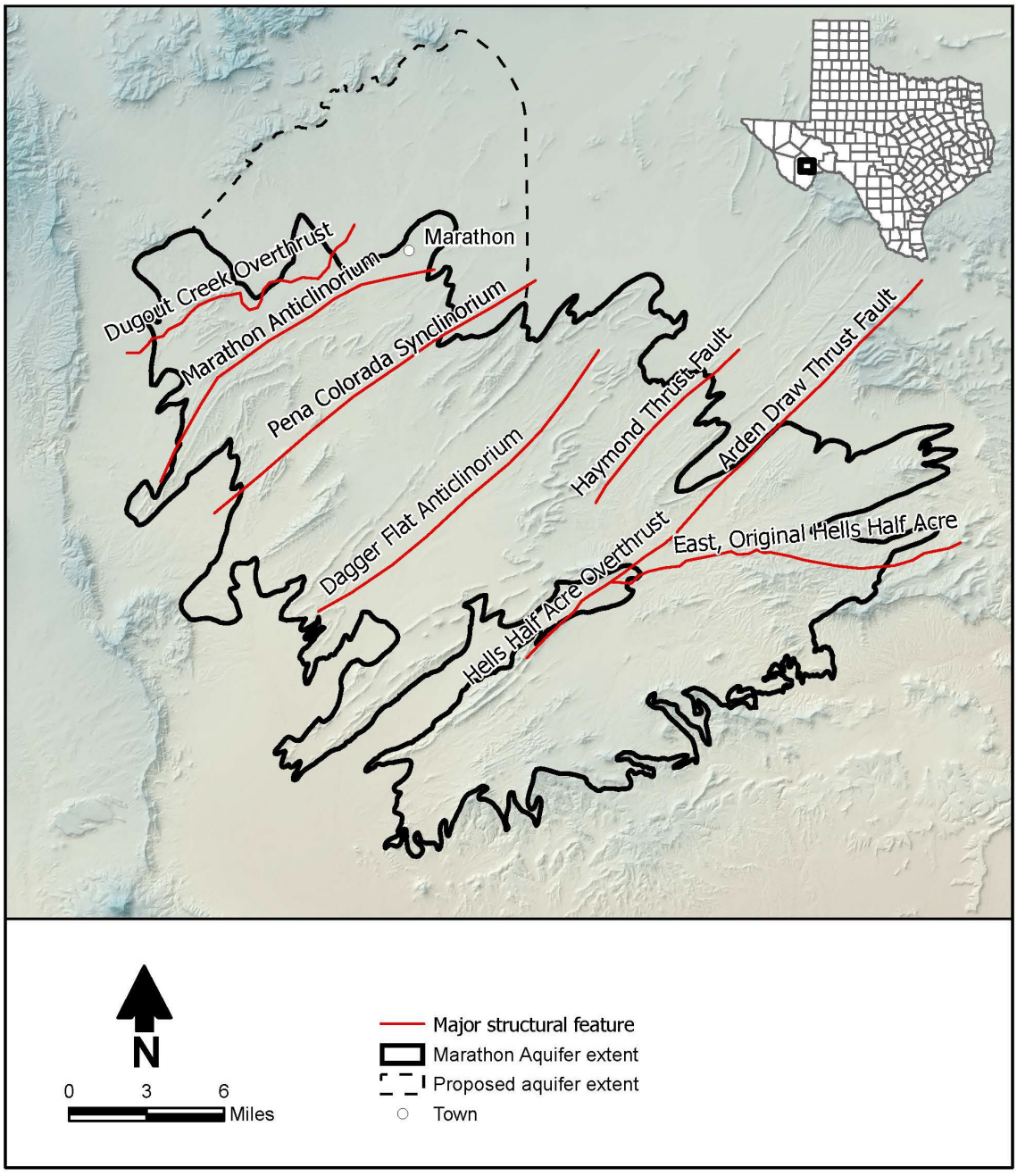

Figure 2-21. Locations of main structural features within the Marathon Aquifer.

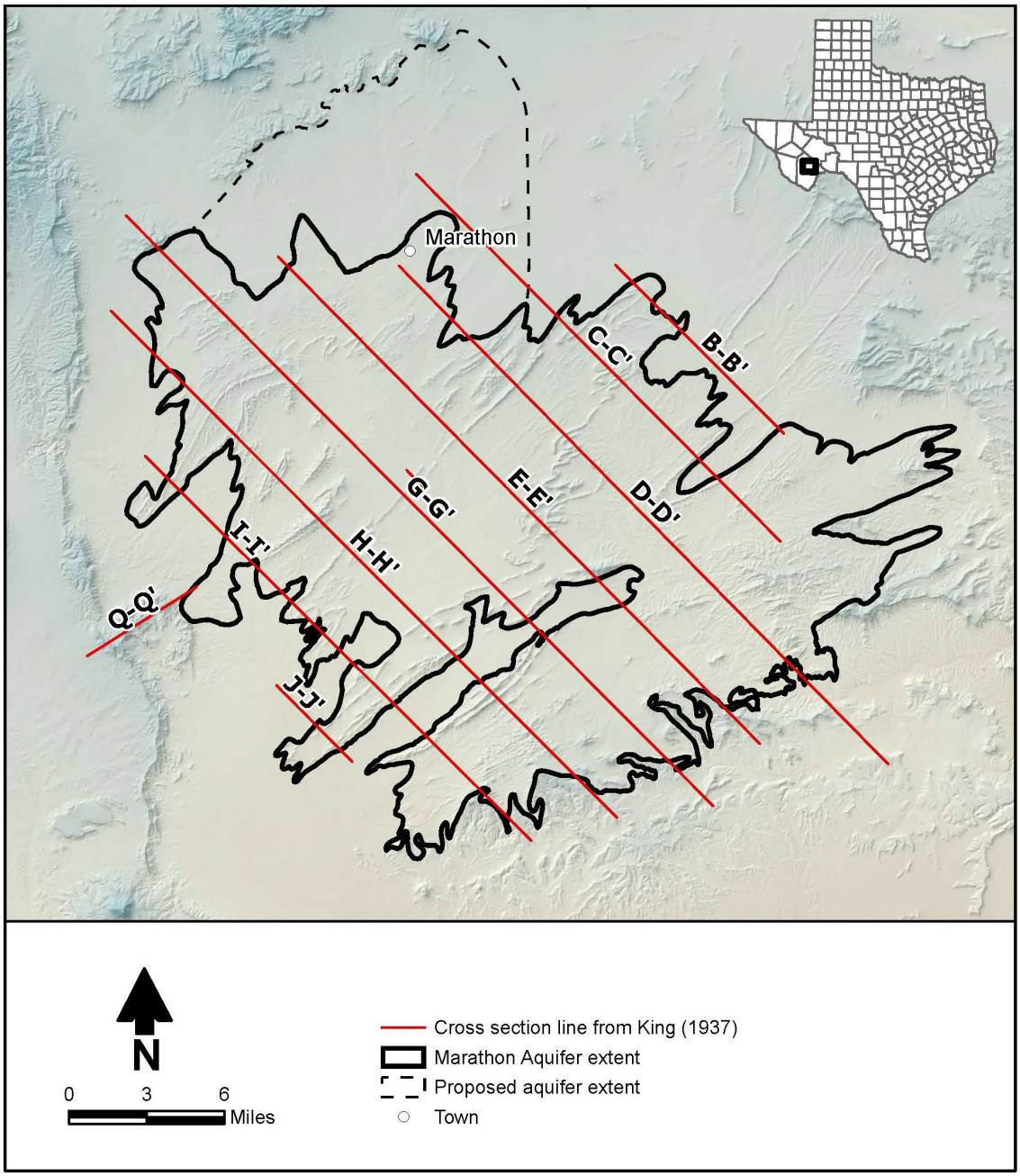

Figure 2-22. Locations of King (1937) cross sections.

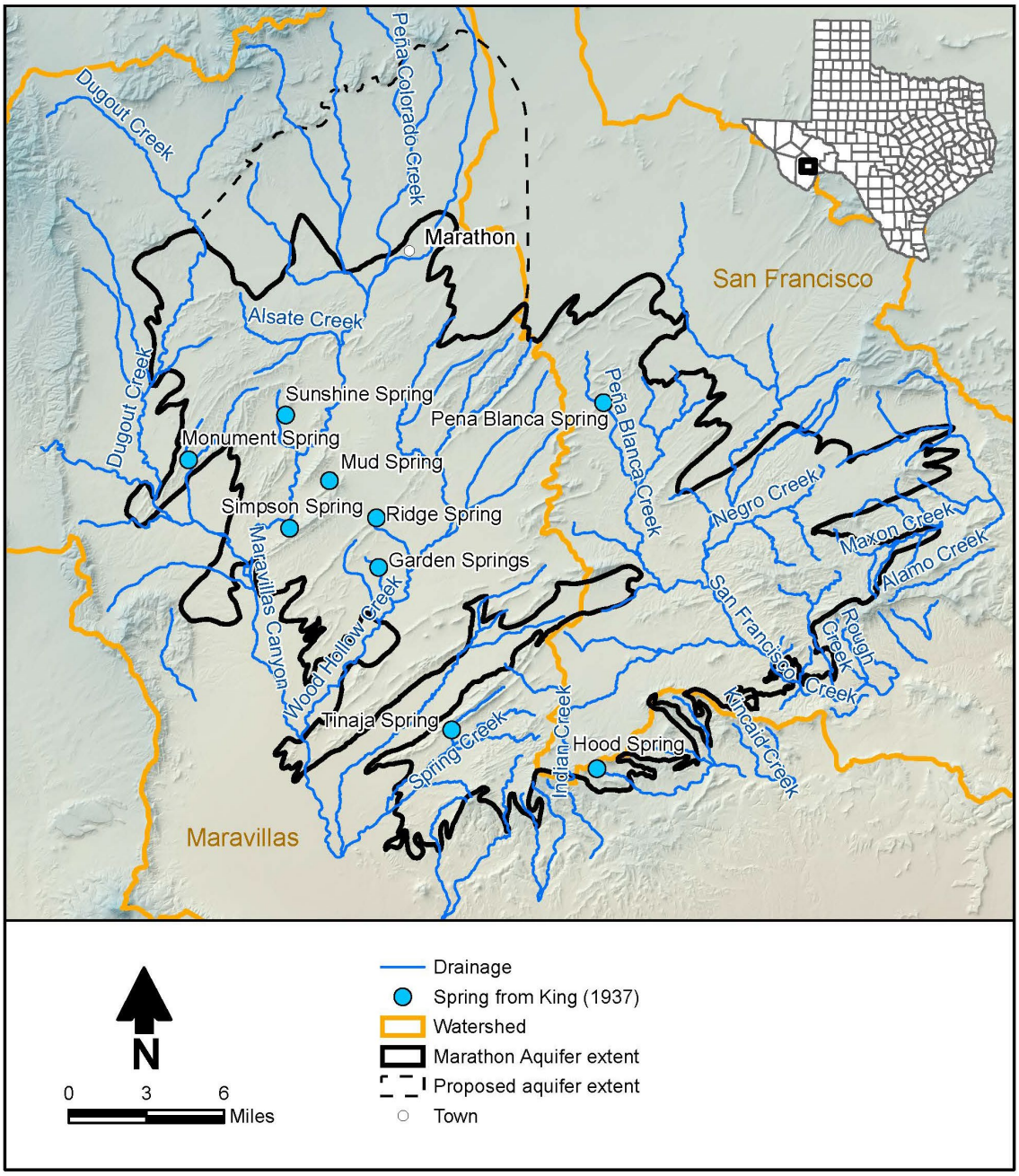

Figure 2-23. Drainages within the Marathon Aquifer study area and springs identified in King (1937).

2.2.1.1 Upper Cambrian

The Dagger Flat Sandstone is the oldest rock in the Marathon region, and consists of massive sandstones overlain by flaggy and thinly laminated brown and greenish micaceous sandstones weathering to angular blocks and flags, with significant amounts of interbedded shale, particularly toward the top of the unit. This formation's fossils are poorly preserved. The base of the Dagger Flat sandstone is not exposed and the relationship with the underlying older Cambrian rocks is not known. The maximum observed thickness of this formation is 300 feet.

The most extensive exposures Dagger Flat Sandstone occur on the Buttrill Ranch and near Three-mile Hill (Figures 2-19 and 2-20), in the vicinity of cross-sections H–H' and I–I' (Figure 2-22). The Dagger Flat Sandstone is overlain by Marathon Limestone. The contact with the overlying Marathon Limestone is not distinct, and is complicated by local folding.

2.2.1.2 Ordovician

The Ordovician formations consist of the Marathon Limestone, Alsate Shale, Fort Pena Formation, Woods Hollow Shale, and Maravillas Chert. Within some areas, Barnes (1979) and Anderson and others (1982) map the Dagger Flat Sandstone and Marathon Limestone as one unit. They also map the Alsate Shale and the overlying Fort Pena Formation as a single unit, and in some areas they map the Woods Hollow Shale and the Fort Pena Formation as a single unit. The following descriptions are from King (1937).

2.2.1.2.1. Marathon Limestone

The Marathon Limestone is the major groundwater producing formation in the Marathon Basin. This formation consists of flaggy limestone weathered to an ashen-gray or bluish color, some of which contain graptolites. Generally thin layers of shale separate most of the limestone layers with a few thicker greenish-shaley intervals. The formation contains argillaceous intervals that make up one-third or one-half its total thickness. Locally, layers of sandstone and numerous beds of intraformational conglomerate occur between the limestones. For formation description purposes, King (1937) divided the Marathon Limestone into three members, called the Upper, the Monument Spring dolomite, and the Lower members.

Aerial photographs of Marathon Limestone outcrops are lighter-colored than adjacent formations, but are streaked with faint light and dark bands that mark the outcrops of individual beds (King, 1937). The Marathon Limestone ranges between 500 and 1,000 feet in thickness, but thins to 350 feet in the southernmost exposures. The formation is highly folded and crumpled, and in some areas weaker beds are cut out by squeezing or faulting.

The most extensive exposures in the Marathon Limestone occur near the axis of the northeast-southwest trending Marathon and Dagger Flat anticlinoria and within the eastern limb of the Pena Colorada Synclinorium (Figures 2-18 and 2-21). Marathon Limestone outcrops occur in the vicinity of King (1937) cross sections C–C', D–D', E–E', F–F', G–G', H–H', and I–I' (Figure 2-22).

Marathon Limestone outcrops occur along the streets and within vacant lots of Marathon, and from Marathon west to the Robert Ranch where the flaggy, ashen-gray limestone outcrops along the crest of the Marathon anticlinorium, in nearly level plains, and/or in rolling hills (Figures 2-19 and 2-21). Marathon Limestone basal beds rest on Dagger Flat sandstone about a mile southwest of the railway station in the town of Marathon.

Within the Marathon Anticlinorium (Figure 2-21), the Marathon Limestone is sharply separated from the Alsate Shale by coarse conglomerate. The Monument Spring dolomite member is persistent and up to 90 feet thick. Along the drainage of Alsate Creek (Figure 2-23), the Marathon Limestone below the base of the conglomerate is channeled and broken. The conglomerate is deposited in cavities and interstices.

Within the Dagger Flat anticlinorium (Figure 2-21), the Marathon Limestone ranges from 950 feet in the northeast and 350 feet in the south. The upper contact for the Marathon Limestone is a conglomerate with slightly different character limestones above and below the conglomerate. The Monument Spring dolomite member is only a few feet thick in the northern part of the area and is absent in the south.

2.2.1.2.2. Alsate Shale

The Alsate Shale is a distinctive thin formation overlying the Marathon Limestone, set off below and above by conglomerates and is characterized by graptolites. The formation consists of two facies; the northern exposures are mostly shale, but the southern exposures contain numerous limestone ledges.

Within the Marathon Anticlinorium (Figure 2-21), the Alsate Shale consists of 5 to 18 feet of conglomerate, overlain by 20 to 40 feet of shale. The change of lithology from shales of the massive sandy limestones and intercalated conglomerates of the Fort Pena Formation is striking. This may be evidence that the two formations are separated by a considerable unconformity, which probably represents the later part of lower Ordovician.

The most extensive exposures in the Alsate Shale occur along the structural limb flanks of the northeast-southwest trending Dagger Flat and Marathon anticlinoria, and southeast of the Arnold Ranch about 1.5 miles along the Dugout Creek Overthrust (Figures 2-18, 2-19, and 2-21). The Alsate Shale outcrops are in the vicinity of King (1937) cross sections C–C', D–D', E–E', F–F', G–G', and H–H' (Figure 2-22).

Within the Marathon Anticlinorium, the Alsate Shale is thickest along anticlinal and synclinal axes. The thickness difference suggests that the Alsate Shale may have acted as a plastic cushion between the two more competent members—the Marathon Limestone below and Fort Pena Formation above.

Within the Dagger Flat Anticlinorium, the Alsate Shale is 100 to 145 feet thick. In this area, ledges of limestone like those in the Fort Pena Formation are a conspicuous part of the formation, with each limestone separated by about 3 to 8 feet of poorly exposed shale. The gray limestones generally form 0.5- to 1-foot beds that are finely granular or sandy.

2.2.1.2.3. Fort Pena Formation

The Fort Pena Formation ranges from 125 to 200 feet in thickness and consists primarily of alternations of thick-bedded limestone—locally sandy with bedded bluish and purplish chert, with some thin partings of shale and one or more beds of coarse conglomerate near the base. Aerial photographs of the outcrops of the Fort Pena Formation stand out as a narrow band that is darker than the outcrops of adjacent formations. The Fort Pena Formation is the dominant ridge maker in the Paleozoic sequence below the novaculite, and rises in low hogbacks out from the generally level country within the Marathon and Dagger Flat anticlinoria.

The most extensive exposures in the Alsate Shale occur along the structural limb flanks of the northeast-southwest trending of the Dagger Flat and Marathon anticlinoria and southeast of the Arnold Ranch about 1.5 miles along the Dugout Creek Overthrust (Figures 2-19 and 2-21). The Fort Pena outcrops along most of the King (1937) cross sections (Figure 2-22).

Within the Marathon Anticlinorium, the Fort Pena Formation outcrops between Marathon and the Roberts Ranch (Figures 2-18 and 2-19) as low but prominent ridges. Shales increase in prominence toward the top of the formation, with the upper part consisting of many thin beds of reddish or bluish granular chert, and the shale beds increase in thickness near the contact with the overlying Woods Hollow Shale.

Within the Dagger Flat Anticlinorium, the Fort Pena Formation is divisible into several members. The lower member consists of thick-bedded gray-brown granular limestone, with some thin-bedded chert. The middle member consists of about 15-foot-thick, dominantly shales that create a sag in the hogback ridge. The upper member consists of bluish gray to reddish, massive chert in several 3- to 4-foot ledges followed by thin limestones and interbedded shales that grade conformably into the Woods Hollow Shale.

2.2.1.2.4. Woods Hollow Shale

The Woods Hollow Shale consists of greenish clay shales interbedded with thinly laminated gray or yellowish sandy limestone and limy sandstone. Some beds are nodular and coarsely granular, conglomeratic limestone, crowded with fragmental fossils. Locally, in the southwestern part of the Marathon Basin, shales may include large, embedded boulders that contain Cambrian and Lower Ordovician fossils. The Woods Hollow Shale ranges in thickness from 300 to 400 feet.

This formation usually forms valleys between the hogbacks of the Fort Pena Formation and the higher ridges of the Maravillas Chert and Caballos Novaculite. In most places, the Woods Hollow Shale is covered by soil and crops out only in gullies and creek banks.

The most extensive exposures in the Woods Hollow Shale occur along the structural limb flanks of the northeast-southwest trending of the Dagger Flat and Marathon anticlinoria and between the Dagger Flat Anticlinorium and the Hells Half Arce Overthrust (Figures 2-18 and 2-21). The Woods Hollow Shale outcrops are in the vicinity of nearly all of the King (1937) cross sections (Figure 2-22).

Strong structural differences between the Fort Pena and Marathon formations below and the Caballos Novaculite and Maravillas Chert above suggest that the incompetent shales of the Woods Hollow Formation had a cushioning effect, allowing the overlying and underlying strata to be deformed differently. The intensity and complexity of these larger structural features is reflected by the intense contortion of the shales in the local exposures of the formation. Dip differences the Maravillas and Woods Hollow formations are probably of tectonic origin and result from the gliding of competent beds over incompetent beds as the rocks were being deformed. The Woods Hollow Shale is separated from the overlying Maravillas Chert by a sharp lithologic break representing a transition from shale and sandy limestone deposition to chert and massive limestone deposition.

2.2.1.2.5. Maravillas Chert

The Maravillas Chert crops out on the inner slopes of the novaculite hogbacks and consists of interbedded limestone and black, bedded chert, with the chert predominating toward the top. In the northwestern part of the study area, this formation has a thick, coarse, basal conglomerate along with other conglomerate beds higher in the section. Barnes (1979) and Anderson and others (1982) map the Maravillas Chert and the overlying (Devonian) Caballos Novaculite as one unit.

The Maravillas Chert ranges in thickness from 100 to 200 feet in the Marathon Anticlinorium (Figure 2-21), but thickens southward to 400 feet. South of Marathon, the upper part of the formation is about 170 feet thick and consists of little other than black, dull-lustered, bedded chert.

The most extensive exposures in the Maravillas Chert occur as ridges paralleling the northeast-southwest trending of the Dagger Flat and Marathon anticlinoria, along the Dugout Creek Overthrust, between the Dagger Flat Anticlinorium and the Hells Half Arce Overthrust (Figure 2-21), between Iron and Leonard Mountains and the town of Marathon and southeast of the Tinaja Mountains (Figures 2-19 and 2-20). The Maravillas Chert outcrops are in the vicinity of all of the cross sections in Figure 2-22.

In the northeastern part of the Marathon Anticlinorium (Figure 2-21), the lower or calcareous part of the Maravillas Chert is sharply offset from the upper or cherty part. Within the Dagger Flat Anticlinorium, the conglomerate beds of the Maravillas Chert are fewer and thinner and the transition between the lower calcareous and the upper cherty parts of the formation is not sharply marked. The vitreous buff, brown, or gray chert of the lower member of the Caballos Novaculite consistently overlies the dull, black chert sharp contact of the Maravillas Chert.

2.2.1.3 Devonian

The Maravillas Chert and Caballos Novaculite are combined as one map unit by Barnes (1979) and Anderson and others (1982). The Caballos Novaculite, a resistant white formation, is the chief ridge former in the Marathon Basin. The Caballos Novaculite is thought to span the entire Silurian and Devonian systems (Wilde, 1990). This formation was subdivided by King (1937) into five members: a lower chert member at the base, a

lower novaculite member, a middle chert member, an upper novaculite member, and an upper chert member at the top. The members change in thickness from northwest to southeast across the area, so various facies of the formation can be distinguished. The maximum thickness ranges from 600 feet in the southern part to 200 feet in the extreme northwestern part of the basin.

The novaculite beds are more dominant in the south, while bedded cherts with shale partings are more dominant in the northwest. The Caballos Novaculite underlies the Tesnus Formation with considerable unconformity that probably represents most if not all Mississippian time.

The most extensive exposures in the Caballos Novaculite occur as ridges paralleling the northeast-southwest trends of the Dagger Flat and Marathon anticlinoria, along the Dugout Creek Overthrust, between the Dagger Flat Anticlinorium and the Hells Half Acre Overthrust, between Iron and Leonard Mountains and the town of Marathon, and southeast of the Tinaja Mountains (Figures 2-18, 2-20, and 2-21). Caballos Novaculite outcrops occur in the vicinity of all of the King (1937) cross sections in Figure 2-22.

On the southeast flank of the Marathon Anticlinorium, the lower novaculite is prominent and is represented by a thick member of bedded chert at such localities as Monument Spring and Fort Pena Colorada, and on Simpson Springs and East Bourland Mountains (Figures 2-18, 2-20, 2-21, and 2-23). The Caballos Novaculite is generally 300 to 400 feet thick in this region, but reaches a maximum of 520 feet at Monument Spring (Figure 2-23). Along the northwest flank of the Dagger Flat Anticlinorium, the lower novaculite member is dominant and is about 60 feet thick, while the upper novaculite thickens from 5 feet in the northwest to about 25 feet in the Woods Hollow Mountains (Figures 2-20 and 2-21). There is an unconformity between the Caballos Novaculite and the overlying Tesnus Formation.

2.2.1.4 Pennsylvanian

The Pennsylvanian formations consist of the Tesnus Formation, the Dimple Limestone, the Haymond Formation, and the Gaptank Formation. Summaries of these units are provided in the following subsections.

2.2.1.4.1. Tesnus Formation

The Tesnus Formation is a thick sequence of interbedded sandstone and shale with thin and thick beds, and is nearly barren of fossils. Because of the generally nonresistant character of its sandstones and shales, the Tesnus Formation occupies the valleys and depressions on the plains. The Tesnus Formation is usually several thousand feet thick, but its thickness varies. In the northwestern part of the basin, the formation is about 300 feet thick and consists of nearly all black shale with few interbedded sandstone layers.

Along the east side of the Marathon Basin, east of the novaculite ridges that bound the Dagger Flat Anticlinorium on the southeast (Figure 2-21), the Tesnus Formation is folded into broad open anticlines and synclines. The formation thickness can exceed 6,500 feet; the composition is predominantly sandstone with many arkose layers and several prominent massive layers of white quartzite.

The Tesnus Formation outcrops throughout the Marathon Aquifer study area except for west of the Dugout Creek Overthrust and within a few miles along the northeast to southwest axis of the Marathon and Dagger Flat anticlinoria (Figures 2-18 and 2-21). Tesnus Formation outcrops occur in the vicinity of all of the King (1937) cross sections illustrated in Figure 2-22.

The upper three quarters of the Tesnus Formation is predominantly sandstone occurring as low parallel massive ledges that crop as rugged ridges in the region of Hells Half Acre and Devils Backbone (Figure 2-21). The sandstone ledges consist of compact, greenish quarzitic sandstone and coarse-grained, friable, buff arkose, with small amounts of interbedded shale. There are a few jagged hogbacks of cream-colored quarzitic sandstone. These sandstone ledges are separated by shallow valleys carved from the interbedded shales (King, 1937). Sandstone bed thickness is up to 40 feet, although most are between 1 and 5 feet thick (McBride and Thomson, 1964).

Many of the massive sandstones are crosscut with lines of shear and fracture and include veins of quartz and calcite. Evidence of low-grade metamorphism is observed in the thinner beds with the occurrence of secondary mica. The basal shale member occupies the lower quarter of the formation. Aerial photographs of this area having outcrops of the sandstones and shales stand out as alternating narrow light and dark bands, revealing the structure of the formation.

Along the lower San Francisco Creek (Figure 2-23) and south of the large fault that bounds Hells Half Acre on the north (Figure 2-21), Tesnus Formation folds are obscure and closely packed, and the overlying Dimple Limestone is absent. Within the Pena Colorada Synclinorium or the northwest side of the Dagger Flat Anticlinorium (Figure 2-21), the Tesnus Formation consists predominantly of shale and is around 2,000 feet thick.

In the Dugout Creek area (Figure 2-23), the Tesnus Formation is about 300 feet thick and is nearly continuous from Monument Spring around the southwest end of the Marathon Anticlinorium to the Dugout Creek area on its northwest flank. In this area, the Tesnus Formation consists of greenish clay shales and indurated blue-black shales, interbedded conglomerate, and some beds of dull-lustered chert.

The Tesnus Formation is probably conformable with the overlying Dimple Limestone and is separated by a transition zone of interbedded limestone and shale. The contact is the lowest limestone layer interbedded in the shale.

2.2.1.4.2. Dimple Limestone

The Dimple Limestone consists of massive, resistant limestones that occur as widely exposed, narrow, sinuous belts of outcrop in the eastern portion of the Marathon Basin. The formation is a sequence of interbedded limestones, dark indurated shales, thin pebble conglomerates, and black cherts (Thomson and Thomasson, 1964). The limestones are dominantly gray, granular, and locally sandy with scattered seams of chert pebbles. Fossils are common.

Within the western part of the Marathon Basin, the Dimple Limestone is only 100 feet thick, and consists mainly of dark-gray granular limestones, which crop out as ledges several feet thick and contain seams of fine chert pebbles and crinoidal fragments. There are many intervals of thin-bedded or flaggy sandy brown and siliceous limestones with interbedded indurated greenish shale.

The Dimple Limestone outcrops within the southern areas between the Marathon Anticlinorium and Dugout Creek, and between the Marathon Anticlinorium and the Pena Colorada Synclinorium (Figures 2-21 and 2-23). It also outcrops north of the town of Marathon between Iron and Leonard Mountains, west and paralleling Arden Draw Thrust Fault and paralleling and south along the northern half of the Hells Half Acre Overthrust (Figures 2-18, 2-20, and 2-21).

The Dimple Limestone outcrops are in the vicinity of King (1937) cross sections B–B', C–C', H–H', and I–I' (Figure 2-22).

South of Haymond Station (Figure 2-19), the Dimple Limestone is less than 500 feet thick (Thomson and Thomasson, 1964). At this location, the Dimple Limestone consists of a main mass of dark gray, finely granular limestone with beds 1 to 4 feet thick, interbedded with many partings of dark indurated shale, capped with a dark indurated shale 150 feet thick on top and a 50-foot-thick dark indurated shale at the base.

Additional southeastern exposures are small patches surrounded by outcrops of the Tesnus Formation within the faulted complex of Hells Half Acre and Devils Backbone (Figure 2-21). The Dimple Limestone has gradational contacts with the Haymond (overlying) and Tesnus (underlying) formations; the contacts are selected at the highest and lowest limestone beds.

2.2.1.4.3. Haymond Formation

The Haymond Formation consists of a huge thick sequence of interbedded, fine to very fine grained, olive-brown sandstone, interbedded with thin black shales. The formation also has a thick mudstone interval, called the Boulder-bed Member, which includes massive coarse sandstone, chert conglomerate, and large exotic (sedimentary, volcanic, intrusive, and metamorphic) and erratic blocks of rock (Dimple Limestone, Tesnus Formation, Caballos Novaculite, and Maravillas Chert). Erratic blocks of Dimple Limestone within the Haymond Formation are up to 130 feet long. The maximum thickness of the preserved Haymond Formation is 4,200 feet (King, 1937; McBride, 1964a and 1964b). The outcrop extent of the Haymond Formation is more restricted than that of the Tesnus Formation because it is confined to synclinal remnants, and it is further masked by overlying Quaternary deposits. No complete sections of the Haymond Formation are exposed from the base to top of the formation (King, 1980).

The Haymond Formation outcrops southeast of Dugout Mountain between the Marathon Anticlinorium and Dugout Creek, and between the Marathon Anticlinorium and the Pena Colorada Synclinorium, north of Cochran Mountain, at the northern end of the Haymond Thrust Fault, west of and paralleling the Arden Draw Thrust Fault and paralleling and east

of the northern Hells Half Acre Overthrust (Figures 2-20, 2-21, and 2-23). The outcrops are in the vicinity of King (1937) cross-sections B–B', C–C', H–H', I–I', and Q–Q' (Figure 2-22).

The upper member of the Haymond Formation is more than two-thirds of the formation and is exposed only on the west side of Housetop Mountain (Figure 2-20) (McBride, 1964a and 1964b). This exposure has the rhythmic bedding characteristic but most of the light-colored beds are sandy shales, with sandstone layers. The upper member extends up to the axis of the syncline west of Housetop Mountain and is the highest Paleozoic strata exposed in the region.

The boulder-bed member is used to describe a complex group of interstratified, thin-bedded sandstones and shales, massive arkose, and boulder-bearing mudstone. The Haymond Formation boulder beds only occur in two areas; the first is on the eastern edge of the Marathon Basin along an 8-mile-long outcrop (2,000 feet thick north thinning moving south to 1,000 feet thick) (McBride, 1964a and 1964b). At one locality due west of Housetop Mountain (Figure 2-20), large erratic blocks are so numerous in the 900-foot-thick boulder bed that the outcrop forms a group of rugged hills (King, 1937). The Haymond Formation is gradational into both the underlying Dimple Limestone and the overlying Gaptank Formation (McBride, 1964a and 1964b).

2.2.1.4.4. Gaptank Formation

The Gaptank Formation only crops out in the northern part of the Marathon Basin (Figure 2-18). The formation consists of a complex sequence of interbedded shale, quartzose sandstone, fossiliferous limestone, calcarenite, and limestone conglomerate beds. The lower two-thirds of the formation is primarily interbedded calcarenite sandstone and shale. The upper portion of the formation has distinct facies that change over distances of just a few miles. The formation has been estimated to be from 1,800 to 2,400 feet thick and pinches out moving southwestward (McBride, 1964a and 1964b).

The Gaptank Formation is the uppermost Pennsylvanian formation beneath the Permian Wolfcamp and Leonard Series. The top of the steeply dipping (30 degrees) and tightly folded Gaptank Formation southeast of Dugout Mountain (Figure 2-20) is an angular unconformity with the overlying, more gently dipping (10 to 15 degrees) Permian Wolfcamp Formation (McBride, 1964a and 1964b).

The Gaptank Formation occurs on axis and west of the Dugout Creek Overthrust and along the southern edge of the Glass Mountains, between Iron and Leonard Mountains, south of the Skinner Ranch (Figures 2-19 and 2-20). The Gaptank Formation outcrops are in the vicinity of the northwestern ends of King (1937) cross sections D–D', E–E', and G–G' (Figure 2-22).

The upper part of the Gaptank Formation is exposed along the base of the Glass Mountains escarpment (King, 1980). The unconformable relations are clearly visible at many places in the southwestern part of the Glass Mountains. The Wolfcamp Formation as identified by King (1937) was subsequently subdivided into the Permian Lenox Hills Formation (Ross, 1963). The Gaptank Formation outcrops west of Marathon along the Dugout Creek

Overthrust (Figure 2-21), where it was overridden by a great mass of pre-Carboniferous rocks (King, 1937).

2.2.1.5 Pennsylvanian-Permian Unconformity

The Glass Mountains are type areas for both the Wolfcampian and Leonardian Series, widely used in North America as standard reference sections for the Lower Permian. These Lower Permian stratigraphic units are of global importance and correspond to, and are largely equivalent to, the international Lower Permian Cisuralian Series. Identifying depositional sequences is based on interpreting depositional and paleoecologic record of sediments, exposure surfaces, and eroded features associated with the unconformities at sequence boundaries (Ross and Ross, 2003). Reed (1990) provides an excellent description of orogenic and depositional events in the Marathon Basin during this Wolfcampian time.

2.2.1.6 Permian

The Marathon Aquifer study area Permian rocks (Hess Limestone and younger) (Table 2-1) all occur in the southern Glass Mountains (Figure 2-20). Unlike the older Paleozoic rocks, the Permian rocks have undergone little deformation and dip northwestward or northward at angles of 15 degrees or less. However, their inclination is steeper than that of the Cretaceous rocks that overlie them unconformably (King, 1980). Permian rocks in the Marathon Aquifer study area consist of the Leonard Hills Formation (Wolfcamp Series) and the Skinner Ranch, Hess Limestone, and Cathedral Mountain formations (Leonard Series) (Table 2-1).

2.2.1.6.1. Lenox Hills Formation

The Neal Ranch Formation (King, 1980) was renamed to the Lenox Hills Formation by Ross (1963). The upper part of the Wolfcampian Series is represented by the Lenox Hills Formation, named for outcrops in the western Glass Mountains originally mapped as western facies of the Wolfcamp Formation (King, 1937; Ross and Ross, 2003). The lowest Lenox Hills depositional sequence filled the topographic relief on the eroded surfaces of the Dugout fold belt (Gaptank Formation) in the western Glass Mountains. The Lenox Hills Formation outcrops in the Lenox Hills and to the southwest and northeast along the base of the Glass Mountains (Ross and Ross, 2003). Basal Wolfcampian carbonates reflect the same depositional environments as the underlying upper Gaptank Formation limestones (Reed, 1990).

The Lenox Hills Formation occurs on the northwestern edge of the proposed Marathon Aquifer extension near Dugout Mountain, Cathedral Mountain, Iron Mountain, and Leonard Mountain (Figure 2-20). The Lennox Hills Formation outcrops are in the vicinity of the northwestern end of King (1937) cross section G–G' (Figure 2-22).

The Lenox Hills Formation consists of conglomerate, shale, limestone, and dolomite, varying widely in proportion from place to place. This type section is 276 feet thick, of which 121 feet consists of alternating chert conglomerate and coarse-grained calcarenite beds that rest on 155 feet of conglomerate. The Lenox Hills Formation thickness ranges from 30 to 675 feet, and is highly variable between locations (Anderson and others, 1982).

2.2.1.6.2. Skinner Ranch

Anderson and others (1982) map the Skinner Ranch Formation and Hess Limestone as a single unit. The Skinner Ranch Formation, calcarenite, thick bed of limestone, and pebble conglomerate are in the lower part, with minor amounts of interbedded shale and thickness of 225 to 1,600 feet, and merge eastward with dolomitized, thin-bedded Hess Limestone (Anderson and others, 1982).

The Skinner Ranch Formation occurs on the northwestern edge of the proposed Marathon Aquifer extension near Dugout Mountain, Cathedral Mountain, Iron Mountain, and Leonard Mountain (Figure 2-20). The Lennox Hills Formation outcrops are in the vicinity of the northwestern end of King (1937) cross section G–G' (Figure 2-22).

On the southwestern face of Leonard Mountain (Figure 2-20), the type section for the Skinner Ranch Formation consists of approximately 690 feet of limestone pebble, cobble, and boulder conglomerates, with abundant chert pebbles, some interbedded siliceous siltstones, and several displaced biohermal blocks. In the Lenox Hills and Dugout Mountain exposures, the Skinner Ranch Formation is subdivided into four members (Ross and Ross, 2003).

2.2.1.6.3. Hess Limestone

As noted above, Anderson and others (1982) consider the Hess Limestone and the underlying Skinner Ranch Formation as a single unit. The Hess Limestone is a shallow water, backreef platform carbonate that formed on the eroded surface of the upper Lenox Hills Formation in the eastern Glass Mountains (Figure 2-20) (Ross and Ross, 2003; King, 1980). This formation forms much of the bulk of the pre-Cretaceous rocks of the Glass Mountains in the study area and crowns the southern escarpment overlooking the Marathon Basin to the south. Hess Limestone outcrops are often capped by Cretaceous outliers within and adjacent to the study area. Hess Limestone thickness ranges from 1,600 to 2,300 feet (Anderson and others, 1982).

The Hess Limestone occurs on the northwestern edge of the proposed Marathon Aquifer extension near Dugout Mountain, Cathedral Mountain, Iron Mountain, and Leonard Mountain (Figure 2-20). The Lennox Hills Formation outcrops are in the vicinity of the northwestern end of King (1937) cross section G–G' (Figure 2-22).

The main body of the Hess Limestone, within Wolfcamp Hill (Figure 2-20) eastward, is a thick mass of thin-bedded limestones containing few fossils. The lower Hess Limestone, equivalent to the Lenox Hills Formation, is composed of interbedded red and green shale with thin beds of sandstone, becoming more prominent eastward. The basal unit of the Hess Limestone is a conglomerate of limestone and chert pebbles and cobbles (King, 1980). The thickness of the conglomerate varies considerably in the basal unit, ranging from more than 200 feet to less than 50 feet, or even disappearing, in some locations, which may suggest deposition occurred over an eroded mild relief topography (Ross and Ross, 2003).

The Hess Limestone is separated from the overlying Cretaceous rocks by an angular unconformity; the divergence is slight, as the formation dips low to the north, generally at

an angle of 5 degrees or less (King, 1980). Locally, the upper surface of the Hess Limestone has karst features (Ross and Ross, 2003).

2.2.1.6.4. Cathedral Mountain

The Cathedral Mountain Formation (equivalent to the Leonard Formation of King [1937]) occurs along a ridge within the northwestern part of Leonard Mountain and extends northwestward across a valley and up an escarpment to the base of the Road Canyon Formation (Ross and Ross, 2003). The Cathedral Mountain Formation is poorly exposed and consists of siliceous shale, interbedded limestone, and small pebble conglomerate weathering to pink and red (Anderson and others, 1982) with a thickness up to 1,150 feet (Ross and Ross, 2003).

The base of the Cathedral Mountain Formation is a distinctive 30- to 80-foot-thick unit of coarsely recrystallized clastic limestone with floating chert pebbles and large-scale cross-beds. The basal unit is overlain by up to 250 feet of thick dark brown to black bituminous shales and siltstones with two or more levels of isolated bioherms, known for their silicified fossils. The upper part of the Cathedral Mountain Formation, just beneath the angular mid-Permian unconformity, is a 50- to 65-foot-thick laminated, platy-weathering, bituminous limestone (Ross and Ross, 2003).

2.2.1.7 Cretaceous

Cretaceous rocks currently encircle the Marathon Basin, but at one time they extended entirely over the crest of the Marathon Dome. The Cretaceous rocks are dipping away from and have been eroded off the higher portions of the dome. This selective erosion was probably caused by the removal of the weaker, less resistant underlying Paleozoic formations (King, 1937). Cretaceous Formations that occur at the edge of the Marathon Aquifer are the Glen Rose Formation, the Maxon Sandstone, the Del Carmon Limestone, and the Telephone Canyon Formation.

2.2.1.7.1. Glen Rose Formation

The Glen Rose Formation occurs along the eastern and southern portions of the Marathon Aquifer study area, and at Cochran mountain on the west side of the study area (Figures 2-18 and 2-20). On Housetop Mountain (Figure 2-20), the Glen Rose Formation is 312 feet thick.

The Glen Rose Formation outcrops at House Top Mountain, east of Tesnus, at Maxon, at Tres Hermanas Mountain, and east of Hood Spring (Figures 2-18, 2-20, and 2-23). In the southwestern corner of the Marathon Aquifer study area, the Glen Rose Formation outcrops on the northeastern end of the Santiago Mountains, east of Del Norte Gap, and around the Cochran Mountain (Figure 2-18 and 2-20). The formation outcrops are in the vicinity of King (1937) cross sections D–D', E–E', G–G', H–H', I–I', and Q–Q' (Figure 2-22).

Along the southeastern edge of the Marathon Aquifer study area, the Glen Rose Formation is up to 500 feet thick and rests on the eroded surface of the Mississippian Tesnus Formation (Table 2-1).

2.2.1.7.2. Maxon Sandstone

The Maxon Sandstone crops out as one or more prominent ledges midway up the Cretaceous rock scarps that rim the Marathon Basin. It has a similar extent to that described above for the Glen Rose Formation. The ledges are cut by vertical joints that run through 25 feet or more of strata, which causes the rock to break off in great cubical blocks.

The sandstone has a thickness of nearly 160 feet along the southern edge of the Marathon Aquifer study area, where it transitions into sandy shale and marl (King, 1980). The sandstone is a prominent brown, well-indurated coarse- to medium-grained sandstone with crossbedding and a few shaley layers. No fossils have been found in the Maxon Sandstone.

2.2.1.7.3. Del Carmen Limestone and Telephone Canyon Formation

Barnes (1979) and Anderson and others (1982) map the Del Carmen Limestone and the Telephone Canyon Formation as a single unit. The unit is a fine-grained, massive limestone, with large (10-inch) chert nodules, with interbedded brownish shales. The unit is fossil rich and has a thickness up to 200 feet; it forms sheer escarpments (Anderson and others, 1982).

The Del Carmen Limestone and Telephone Canyon Formation outcrop southeast of and paralleling the Tinaja Mountains (Figures 2-18 and 2-20). The Del Carmen and Telephone Canyon outcrops are in the vicinity of the eastern edges of King (1937) cross sections D–D', E–E', G–G', H–H', and I–I' (Figure 2-22).

2.2.1.8 Tertiary

Tertiary intrusive igneous rocks occupy small areas within the Marathon region (Figure 2-18). These rocks intruded into all the sedimentary rocks from the oldest to the youngest. The three major intrusive plugs are Iron Mountain, the Altuda Mountain uplift just west of the study area, and Santiago Peak (Figure 2-20). Along the southern Marathon Basin rim, smaller plugs cut the Paleozoic and Cretaceous rocks with a few plugs and dikes within the basin itself (Figure 2-18). All the intrusive igneous rocks are porphyritic, and most of them appear to be of intermediate composition (King, 1937).

2.2.1.9 Quaternary

More than a quarter of the study area is covered by a thin blanket of alluvial deposits of Quaternary age. This cover is most extensive in the northern and eastern portions of the study area. The Quaternary deposits are of Pleistocene and Holocene ages; the younger is the most extensive. Other Quaternary deposits are considerably younger (King, 1980). The higher gravel may be Pleistocene. The alluvial deposits consist chiefly of stream sediments laid down on the lowlands during times when wide areas of plains were being weathered down near base level. Some deposits formed terraces that stand above the present stream grade; others are more recent time and were redeposited in valleys during the present cycle of erosion.

In the northern part of the Marathon Basin, near bases of the mountains, the sediment deposits merge into broad alluvial fans. Local water wells suggest the thickness may reach 100 feet. In the southern Marathon Basin, along Pena Blanca Creek (Figure 2-23) in Dagger Flat and other lowland areas, the streams are entrenched to a depth of 50 or 100 feet and there is a gravel-covered terrace of limited extent 25 or 50 feet below the land surface. In most areas of Marathon Basin covered by Quaternary sediments, the thickness of the deposits is rarely greater than 25 feet, but they may be thicker on the lower course of Maravillas Creek (Figure 2-23).

In areas drained by San Francisco Creek and its tributaries (Figure 2-23), older terrace deposits are 100 feet or more above the existing modern drainage; these units occur as small to large remnants on the low hilltops of tilted Paleozoic rocks (King, 1980).

The occurrence of boulders derived from formations outside the drainage area implies either there has been a change in drainage or that there has been a change in the extent of the formations from which the boulders were derived.

2.2.2 Structure

The major structural features of the Marathon Basin are revealed by the hogbacks of the Caballos Novaculite and the Dimple Limestone, which are the remnants of substantially denuded mountain structures. Strata of the Marathon Basin generally have not been metamorphosed. The sandstones and shales are somewhat indurated, and the shales approach slates to the southeast (King, 1937). Detailed descriptions of the evolution of Paleozoic regional tectonics of the Marathon Basin are provided by Ross (1986), Wuellner and others (1986), Tauvers (1988), Hickman and others (2009), and Chapman and McCarty (2013).

The rocks of the Marathon Basin are thrown into northeastward-trending folds, overturned toward the northwest. Many of these folds are broken by thrust faults. The faulting culminated on the northwest in the nearly flat-lying Dugout Creek overthrust; the estimated displacement is more than 6 miles. Farther southeast, there are other large thrusts also with miles of displacement; some of these thrust faults are folded and therefore older than the frontal overthrust. The folds are also shattered by transverse flaws and tear faults, some of which have large horizontal displacements. Folds and faults have a slightly arcuate form (King, 1937).

King (1937) subdivided the Marathon Basin into major structural areas he called the Marathon Anticlinorium, the Pena Colorada Synclinorium, the Dagger Flat Anticlinorium, the synclinorial area between Tesnus and Hells Half Acre Fault, and areas to the east outside the Marathon Aquifer boundary. This last region, which is the southeastern portion of the Marathon Aquifer study area, is called the Hells Half Acre Overthrust in this report.

Figure 2-24 illustrates the locations of these four general regions. Figure 2-8 is a schematic of a northwest to southeast cross section modified from a figure in King (1937). The location of the cross section in Figure 2-25 is marked on Figure 2-24. In addition, the

geologic units in Figures 2-24 and 2-25 are shaded such that the blue units tend to be water-bearing (aquifers) and the brown units tend to be non-water-bearing (aquitards).

Tauvers (1988) presents updated interpretations of the Marathon Basin framework. He subdivides the Marathon Basin into three stratigraphically and structurally defined domains called the western, eastern, and southern domains based on Muehlberger and others (1984). These domains improve the understanding of the structural and temporal evolution of the Marathon Basin, but do not advance the understanding of the Marathon Aquifer hydrogeology (i.e., water-producing rocks less than about 1,000 feet below surface) beyond information provided in King (1937 and 1980).

The movements that created these structural features were pulsatory and extended through a considerable span of Pennsylvanian time. Deposition was nearly continuous during the Pennsylvanian, so many of the movements are recorded in the sedimentary rocks. Early Permian age formations lie unconformably on the folds along the north side of the Marathon Basin near the Glass Mountains (King, 1937).

To simplify and coordinate the excellent lithologic formation and local structural descriptions provided by King, the work of King (1937) is used to outline the Marathon Aquifer study area structure. Unless otherwise noted, the descriptions provided in the following subsections are summarized and paraphrased directly from King (1937). As illustrated by these summaries, the structure of the rocks that comprise the Marathon Aquifer is extremely complex.

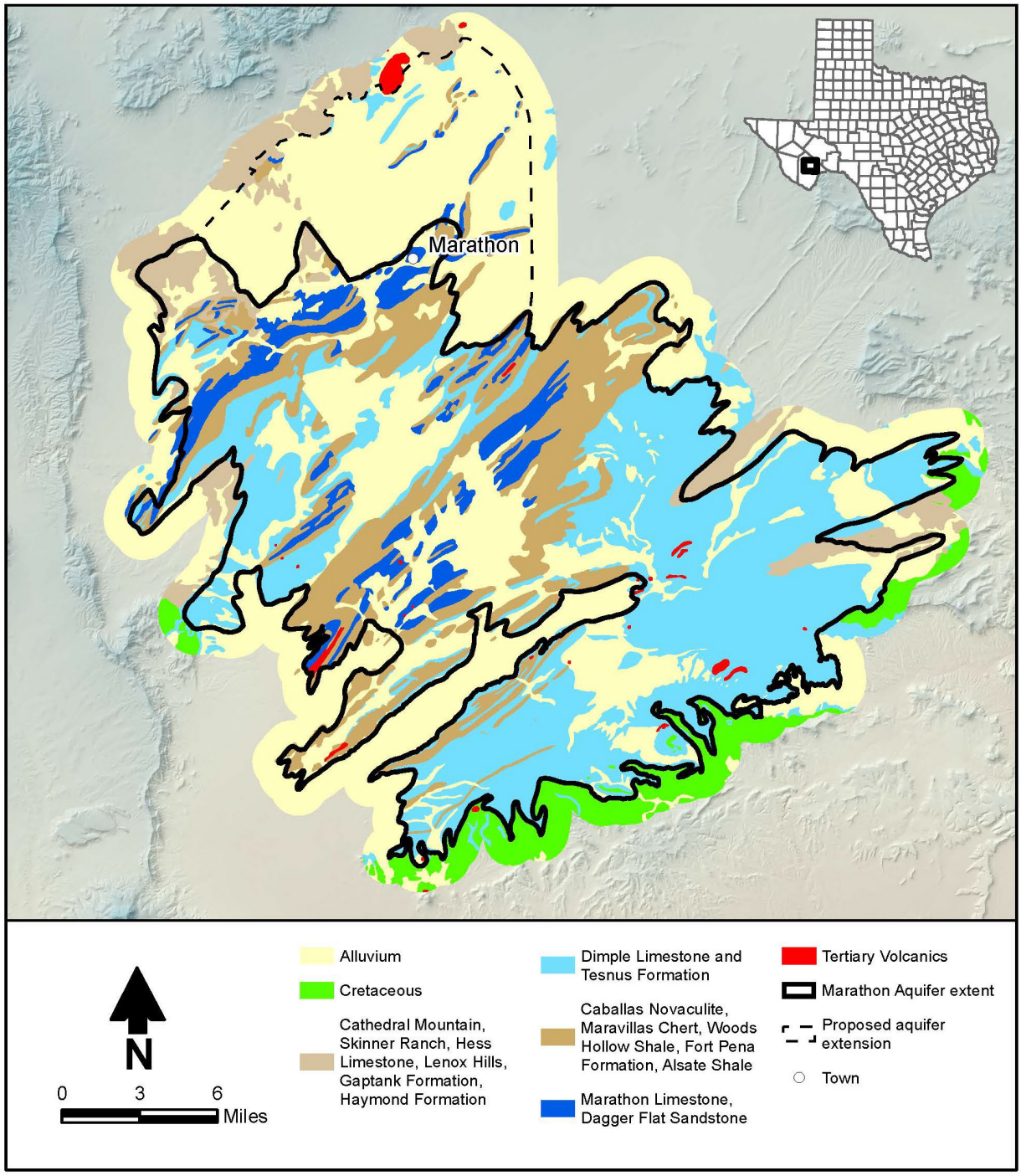

Figure 2-24. Major structural areas used to divide the Marathon Aquifer after King (1937). Blue and purple units tend to be aquifers, while brown units tend to be aquitards. Tan unit (alluvium) can be an aquifer where saturated.

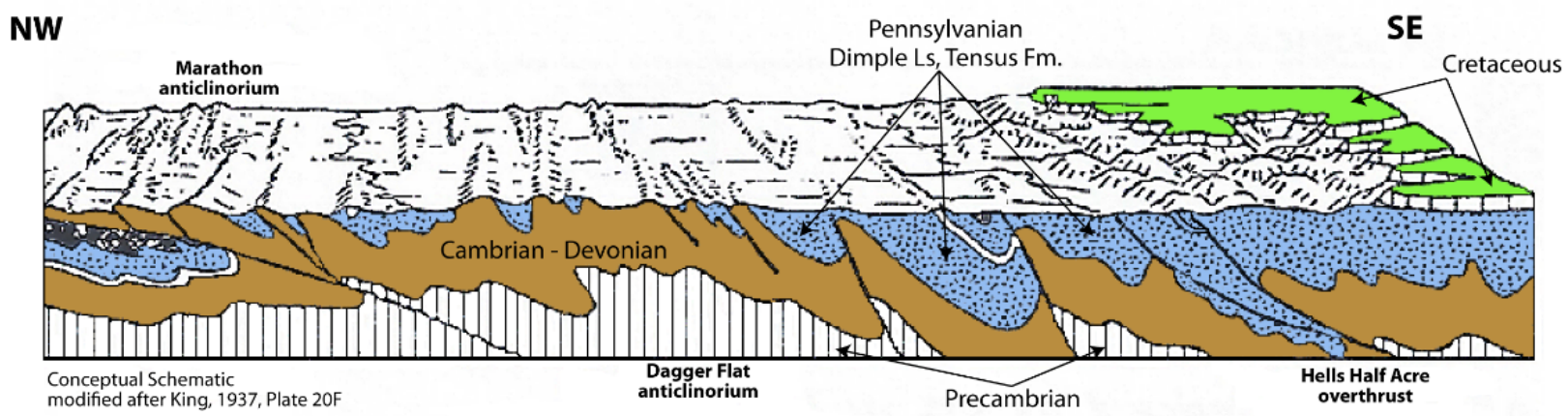

Figure 2-25. Northwest to southeast structural cross section after King (1937). Location of section is shown on Figure 2-7. Blue units tend to be aquifers, while brown units tend to be aquitards.

2.2.2.1 Marathon Anticlinorium and the Dugout Creek Area

The Marathon Anticlinorium occurs in the northwestern part of the Marathon Basin and lies across the belt of upwarping (Figure 2-24). Folds within the anticlinorium pitch both northeast and southwest. In the northwestern part of the anticlinorium, the Dugout Creek Overthrust is exposed at land surface due to upwarping. Here, older Paleozoic formations overlie younger Pennsylvanian formations. Dips on the southeast flanks of the Marathon Anticlinorium range from 30 to 45 degrees southeast, and the northwest limbs either dip steeply northwest or are overturned.

The Dugout Creek Overthrust is exposed about 7 miles west of Marathon (Figure 2-21). The fault plane is nearly flat. Chert of the Caballos and Maravillas formations cap the hills; upper Pennsylvanian shales and thin sandstones form the slopes and valleys. To the southeast, the fault dips at a low angle beneath the surface. To the east, the outcrop is covered by alluvium in most places. North of Hargus Ranch and at several places a few miles northwest of Decie Ranch (Figure 2-19), there are small outliers of the overthrust, consisting mostly of novaculite, resting on the Gaptank Formation. The Gaptank and Haymond formation shales and sandstones that lie beneath the overthrust are mostly incompetent and have small, deformed folds and thrusts. Where the thrusts moved across shale, there is rarely breccia and are only slightly indurated. Thin series of interbedded limestone beds are bent, broken, and repeated. Planes of the thrusts and axial planes of the folds dip to the southeast. There is no evidence at any place of metamorphism.

The structurally highest area is northwest, near the base of the Permian escarpment. Here, beds of the Haymond Formation are brought up in two anticlinoria—one on Decie Ranch (Figure 2-19) and the other south of Dugout Mountain (Figure 2-20). The north flank of the anticlinorium south of Dugout Mountain is overturned and dips approximately 35 degrees to the south. The higher Gaptank beds (Pennsylvanian–Permian contact) are exposed to the southeast in a local synclinorial area. Permian rocks with coarse thick basal conglomerate lie unconformably on the overturned beds on the face of Dugout Mountain. North of Decie Ranch, the Permian conglomerates rest locally on the Caballos Novaculite and the Dimple Limestone of the thrust sheet. In other locations, the Permian conglomerates overlie the Pennsylvanian sandstones.

A system of pronounced en echelon tear faults extend from the front of the thrust at Alsate Creek (Figure 2-23) for nearly 10 miles to the southeast, apparently the result of differential movement between two parts of the overriding mass. The faults are downthrown on their northeast side. Rocks on the northeastern side of the Marathon Anticlinorium are strongly folded but not greatly faulted; on the southwestern side, the strata are broken into numerous thrust faults.

On the northwest flank of the anticlinorium west of Alsate Creek (Figures 2-21 and 2-23), the lower Ordovician Alsate Shale is unusually thick. This incompetent layer probably acted as a gliding plane, such that the Marathon beds are more intricately deformed than the massive limestones of the overlying Fort Pena. The Fort Pena and older beds are more complexly deformed than the overlying Maravillas and Caballos formations, probably as a result of the gliding of the Woods Hollow Shale serving as a cushion between two series

that were differentially deformed. The Fort Pena and Woods Hollow shales are greatly squeezed and crumpled.

Between Marathon and Fort Pena Colorada (Figure 2-19), the Maravillas Chert and Caballos Novaculite occur in open folds different from the isoclinal structure of the older Upper Ordovician to Upper Cambrian rocks. In this region, there are four anticlines within a 3-mile distance that cross the strike. Strata on the northwest limb have steep or vertical dips, but arch gently over the crest to joining gently dipping beds on the southeast limb. The folds are considerably broken by tear faults, some of which some offset local anticlinal and synclinal axes.

2.2.2.2 Pena Colorada Synclinorium

The Pena Colorada Synclinorium area has a width of about 6 miles and separates the Marathon Anticlinorium from the Dagger Flat Anticlinorium (Figures 2-24 and 2-25). The Pena Colorada Synclinorium generally consists of broad areas of Tesnus Formation, with anticlines of Caballos Novaculite and older rocks rising through it. The northwest flank of the anticlinorium is bounded by Caballos Novaculite strata dipping gently southeast off the marginal folds of the Marathon Anticlinorium. The southeast flank of the anticlinorium is bounded by outcrop of overturned Caballos Novaculite strata on the northwest flank of the Dagger Flat Anticlinorium.

Formation outcrops within this area are openly folded and are not greatly faulted. Most are nearly symmetrical and show little overturning of strata. These folds pitch southwest at the southwest end and northeast at the northeast end, like the Marathon and Dagger Flat anticlinoria.

Close to Wood Hollow Tank due south of Marathon is a central depressed area, covered by terrace gravel but with Tesnus Formation exposed (Figures 2-18 and 2-20). Near the southwest end of the synclinorium, east of Monument Spring (Figure 2-23), broad synclinal areas of Dimple and Haymond formations outcrop. The Tesnus through the Gaptank formations within the synclines are more sharply folded than the underlying Caballos Novaculite, and are broken by small thrust faults. A grouping of sharp synclinal folds of Dimple Limestone forms the crest of West Bourland Mountain.

Southeast of the Dimple Limestone outcrops are two anticlinal ridges named East Bourland Mountain and Simpson Springs Mountain (Figure 2-20). These ridges are composed of Caballos Novaculite and Maravillas Chert. The Woods Hollow Shale outcrops in narrow axial basins along their crests. East Bourland Mountain is a simple fold, which is somewhat overturned toward the northwest. The northeastern end of East Bourland Mountain has been downthrown several hundred feet by an en echelon tear fault. Simpson Springs Mountain is composed of three closely compressed en echelon anticlines severed on the northeast by a fault. Folded and contorted Woods Hollow Shale outcrops along the axes of these two anticlinal ridges contains large erratic boulders of Cambrian and Ordovician limestone.

Moving northeast, Wood Hollow Mountains (Figure 2-20) rise; this synclinorium consists of anticlinal ridges of chert and novaculite, separated by narrow synclinal valleys of Tesnus Formation shales. Dips are steep on the flanks of the anticlines, but are greater on the northwest side. The rocks are cut by numerous north-northwest tear faults; many of the faults have considerable horizontal displacement.

2.2.2.3 Dagger Flat Anticlinorium

The Dagger Flat Anticlinorium (Figure 2-24) has been uplifted the highest (Buttrill Ranch, Figure 2-19) within the Marathon Basin, and large areas of the Cambrian Dagger Flat Sandstone are exposed in the center of the structure. The structure extends for 25 miles in the northeasterly direction across the center of the Marathon Basin and has a maximum width of about 6 miles. It is bounded by long straight ridges of Caballos Novaculite that become convoluted and zigzag outcrops at the northeastern and southwestern ends that dive below the surface beneath the Carboniferous (Mississippian and Pennsylvanian) rocks.

The Caballos Novaculite and Maravillas Chert fold over the anticlinorium and were broken into flat slices that slid forward over each other and then were folded. The underlying strata occur in narrow, sharp isoclinal folds. The Caballos Novaculite is thinner at the folds of the crest than it is on the flanks. The Tesnus Formation is about 2,000 feet thick on the northwest flank and about 6,500 feet thick on the southeast flank. The Maravillas Chert that outcrops within the central lowland of the anticlinorium was folded into numerous sharp, narrow anticlines and synclines; most are isoclinal, with dips on both flanks of 70 to 80 degrees to the southeast.

Some northeastern anticlines in the Dagger Flat Anticlinorium are broken by thrust faults on their northwest flanks. As many as four Marathon Limestone and Dagger Flat anticlinal folds occur within 1 mile across of strike across these rocks; the synclines contain Woods Hollow and Fort Pena formations. The Woods Hollow Shale has been greatly contorted and squeezed. There is outcrop several miles in width at the northeast end of the anticlinorium, west of Lightning Ranch.

In the Pena Blanca Mountains (Figure 2-20), which represent the southeast flank of the anticlinorium, there is some backward folding where the anticlines have been somewhat overturned toward the southeast and locally broken on the southeast side by steep thrust faults that dip northwest. In other locations, the dips are steeply southeast.

Dagger Flat Anticlinorium (Figure 2-24) folded overthrusts of the younger rocks with the repetition of the Caballos and Maravillas formations along the crest of the anticlinorium, and is found at both its northeast and southwest ends. Folder overthrust example locations include the Warwick and Lightning Hills to the south at the Pena Blanca Mountains and to the southwest at Three-mile Hill (Figure 2-20) and at Garden Springs (Figure 2-23). Folded overthrusts appear to be almost wholly confined to the competent Maravillas and Caballos strata. The Caballos and Maravillas formations have numerous tear faults that have a general northwest trend.

Several anticlinal folds occur southeast of the Dagger Flat Anticlinorium (Figure 2-24), in which Maravillas and Caballos strata are exposed and are surrounded by the Tesnus Formation. At Horse Mountain (Figure 2-20), a symmetrical eastward-plunging fold with the crest that was dominantly covered Caballos Novaculite, the dips on the north and south flanks are between 60 and 80 degrees.

2.2.2.4 Hells Half Acre Overthrust

The Hells Half Acre Overthrust area (Figure 2-24) consists of anticlinal and synclinal basins with broad folds, thrust faults, and locally highly contorted, faulted, and fractured rocks. This stratigraphic sequence includes formations between the Devonian Caballos Novaculite through Pennsylvanian Haymond Formation, with the overlying, unconformable Cretaceous formations at the Marathon Aquifer study area boundary east to the south.

Downcutting by San Francisco Creek (Figure 2-23) has eroded excellent exposures over wide areas of thick sequences of Tesnus Formation and Dimple Limestone north of Hells Half Acre (Figure 2-20). The Dimple Limestone is well exposed, forming sharp hogbacks in the southern part of the area, and the top of the basal shale member of the Tesnus Formation can be mapped. The folds are broad and open and have an amplitude of several miles, with dips ranging from 30 to 60 degrees on the southeast flanks of the anticlines, and dips on the northwest flanks as low as 45 degrees. Dips are nearly flat in some places near the synclinal axes. The anticlines tend to be narrower and sharper than the synclines. Some northwest limbs are broken by steep thrust faults.

The syncline southeast of Haymond extends into the synclinorium between the novaculite areas of Horse Mountain and the Pena Blanca Mountains (Figure 2-20). The southeast side of the syncline southeast of Haymond is broken by the Arden Draw thrust fault (Figure 2-21), which passes beneath the Cretaceous rock cover half a mile northwest of the summit of House Top Mountain (Figure 2-20).

The Arden Draw Fault (Figure 2-21) is the basal shale member of the Tesnus that is thrusted up against upper Tesnus. The fault is lost in the basal shales several miles west of Twin Peaks (Figure 2-20) just north of Horse Mountain. The Arden Draw Fault dips at high angles to the southeast like the Haymond Fault. These faults may be overturned limbs of anticlines with a dominantly vertical movement. The throw on each fault is several thousand feet or more. The hogbacks of Dimple Limestone northwest and southeast of Haymond Station are cut by several small tear faults.

South to southeast of the Arden Draw Thrust Fault and approaching the Hells Half Acre Fault (Figure 2-21) the folds are closely compressed. Structure is obscure, partly because of the intense deformation and the repetitive character of the Tesnus Formation sandstones that crop out over most of the area.

The Hells Half Acre Fault (Figure 2-21) extends along the north side of Hells Half Acre and crosses San Francisco Creek near its junction with Negro Creek (Figure 2-23). The fault trace is obscure because Tesnus Formation occurs on both sides of the fault. Rocks on the north are folded into open anticlines and synclines with a northeast strike truncated by the

Hells Half Acre fault. Rocks on the south have east to northeast strike and are closely folded. A mile south of the fault and east of San Francisco Creek, the strata are so disordered that it is impossible to map sandstone ledges more than a few hundred yards. The trace of the fault is sinuous.

The major structural boundary created by the Arden Draw Thrust Fault and the Hells Half Acres Overthrust Fault (Figure 2-21) was reinterpreted by Muehlberger and others (1984). Their interpretation is that the Hells Half Acres Overthrust Fault (structural boundary) does not continue to the east as mapped by King (1937), but instead connects with the Arden Draw Thrust Fault to the north. This interpretation is still being investigated through communication with one of the authors of Muehlberger and others (1984), which may result in modification of Figure 2-21.

Hells Half Acre Fault (Figure 2-21) probably continues southwestward into the thrust faults bounding the northern flank of the Tinaja Mountains (Figure 2-20). The mountain ridges consist of Caballos Novaculite folded and broken by closely spaced parallel thrust faults. The Hells Half Acre Fault marks a line of major overthrusting supported by wedges of Maravillas, Caballos, and Dimple formations included in the fault plane on the south side of the fault. Numerous Tertiary porphyry diapirs occur along the north flank of the mountains; these features likely ascended along the thrust planes.

Two white quartzite Tesnus Formation layers form the Devils Backbone (Figure 2-20), which outcrops in several sharply faulted anticlines and synclines. Wedges of Dimple Limestone are found along the largest of the faults, named the Devils Backbone Fault. On the ridges between San Francisco Creek (Figure 2-23) and the Cretaceous and southeast of Devils Backbone on the Tres Hermanas Mountains (Figure 2-20), several large Tesnus Formation overturned sandstone folds outcrop.

West and southeast of the Tinaja Mountains, the Tesnus Formation outcrops in several obscure folds along with narrow belts of Caballos Novaculite. The Caballos Novaculite outcrops were probably carried up along faults and resemble the thrust slices in the Tinaja Mountains. Farther south, the Paleozoic strata pass unconformably beneath the Cretaceous limestones, beyond which their structural features are unknown.

3 Previous Work

3.1 Geology

The geology of the Marathon Basin has been intensely studied for over 80 years. The most comprehensive field studies are King (1937 and 1980), which provide detailed structural history, maps, cross sections, stratigraphy, lithology, outcrop, and fossil descriptions. Flawn (1956) provides the outline of Marathon Uplift, and Flawn and others (1961) provides historically compiled history and well data of the Ouachita System. Ellison and others (1964) describe the stratigraphic deposition within the Marathon Aquifer area. Dickerson and Muehlberger (1985), Dickerson (1987), Muehlberger and Dickerson (1989), and Dickerson (2013) investigated the tectonics of the Marathon Basin. LaRoche and Higgins (1990) investigated the hydrocarbon potential of the basin. Chapman and others (2013) provide detailed structural analyses of the northwestern quadrant of the basin. Ewing (2016) provides a good summary of the Marathon Basin geologic evolution and history.

While teaching at the University of Texas in Austin, Dr. Bill Muehlberger focused on understanding the structure and stratigraphy of the Marathon Basin. He supervised nine master's theses and one doctoral dissertation referenced as Byrd (1958), Bjorklund (1962), Houser (1967), Demis (1983), Leason (1983), Kraft (1984), Coley (1987), Duncan (1987), Tauvers (1988), and Diggs (1989).

Project team access to these studies was limited due to COVID-19 restrictions imposed at University of Texas Walter Geology Library in Austin from spring 2020 to the current time. Team member Dr. Pat Dickerson was able to borrow the Tauvers (1988) dissertation from the library in late July 2021; this dissertation integrated and summarized most of the earlier University of Texas work.

The West Texas Geological Society conducted three field trips to the Marathon Basin (Adams and Frenzel, 1952; Lewis and Barton, 1946; Maxwell and others, 1949) to study road outcrops and the structural geology. These geological field trip publications provide a guide to outcrops in the Marathon Basin.

There are two 1:250,000 scale Geologic Atlas of Texas sheets for the Marathon Basin study area: the Fort Stockton sheet (Anderson and others, 1982) and the Emory Peak–Presidio sheet (Barnes, 1979).

Review of the previous published geological studies, related references, and available data indicated that sufficient detailed, peer-reviewed geologic information was available to complete the stratigraphic and structural framework of the Marathon Aquifer, and that additional work or interpretations regarding these issues was not required. The geology presented in this report is based largely on the outstanding field work of Dr. Phillip B. King. In order to complete his analysis, Dr. King had to be able to conduct complex structural interpretations in the field, as well as identify minerals, rock types, sedimentary features and textures, and fossils. Dr. King was assisted in the field by R.E. King; they began working

in the Marathon Basin in 1929 and ended their field work in 1931. Previous studies by Udden (1917), Sellards (1933), and Baker (1928) provided the geological and paleontological foundation for the Marathon Basin (King, 1937).

King (1937) mapped the Marathon Basin region using an elaborate system of pacing traverses and partly by recording the observations on enlargements of the topographic sheets. Stratigraphic sections were often described by pacing used in conjunction with a Brunton compass; at exceptionally good outcrops, tape measures were used.

King produced a second Marathon Basin publication (King, 1980) for the U.S. Geological Survey. This publication refined some of the interpretations in King (1937) using aerial photographs and available ground surveys, which increased overall precision of the work. This second publication is focused on the geological description of the eastern Marathon Basin.

3.2 Hydrogeology

Study of the hydrogeology of the Marathon Basin has been limited, likely because (1) the Marathon Aquifer is relatively small compared to other designated aquifers in Texas, (2) the water demand is limited, and (3) access to private property in the region to study the water resources is difficult or not permitted by the landowners in some cases. The first published study of the Marathon Aquifer hydrogeology was conducted by the Texas Water Board of Engineers (DeCook, 1961). This study provides data on over 300 water wells and 11 springs, and is the dataset that forms the basis of much of the information within the TWDB Groundwater Database. Muse (1966) also provides useful water level information. Additional Marathon Aquifer publications include Smith (2001) and George and others (2011). There are no published groundwater models of the Marathon Aquifer.

4 Hydrologic Setting

This section presents the information compiled and analyzed for developing the conceptual model of groundwater flow in the Marathon Aquifer.

4.1 Hydrostratigraphy and Hydrostratigraphic Framework

4.1.1 Hydrostratigraphic Units

Aquifers and aquitards that occur in the Marathon Aquifer region are the result of interactions of rock composition and the cumulative effects of a complex geologic history that has produced numerous fractures, faults, and folds. Lithology influences the mechanical properties of the rock, which affect the susceptibility of the rock to fracturing and determine whether the rock exhibits a brittle or ductile response to stress. Prior tectonic and structural events have resulted in the development of localized, well-developed fracture and joint permeability systems. Minor karstification (cavities) within the Marathon Limestone has also occurred, as confirmed by local well drillers.

Grouping formations by age and water well productivity is a useful starting point for conceptualizing the aquifer system, although it must be kept in mind that the stratigraphic units vary significantly, and some units may include both aquifer and aquitard intervals. For example, TWDB well records may indicate if water is produced from limestones of the upper or the lower Marathon Formation. Bentonites at the top and the mega-conglomerate in the middle of the Marathon Limestone are unlikely to produce water.

The dominant groundwater-producing Paleozoic formations mapped in the Geologic Atlas of Texas sheets (Barnes, 1979; Anderson and others, 1982) are the Ordovician Marathon Limestone (367 MRTN) and the sandstone of the Pennsylvanian Tesnus Formation (327 TSNS). These Paleozoic formations are lithified if unaltered and generally have low primary porosity. The Marathon Limestone is the primary aquifer in the anticlinorial belts, where it occurs at the surface or at shallow depths. Where the Marathon Limestone occurs at significant depth in the synclinorial belts, the younger and less productive Pennsylvanian formations are the primary aquifer units (DeCook, 1961).

Table 4-1 summarizes the conceptual hydrostratigraphic units identified based on existing information. Compositions and physical characteristics of the hydrostratigraphic groups are summarized in the following subsections.

Table 4-1. Hydrostratigraphic column for the Marathon Aquifer.

Period and Series	Model Layer	Predominant Hydrogeologic Character	Formation/ Geologic Unit	Primary Lithology
Quaternary	1	Aquifer	Alluvial types	Gravel, sand, silt, clay
Tertiary	2	Aquitard	Volcanic intrusives	Volcanic, intrusive rocks
Cretaceous, Lower Trinity	3a	Aquitard – not saturated in study area	Del Carmen and Telephone Canyon	Limestones, chert, and shales
			Maxon Sandstone	Sandstone and marl
			Glen Rose	Limestone, marl, chert, conglomerate
Permian, Leonard			Cathedral Mountain	Shale, limestone, and pebble conglomerate
			Skinner Ranch and Hess Limestone	Limestone and pebble conglomerate
Permian, Wolfcamp			Lenox Hills	Conglomerate, shale, and limestone
Upper to Lower, Pennsylvanian	3b	Aquitard	Gaptank	Limestone, sandstone conglomerate
			Haymond	Sandstone, shale, boulder beds
Lower Pennsylvanian to Upper Mississippian	4	Aquifer	Dimple Limestone	Limestone and shale
			Tesnus	Sandstone and shale
Devonian to Upper Ordovician	5	Aquitard	Caballos Novaculite	Novaculite and chert
			Maravillas Chert	Chert conglomerate
			Woods Hollow Shale	Shale
			Fort Pena	Limestone, chert, and shale
			Alsate Shale	Shale, limestone, and sandstone
Lower Ordovician to Upper Cambrian	6	Aquifer	Marathon Limestone	Limestone, sandstone, and conglomerate
			Dagger Flat Sandstone	Sandstone

4.1.1.1 Layers 1 and 2

Shallow Quaternary alluvial deposits that blanket large portions of the Marathon Aquifer region provide groundwater to wells where sufficient saturation exists. The alluvium is estimated to have a maximum thickness of about 100 feet; the saturated thickness is less, and may be zero in many places, particularly in upland areas. Alluvial wells generally produce less than 20 gallons per minute, and their yield may be susceptible to drought.

There are no known wells that produce water from volcanic intrusive rocks in the Marathon Aquifer, although these rocks may produce small quantities of water if they are sufficiently fractured.

4.1.1.2 Layer 3

The Cretaceous units in Table 4-1 are marked as an aquitard because they are not saturated in the Marathon Aquifer area, but are included in the hydrostratigraphic model for completeness. North and east of the Marathon Aquifer, the Skinner Ranch, Hess, and Lenox Hills formations are dominantly massive limestones with common beds of red and green shale. The strata were folded and thrusted in the late Paleozoic episode, and then the carbonates were fractured again during Laramide doming of the region. Thick homogeneous limestone layers and common shale beds (up to 100 feet thick) contribute to the function of these formations as aquitards. However, fracture porosity and permeability in limestones at structural junctions could favor groundwater production where these rocks are saturated.

4.1.1.3 Layer 4

The lower Pennsylvanian Dimple and Tesnus formations are thick, laterally extensive turbidite sequences throughout the Marathon Basin. The intersections of northeast-trending geologic structures and northwest-striking tear faults, such as along the southern limb of the Marathon Anticlinorium (Figure 2-4), are potential sites for fractured-rock aquifers, possibly with shaley alluvium or Haymond clay shales as aquitards.

4.1.1.4 Layer 5

The middle Ordovician Fort Peña and Woods Hollow formations, the upper Ordovician Maravillas Formation, and the upper Silurian to lower Mississippian Caballos Novaculite are mapped together in the primary reference for the basin (King, 1937). Based on TWDB well records indicating limited well yields, they are placed in a single group conceptualized as primarily an aquitard. Of the collected formations, only the Woods Hollow Shale is consistently an aquitard. Field observations in the northwestern portion of the Marathon Aquifer are relevant for assessing the aquifer and aquitard potential of these units (Dickerson, 2012).

Composition of the Fort Peña Formation is variable. Much of the formation is thin- to medium-bedded, clean to sandy limestone with thin shale interbeds. If fractured, or if water-bearing fractured beds are fault-connected, the unit can locally be an aquifer. Bentonite layers in the upper portion of the formation could serve as aquitards, and the swelling clays could also occlude aquifer porosity and/or impede flow through fractures. Coarse conglomerate layers to boulder beds are present throughout the formation, and these units are variably cemented and are probable aquitards.

The Woods Hollow Shale is thin-bedded, ductile, greenish-gray clay shale with sandy and calcareous intervals. It is an effective aquitard, and it also serves as a decollement for thrust faults in the complex, by which permeable units can be juxtaposed with the shale.

The Maravillas Chert consists of fossiliferous limestone and conglomerate in the lower part of the formation, overlain by massive black chert with some carbonate interbeds. The chert generally replaces limestone and does not preserve primary porosity. All of these units are pervasively fractured. The lower sequence of the Maravillas Chert may be an aquifer unit where it is in contact with underlying Woods Hollow Shale.

Novaculite and chert predominate in the Caballos Novaculite, although multiple shale interbeds occur in the lower chert member (e.g., in the Dugout Creek area). The Caballos Novaculite, like the Maravillas Chert, is an intensely fractured unit, though it does not tend to produce large quantities of water. Springs issue from the base of the Caballos Novaculite, potentially where the lower fractured chert is in contact with shale aquitards or silicified limestones at the top of the Maravillas Formation.

4.1.1.5 Layer 6

In the Dagger Flat and Marathon anticlinoria, the Dagger Flat Formation is an extensive, moderately well-sorted quartzose sandstone and sandy shale. Well cemented with calcite, it is susceptible to fracturing and aquifer development in favorable structural settings. Shale or lime mudstone of the overlying Marathon Formation could locally function as aquitards.

The Marathon Formation consists of lower and upper sequences of thin-bedded lime mudstones interlayered with thin shales. The flaggy, brittle carbonates form a fractured aquifer in the Marathon Anticlinorium. Reported karstified areas with higher well yields are probable solution features at fault intersections.

Conglomerate beds are common throughout the Marathon Limestone. Monument Spring Member, up to 90 feet thick, occurs between the upper and lower limestone sections. This member is composed of large silicified boulders and blocks in a dolomite matrix, which could be an aquitard internal to the limestone sequence. For aquifer intervals in fractured upper Marathon limestones, bentonites in the uppermost formation could serve as aquitards, but with the same caveats as for the Fort Peña Formation. Massive conglomerates, well-indurated green shale, and limestone beds of the Alsate Shale overlie the Marathon Formation and can function as a highly variable aquitard.

4.1.2 Geophysical Logs

The TWDB Brackish Resource Aquifer Characterization System, the Texas Bureau of Economic Geology, and the Texas Railroad Commission geophysical log libraries were researched for logs within and in the vicinity to the Marathon Aquifer study area. North (mostly in Pecos County) and directly south of the Marathon Aquifer study area there are a few small oil and gas plays that have a high density of geophysical logs.

King (1980) researched available geophysical logs for the Marathon Basin region and identified 10 geophysical logs within his study area for which he provided formation picks.

Within 20 miles of the Marathon Aquifer study area outline, 13 geophysical logs and 1 mud log were located (Figure 4-1); these logs are provided in the project geodatabase. Only 8 of the 10 geophysical logs identified by King (1980) could be located and are included in the geodatabase. No geophysical log formation picks were made using these logs because additional, deeper subsurface formational interpretation was not required.

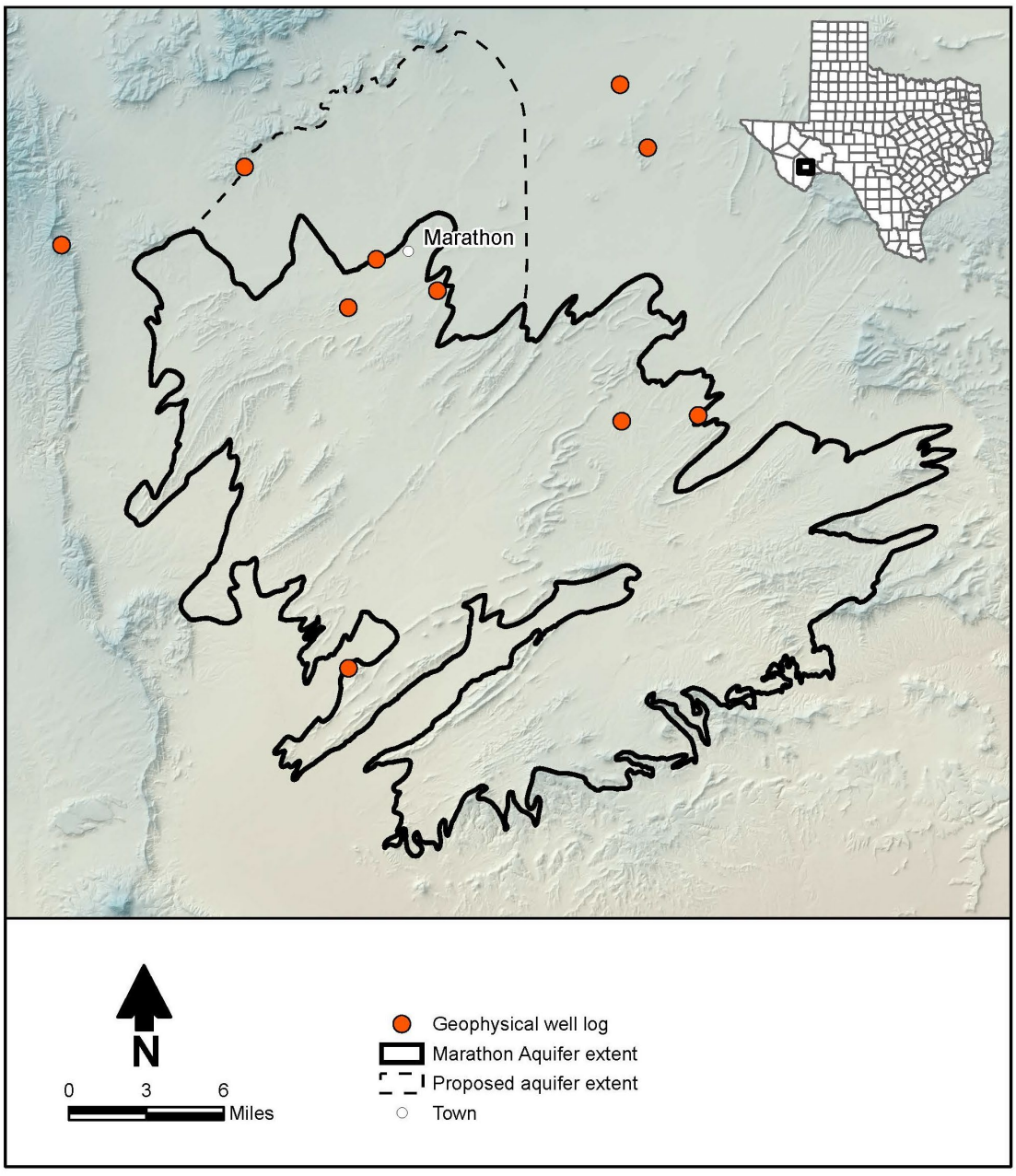

Figure 4-1. Location of geophysical logs provided in the project geodatabase.

4.1.3 Leapfrog Model

As part of the conceptual model development, a hydrostratigraphic framework is created to form the geometry for a future flow model. To examine the project data and test the geometry in three-dimensional space, a three-dimensional geologic model was created using the software package Leapfrog Works® by Seequent. The three-dimensional geologic model is a digital representation of the hydrostratigraphic structure. The hydrostratigraphic layers are those summarized in Table 4-1. Once the composition and number of layers were established, the Leapfrog model was constructed using a variety of data sources. The data sources used and the approach to developing the Leapfrog model are described in the following subsections.

4.1.3.1 Methodology

The lateral extent of the three-dimensional geologic model is the study area as defined by the Marathon Aquifer extent with an addition to the northeast of Marathon, Texas, plus a 1-mile buffer around the aquifer boundaries (Figure 2-1). The vertical extent is defined from the topography to a horizontal plane surface set at an elevation of 2,000 feet above mean sea level.

An a 30-meter digital elevation model grid obtained from the USGS National Map Seamless Server (https://apps.nationalmap.gov/viewer/) defines the land surface of the three-dimensional geologic model. Surface geology maps (Plates 23 and 24 of King, 1937) served as general guides for the interpretation of surface geology. The historical maps were scanned, georeferenced, and imported into a three-dimensional workspace, and then draped on top of the digital elevation model (Figure 4-2).

Figure 4-2. Extent of the Leapfrog model with a scanned map (Plate 23 of King, 1937) draped on a U.S. Geological Survey 30-meter digital elevation model. The extent of the Marathon Aquifer is shown as a red line.

Selected shapefile data exported from the Geologic Atlas of Texas (https://txpub.usgs.gov/txgeology/) provided a second reference for the surface expression of the grouped geologic units. The shapefiles were imported into the three-dimensional workspace and the elevation of each point and line segment was set to the topography.

Using a combination of the surface geology maps and the Geologic Atlas of Texas shapefiles, the model surface geology was interpreted by comparing the two data sources and blending them together through hand-drawing polylines using drawing tools in Leapfrog. During this process, care was taken to preserve the major features while generalizing some of the finer detail. This was done while keeping in mind an interpretation of the subsurface structure. Defining the hierarchy of the three-dimensional geologic model surfaces (i.e., how the software will direct the surfaces to interact in space that result in digital volumetric shapes) was also an important consideration in the construction of the model files.

To create the subsurface interpretations, 19 cross sections (A–A' through S–S') from King (1937) were scanned, georeferenced, and imported into the three-dimensional workspace (Figure 4-3).

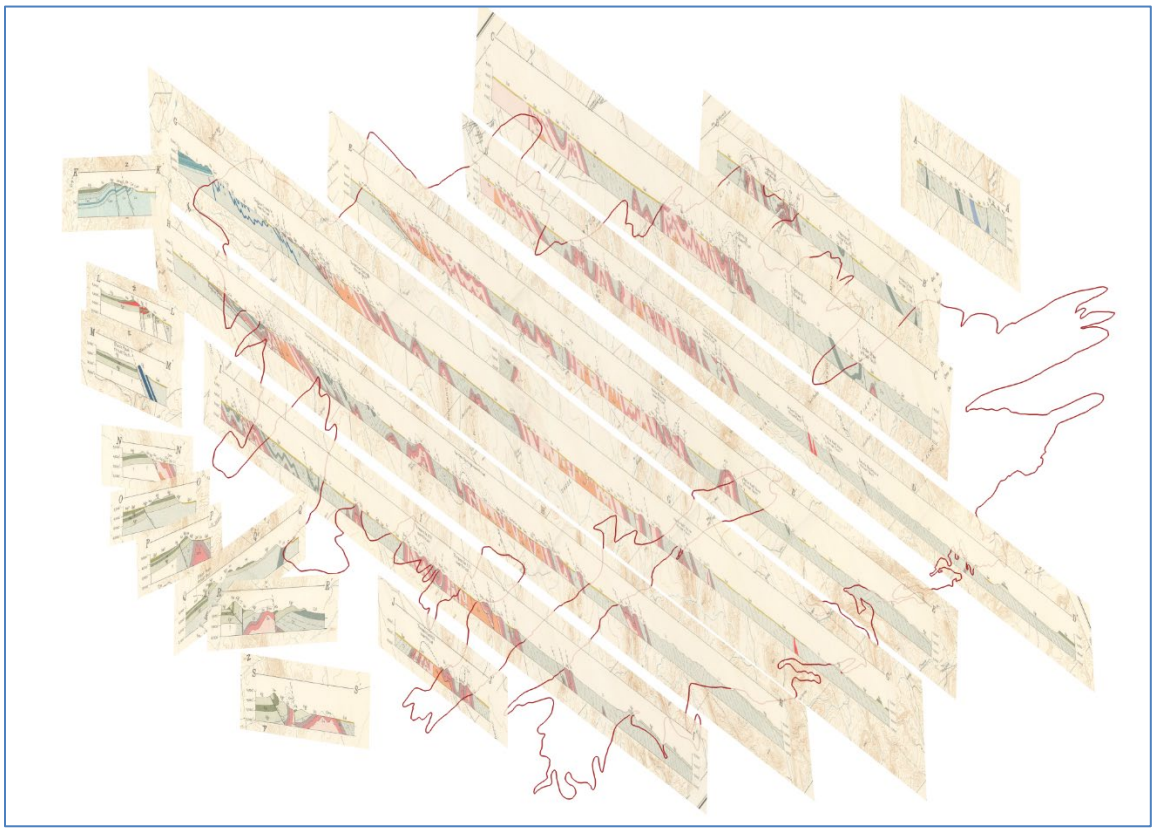

Figure 4-3. Scanned and georeferenced cross-sections from King (1937) shown in three-dimensional space. The Marathon Aquifer outline is shown in red.

Three-dimensional drawing tools available within the Leapfrog software were used to mark subsurface contacts between units from the scanned, georeferenced cross sections. The subsurface contacts were combined with the digitized surface outcrops to create the model layer surfaces (Figure 4-4).

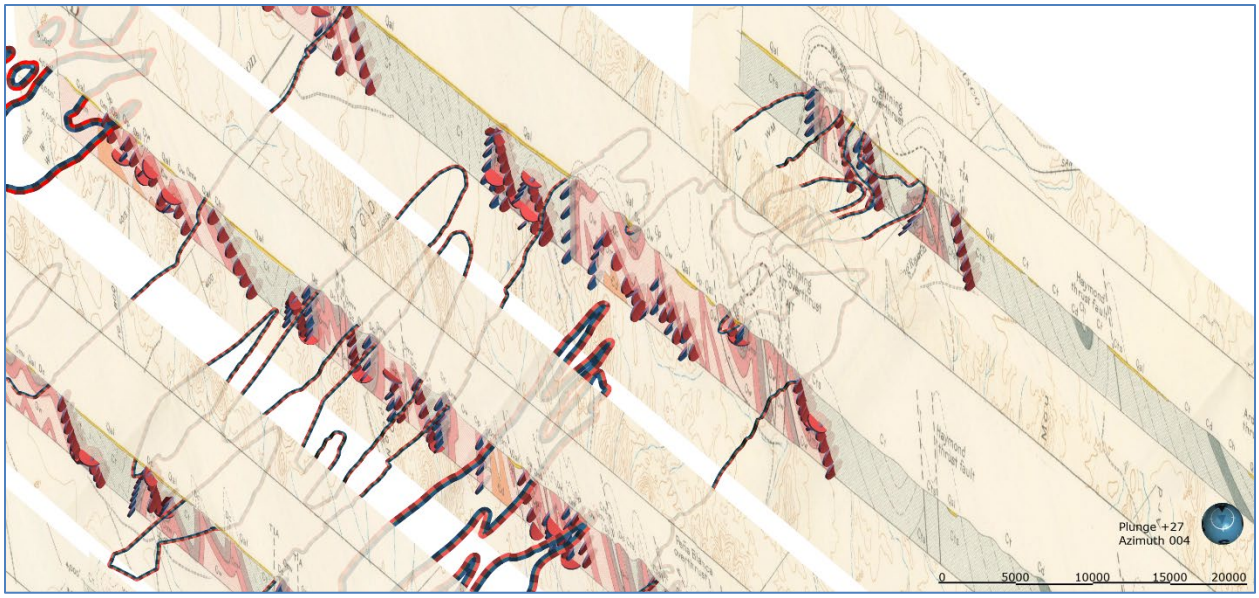

Figure 4-4. A close-up view of structural control points (shown as red disks) that mark subsurface contacts on the georeferenced cross-sections. Outcrops are defined by polylines (shown as dotted red and green lines) created by importing and editing shapefiles from the Geologic Atlas of Texas.

The model layer surfaces form the boundaries of each hydrostratigraphic layer. Some of the hydrostratigraphic layers consist of multiple geologic units grouped together (Figure 4-5 and Table 4-1) based on the relative age and general water-bearing characteristics of the units.

Code	Colour
1_Alluvium (Qal)	
2_Igneous (Ti)	
3a_Telephone Canyon, Glen Rose, Skinner Ranch, Hess, Lenox Hills (Ke, Kgr, Cw)	
3b_Gaptank, Haymond (Cg, Ch)	
4_Dimple, Tensus (Cd, Ct)	
5_Caballos, Maravillas, Fort Pena, Woods Hollow, Alsate Shale (Dc, Omv, Op, Ow, Oa)	
6_Marathon and Dagger Flat (Om, -Cd)	

Figure 4-5. Groupings of geologic units in three-dimensional geologic model, as shown by a screenshot from Leapfrog Works® software.

The surfaces were defined as contacts or intrusions in Leapfrog modeling software and a hierarchy was established (Figure 4-6), which indicates which surface takes precedence when multiple surfaces interact.

Contact surface chronology:

Contact surface
2_Igneous (Ti)
4_Dimple, Tensus (Cd, Ct) - 1_Alluvium (Qal) contacts
4_Dimple, Tensus (Cd, Ct) - 3a_Telephone Canyon, Glen Rose, Skinner Ranch, Hess, Lenox Hills (Ke, Kgr, Cw) contacts
Unknown - 3b_Gaptank, Haymond (Cg, Ch) contacts
5_Caballos, Maravillas, Fort Pena, Woods Hollow, Alsate Shale (Dc, Omv, Op, Ow, Oa) - 6_Marathon and Dagger Flat (Om, -Cd) contacts
4_Dimple, Tensus (Cd, Ct) - 5_Caballos, Maravillas, Fort Pena, Woods Hollow, Alsate Shale (Dc, Omv, Op, Ow, Oa) contacts

Figure 4-6. The contact surface chronology in the Leapfrog three-dimensional geologic model. The contact surfaces were modeled as either erosional surfaces (red icons) or intrusions (green icons). These types of contact surfaces refer to how the software is programmed rather than a classification of units by geologic process.

4.1.3.2 Results

The resulting three-dimensional geologic model has seven distinct units with volumetric shapes that include complex structural upthrusts and folded units (Figure 4-7) that correspond to the units in the stratigraphic column (Figure 4-5). The three-dimensional geologic model is provided as a Leapfrog application file, which contains an example of the geometry converted into a MODFLOW grid (Figure 4-8).

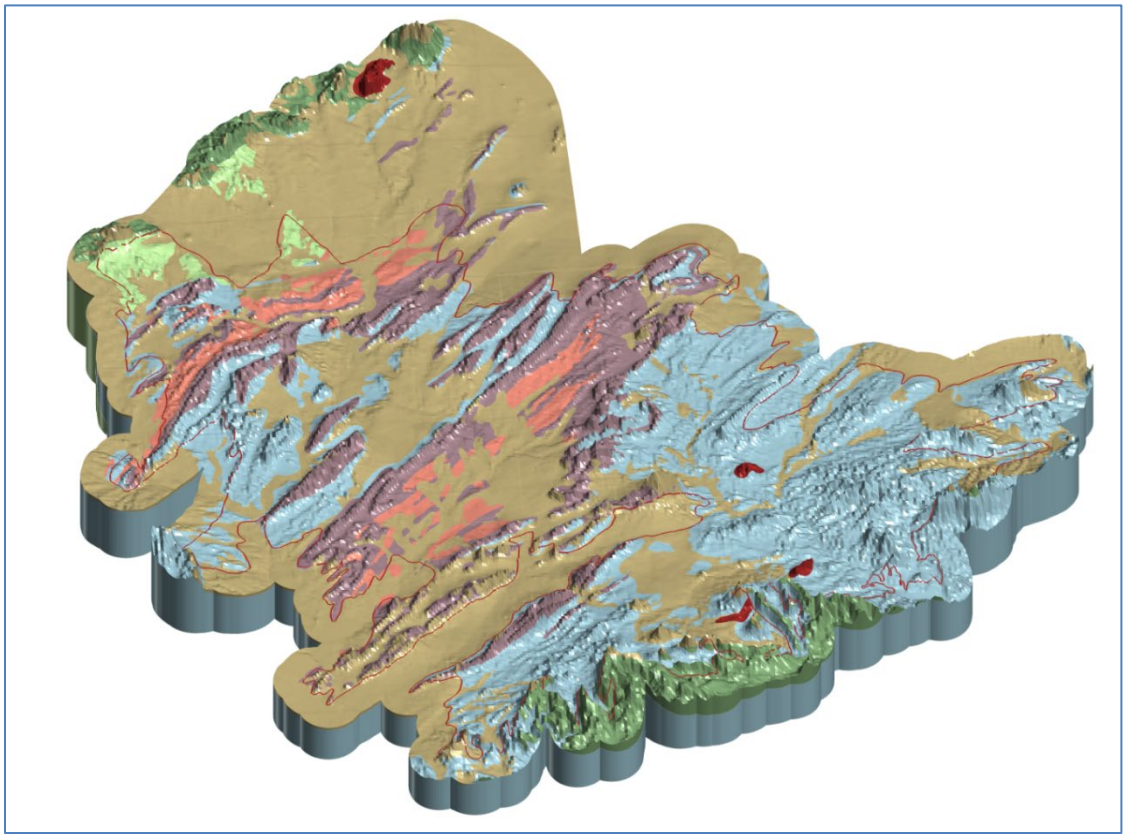

Figure 4-7. Completed volumes in three-dimensional geologic model, as shown by a screenshot from Leapfrog Works® software. The outline of the Marathon Aquifer is shown as a thin red line. Geologic units correspond to the codes used in Figure 4-5.

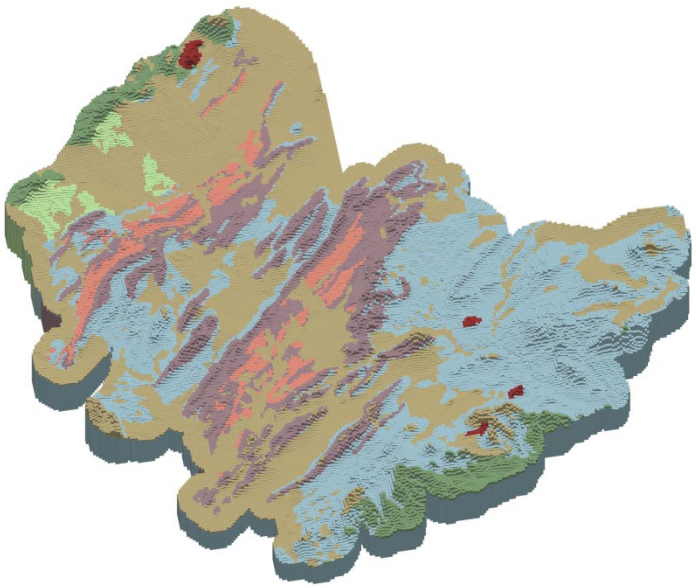

Figure 4-8. MODFLOW grids can either be imported or created in the Leapfrog Works® software. For example, a 660 foot MODFLOW grid based on the recharge model grid (Section 5.3) was created from the geometry of the three-dimensional geologic model, shown above.

Four representative cross sections (two northwest to southeast and two northeast to southwest) generated using the Leapfrog model are provided in Figures 4-9 through 4-12.

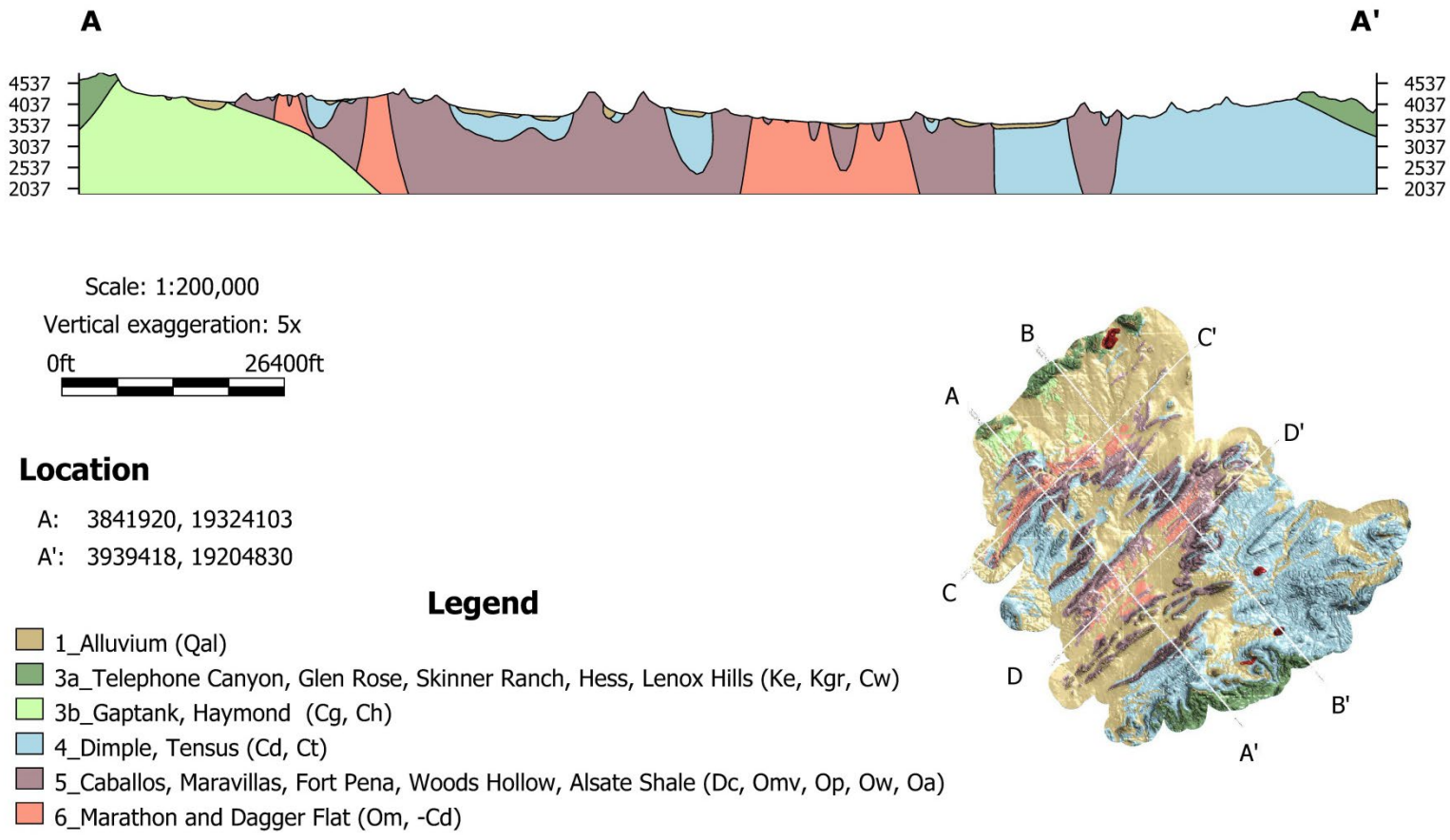

Figure 4-9. Leapfrog northwest-southeast cross section A-A'.

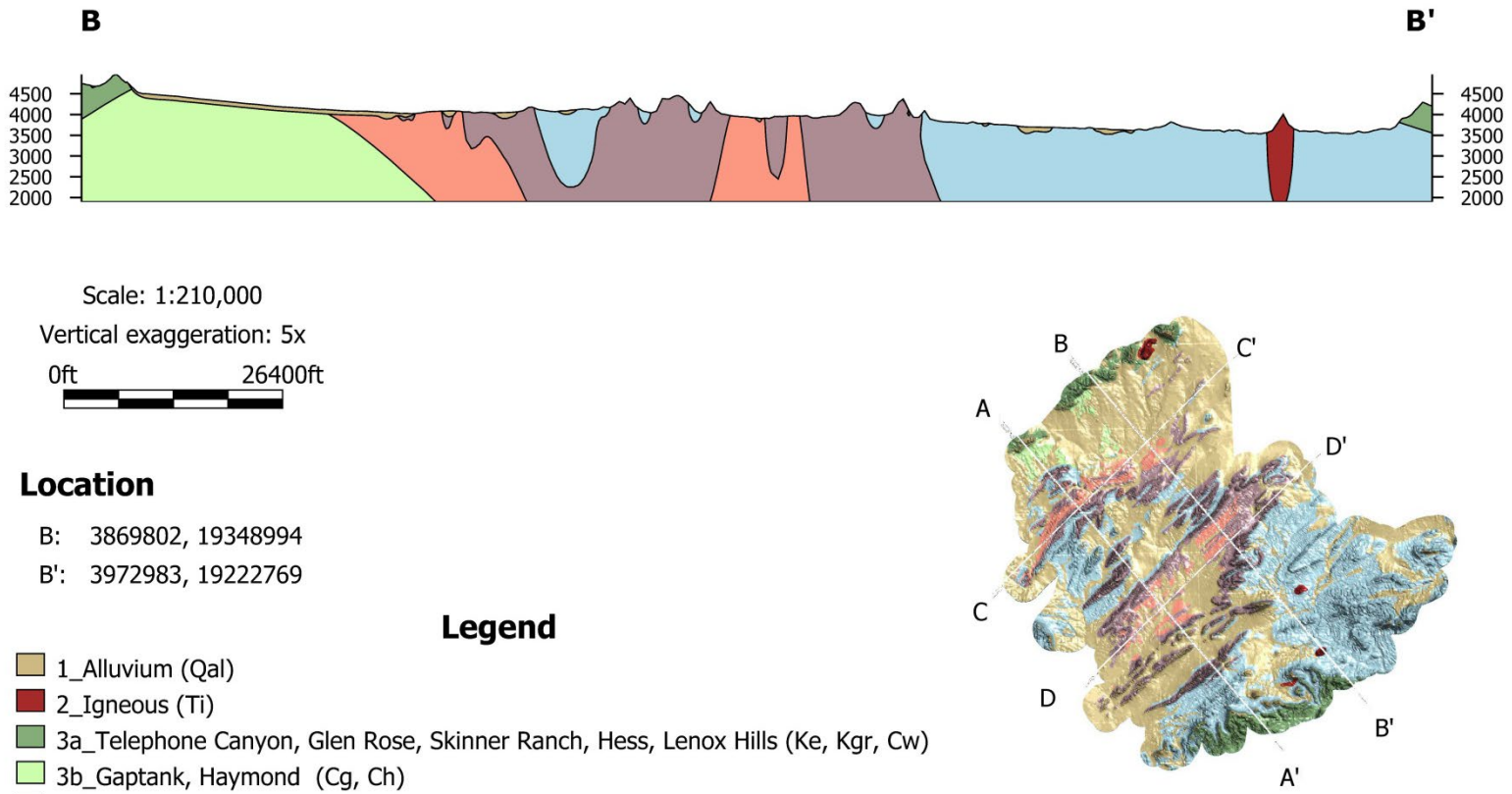

Figure 4-10. Leapfrog northwest-southeast cross section B-B'.

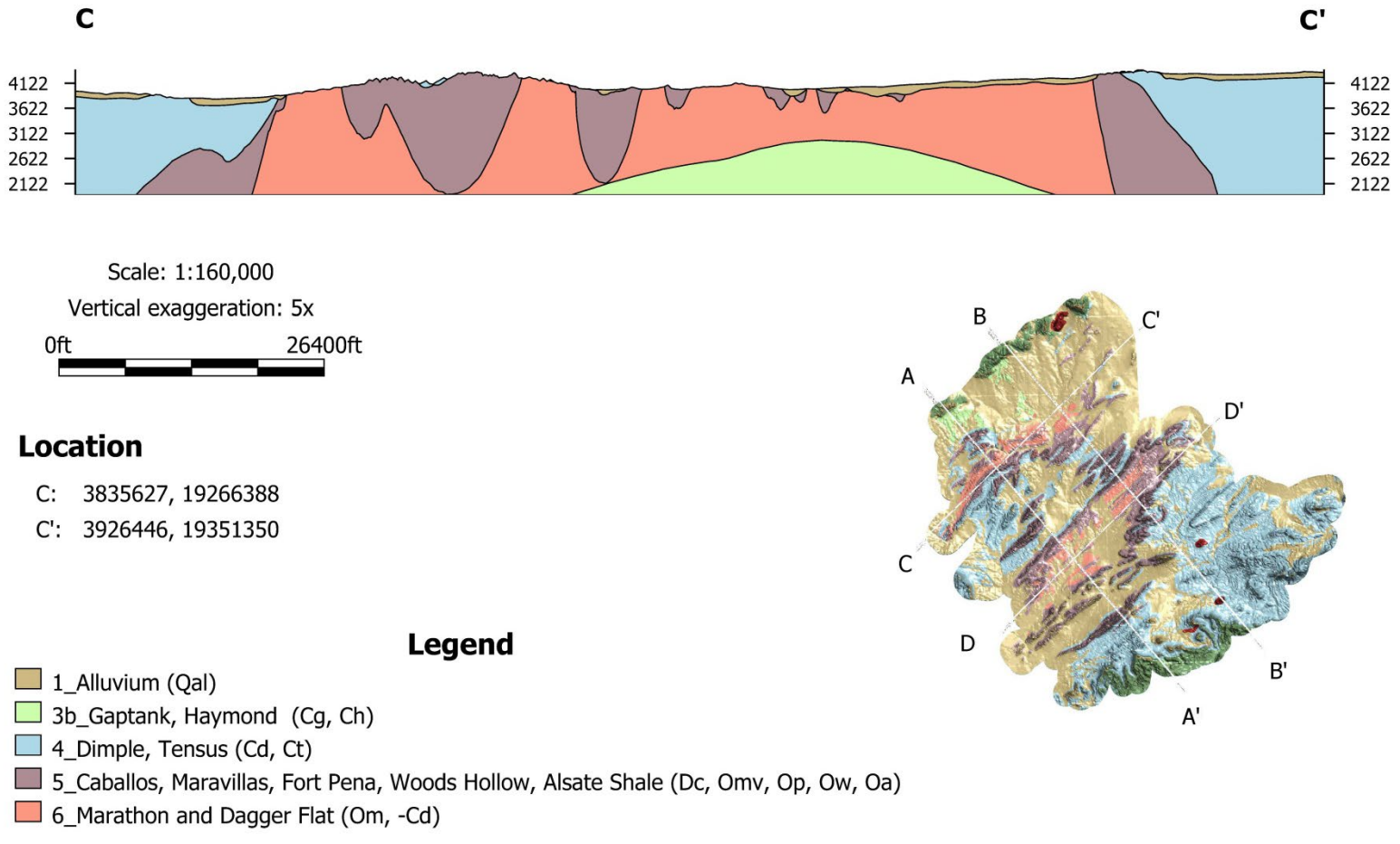

Figure 4-11. Leapfrog southwest-northeast cross section C-C'.

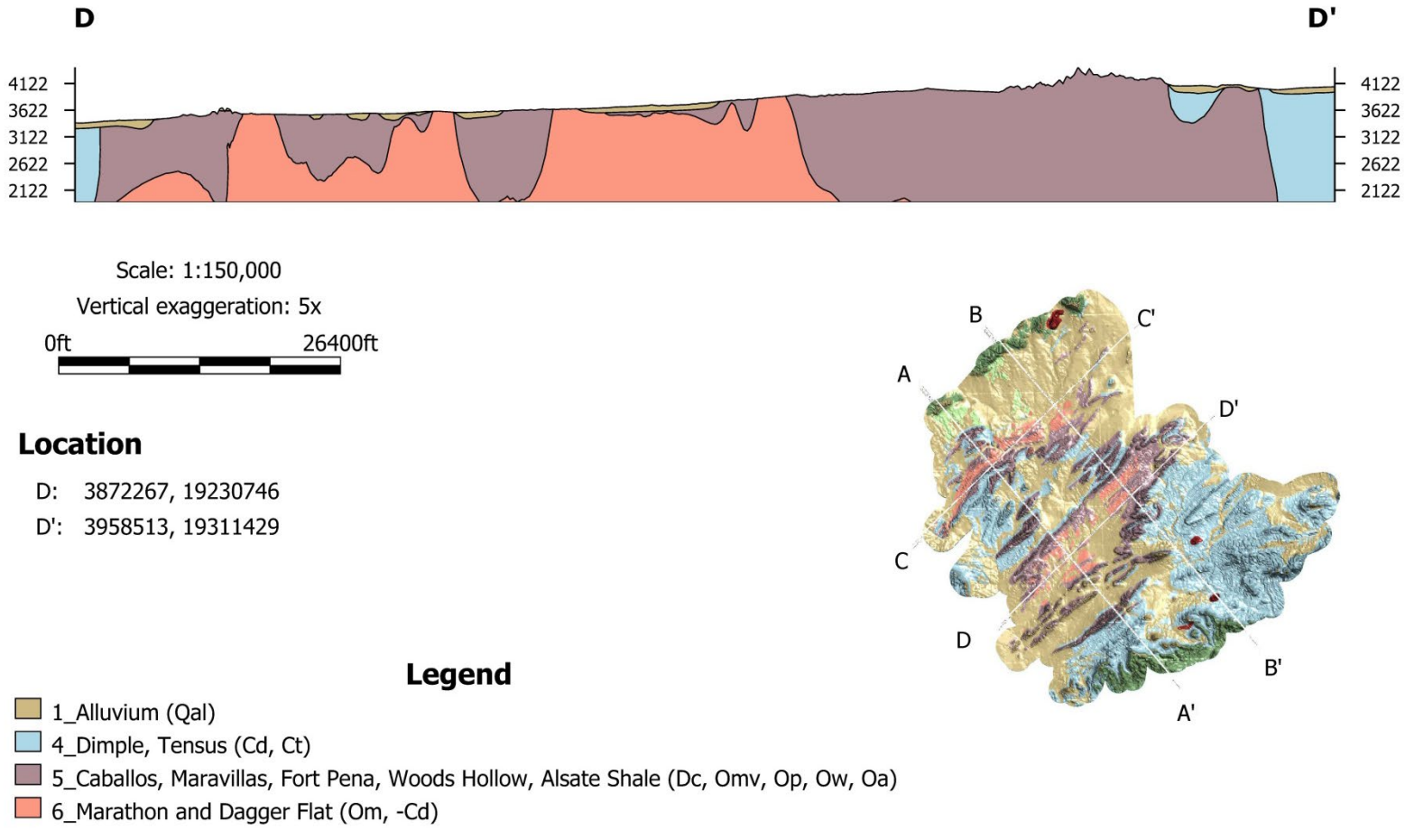

Figure 4-12. Leapfrog southwest-northeast cross section D-D'.

4.2 Water Levels and Regional Groundwater Flow

4.2.1 Water Levels from Existing Data Sources

As of March 2021, the TWDB groundwater database included 183 wells within the Marathon Aquifer and proposed aquifer expansion area, while the Texas Department of Licensing and Regulation submitted driller report database included 73 additional water wells. A total of 22 wells are listed in both the TWDB groundwater database and the Texas Department of Licensing and Regulation database. The geographic distribution of these well datasets is shown in Figure 4-13.

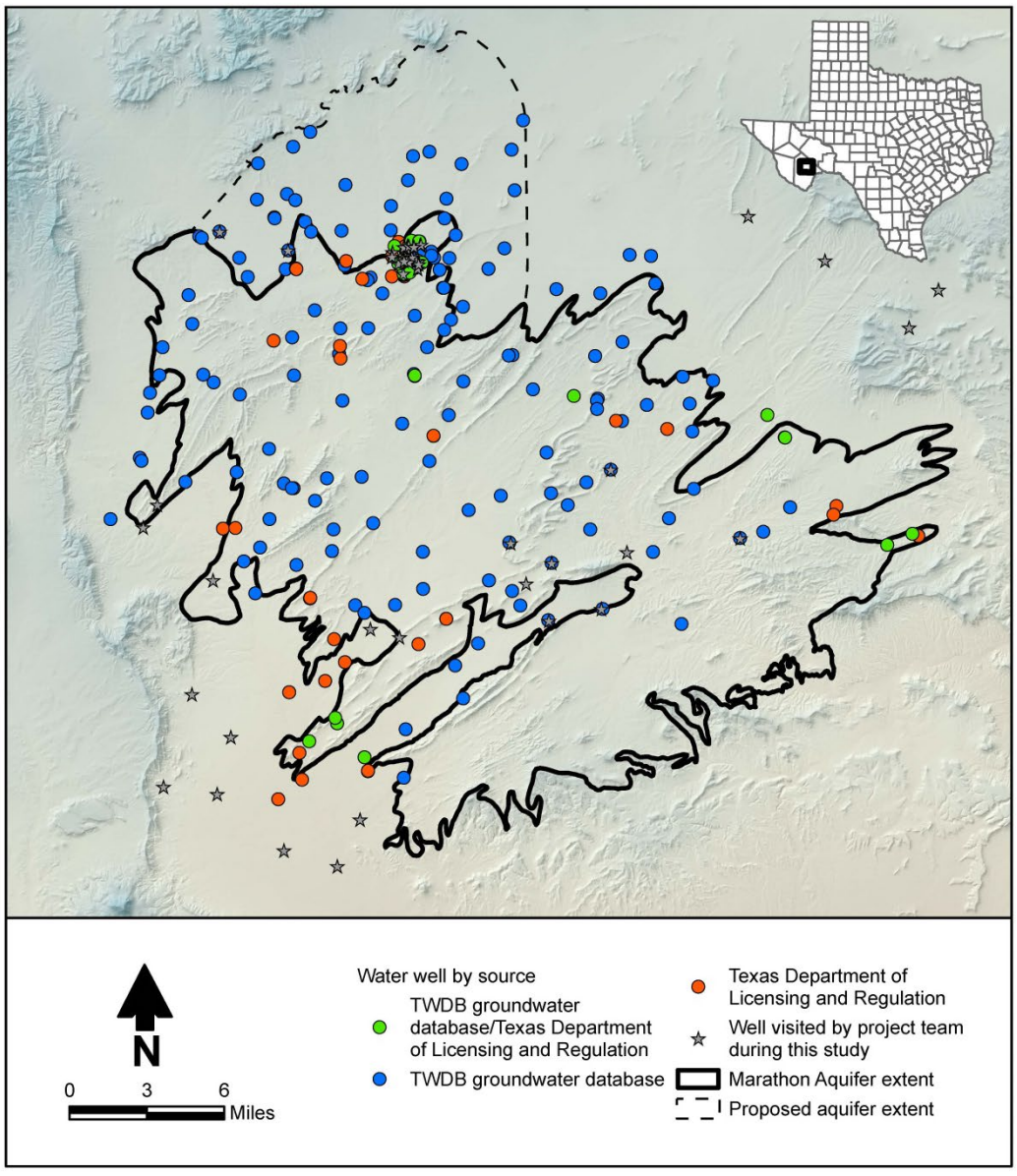

Figure 4-13. Location of documented water wells in the Marathon Aquifer study area.

The Texas Commission on Environmental Quality plotted water well database was also reviewed. However, wells from this dataset were not included in the Marathon Aquifer analysis due to imprecise location information and the absence of relevant aquifer information.

Every TWDB groundwater database well (including the 22 wells from the Texas Department of Licensing and Regulation database) was reviewed for production and stratigraphic data. Production data generally consisted of driller estimates, except for three multi-well Marathon Limestone pump tests and three specific capacity tests in Marathon. Stratigraphic data were limited, as most wells are shallow and do not penetrate multiple stratigraphic units.

Based on the well depth and location and a review of available data, each well was assigned a source aquifer designation that corresponded to one of the following Marathon Aquifer units: Alluvium, Gaptank Formation, Haymond Formation, Dimple Limestone, Tesnus Formation, Caballos Novaculite - Maravillas Chert, Woods Hollow Shale, Fort Pena Formation, Marathon Limestone, or Unknown when a production interval could not be determined.

Aquifer designations were determined by reviewing scanned documents and driller report completion notes, stratigraphic descriptions, and surface geology. Table 4-2 provides a summary of the aquifer designations and number of wells assigned to each aquifer, while Figure 4-13 illustrates the geographic distribution of these water wells.

Table 4-2. Marathon Aquifer TWDB and Texas Department of Licensing and Regulation wells by geologic unit

Aquifer Designations	Water Wells
Alluvium	40
Gaptank Formation	14
Haymond Formation	8
Dimple Limestone	6
Tesnus Formation	57
Caballos Novaculite and Maravillas Chert	12
Woods Hollow Shale	13
Fort Pena Formation	5
Marathon Limestone	61
Unknown	18

As indicated in Table 4-2, the majority of the existing recorded wells are completed in the alluvium, Tesnus Formation, and Marathon Limestone, which are aquifer units identified in Table 4-1. However, there are also a lesser number of wells completed in what are generally considered to be aquitard units, such as the Gaptank and Haymond formations.

This is not surprising, as the formations considered to be aquitards may produce small amounts of water from fracture zones, even though they are not as productive as some of the other formations. In the Marathon Aquifer area, as with many rural areas, land owners will often drill to the depth where they first encounter a source of water sufficient for their needs, and for local livestock or domestic use, relatively small well yields will suffice.

4.2.2 Water Level Data Collection

The project team and Mr. Tim Leary were able to compile a total of 35 new water level measurements from 13 separate stakeholders geographically dispersed throughout the Marathon Aquifer study area. In addition, Mr. Cody Bjornson from the TWDB collected Marathon Aquifer water level measurements during July 27 to July 29, 2021; these data added 9 additional water level locations, improving the geographic distribution of water levels within the study area. A table of the 2021 Marathon Aquifer measured water levels is provided in Appendix A.

A few large geographic areas without 2021 water levels within the Marathon Aquifer study area were identified and 11 supplemental 2019 and 2020 Texas Department of Licensing and Registration water levels were used to fill these data gaps to create the final Marathon Aquifer study area water level dataset. A listing of the 55 Marathon Aquifer water levels for the 2019 to 2020 period is also provided in Appendix A. Figure 4-14 illustrates the location of wells where water level measurements were obtained between 2019 and 2022.

4.2.3 Proposed Aquifer Expansion

In the TWDB groundwater database and the Texas Department of Licensing and Regulation datasets, there are at least 8 Marathon Limestone water wells and 26 wells producing from other Marathon Aquifer stratigraphic units within the proposed extension area. There are no apparent barriers to groundwater flow that separate this proposed extension area from the Marathon Aquifer to the south as currently delineated by the TWDB. Based on this, and an analysis of the TWDB and Texas Department of Licensing and Regulation water well data, in conjunction with the observation that the Marathon Limestone outcrops outside of the official TWDB Marathon Aquifer extent (Anderson and others, 1982), it is proposed that the Marathon Aquifer extent be extended on the north side of the current extent between the town of Marathon and the Glass Mountains. This region is identified by the proposed aquifer extent line on the figures. Within the proposed extension, the Marathon Limestone and other Marathon Aquifer units, such as the Tesnus Formation and Dimple Limestone, crop out or are overlain by alluvium.

The proposed expansion includes an area of approximately 60 square miles.

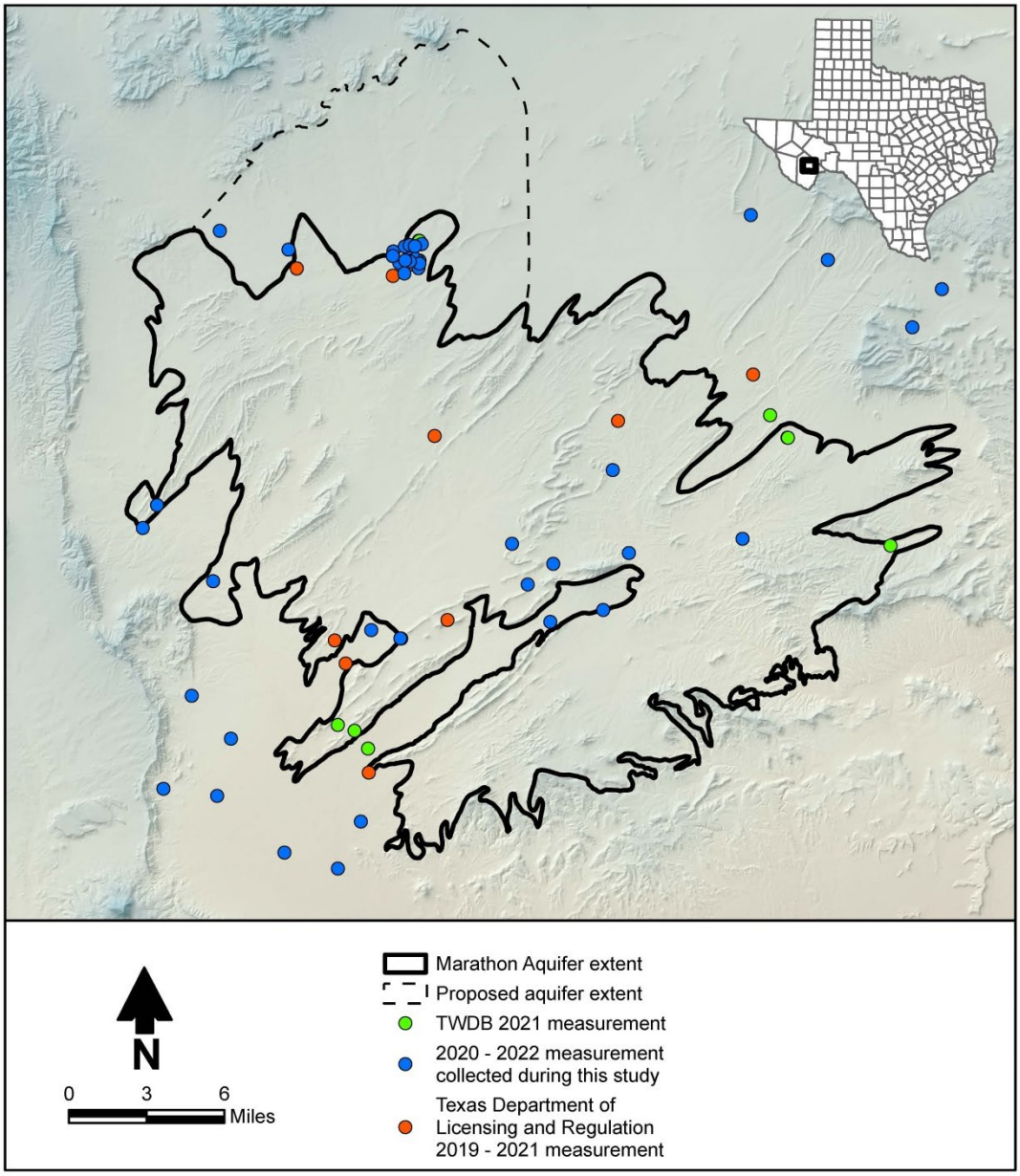

Figure 4-14. Locations of water wells with recent (2019-2021) water levels.

4.2.4 Water Level Changes through Time

DeCook (1961) states that water levels on the Marathon area fluctuate chiefly in response to changes in the rates of recharge and discharge. He measured water levels at four wells over the period September 1956 through November 1957 and observed "very little net change in water level during this period" (DeCook, 1961, p. 18).

Available information on changes in water levels through time is limited. Two well hydrographs were constructed from water levels in the TWDB groundwater database

(Figure 4-15). Well 52-55-104 is the town of Marathon public supply well 1. Water levels at this well have fluctuated over a range of about 20 feet for the period 2007 to early 2022. The highest water levels recorded during this more recent period are about 10 feet lower than the earliest recorded water level of 3,974 feet above mean sea level in 1969, when the well was installed, indicating that over the long term, there has been some moderate water level decline at this well.

The second hydrograph is also for a Marathon public supply well installed in 2015 near supply well 1. Observed water levels at this location fluctuate over the period 2016 through early 2022, but there is no clear upward or downward trend. As would be expected, the observed water levels at this well are similar to those at well 1.

Some of the water levels measured during this study were obtained at wells that had prior water level information from either the TWDB groundwater database or the Texas Department of Licensing and Regulation submitted drillers reports database. A total of 14 of these wells were identified (Figure 4-15); reported water levels are summarized in Table 4-3. Of the 14 wells, 9 exhibited a water level decline from the prior measurement and 5 exhibited a water level increase. Of these wells, 3 wells owned by Mr. Leary provide information over the longest period of time; 2 of these wells had measurements from 1957 (wells 52-64-701 and 52-63-503), and 1 had a measurement from 1973 (well 52-63-901). The first 2 wells showed almost no change in water levels over the 64-year span of time—one increased by 9 feet and the other declined by 2 feet. Water level at the third well, however, declined by 46 feet. Details regarding this well are not available, but it is likely in a low-permeability aquifer (or confining) unit with limited recharge potential.

Overall, because water use in the Marathon Aquifer is primarily for domestic and stock purposes, water levels are not expected to exhibit consistent upward or downward trends, but rather should primarily fluctuate based on changes in groundwater recharge. The exception to this would be the town of Marathon, where there is a public water system and water use for other purposes common to a small community. Based on the water levels at Marathon supply well 1 and some of the other wells in the town (Table 4-3), some moderate water level decline appears to have occurred over time.

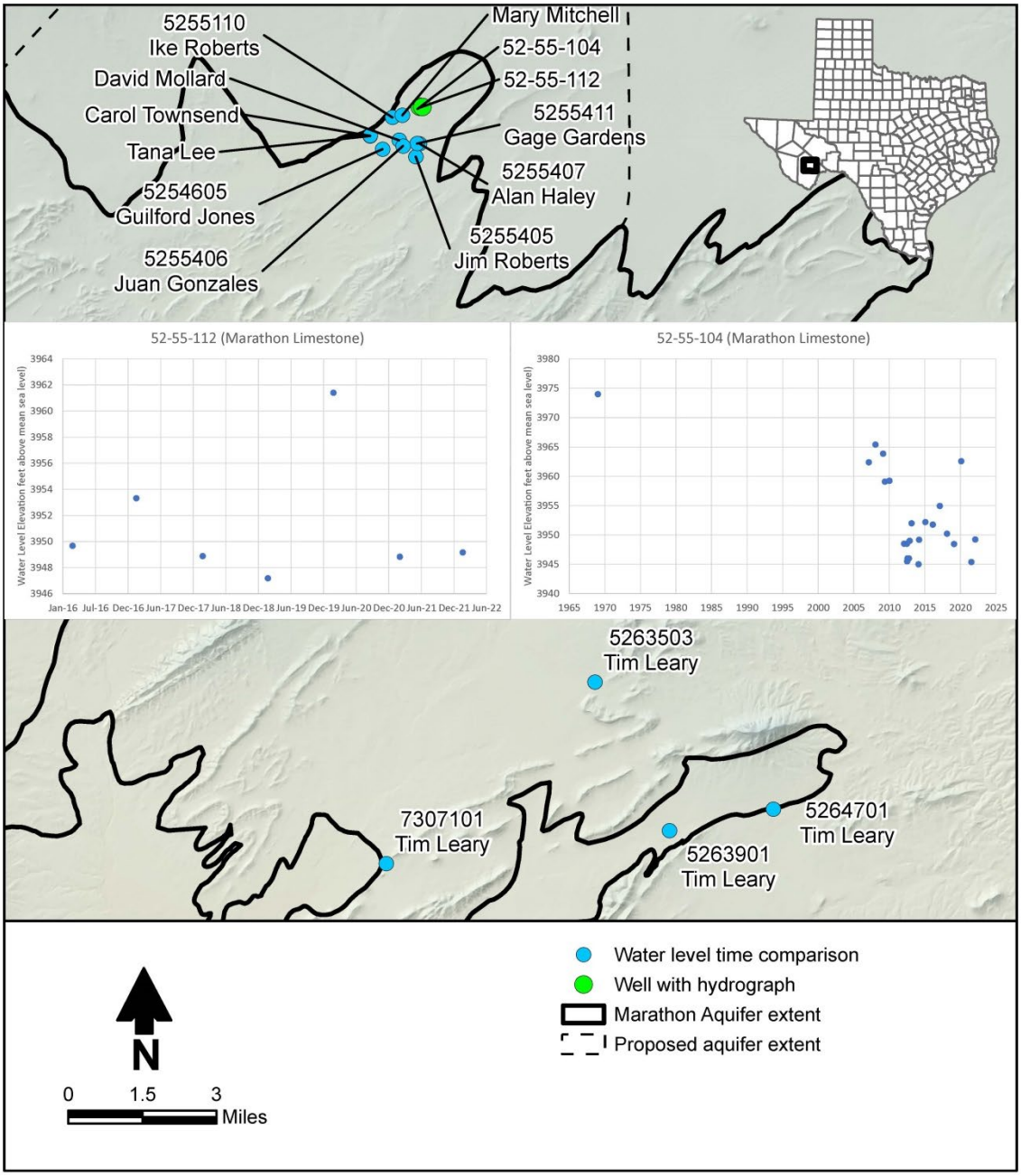

Figure 4-15. Well locations with multiple observed water levels (Table 4-3).

Table 4-3. Water level comparison over time.

State Well Number	Current Owner	Well Depth (feet)	First Measurement		Second Measurement		Change (feet)	Percent Change in Water Column
			Date	Depth to Water (feet)	Date	Depth to Water (feet)		
	David Mollard	343	5/9/2019	146	5/4/2021	142	4	2.0%
5255407	Alan Haley	185	3/21/2006	110	5/5/2021	121	–11	–14.7%
5255405	Jim Roberts	205	12/13/2006	123.17	5/4/2021	134	–11	–13.2%
5254605	Guilford Jones	515	10/27/2004	75	7/19/2021	105	–30	–6.8%
5255411	Gage Gardens	425	4/28/2009	108.1	6/16/2021	120	–12	–3.8%
7307101	Tim Leary	Unknown	7/28/2021	27	8/3/2021	12	15	—
5264701	Tim Leary	Unknown	9/16/1957	95.9	8/4/2021	87	9	—
5263503	Tim Leary	Unknown	9/16/1957	67.9	8/7/2021	70	–2	—
5263901	Tim Leary	Unknown	4/7/1973	30	8/8/2021	76	–46	—
	Tana Lee	250	4/18/2017	84	3/19/2022	89	–5	–3.0%
5255110	Ike Roberts	Unknown	6/21/2011	120.55	2/25/2022	109	12	—
5255406	Juan Gonzales	225	11/15/2006	100	4/3/2022	117	–17	–13.6%
	Mary Mitchell	278	4/4/2008	139	3/25/2022	151	–12	–8.6%
	Carol Townsend	230	4/18/2017	84	3/19/2022	83	1	0.7%

4.2.5 Water Level Maps

A regional groundwater level contour map was constructed based on available measurements at wells and the estimated land surface at spring believe to be representative of regional (not perched) aquifers (Figure 4-16). At most of these wells, only one water level measurement was available; if multiple measurements were available the more recent value was used in the contouring. Although wells are identified by hydrostratigraphic unit, based on the fact that all wells are relatively shallow (less than 500 feet and many are less than 200 feet) it is assumed that there is sufficient fracturing of the near-surface bedrock units such that groundwater flow can occur.

Figure 4-17 shows the estimated regional groundwater flow direction and groundwater divide based on the water level data and regional water level map shown in Figure 4-16. As shown in Figure 4-17, in the western portion of the aquifer (approximately coincident with the Maravillas Creek watershed), groundwater flow tends to be to the south-southwest and in many places parallel to the distinct series of ridges and hills comprised most often of Caballos Novaculite, Maravillas Chert and other rocks of hydrostratigraphic unit 5. However, it is believed that these formations are sufficiently fractured that groundwater can migrate through these features at depth. A portion of the observed southwestward flow component is likely attributable to the alluvium that overlies the fractured rocks between the ridges, which can act a higher-permeability aquifer unit where it is saturated.

Within the eastern portion of the aquifer, approximately coincident with the San Francisco Creek watershed, groundwater tends to flow south and east. In this area, Hell's Half Acre is a region of higher water levels, and groundwater flow is radially outward from this area. This area also has a number of springs identified from the U.S. Geological Survey National Hydrography Dataset.

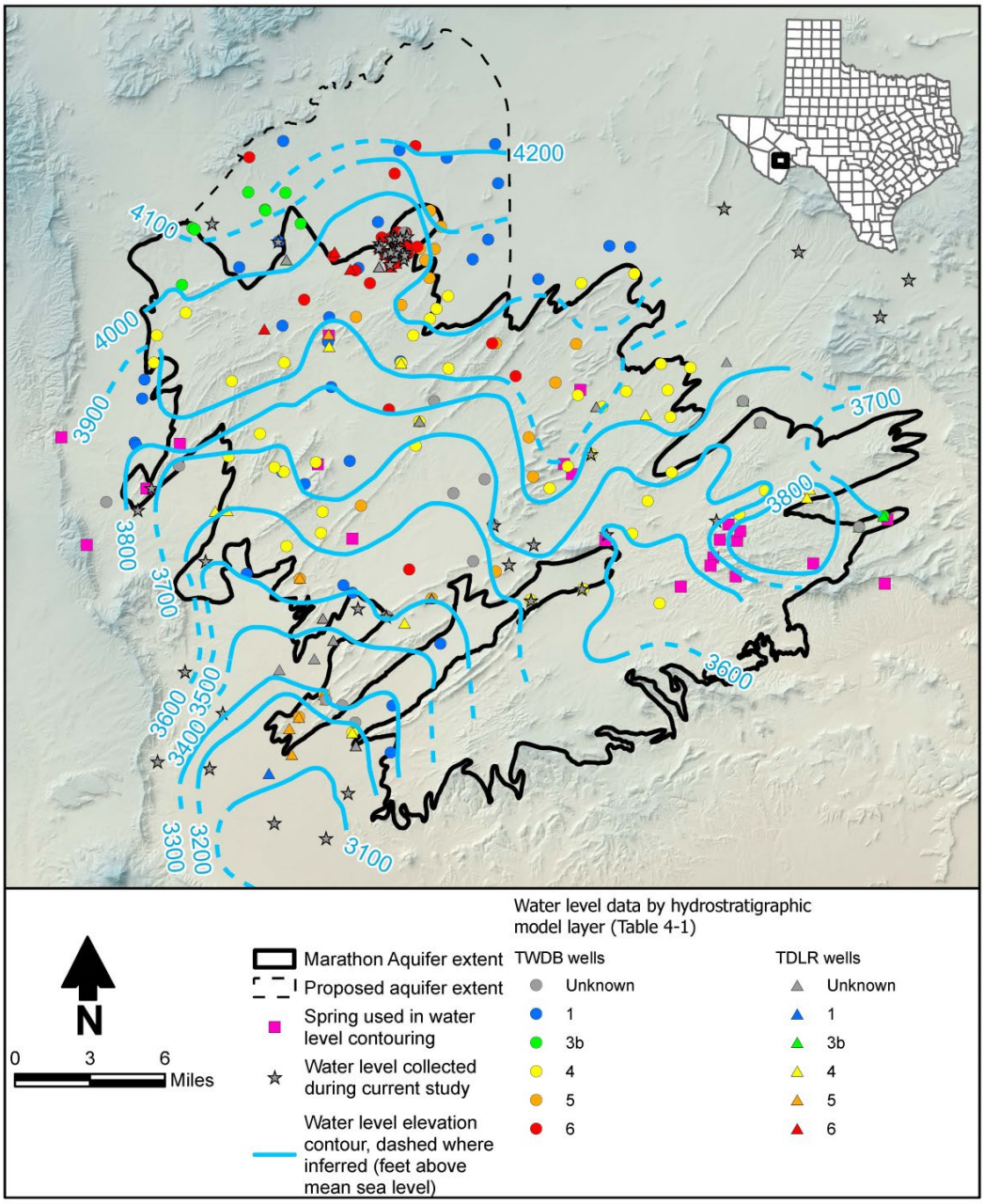

Figure 4-16. Regional Marathon Aquifer water levels.

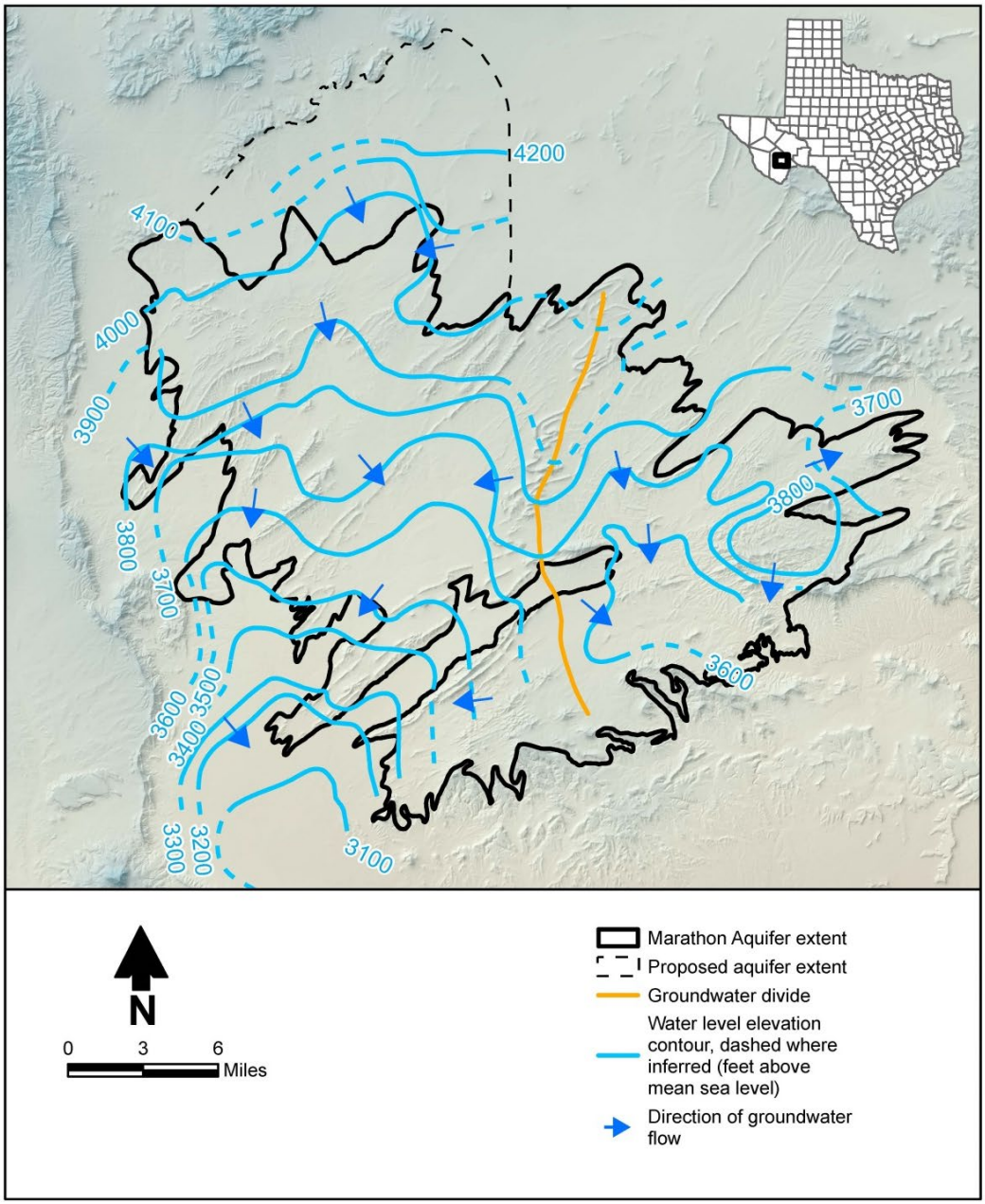

Figure 4-17. Regional groundwater flow direction and groundwater divide.

4.3 Recharge

Groundwater recharge to the Marathon Aquifer was estimated to be approximately 35,000 acre-feet per year by DeCook (1961) and approximately 25,000 acre-feet per year by Smith (2001). A more rigorous estimate of groundwater recharge based on climatic and physiographic data was developed for this study using the Distributed Parameter Watershed Model. Daniel B. Stephens & Associates, Inc. developed the Distributed Parameter Watershed Model based on the Mass Accounting System for Soil Infiltration and Flow model developed by Sandia National Laboratories (2007) for the Yucca Mountain Project. The Distributed Parameter Watershed Model is similar in concept to water balance models used by the U.S. Geological Survey (e.g., Precipitation Runoff Modeling System [Leavesley and others, 1983], INFIL [Hevesi and others, 2003], Basin Characterization Model [Flint and Flint, 2007]). The Distributed Parameter Watershed Model uses a daily time step over regular grid cell sizes that are user-defined. The model generally relies on the widely accepted FAO-56 procedure for computing actual evapotranspiration from the reference evapotranspiration estimated using the Penman-Monteith method (Allen and others, 1998). Water budget components accounted for in the model include precipitation, bare soil evaporation, transpiration, runoff, run-on, snow accumulation, snowmelt, snow sublimation (direct evaporation of snow into the atmosphere), soil water storage, and net infiltration. A bedrock boundary is placed at the bottom of Distributed Parameter Watershed Model cells with shallow soil depths; this boundary may restrict infiltration when the saturated hydraulic conductivity of the bedrock is less than that of the soil.

Surface water runoff is estimated by the model when either the rate of precipitation exceeds the saturated hydraulic conductivity of the soil (infiltration excess or Hortonian runoff) or the soil-water content of the soil exceeds the water-holding capacity of the soil (saturation excess or Dunnian runoff). Surface water runoff is routed between model cells based on topography obtained from a digital elevation model. The Distributed Parameter Watershed Model accounts for focused runoff by modeling washes and streams as a separate water balance calculation within each model cell. Where washes and streams are present, runoff is routed from overland flow to the washes and streams within a model cell, and then runoff is routed to the wash and stream in the next downstream cell. All routing is based on topography only. The model does not simulate interflow in the subsurface between the model cells; the only hydrologic connection between cells occurs as the surface water component.

The Distributed Parameter Watershed Model domain consists of the portions of the Maravillas Creek and San Francisco Creek watersheds that overlie the Marathon Aquifer. A recharge model grid size of 40,469 square meters (⅛ mile by ⅛ mile) was deemed to be adequate for the goals of this study. The time period of simulation is water years 1981 through 2021 (41 years from October 1980 through September 2021) to correspond to readily available climatic data required as model input.

The model is constructed and executed using metric units to efficiently capitalize on existing data sources. A schematic representation of model operation is provided in Figure 4-18.

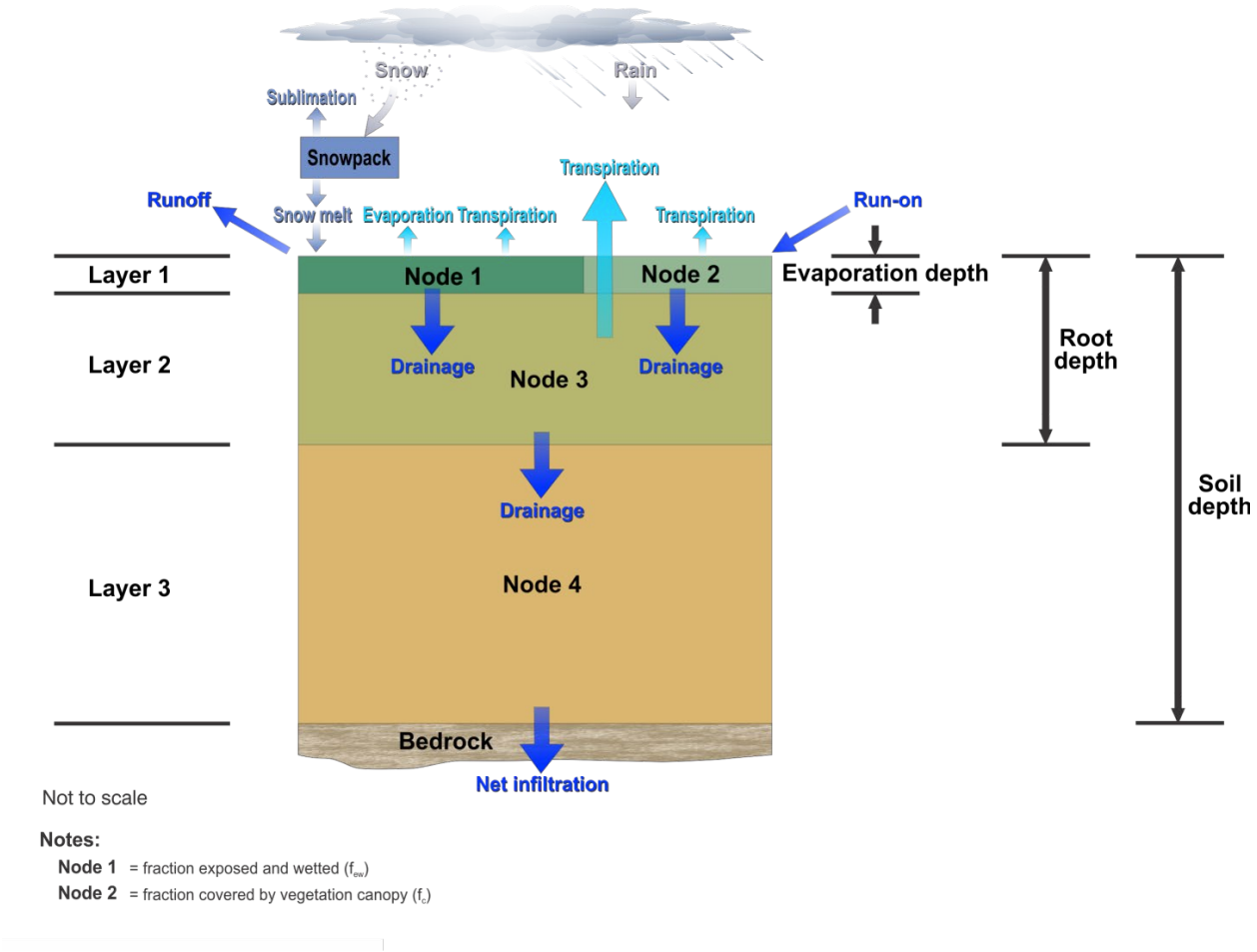

Figure 4-18. Schematic representation of Distributed Parameter Watershed Model operation.

4.3.1 Recharge Model Inputs

To estimate the spatial and temporal distribution of groundwater recharge, the Distributed Parameter Watershed Model assimilates published data from multiple sources. The primary model inputs and data sources are outlined in the following subsections. Tables summarizing primary model inputs are provided in Appendix B due to the large number of model inputs that had to be documented.

4.3.1.1 Climate

For each grid cell in the modeling domain, the Distributed Parameter Watershed Model requires daily minimum and maximum temperatures, precipitation amount and duration, and wind speed. Reliable estimation of climate data in both space and time from sparse weather stations is complex. Standard practice is to rely on climate models published by specialists. Two widely used climate models are the Parameter Elevation Regression on Independent Slopes Model (PRISM Climate Group, 2004) and the North American Land Data Assimilation System (Xia and others, 2009 and 2012).

The daily variation of climate was input to the Distributed Parameter Watershed Model for the Marathon, Texas National Oceanic and Atmospheric Administration weather station location. Daily total precipitation and minimum and maximum air temperature at the station were obtained from the data record reported by the National Oceanic and Atmospheric Administration. Mean daily wind speeds were obtained for the station location from North American Land Data Assimilation System. The daily durations of precipitation were obtained from North American Land Data Assimilation System when available or were based on monthly regressions between the North American Land Data Assimilation System and National Oceanic and Atmospheric Administration data. For the daily durations, 20 percent were obtained directly from the North American Land Data Assimilation System and 80 percent were estimated based on monthly regressions. Gaps in the daily climate input to the Distributed Parameter Watershed Model were filled using the estimates at the reference station location provided by the Parameter Elevation Regression on Independent Slopes Model.

The Parameter Elevation Regression on Independent Slopes Model was used to spatially distribute precipitation over the Distributed Parameter Watershed Model domain. Parameter Elevation Regression on Independent Slopes Model reports mean annual precipitation at 800-meter grid cell resolution over the Continental United States for the 30-year period from 1991 through 2020. Each Distributed Parameter Watershed Model grid cell is mapped to the Parameter Elevation Regression on Independent Slopes Model grid cells based on the centroid of the Distributed Parameter Watershed Model cell.

The mean annual precipitation simulated by the Distributed Parameter Watershed Model for water years 1981 through 2021 was 14.5 inches over the model domain, and ranged from 20.3 inches in the higher elevations to the northwest in the Del Norte Mountains to 12.1 inches along the lower elevations of the southern boundary of the model domain. The driest water year on record from 1981 through 2021 was 2011. The wettest water year on record from 1981 through 2021 was 1987.

Based on the relation between Parameter Elevation Regression on Independent Slopes Model air temperature and elevation, the lapse rate for air temperature was estimated at 4.890×10^{-3} degrees Celsius per kilometer.

In arid and semiarid regions, the dew point may be less than the daily minimum air temperature. This difference is known as the dew point offset. The dew point offset can be specified in the Distributed Parameter Watershed Model as a constant, using a harmonic function, or can be entered as daily values. The dew point offset is for the reference grass surface used in the reference evapotranspiration in the FAO-56 Penman-Monteith method, which may be a wetter surface than found naturally in the Distributed Parameter Watershed Model domain. Therefore, although weather stations over natural vegetation may show a large dew point offset, the dew point offset should not be greater than 5 degrees Celsius. A constant dew point offset of 2 degrees Celsius was assumed for the Marathon Aquifer area.

The Hargreaves' coefficient for estimating incoming solar radiation (degrees Celsius$^{-0.5}$) typically ranges from 0.16 to 0.19 (Allen and others, 1998). The Hargreaves' coefficient can be estimated from observed solar radiation data, but there were no observed solar radiation data for the Marathon area. When solar radiation data are not available, a value of 0.16 is recommended for 'interior' locations, where land mass dominates and air masses are not strongly influenced by a large water body (Allen and others, 1998). A value of 0.16 was selected for Marathon Aquifer area.

The turbidity coefficient for solar radiation ranges from 0 to 1, where 1 represents clean air and values less than or equal to 0.5 represent extremely turbid, dusty, or polluted air (Allen and others, 2005). The turbidity coefficient is constant and uniformly applied over the model domain. A value of 0.59 for the turbidity coefficient was obtained from HOMER Energy 2022, which is the average value for Midland, Texas.

The snowmelt factors can be constant or can vary over the year with a minimum rate on December 21 and a maximum rate on June 21. The minimum rate is typically 2 millimeters per degree Celsius for each degree above 0 degrees Celsius, and the maximum rate is typically 5.2 millimeters per degree Celsius for each degree above 0 degrees Celsius (Schroeder and others, 1994). Typical values of 2 millimeters per degree Celsius and 5.2 millimeters per degree Celsius were selected for the model.

The Distributed Parameter Watershed Model has options to estimate sublimation of snow using the methodologies in the Mass Accounting System for Soil Infiltration and Flow model or the INFIL model. In the Mass Accounting System for Soil Infiltration and Flow model, sublimation is a constant coefficient of the snow pack. In the INFIL model, the sublimation can vary depending on air temperature and the reference evapotranspiration (Hevesi and others, 2003). The INFIL methodology was selected, and the fraction of reference evapotranspiration that becomes sublimation was set to 1.0 for temperatures at or below freezing and for temperatures above freezing.

4.3.1.2 Palmer Drought Severity Index

The Marathon Aquifer is located within Texas Climate Division 5. According to the Palmer Drought Severity Index, water years 2012 through 2014 were in drought, and water years 2015 through 2016 were wetter than average (Figure 4-19).

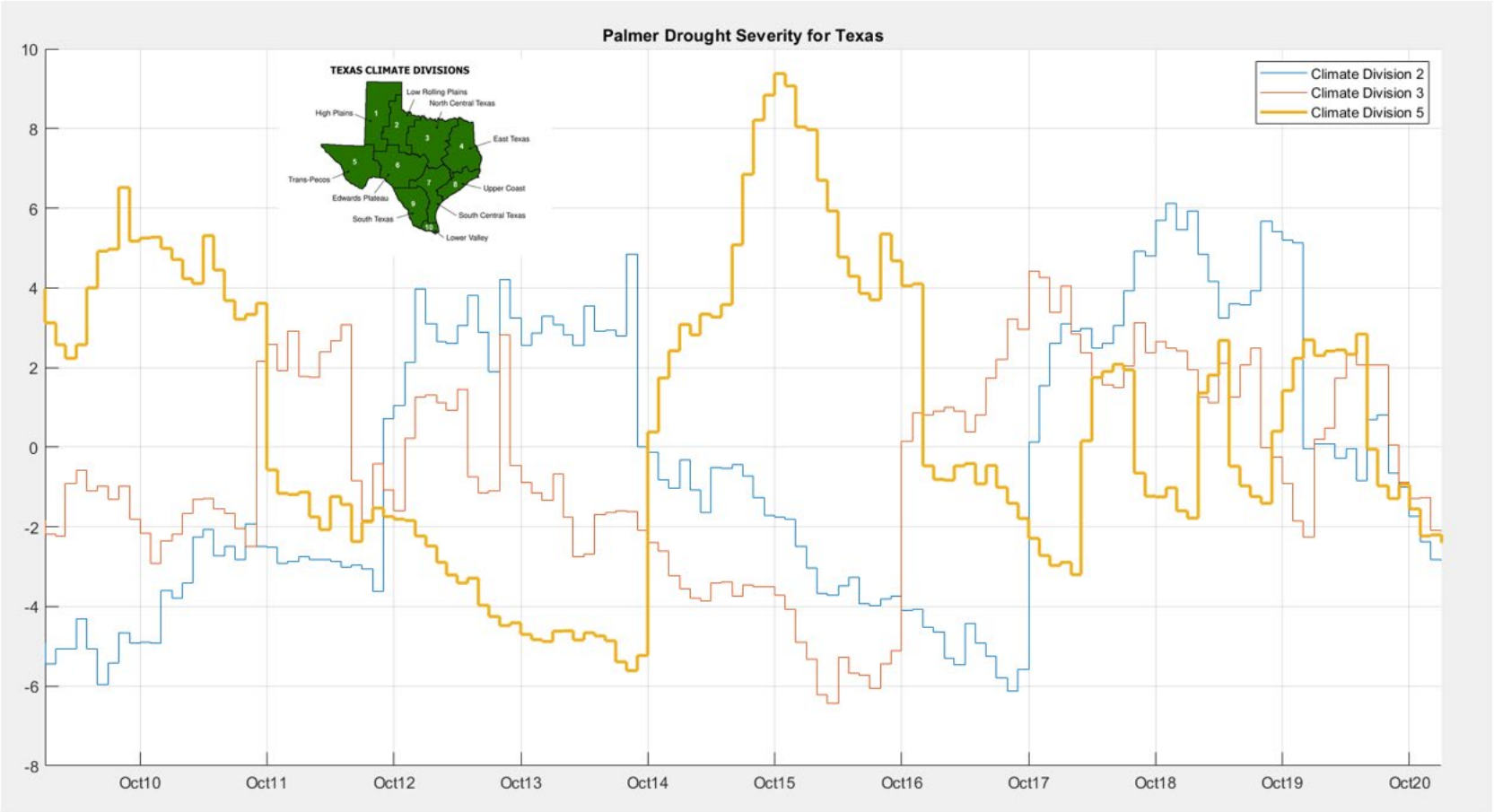

Figure 4-19. Palmer Drought Severity Index for Texas Climate Division 5.

The precipitation estimated by the Distributed Parameter Watershed Model was compared to data from three weather stations within or adjacent to the model domain. The stations include the Elephant Mountain WMA Remote Automated Weather Station located at an elevation of 4,476 feet above mean sea level on the western boundary of the model domain, the Housetop Mountain station located at an elevation of 4,320 feet above mean sea level on the eastern boundary of the model, and the Alan Haley station located at an elevation of 4,075 feet above mean sea level in Marathon. For comparison, the Marathon, Texas National Oceanic and Atmospheric Administration station (Station No. USC00415579) is located at an elevation of 3,989 feet above mean sea level. The Elephant Mountain Remote Automated Weather Station is operated by the U.S. Bureau of Land Management, and reports hourly data from September 2013 through present. The Housetop Mountain station is read daily from a graduated glass gauge, and the occurrence of precipitation is recorded in hand-written records from May 2005 through December 2019. The Alan Haley station is a digital weather station with monthly total precipitation from January 2015 through December 2020. The Elephant Mountain Remote Automated Weather Station and the Housetop Mountain station are not within the Distributed Parameter Watershed Model grid, but are within 1,500 feet of the Distributed Parameter Watershed Model boundary. For these stations, the closest grid cell in the Distributed Parameter Watershed Model was selected for comparison.

Figure 4-20 shows a comparison of the cumulative daily precipitation between the Distributed Parameter Watershed Model and the Elephant Mountain Remote Automated Weather Station over the period of record available from the Remote Automated Weather Station. The cumulative precipitation records are generally in good agreement except for summer 2019, when more precipitation was observed at the Marathon, Texas reference station than was observed at the Elephant Mountain Remote Automated Weather Station. The Distributed Parameter Watershed Model may be overestimating recharge in the vicinity of the Elephant Mountain Remote Automated Weather Station for summer 2019.

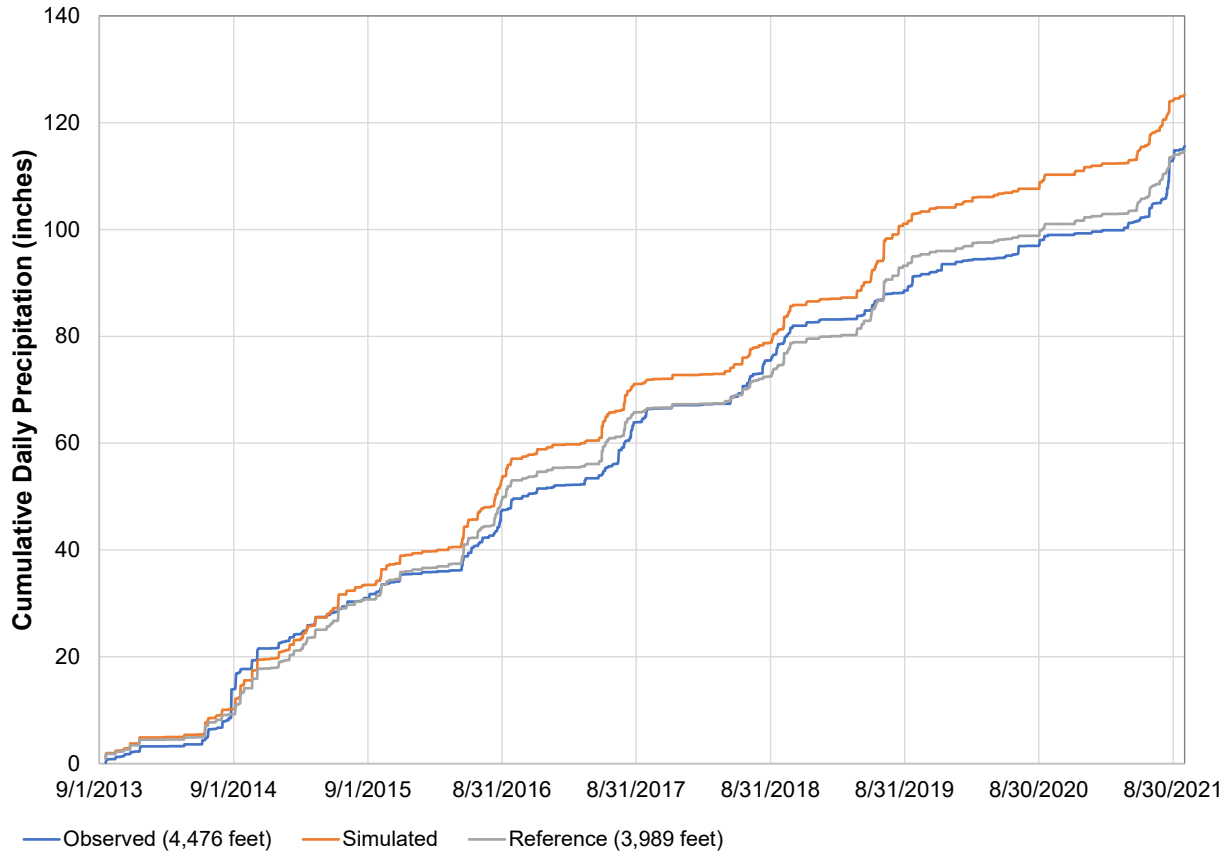

Figure 4-20. Comparison of observed cumulative daily precipitation at Elephant Mountain Remote Automated Weather Station and cumulative daily precipitation simulated by the Distributed Parameter Watershed Model.

Figure 4-21 shows a comparison between the cumulative daily precipitation observed at the Housetop Mountain station and the simulated precipitation in the Distributed Parameter Watershed Model. The data gap from September 23, 2010 through January 8, 2012 in the observed record was removed from the simulated record for the comparison. The result shows that the Distributed Parameter Watershed Model is generally in good agreement with the observed record except for summer 2018, when there was more precipitation observed at Housetop Mountain than was observed at Marathon, Texas and simulated by the Distributed Parameter Watershed Model. The Distributed Parameter Watershed Model may be underestimating recharge for summer 2018 in the vicinity of Housetop Mountain.

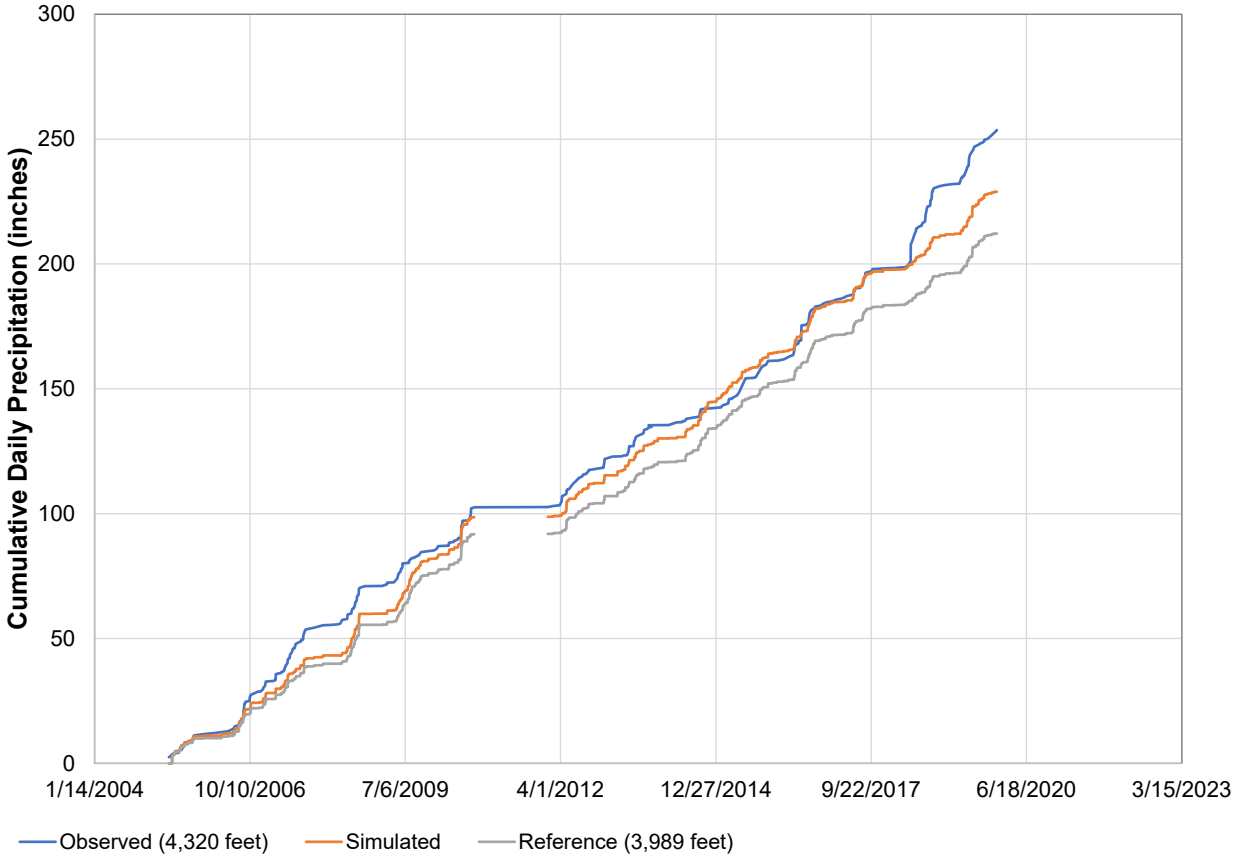

Figure 4-21. Comparison of observed cumulative daily precipitation at Housetop Mountain station and cumulative daily precipitation simulated by the Distributed Parameter Watershed Model.

Figure 4-22 shows a comparison between the cumulative monthly precipitation observed at the Alan Haley station and the simulated precipitation in the Distributed Parameter Watershed Model. The Alan Haley station is located in Marathon about 2 miles east of the Marathon National Oceanic and Atmospheric Administration station used as the reference station for the Distributed Parameter Watershed Model. The Alan Haley station had incomplete records for the months of August 2019, September 2019, and December 2019 but the totals for these three months at the Alan Haley station were more than the total observed at the Marathon National Oceanic and Atmospheric Administration station, so these months were not removed from the comparison. The comparison shows that the Distributed Parameter Watershed Model may be overpredicting the precipitation in Marathon Aquifer, but the Marathon National Oceanic and Atmospheric Administration station on the west side of Marathon that is input to the Distributed Parameter Watershed Model is likely more accurate.

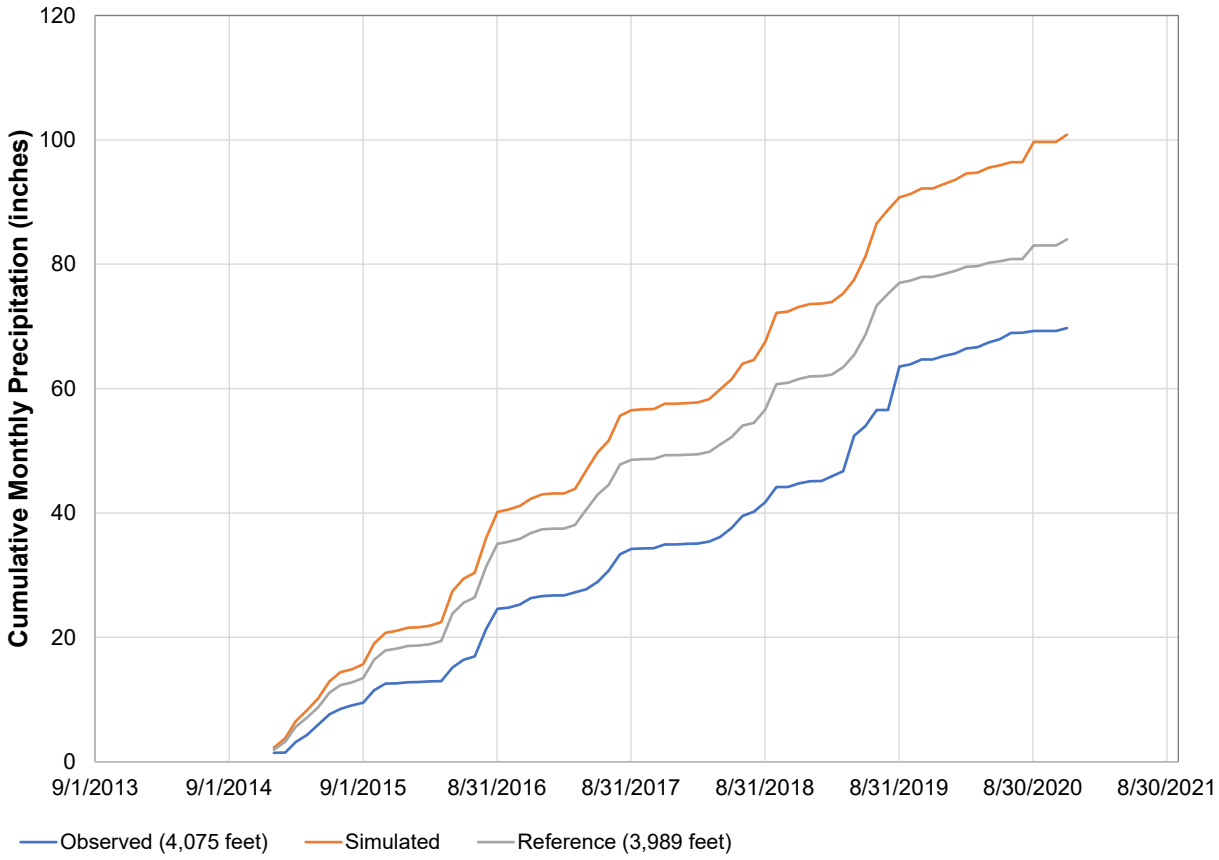

Figure 4-22. Comparison of observed cumulative daily precipitation at Alan Haley station and cumulative daily precipitation simulated by the Distributed Parameter Watershed Model.

4.3.1.3 Topography

Topography data used in the Distributed Parameter Watershed Model include the slope, azimuth, and elevation of the land surface for each model grid cell. The topography is part of the recharge model calculations of reference evapotranspiration (also known as potential evapotranspiration). For example, south-facing slopes will typically have higher evapotranspiration than north-facing slopes in the northern hemisphere due to increased solar radiation. The routing of surface runoff in the recharge models is also based on averaged grid cell elevations.

Topography data in the model were derived from the U.S. Geological Survey 30-meter digital elevation model (Figure 2-5) by averaging elevations, slopes, and azimuth onto the ⅛-mile square grid cells.

Each grid cell in the Distributed Parameter Watershed Model was assigned an active channel wash width to calculate the proportion of the grid cell that is a wash versus the proportion of the grid cell that is between washes (interwash). The wash width was set to zero for grid cells that had a flow accumulation of less than five upstream contributing grid cells and was set to a maximum of 10 meters for grid cells that had a flow accumulation of

200 or more upstream contributing grid cells. For flow accumulations between 5 and 200, the wash width was linearly interpolated.

4.3.1.4 Drainages

The drainages in the model domain are primarily ephemeral, with some limited reaches that receive intermittent or perennial groundwater discharge. The two primary drainages in the model domain are Maravillas Creek and San Francisco Creek. Major tributaries to San Francisco Creek include Pena Blanca Creek. Major tributaries to Maravillas Creek include Kincaid Creek (also known as Bear Creek), Woods Hollow (also known as Reynolds Creek or Dagger Flat Draw), Pena Colorado Creek, and Dugout Creek. Another named drainage is Maxon Creek, which is tributary to San Francisco Creek outside of model domain.

4.3.1.5 Soils

Soils data used by the Distributed Parameter Watershed Model include saturated hydraulic conductivity, soil depth to bedrock, saturated and residual water contents, and the van Genuchten curve parameters. These data were obtained directly or estimated based on soils data published by the U.S. Department of Agriculture Soil Survey Geographic database (SSURGO)(Natural Resources Conservation Service, 2020), which contains electronic data from field surveys conducted by the U.S. Department of Agriculture for the model domain. Saturated hydraulic conductivity values for soils used in the Distributed Parameter Watershed Model are provided in Figure 4-23.

SSURGO provides texture data (percent sand, silt, and clay), saturated hydraulic conductivity, dry and wet bulk density, saturated water content, and water contents at ⅓ bar and 15 bars for each soil horizon. SSURGO also reported the soil depth to bedrock where bedrock was within 2 meters of the ground surface. Using a geographic information system tool, a weighted average for soil texture, wet bulk density, and the saturated hydraulic conductivity was estimated within a SSURGO map unit based on the soil horizon thickness. The saturated water contents were estimated from the wet bulk density by converting to a dry bulk density using the method of Heuscher and others (2005) and then estimating the saturated water content based on a typical rock grain density of 2.65 grams per cubic centimeter. The residual water contents and van Genuchten curve parameters were estimated based on soil texture for each SSURGO map unit using the Rawls and Brakensiek pedotransfer method (Rawls and Brakensiek, 1985; Rawls and others, 1992; Carsel and Parrish, 1988; Lee, 2005).

Within the recharge model area, there were 47 map units in SSURGO. Grid cells were assigned a soil type based on the predominant Soil Survey Geographic map units present at each recharge model cell centroid.

SSURGO reports the depth and type of the first restrictive layer for depths up to 2 meters below the land surface. The restrictive layer type is typically bedrock but, in some locations, SSURGO reports the restrictive layer as petrocalcic (e.g., caliche or hardpan). Where the restrictive layer was reported as bedrock, the soil depth in the Distributed Parameter Watershed Model was set to the depth of the restrictive layer. For all other soils,

including soils underlain by petrocalcic restrictive layers, the soil depths were assumed to be equal to the maximum vegetation rooting depth of 10 meters.

In soils that have washes, the soil properties of the wash are specified separately from the remaining area of the cell, which is referred to as the interwash. Soils within washes were assumed to have the hydraulic properties of sand as provided by Carsel and Parrish (1988). The depth of soil for washes is set by the Distributed Parameter Watershed Model to be the same as the adjacent interwash soil.

The field capacity pressure point partitions the soil zone between the gravity and capillary reservoirs. The gravity reservoir is the water content between saturation and the field capacity water content. In the gravity reservoir, the water drains by gravity at rate less than or equal to the vertical saturated hydraulic conductivity of the soil under a unit gradient (Darcy's Law). There is no evapotranspiration from the gravity reservoir. The capillary reservoir is the water content between the field capacity and the wilting point water contents. There is no drainage of water from the capillary reservoir. Water in the capillary reservoir is only removed by evapotranspiration. The field capacity and wilting point pressure points are uniformly distributed for the model domain and are used to calculate the corresponding water contents based on the residual and saturated water contents and the van Genuchten curve numbers (α and n) specified for each soil. Typical field capacity of ⅓ bar and a typical wilting point of 15 bar were selected (Karkanis, 1983).

The depth of evaporation or "evaporation layer depth" [Ze] is the depth of the surface soil layer that is subject to drying by way of evaporation (Allen and others, 1998). The evaporation layer depth is set uniformly over the Distributed Parameter Watershed Model domain, and typically ranges from 10 millimeters (coarse soil) to 15 millimeters (fine soil) (Allen and others, 1998). The large value of 15 millimeters was selected, which reduces groundwater recharge.

The fraction (p) of total available soil water that can be depleted from the root zone before moisture stress (reduction in evapotranspiration) occurs ranges from 0 to 1, and is typically set to a value of 0.5. The Distributed Parameter Watershed Model has the option to keep the value of p constant or to vary the value of p with the rate of potential evapotranspiration as given in FAO-56 (Allen and others, 1998). An intermediate value of 0.5 was selected.

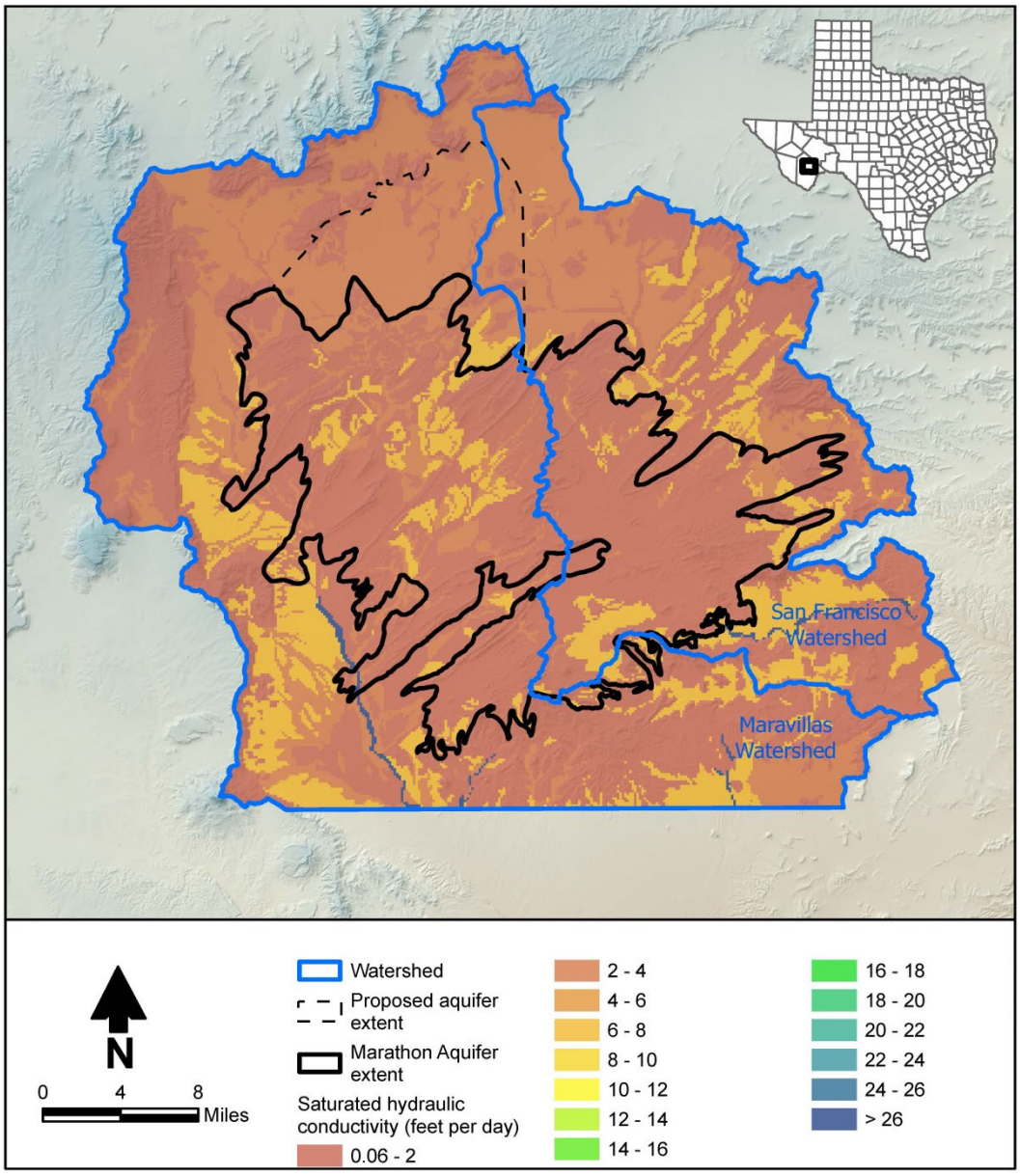

Figure 4-23. Soils saturated hydraulic conductivity values used in the Distributed Parameter Watershed Model.

4.3.1.6 Bedrock Vertical Hydraulic Conductivity

Bedrock underlying the soils of the Distributed Parameter Watershed Model domain may restrict net infiltration when the vertical saturated hydraulic conductivity of the underlying bedrock is less than the soil infiltration rate and soils are shallow. Bedrock data used in the Distributed Parameter Watershed model are the saturated hydraulic conductivities of the bedrock underlying the soils (Figure 4-24). The bedrock geology for each grid cell is based on the 1:250,000 scale Geologic Atlas of Texas sheets. The bedrock hydraulic conductivities were initially estimated based on the unit lithology (e.g., sandstone or shale) and the ranges

published by Domenico and Schwartz (1998). The Glen Rose Formation, Lenox Hills Formation, Skinner Ranch Formation and Hess Limestone were reduced by factor of 10 because these formations are typically not as permeable/productive as the Marathon Limestone (Section 4.1). The hydraulic conductivity values for the Caballos Novaculite, Maravillas Chert, and Maravillas Formation were set to 0.01 foot per day based on pervasive fracturing in these formations. A portion of the recharge simulated to occur to these formations may emanate as perched springs and seeps at the base (Woods Hollow Shale) and may not ultimately enter regional water.

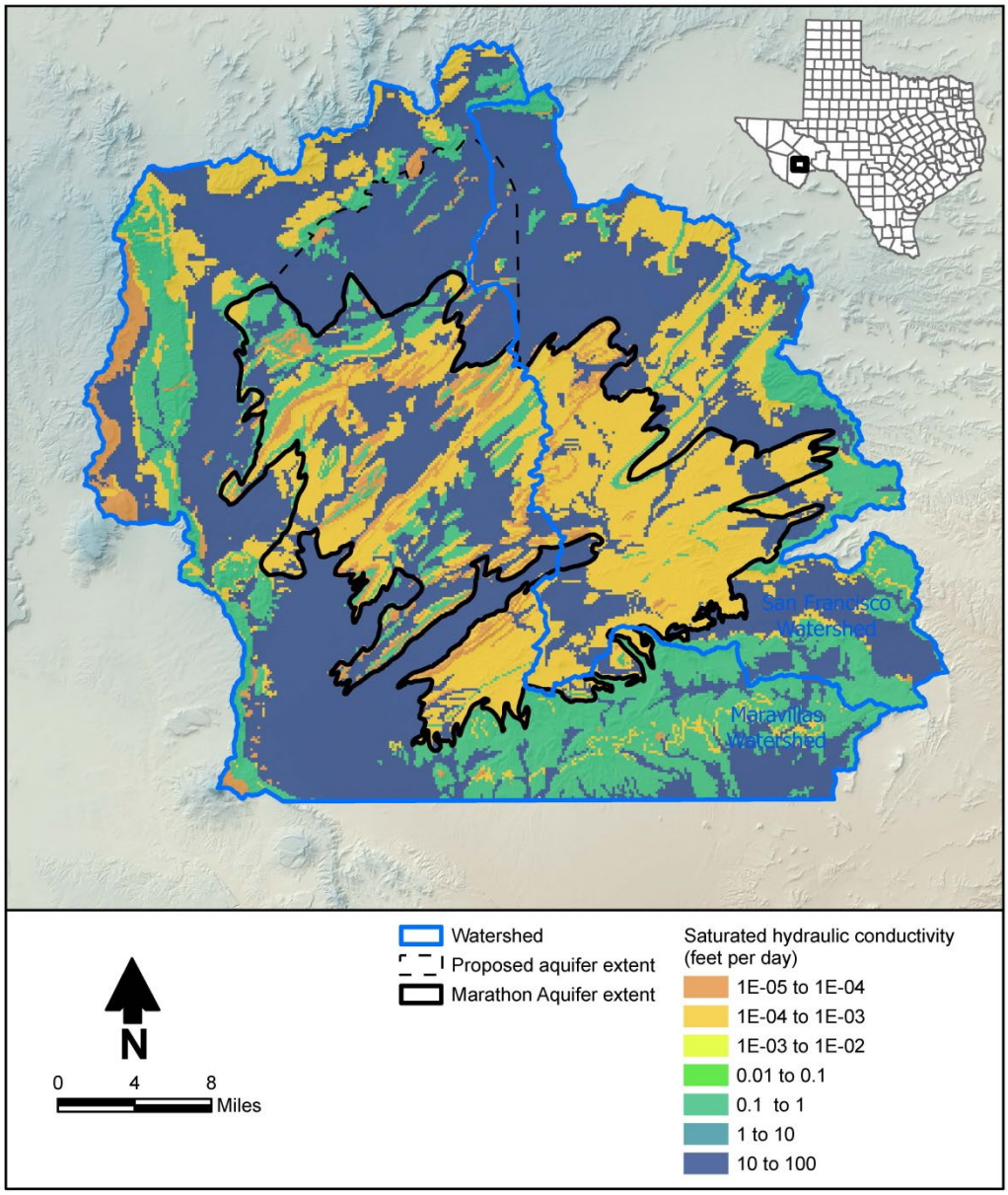

Figure 4-24. Bedrock hydraulic conductivity values used in the Distributed Parameter Watershed Model.

4.3.1.7 Vegetation

Vegetation data used in the Distributed Parameter Watershed Model include the rooting depth and plant height for each class of vegetation and the density of vegetation in each model grid cell. Vegetation classes were obtained from the National Land Cover Database (Homer and others, 2012) (Figure 2-12). The dominant vegetation types are shrub/scrub (89 percent of model area) and herbaceous (10 percent of the model area) (grasses, forbs, and cacti). Table B-2 (Appendix B) summarizes the rooting depths and maximum plant height for vegetation class in the Marathon Aquifer region. The rooting depths for the dominant vegetation types are the upper end estimates based on an analysis published by Schenk and Jackson 2002 for the Western United States (including West Texas) to estimate rooting depth by vegetation class from mean annual precipitation and potential evapotranspiration.

Plant heights were estimated from similar vegetation classes described in Allen and others (1998). Plant heights range from 0.10 meter (0.33 foot) for developed areas to 10 meters (33 feet) for evergreen forests. The vegetation density was obtained from monthly Moderate Resolution Imaging Spectroradiometer satellite observations of the leaf area index for the representative wet water year of 2015 (U.S. Geological Survey, 2016). The monthly leaf area index data were provided as input to the Distributed Parameter Watershed Model.

The albedo of the land surface ranges from 0 to 1, and is the fraction of solar radiation that is reflected from the land surface. Albedo of the land surface was set to a uniform value of 0.23 in the Distributed Parameter Watershed Model as is used in FAO-56 (Allen and others, 1998).

Vegetation density and phenology were obtained from satellite measurements of leaf area index. Leaf area index is the ratio of one-sided leaf area over the total land area. Values of leaf area index were obtained from datasets published by the National Aeronautics and Space Administration from the Moderate Resolution Imaging Spectroradiometer satellites (U.S. Geological Survey, 2016) on a monthly basis for the wet water year of 2015 (October 2014 through September 2015). The pattern of leaf area index measured by the Moderate Resolution Imaging Spectroradiometer satellites was also used to determine the phenology for the vegetation associations (initiation of leaves, peak growing season, decline in growth, and dormant season) on a monthly basis. The leaf area index data were provided as input to the Distributed Parameter Watershed Model.

4.3.2 Simulation Results

The final estimated groundwater recharge is presented for mean annual conditions for the period 1981 through 2021, the lowest water year of recharge (water year 2011), and the highest water year of recharge (water year 2004). Figure 4-25 illustrates mean annual precipitation over the watershed model study area. Figure 4-26 presents the mean simulated recharge. As indicated in Figure 4-24, higher recharge generally occurs where soils are thin and soil hydraulic conductivity and bedrock hydraulic conductivity are highest, as would be expected. In addition, higher rates of recharge occur along drainages

because (1) the drainages occur in alluvial sediments (bedrock at those locations), which has high permeability, and (2) storm flows are collected in the drainages and provide source water to be recharged.

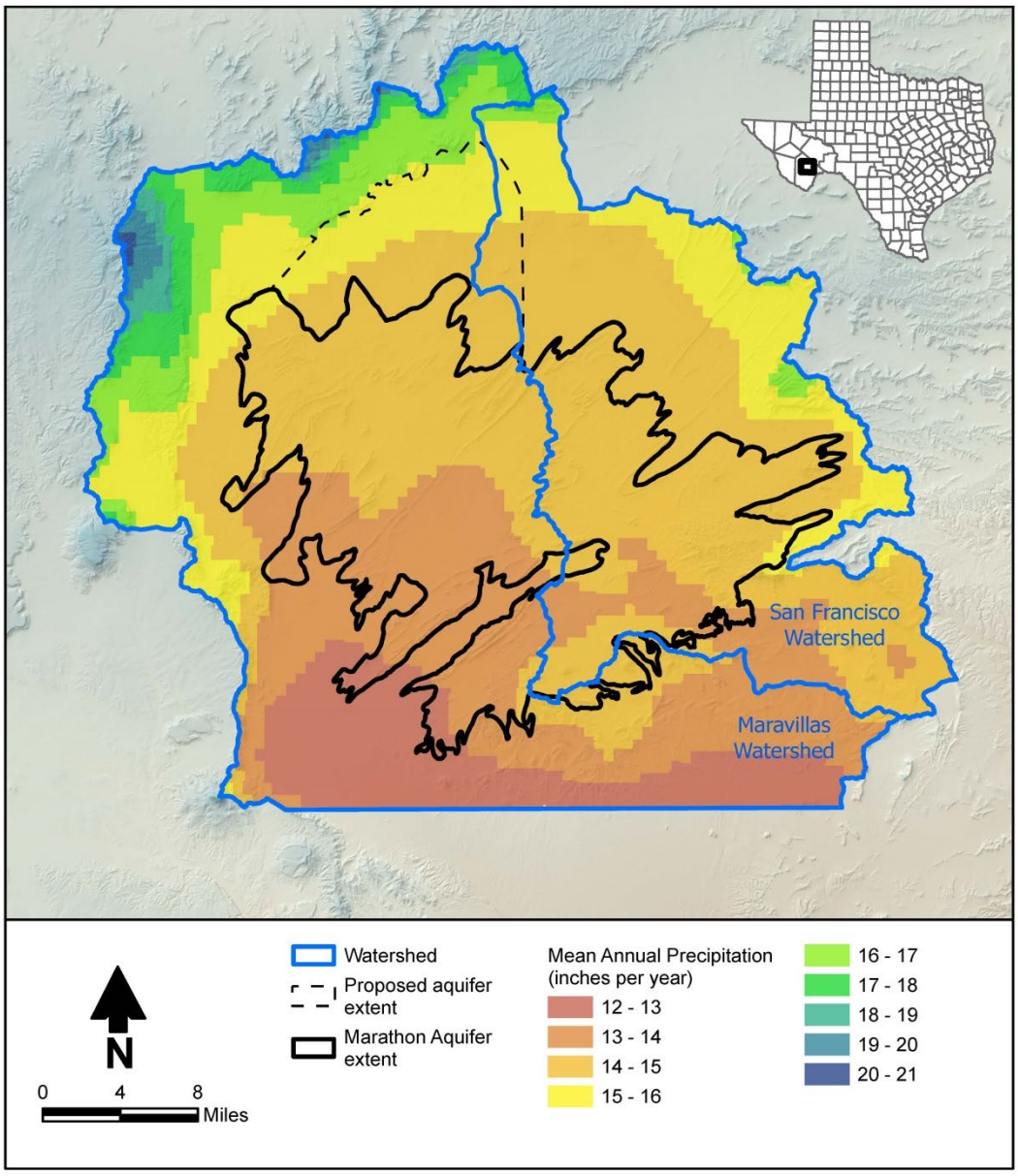

Figure 4-25. Mean annual precipitation in the Marathon Aquifer study area.

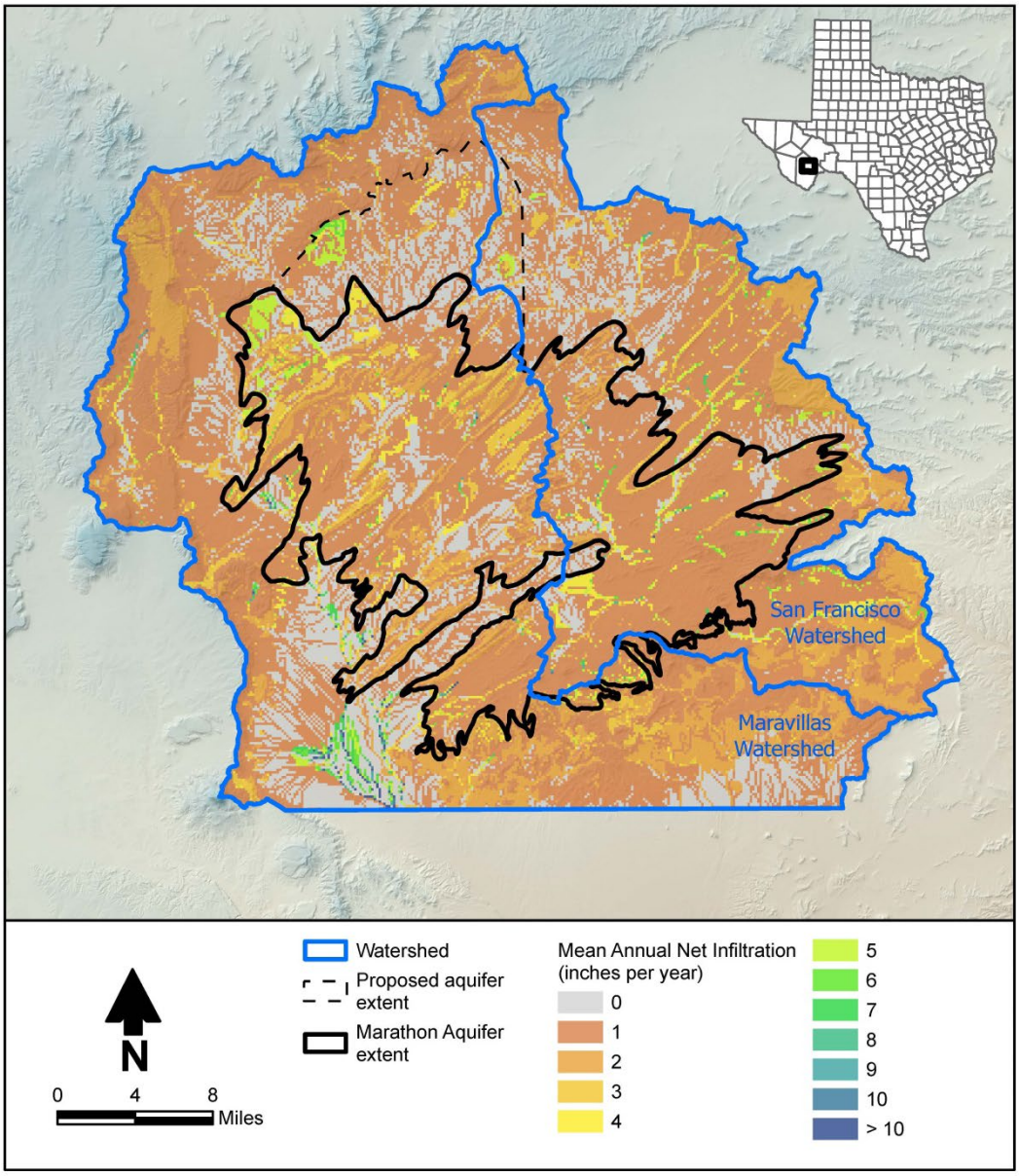

Figure 4-26. Mean annual net infiltration simulated by the Distributed Parameter Watershed Model.

Figure 4-27 presents the simulated recharge for the driest year in the simulation period, 2011. Figure 4-28 presents the simulations results for the 2004, the year of highest recharge, which was the year of second highest precipitation. The fact that the year of second highest precipitation leads to the most recharge illustrates the importance of precipitation timing in the recharge calculation.

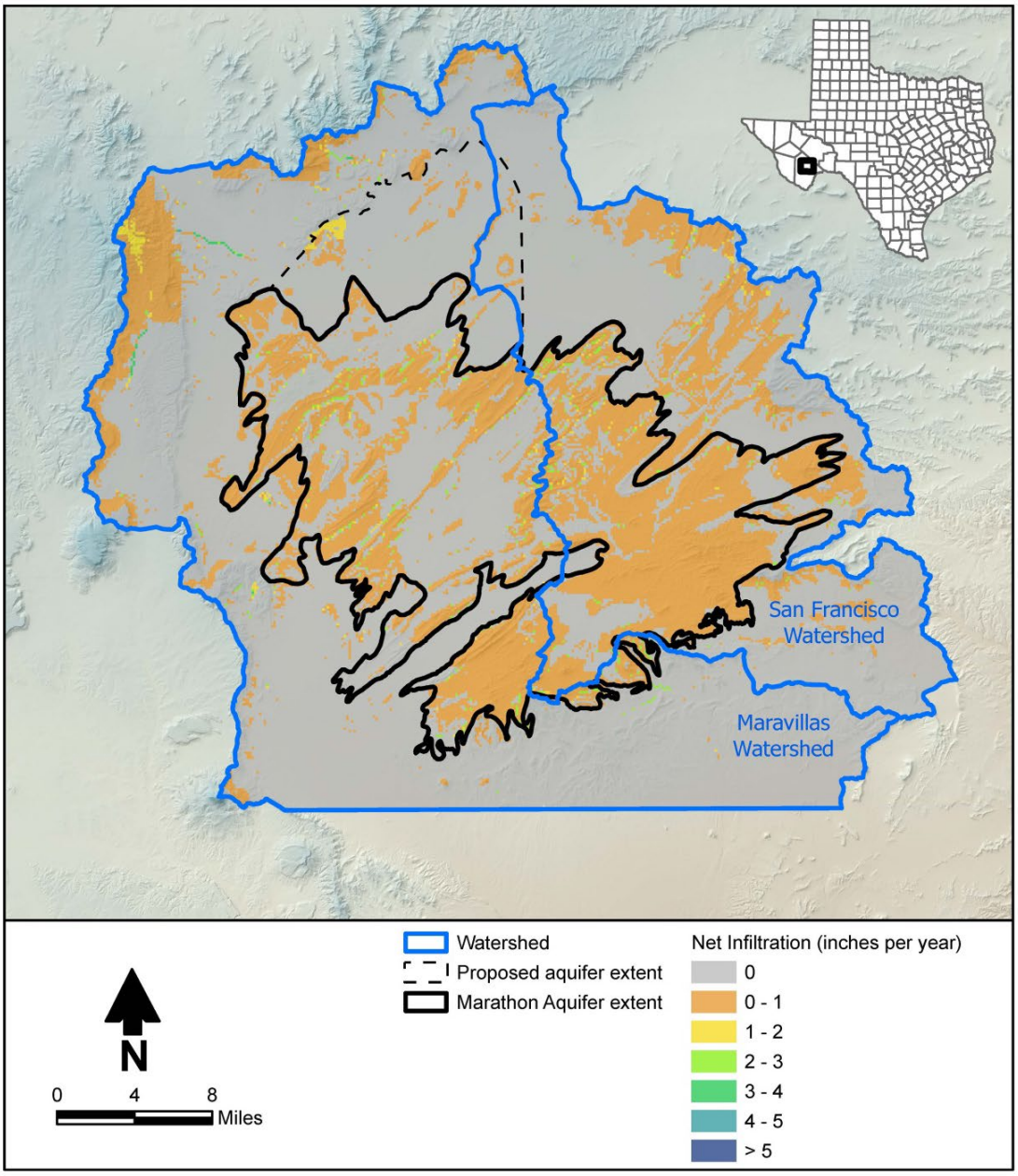

Figure 4-27. Simulated net infiltration for dry year 2011.

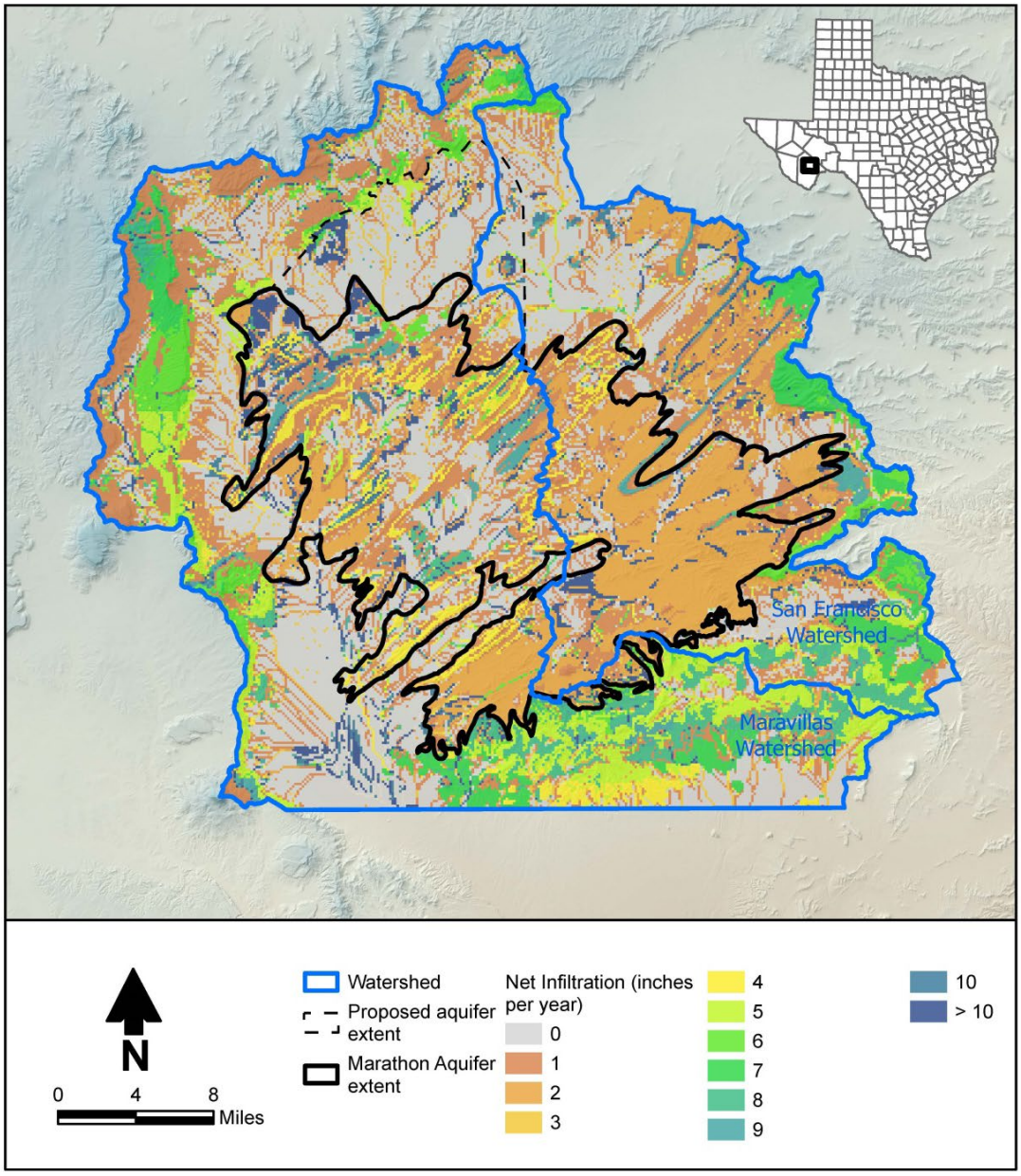

Figure 4-28. Simulated net infiltration for wet year 2004.

The mean annual groundwater recharge over the entire Distributed Parameter Watershed Model domain for 1981 through 2021 is estimated at 48,864 acre-feet per year (5.2 percent of precipitation). For the portion of the Distributed Parameter Watershed Model domain overlying the Marathon Aquifer (including the proposed extension), recharge is estimated at 21,284 acre-feet per year (4.7percent of precipitation and run-on). The recharge for the entire model domain was 3,850 acre-feet (2.4 percent of precipitation) in water year 2011 and 184,183 acre-feet (10.6 percent of precipitation) in water year 2004. Table 4-4 gives the simulated water balance for the model domain for each water year. Table 4-5 gives the simulated water balance over the Marathon Aquifer for each water year.

Table 4-4. Annual simulated water balance over the Distributed Parameter Watershed Model domain.

Water Year	Annual Water Balance Component (acre-feet)					
	Precipitation	Actual Evapo-transpiration	Runoff Out of Model Domain	Sublimation	Net Infiltration	Change in Soil Water Storage
1981	1,278,745	1,200,950	12,659	22,662	29,804	12,670
1982	1,050,244	928,286	48,612	0	77,784	-4,437
1983	807,647	739,322	8,876	784	25,361	33,303
1984	1,277,958	1,138,698	7,236	5	75,957	56,062
1985	1,399,092	1,318,228	2,500	15,725	52,286	10,353
1986	1,271,455	1,182,476	1,735	2,811	87,183	-2,749
1987	2,024,471	1,853,637	11,380	962	183,217	-24,724
1988	831,549	817,754	3,369	3,424	47,412	-40,409
1989	713,387	699,788	1,363	0	27,372	-15,137
1990	1,167,619	925,289	3,967	8	107,473	130,881
1991	1,383,877	1,263,782	19,491	0	158,667	-58,063
1992	1,029,239	1,067,456	333	5,893	30,905	-75,350
1993	480,568	491,143	102	1,651	6,828	-19,156
1994	373,455	370,436	53	455	3,898	-1,388
1995	501,294	475,696	522	14	20,281	4,781
1996	955,451	825,692	14,396	0	47,275	68,088
1997	547,574	535,107	22,838	0	18,423	-28,795
1998	203,146	238,053	4,545	0	4,261	-43,714
1999	699,213	591,794	76,554	0	22,456	8,409
2000	455,447	443,347	33	0	18,853	-6,786
2001	763,755	654,632	34,210	9,456	67,466	-2,007
2002	486,435	473,004	649	6,744	9,280	-3,242
2003	1,444,127	1,261,514	57,015	4,478	80,015	41,103
2004	1,742,351	1,411,078	25,701	0	184,183	121,389
2005	862,613	893,371	68,496	872	47,127	-147,252
2006	744,273	722,479	1,686	0	17,396	2,713
2007	1,219,284	1,070,979	80,286	3,846	48,679	15,493
2008	1,106,075	928,662	25,723	9,144	64,749	77,798
2009	1,105,643	1,136,845	19,056	61	36,954	-87,273
2010	1,275,824	1,092,255	62,018	10,198	95,867	15,486
2011	161,820	189,100	47	0	3,850	-31,176
2012	813,032	703,908	1,323	4,175	41,703	61,923
2013	920,526	900,914	381	14,648	45,664	-41,081
2014	801,881	672,406	396	14,136	36,799	78,144
2015	1,124,591	1,153,050	16,930	14,683	39,087	-99,158

Table 4-4. Annual simulated water balance over the Distributed Parameter Watershed Model domain.

Water Year	Annual Water Balance Component (acre-feet)					
	Precipitation	Actual Evapo-transpiration	Runoff Out of Model Domain	Sublimation	Net Infiltration	Change in Soil Water Storage
2016	1,399,574	1,304,737	9,053	163	45,356	40,266
2017	878,234	806,316	72,835	0	19,083	-19,999
2018	530,556	527,281	996	16,126	9,178	-23,026
2019	1,319,945	1,125,753	138,085	6	37,541	18,559
2020	395,375	410,866	89	0	5,125	-20,704
2021	887,962	787,325	13,170	38,017	22,644	26,806
Mean	937,447	861,790	21,188	4,906	48,864	698

Table 4-5. Simulated water balance for the Marathon Aquifer area.

Water Year	Simulated Water Balance for the Marathon Aquifer (acre-feet)							% Recharge (Net Infiltration/ (Precipitation + Run-On)
	Precipitation	Run-On	Actual Evapo-transpiration	Net Infiltration	Runoff	Sublimation	Change in Soil-Water Storage	
1981	511,720	21,704	480,145	15,373	25,395	9,211	3,344	2.9%
1982	419,258	98,400	367,932	29,494	121,514	0	–1,172	5.7%
1983	321,092	16,581	293,254	13,645	18,043	1	12,752	4.0%
1984	511,401	11,327	454,182	36,931	10,847	0	20,772	7.1%
1985	560,418	3,047	526,903	25,548	2,822	5,947	2,238	4.5%
1986	508,770	5,001	469,415	36,405	7,256	1,271	–623	7.1%
1987	813,475	21,629	739,686	70,916	30,848	352	–6,797	8.5%
1988	330,764	6,662	324,891	21,854	6,231	1,241	–16,795	6.5%
1989	282,950	2,753	273,850	15,541	2,495	0	–6,184	5.4%
1990	466,754	11,245	370,465	38,677	17,214	0	51,562	8.1%
1991	554,261	41,160	502,497	59,873	53,258	0	–20,266	10.1%
1992	410,758	3	420,969	17,574	4	2,438	–30,225	4.3%
1993	188,741	5	190,952	4,231	1	399	–6,837	2.2%
1994	145,398	19	143,772	2,468	1	12	–835	1.7%
1995	197,128	1,091	186,393	9,399	1,035	0	1,389	4.7%
1996	380,900	25,451	331,300	21,152	29,618	0	24,308	5.2%
1997	215,855	49,642	213,778	8,808	52,888	0	–9,910	3.3%
1998	76,483	14,963	91,328	2,035	14,574	0	–16,484	2.2%
1999	277,215	154,497	236,114	11,249	181,921	0	2,712	2.6%
2000	178,576	1	172,261	9,079	12	0	–2,775	5.1%
2001	303,331	67,850	261,433	22,918	83,230	3,985	–288	6.2%
2002	191,115	1,504	184,999	5,037	1,308	2,572	–1,297	2.6%
2003	578,641	104,069	502,274	38,761	125,433	1,708	14,723	5.7%

Table 4-5. Simulated water balance for the Marathon Aquifer area.

Water Year	Simulated Water Balance for the Marathon Aquifer (acre-feet)							% Recharge (Net Infiltration/ (Precipitation + Run-On)
	Precipitation	Run-On	Actual Evapo-transpiration	Net Infiltration	Runoff	Sublimation	Change in Soil-Water Storage	
2004	699,316	49,288	570,204	67,132	63,199	0	48,000	9.0%
2005	343,334	131,261	357,896	23,309	149,493	346	–56,223	4.9%
2006	295,448	3,139	286,649	9,214	2,743	0	–19	3.1%
2007	487,659	152,224	427,388	24,903	181,118	1,395	5,380	3.9%
2008	441,849	49,220	371,603	27,123	58,521	4,267	29,603	5.5%
2009	441,675	34,004	452,405	19,187	36,598	0	–32,456	4.0%
2010	510,538	116,694	438,635	35,407	142,191	4,050	7,116	5.6%
2011	59,761	0	71,162	2,297	0	0	–13,697	3.8%
2012	323,271	2,985	277,801	17,143	4,548	1,746	24,988	5.3%
2013	366,768	167	354,534	23,564	331	5,885	–17,389	6.4%
2014	318,759	12	267,032	17,073	50	5,704	28,909	5.4%
2015	449,342	30,215	454,698	20,669	34,515	5,729	–36,001	4.3%
2016	560,613	12,886	524,422	22,295	12,700	0	14,099	3.9%
2017	349,655	140,760	321,930	9,143	166,073	0	–6,462	1.9%
2018	208,968	2,102	207,034	4,799	1,744	6,328	–8,837	2.3%
2019	528,391	267,694	448,321	18,515	323,586	0	6,208	2.3%
2020	154,268	170	158,470	2,989	110	0	–7,131	1.9%
2021	353,591	24,220	313,333	10,898	28,134	15,304	10,183	2.9%
Mean	373,615	40,869	342,495	21,284	48,576	1,949	234	4.7%

The groundwater recharge simulated by the Distributed Parameter Watershed Model is termed net infiltration, which is the quantity of soil-water that passes through the root zone and enters underlying bedrock. There may be a time delay of months to years for the net infiltration to reach the groundwater aquifers, and the net infiltration may be discharged at springs or seeps or as evapotranspiration along perched zones prior to reaching the deeper (regional) groundwater aquifer.

4.3.3 Sensitivity Analysis

Sensitivity analyses were performed on the Distributed Parameter Watershed Model simulation results for (1) utilization of the ROSETTA pedotransfer method, and (2) an increase in the bedrock vertical saturated hydraulic conductivity in areas with high concentrations of lineaments.

ROSETTA is a popular pedotransfer method that uses artificial neural network analysis coupled with bootstrap re-sampling method to estimate soil hydraulic parameters (Zhang and Schaap, 2017; Schaap and others, 2001). The most recent version of ROSETTA is version 3 (ROSETTA3), which is published in the Python programming language (Zhang, 2017).

ROSETTA3 was run on the weighted depth averaged soil texture (percent sand, percent silt, and percent clay), dry bulk density, and water contents at ⅓ bar and 15 bar reported in the SSURGO database. The estimated water contents and saturated hydraulic conductivity were not adjusted for rock fragments. For this simulation, the mean annual estimate of recharge to groundwater for 1981 through 2021 is estimated at 7.7 percent of precipitation for the entire recharge model domain and at 7.7 percent of precipitation and run-on for the Distributed Parameter Watershed Model overlying the Marathon Aquifer (Figure 4-29).

Areas where there is a high density of fractures may result in increased groundwater recharge. A second sensitivity analysis was performed using the mapped lineaments to identify Distributed Parameter Watershed Model grid cells with a high degree of fracturing and where the bedrock saturated hydraulic conductivity of the bedrock in the Distributed Parameter Watershed Model grid cell was relatively low (e.g., Tesnus Formation, Caballos Novaculite, Maravillas Chert, and the Woods Hollow Shale). The bedrock saturated hydraulic conductivity in these grid cells was increased by a factor of 100. The total area of the grid cells with increased hydraulic conductivity is 3,280 acres.

The recharge for the Distributed Parameter Watershed Model domain increased slightly from 5.2 percent to 5.3 percent of precipitation and for the Marathon Aquifer from 5.1 percent to 5.2 percent of precipitation and run-on. However, locally where the high fracturing occurs in the Distributed Parameter Watershed Model, the recharge increased from an average of 191 acre-feet per year to 659 acre-feet per year (Figure 4-30). The areas of increased recharge due to fracturing generally correspond with the presence of known springs.

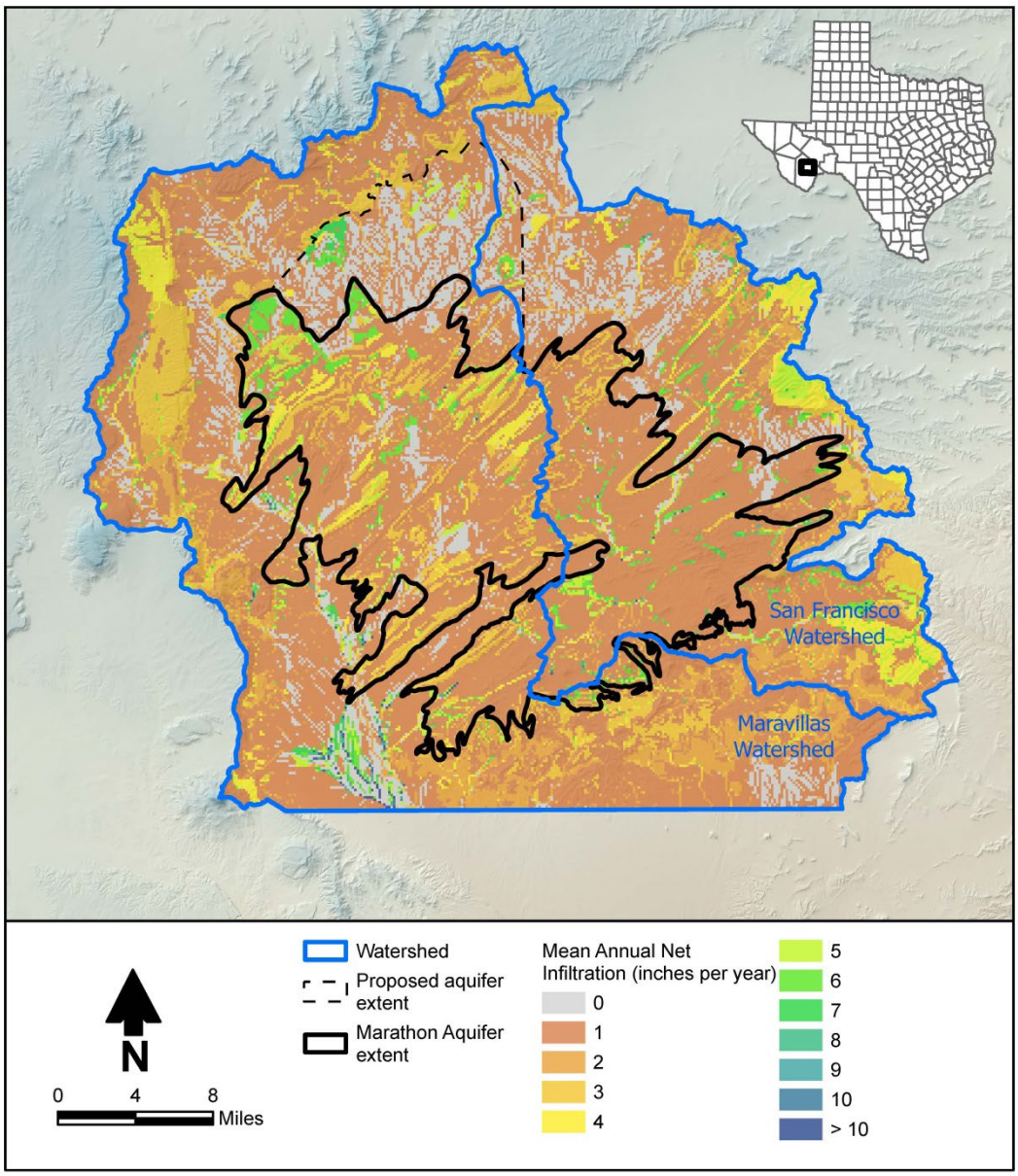

Figure 4-29. Mean annual net infiltration simulated using ROSETTA3 to estimate soil hydraulic parameters.

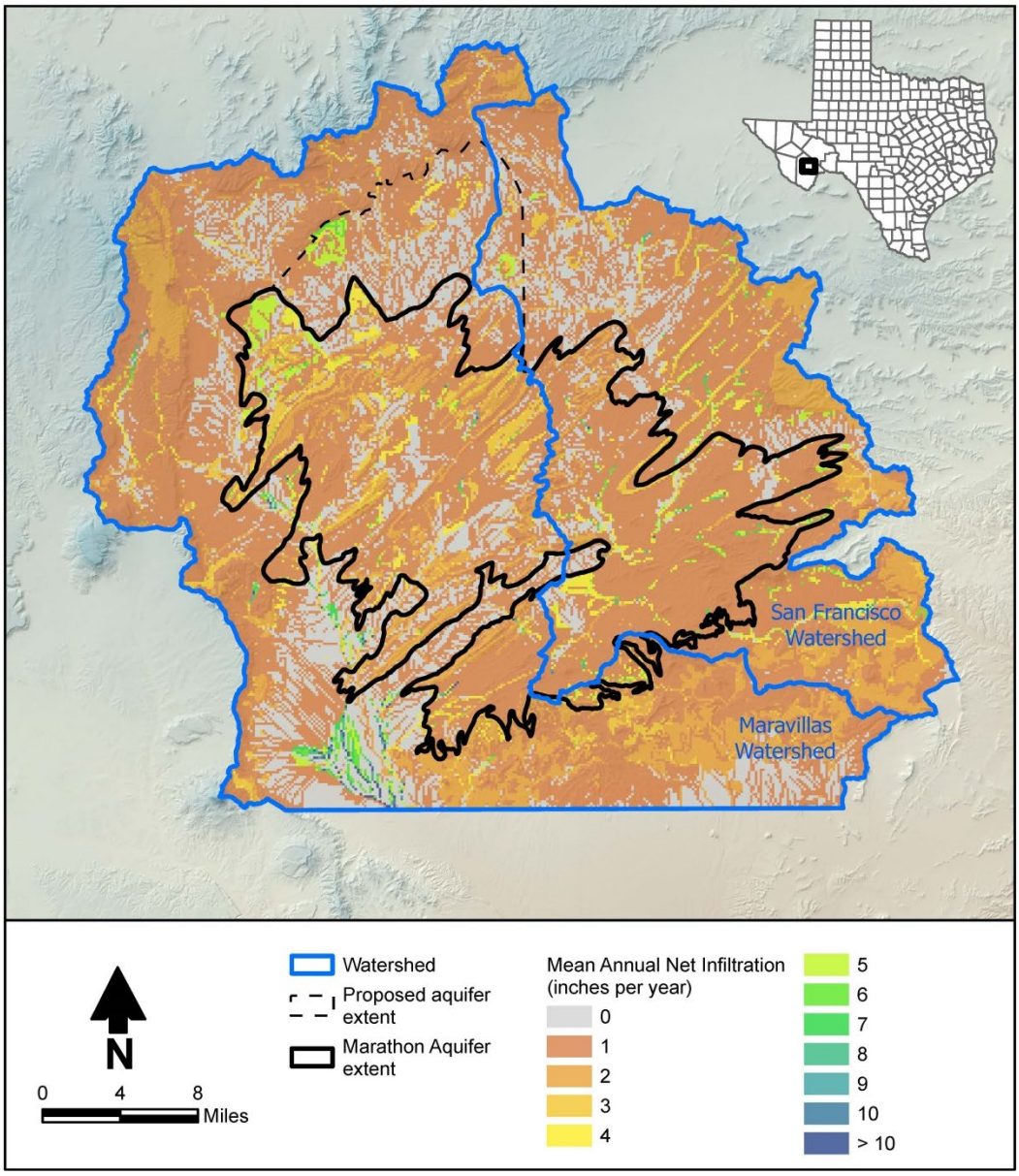

Figure 4-30. Mean annual net infiltration simulated with hydraulic conductivity of the bedrock increased to acocunt for mapped lineaments.

4.4 Rivers, Streams, Springs, Reservoirs, and Other Surface Hydraulic Features

There are no perennial rivers or reservoirs within the Marathon Aquifer extent. The two major drainage systems that cross the aquifer are Maravillas Creek and San Francisco Creek (Figure 4-31). These drainages and their tributaries are ephemeral, with the exception of limited reaches fed by springs or diffuse groundwater discharge. Gauged flow data are not available for either Maravillas Creek or San Francisco Creek.

The primary surface water features in the study in addition to the drainages identified above are springs. Spring locations, reported flows, and other information was compiled from King (1937), DeCook (1961), Brune (1975), Brune (1981), scanned TWDB files from the TWDB groundwater database, and the U.S. Geological Survey National Hydrography Dataset. Reported spring locations were reviewed, and where needed adjusted, based on review of Google Earth imagery in conjunction with U.S. Geological Survey 7.5-minute topographic maps (Figure4-31). DeCook (1961) estimated that the combined flow of 11 springs in the Marathon area in 1957 was about 420 gallons per minute (660 acre-feet per year), with about 70 percent of this total from Pena Colorada Spring.

Brune (1981) describes the springs in the Marathon area as rising mainly from fractured and vugular limestone and alluvial sand and gravel. A summary of Marathon Aquifer springs taken primarily from Brune (1981) is provided in Table 4-6. Many of these springs are associated with the Maravillas Formation chert and limestone, and a number of springs occur where there is a contact of the Maravillas Formation or other saturated geologic unit with the Caballos Novaculite, which forces water to the surface (Brune, 1981; DeCook, 1961). Many of the discharge estimates provided in DeCook (1961) and Brune (1981) are from 1957, which is at the end of a significant period of drought.

The largest spring in the study area is Pena Colorada Spring, also called Rainbow Cliff Springs. As noted in Brune (1981), the name of this spring is often misspelled as Colorado (as is done in the TWDB groundwater database). This spring emanates from gravel deposits where Pena Colorada Creek crosses the Caballos Novaculite. There is now a small lake at this location, formed by a dam in Fort Pena Colorada Park, about 4 miles south of the town of Marathon (Figure 4-31). Reported flow from this spring ranges from 151 to 444 gallons per minute (Table 4-6), and DeCook (1961) estimated an average flow of 300 gallons per minute. Review of aerial photography in Google Earth indicated perennial or shallow groundwater conditions in Pena Colorada Creek about 1 mile downstream of the spring. Pena Colorada Spring maintained a strong flow even at the end of the mid-1950s drought, and is a significant discharge point for regional groundwater.

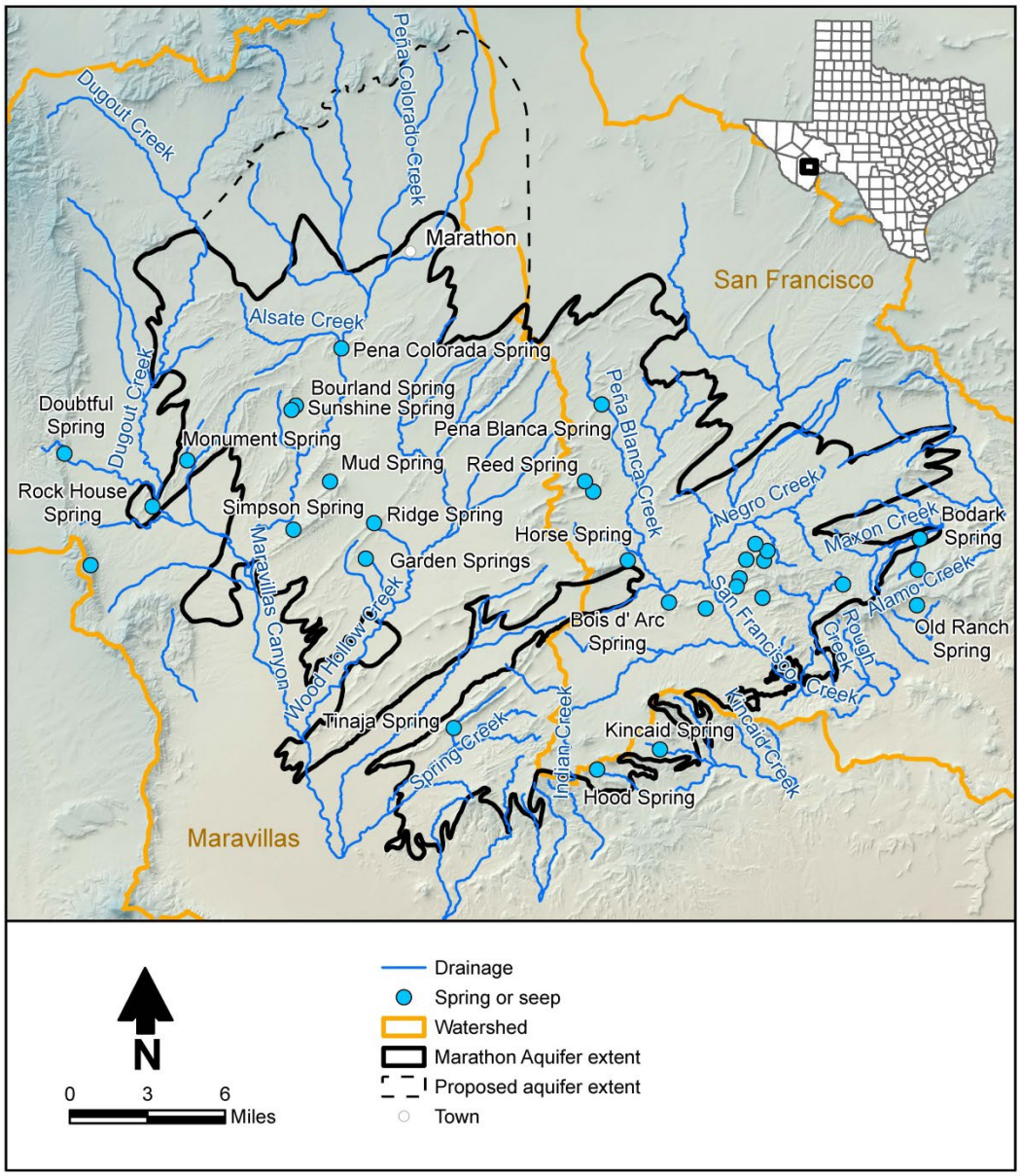

Figure 4-31. Drainages and springs in the Marathon Aquifer area.

Table 4-6. Springs in the Marathon Aquifer area.

Name	Alternative Name	Reported Flow		Geologic Setting	Comments
		Year	Flow (gpm)		
Pena Colorada Springs	Rainbow Cliff Springs	1957	151–444	Pena Colorada Creek alluvium crosses Caballos Novaculite	See report narrative. Largest Marathon Aquifer spring.
		1976	333		
Pena Blanca Springs	White Cliff Springs	1957	21	Water emanates from fractured Maravillas Formation chert and limestone where they contact Caballos Novaculite	Two dams have been built to store the spring water.
		1976	21		
		1977	15		
Reed Springs		1957	5	Discharges from the Tesnus Formation sandstone, which dips to the northeast on top of Caballos Novaculite	
		1977	3		
Garden Springs		1957	3		
Ridge Springs		1937	240–320	Flow is from faults in the Maravillas Formation limestone in the Garden Springs Overthrust area	The springs occur in a pass through a ridge of Caballos Novaculite; hence the name Ridge Springs. Flow ceased during the drought of the 1950s. Second largest spring flow reported for Marathon Aquifer. Perched water table (see report narrative).
		1976	95		
Garden Springs		1957	2		Water collects in a tank and marshy areas.
		1976	27		
Rock House Spring		1957	25		Western side of the study area
Monument Springs	Collins Springs	1957 and 1976	21	Flow is from Maravillas Formation limestone which dips to the southeast, water is forced to the surface to flow over Caballos Novaculite	Water tastes fresh but has a slight hydrogen sulfide odor, and some white precipitate present.

gpm = Gallons per minute

Table 4-6. Springs in the Marathon Aquifer area.

Name	Alternative Name	Reported Flow		Geologic Setting	Comments
		Year	Flow (gpm)		
Tinaja Springs	Waterhole Springs		3	Flow from Maravillas Formation Limestone; water is pooled by the Caballos Novaculite	Used for livestock watering and provides base flow to Spring Creek.
Sunshine Springs		1957	5		Located very close to Bourland Spring
Cottonwood Springs		1977	25	Occurs where Hell's Half Acre thrust fault brings the Caballos Novaculite to the surface	About 4.3 miles southeast of the Holland Ranch headquarters on Pena Blanca Creek
Horse Spring					Small spring; stopped flowing after a nearby seismograph blast around 1967
Jose Springs		1977	21	Springs emanate from gravel, where a thrust fault brings the Maravillas Chert to the surface	About 5.6 miles southeast of the Holland Ranch headquarters on San Francisco Creek
Hood Spring				Water forced to the surface by near vertical beds of quartzite of the Tesnus Formation	Seep; minimal discharge
Kincaid Spring	Dowlin's Spring?				Spring is gone and replaced by an old windmill
Bois d'Arc Springs	Bowdark Springs?				Flow is very small

gpm = Gallons per minute

The only other spring that has reported flow rates approaching those of Pena Colorada Spring is Ridge Springs. Ridge Springs is interesting because it occurs in a pass through the Caballos Novaculite ridge (Brune, 1981) that forms the north side of Dagger Flat. The spring pool elevation of 3,801 feet above mean sea level is about 100 feet above regional groundwater measured at a nearby well completed in hydrostratigraphic unit 5 (Section 4.2). Although reported flows at this spring are high (95 to 320 gallons per minute), it reportedly failed (stopped flowing) during the drought of the 1950s (Brune, 1981). The flow at Ridge Springs appears to be derived through recharge that occurs on the Caballos Novaculite outcrop, but does not seep down to regional groundwater. A significant northeast-trending lineament was mapped along this ridge, and there is an intersecting northwest-trending lineament in the vicinity of the spring (Figure 4-32). It appears that significant recharge occurs in the fractured novaculite, and water is channeled to the spring location along the geologic structure. In addition, the fact that the spring failed during the 1950s drought indicates a small residence time and limited storage within the fractured perched groundwater system.

These observations imply that even though the Caballos Novaculite is commonly fractured in outcrop allowing for significant recharge, recharge may not reach the Marathon Aquifer. In fact, many springs in the region occur where a given formation abuts the novaculite, indicating that the Caballos Novaculite is often a low-permeability unit, despite the predominance of fractures evident in outcrop.

Other springs that appear to occur above regional groundwater include Monument Springs, Tinaja Springs, and Hood Spring. There may be others as well, but the paucity of water level data from wells and the complex geologic setting makes the identification of perched versus regional water difficult in many areas.

DeCook (1961) also estimated than an undetermined but large amount of groundwater discharges from the Marathon Aquifer into the alluvium of Maravillas, Woods Hollow, Hackberry, and San Francisco creeks and other minor drainages, and then moves through the alluvium as underflow, never surfacing in a distinct spring. This underflow flows to the south toward the Rio Grande. DeCook (1961) also estimated that a large amount of groundwater discharged from the Marathon Aquifer through evapotranspiration, including by direct evaporation along Pena Colorada Creek, Maravillas Creek, and several other creeks where the water table is near land surface.

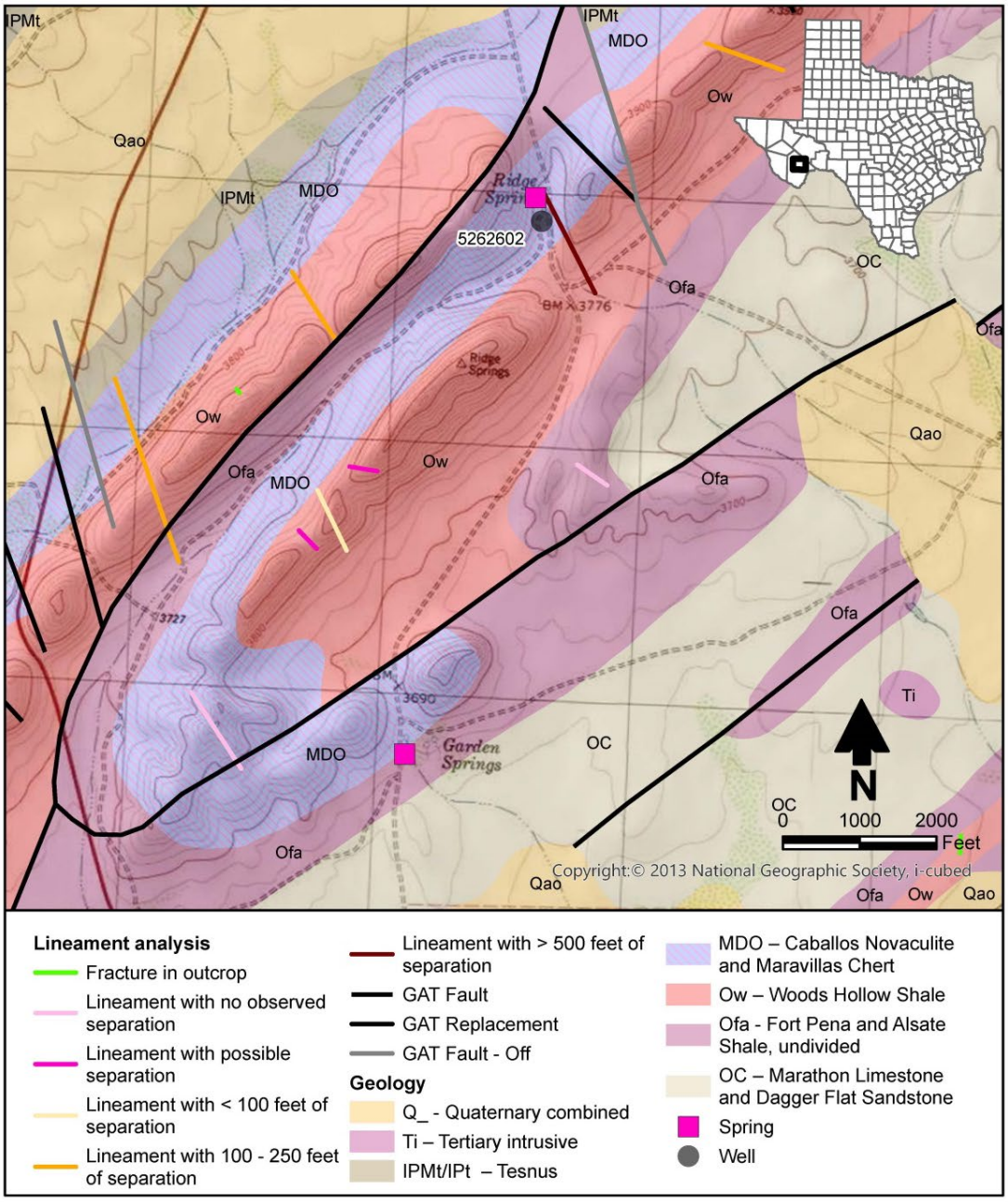

Figure 4-32. Lineament mapping and geologic units near Ridge Spring. GAT is Geologic Atlas of Texas.

4.5 Hydraulic Properties

Available aquifer testing data are very limited for the Marathon Aquifer. As an approximate surrogate for aquifer properties, reported well yields were compiled by geologic formation. Where there were a sufficient number of data points, statistics were calculated. The results of this analysis are provided in Table 4-7. The Marathon Limestone exhibits the greatest median well yield at 43 gallons per minute. The median well yields for other formations are relatively similar, ranging from 9 gallons per minute for alluvium (based on six values) to 20 gallons per minute for the Haymond Formation based on eight values.

Table 4-7. Well yield by formation.

Formation	Number of Wells with Reported Yield	Well Yield (gallons per minute)			
		Minimum	Maximum	Average	Median
Alluvium	6	2	20	10	9
Gaptank	3	5	18	—	—
Haymond	8	1	30	18	20
Dimple	2	2	15	—	—
Tesnus	23	1	100	21	10
Caballos Novaculite and Maravillas Chert	9	2	100	27	16
Woods Hollow Shale	1	25	25	—	—
Fort Pena Formation	1	5	5	—	—
Marathon Limestone	36	15	269	78	43
Dagger Flat Sandstone	0	—	—	—	—

— = Not calculated

4.5.1 Marathon Limestone Aquifer Tests

All of the aquifer test information available for the Marathon Aquifer is for the Marathon Limestone in or near the town of Marathon. The aquifer test data obtained from the TWDB groundwater database and the Texas Department of Licensing and Regulation submitted driller report database are summarized in Table 4-8. The locations of the tested wells are provided in Figure 4-33. In 2009, LBG-Guyton conducted aquifer tests on the Marathon water supply wells 1 and 2, the Gage Gardens supply well, and the Cavness well. In 2000, a single-well test was conducted for the Z Bar Farms well. In January 1957, multiple-well aquifer tests were conducted for the Texas Department of Transportation well, the Dow Chemical Company well 1, and the Southern Pacific Railroad east well. Because water levels in the Marathon Aquifer have not changed significantly through time (Section 4.2.4), the 1957 data are relevant to current conditions.

Table 4-8. Marathon Limestone aquifer properties from pumping tests.

State Well No.	Well Type	Owner	Well Depth (feet)	Date	Depth to Water (feet)	Open Interval (feet)	Pumping Rate (gpm)	Pumping Duration (hours)	Drawdown (feet)	Transmissivity (ft^2/d)	Hydraulic Conductivity (ft/d)	Storage Coefficient (—)
Marathon Public Supply Well 1 Test												
5255104	Pumping (Well 1)	Marathon Water Supply Well #1	468	5/29/2009	166.9	270–282 455–468	260	2	4.2	26,217	87	—
5255105	Observation (Well 2)	Marathon Water Supply Well #2	346	5/27/2009	165.2	340–346	—	—	—	16,684	92	0.00179
Marathon Public Supply Well 2 Test												
5255105	Pumping - single well test	Marathon Water Supply Well #2	346	5/27/2009	165.2	34–346	89	22.6	4.3	12,564	69	—
Gage Gardens Test												
5255411	Pumping well	JP Bryan-Gage Gardens	425	4/27/2009	108.1	—	191	24.2	61.9	2,497	8	—
5255412	Observation well	Buddy and Kristen Cavness	440	2/29/2009	125.9	220–440	—	—	—	9,234	29	0.00295
Cavness Test												
5255412	Pumping - single well test	Buddy and Kristen Cavness	440	5/12/2009	128.5	220–440	135	22.5	2.06	9,495	30	—
Z Bar Farms Test												
5254604	Pumping - single well test	Z Bar Farms, Ike Roberts	110	11/6/2000	28	40–100	100	2	10	2,861	35	—
TX DOT Test												
5255401	Pumping well	TxDOT J. A. McGongil	168	1/19/1957	118.51	8–168	210	41.5	3.6	3,369	68	—
5255422	Observation well	L. S. Dickson	195	1/19/1957	125.46	—	—	—	—	4,519	65	0.0142

gpm = Gallons per minute
ft^2/d = Square feet per day
ft/d = Feet per day
— = Dimensionless

Table 4-8. Marathon Limestone aquifer properties from pumping tests.

State Well No.	Well Type	Owner	Well Depth (feet)	Date	Depth to Water (feet)	Open Interval (feet)	Pumping Rate (gpm)	Pumping Duration (hours)	Drawdown (feet)	Transmissivity (ft^2/d)	Hydraulic Conductivity (ft/d)	Storage Coefficient (—)
Dow Chemical Co. Well No. 1 Test												
5255419	Pumping well	Dow Chemical Co.	502	1/16/1957	139.97	—	40	24	158.18	2,821	8	—
5255413	Observation well	Dow Chemical Co.	446	1/16/1957	57.69	—	—	—	—	—	—	—
5255109	Observation well	A. W. Haley	200	1/16/1957	126.09	—	—	—	—	—	—	—
5255423	Observation well	Forker-Gage Ranch Town Mill	350	1/16/1957	127.63	—	—	—	—	4,465	20	0.000673
Southern Pacific Railroad - East Well Test												
5255524	Pumping well	Southern Pacific RR East well	316	1/22/1957	91.45	—	40	3.7	16.45	1,564	7	—
5255421	Observation well	Southern Pacific RR West well	203	1/22/1957	92.82	20–203	—	—	—	535	5	0.0167

gpm = Gallons per minute
ft^2/d = Square feet per day
ft/d = Feet per day
— = Dimensionless

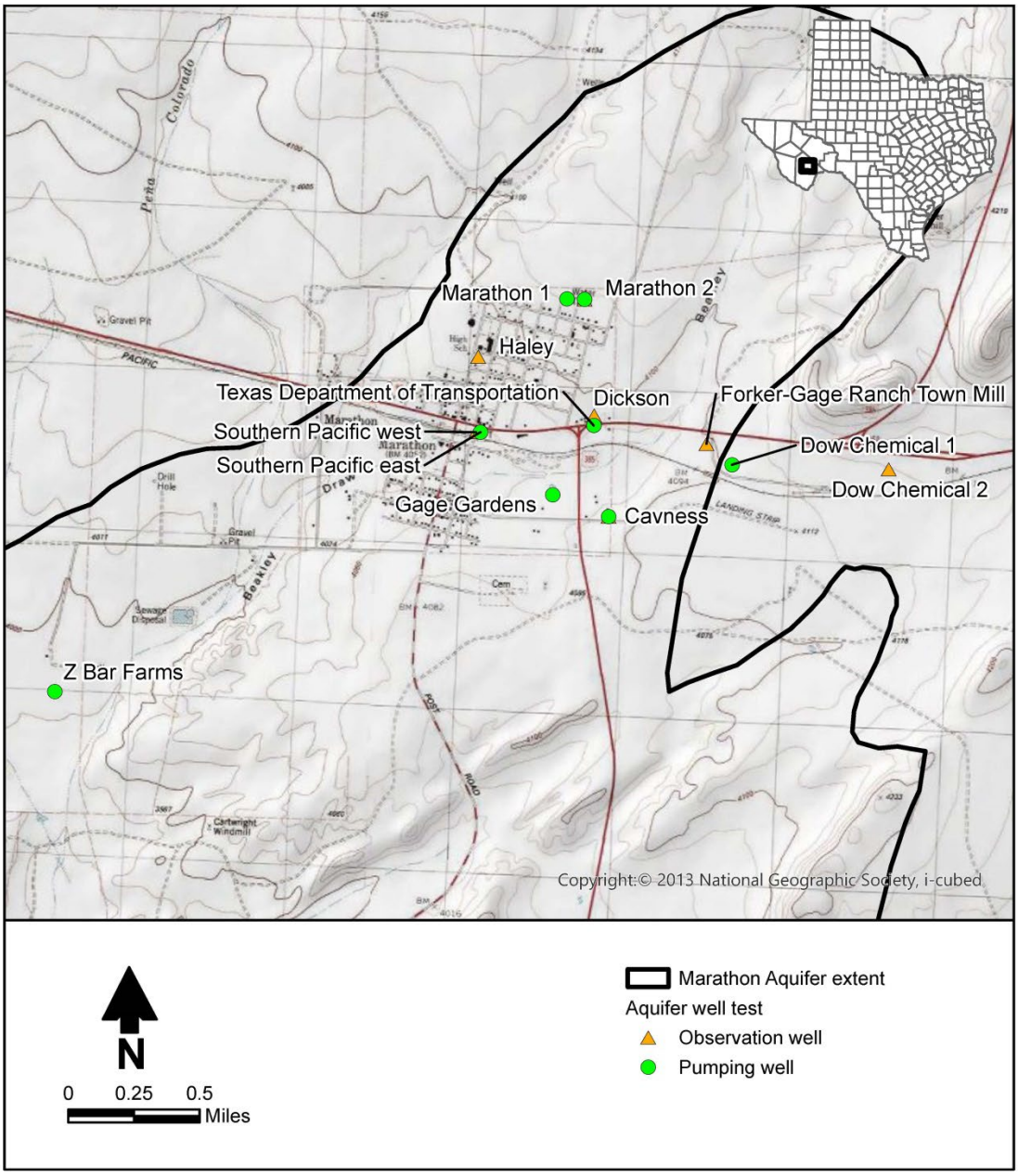

Figure 4-33. Locations of wells used in aquifer tests.

Aquifer properties (i.e., transmissivity and storage coefficient) were generally available from the test records in the TWDB groundwater database. The aquifer properties as interpreted by LBG Guyton Associates on the wells tested in 2009 are reported in Table 4-8. The same is true for the aquifer tests conducted in 1957, although the author of the analysis for those tests is not listed. For some of these tests, aquifer transmissivity is provided for both pumping well drawdown and recovery data. Where this was the case, the aquifer transmissivity from the recovery data was used, as it tended to be higher than that

interpreted from the drawdown data and the value is not influenced by pumping well efficiency.

For the Texas Department of Transportation well test, test data for the pumping well and the L.S. Dickson windmill observation well were analyzed. Water levels were also monitored during the test at the Forker-Gage Ranch Town Mill well (state well number 5255423), but the drawdown was small and data were not analyzed. The test duration of 48 hours listed on the well log includes an initial step test period and 30 minutes of water level recovery (no pumping) prior to the production test. The Dow Chemical Company well 1 test consisted of 5 hours of well development, followed by 40 minutes of water level recovery, followed by a 24-hour pumping test. Aquifer properties for this test were determined for the pumping well and the Forker-Gage Ranch Town Mill observation well. Data for two other wells monitored during this test, Dow Chemical Company well 2 (completed in Woods Hollow Shale) and A.W. Haley, indicated no discernable drawdown due to the test, and data were not analyzed further.

Test data were not previously analyzed for the Z Bar Farms (state well number 5254604) single-well test. Specific capacity is the pumping rate of a well divided by the water level decline (drawdown) at the well that occurs due to pumping. Aquifer transmissivity at this well was estimated from specific capacity using a modified form of the Cooper-Jacob solution for drawdown in a pumping well (Walton, 1970; Mace, 2001). The Cooper and Jacob solution for drawdown in a pumping well (Cooper and Jacob, 1946) can be written assuming consistent units as follows:

$$s = [Q/(4\pi T)] \times \ln(2.25Tt/r^2S) \qquad \text{Equation 1}$$

where s = drawdown in the well
Q = pumping rate of the well
T = aquifer transmissivity
t = time since pumping began
r = radius of the well
S = aquifer storage coefficient

Equation 1 can be rearranged to solve for the specific capacity as follows:

$$Q/s = 4\pi T/[\ln(2.25Tt/r^2S)] \qquad \text{Equation 2}$$

Where all terms in Equation 2 are known or assumed except for transmissivity, the transmissivity can be solved for iteratively. For purposes of the calculation, a well efficiency of 80 percent and a storage coefficient of 0.001 were assumed. The assumed storage coefficient is lower than those observed during other aquifer tests due to the short duration of pumping at the Z Bar Farms well (2 hours); even in an unconfined aquifer, the water levels will respond as if the aquifer is confined for short pumping durations (e.g., Neuman, 1975).

4.5.2 Marathon Limestone Aquifer Properties

Marathon Limestone transmissivity determined from aquifer testing ranges from 535 square feet per day at the Southern Pacific Railroad well 2 to 26,217 square feet per day at Marathon well 1. Average aquifer hydraulic conductivity was estimated by dividing the transmissivity by the saturated thickness of aquifer at the time of the test; this analysis leads to a range in aquifer hydraulic conductivity of 5 to 92 feet per day (Table 4-8).

Although an average hydraulic conductivity can be calculated, it should be noted that Marathon Limestone permeability is largely related to the presence of secondary porosity formed through fracturing and the development of karst features at a given location. Therefore, the majority of aquifer transmissivity is attributable to what may be limited thicknesses of the formation. For example, Marathon water supply well 1, with the highest aquifer transmissivity of all the wells tested, is only screened over two short intervals—from 270 to 282 feet and from 455 to 468 feet below ground surface (25 feet total). The intervals likely correspond to observed solution cavities and related karst features. Nearby Marathon well 2 is screened from 340 to 346 feet below ground surface, covering a zone listed on the well log as "Broken lime w/water." A number of other wells in the area are completed as open hole or have long screened intervals (e.g., wells 5255401 and 5255421 in Table 4-8), and specific zones of water production are not evident.

Five estimates of aquifer storage coefficient are available from the tests; the estimated values range from 0.000673 to 0.0167. The lower value is indicative of confined aquifer conditions, while the higher value is indicative of unconfined aquifer conditions, particularly given the limited duration of test pumping and the fact that the volume of connected pore space within the aquifer is relatively low because it is attributable to secondary porosity (i.e., fracturing and karst features). The Marathon Limestone is likely an unconfined aquifer on the regional scale where it is near surface (such as at Marathon), with a storage coefficient of about 2 to 3 percent (i.e., 0.02 to 0.03).

4.5.3 Aquifer Properties for Other Formations

Available well yield and lithologic data indicate that the hydraulic conductivity of other formations (with the possible exception of alluvium) would be less than that of the Marathon Limestone—in many cases significantly less. Karst conditions have not been identified for any of the other potential aquifer units. Assumed hydraulic conductivity values are used in the recharge modeling based on standard references, but these values should be considered educated estimates at best.

Because other formations that yield water do so because of secondary porosity, their storage coefficient is expected to be similar to that of the Marathon Limestone (i.e., several percent). The alluvium is an exception to this generalization; the alluvium would be expected to have an unconfined storage coefficient (specific yield) of 10 to 20 percent (0.1 to 0.2).

4.5.4 Fracture and Lineament Analysis

Remote sensing analysis can be a useful technique for identifying lineaments that may correlate with areas of higher groundwater production potential (Mogaji and others, 2011). This analysis normally relies on the use of imagery, a digital elevation model, and derivative terrain products (e.g., hillshade, slope, vegetation index) to identify surface expressions of geologic features that suggest the existence of a fracture or lineament. These data can serve as a predictive tool when part of a multi-criteria evaluation that considers other factors such as rock type, slope, lineament density, and groundwater flow (e.g., Liu and others, 2015).

In the Edwards Aquifer, a correlation between increased water well yields and decreased distances from fractures and lineament-trace features determined through remote sensing was observed by Alexander (1990), who also suggests that areas with increased lineament density or intersecting lineaments may provide larger well yields. Similar observations using remotely sensed lineament data have been made elsewhere and in varying rock types (Lattman and Parizek, 1964; Yenne and others, 2015).

Members of the Daniel B. Stephens & Associates, Inc. team have used this method in the past to site productive water wells in the Marathon Aquifer. With the intent of providing a framework that would indicate zones of higher hydraulic conductivity and potential well yield, fractures and lineaments were delineated for the Marathon Aquifer using the approach described in the following subsections.

4.5.4.1 Fracture and Lineament Mapping

The Texas National Agriculture Imagery Program 2020 product was the preferred imagery used for the lineament analysis (U.S. Department of Agriculture, 2020). This dataset provides full coverage of the aquifer extent at 1-meter resolution with red, blue, green, and near-infrared bands for both natural color and infrared analysis. A normalized difference vegetation index that is effective at identifying healthy vegetation was also developed from this imagery.

The West Texas LiDAR 1-meter digital elevation model (U.S. Geological Survey, 2019) was used for the analysis; the 30- and 10-meter digital elevation models were too coarse, as many of the lineament features are less than 10 meters in width. Two hillshade models were developed from these data at azimuths of 45 degrees and 315 degrees from a 45 degree angle above the horizon. Hillshade models consider how an illumination source casts shadows across the landscape by creating a shaded relief surface; they are useful for identifying subtle topographic changes not normally detectable with imagery or a digital elevation model. An attempt was made to automate lineament extraction using the PCI Geomatica software, but because of noise created by graded roads, fence lines, game trails, and so on this approach was unsuccessful.

A 1:4,000 fixed map reference scale was applied when identifying lineament and fracture features. This approach provided a high level of detail and is the approximate maximum limit of resolution before the imagery appeared pixelated, an effect that impaired

lineament feature identification. At this working scale, the minimum mapping unit was approximately 1 millimeter; this allowed for features as small as 4 meters (13.12 feet) wide to be reasonably mapped.

A minimum mapped feature length was also defined. This was 50 feet for fractures, the approximate minimum distance that a line can be drawn using ArcGIS at the reference scale. A higher threshold of 200 feet was used for lineaments. This increased the confidence level of these features by providing enough segment length to differentiate lineaments from other topographic features such as a ridge or stream channel, and helped to eliminate potential dataset artifacts associated with shadows or anthropogenic interference.

Mapping occurred within an ArcGIS workspace by identifying and manually tracing rectilinear or slightly curvilinear features across the Marathon Aquifer landscape. The area was systematically reviewed from north to south and west to east 1 square mile grid at a time. Imagery and elevation data were independently and jointly reviewed by overlaying transparent layers for additional clarity. "On-the-fly" ArcGIS 3D Analyst elevation profile graphs were created as needed to better understand breaks and changes in the topography.

Mapped features were categorized as a fracture or lineament. The term fracture was used to define rectilinear features visible across an exposed rock surface with no observable separation along the feature plane. Fractures were mainly detected using aerial imagery in outcrops as dark narrow lines that cut across the underlying bedding planes.

Lineaments were defined as rectilinear or slightly curvilinear topographic features, distinguishable from the surrounding landscape through a change in surface expression or as a plane with measured plan view separation between two points. Lineaments differ from fractures in that they exhibit lateral separation, could be observed outside of rock outcrop areas, and often appeared as breaks in ridge lines and bedding planes or as linear erosional features that cut across the surrounding landscape. Lineaments were detectable using both imagery and hillshade models, although not always concurrently. Ridge lines, exposed bedding planes, and stream segments were not mapped as lineaments.

Lineament separation was used to differentiate features and was measured using the ArcGIS measure tool as the plan view distance between points with an identical origin, usually two bedding planes or the apex point of a ridge line. Lineaments were subdivided into six categories based on the extent of separation; the six categories are (1) no observed separation, (2) possible separation, (3) less than 100 feet of separation, (4) 100 to 250 feet of separation, (5) 250 to 500 feet of separation, and (6) greater than 500 feet of separation. An additional seventh category was developed for areas where an unconformity was observed with abutting stratigraphic beds at land surface.

This analysis supplements the Geologic Atlas of Texas (1:250,000 scale) faults for the Marathon Aquifer. Geologic Atlas of Texas faults were not mapped as part of this analysis, but were rather appended to the lineament dataset. The one exception to this was when a Geologic Atlas of Texas fault was found to be misplaced by more than 200 feet, likely due to scale and projection changes that have taken place since the faults were initially

interpreted over 50 years ago. These faults are identified as “GAT Fault – Off” within the “Lineament” field, and a correctly located replacement fault is identified as a “GAT Replacement” in the project geodatabase.

Lineament mapping was limited in some areas by anthropogenic and Quaternary cover deposits. The town of Marathon was not mappable because of interference from infrastructure. Regions covered by alluvial fans and other alluvial deposits are also not conducive to the analysis.

4.5.4.2 Lineament Model Grid

Lineaments and fractures were mapped as polyline shapefile features that provide a linear representation where these features were identified. A workflow was developed to convert these locations and their potential impact on groundwater production into a ranked model grid. Mapped fractures are believed to mainly occur as relatively shallow surficial features, and were not included in this analysis.

A lineament damage zone shapefile was developed that provides a more accurate spatial representation of the area of influence for these mapped features. A damage zone was defined as the width of the disturbed area associated with a feature, and is assumed to correlate with subsurface fractured rocks. A damage zone of 15 feet was assigned to lineaments with and without possible separation. This is the minimum mapping unit rounded to the nearest 5-foot increment, and was selected because these were normally very narrow features with unknown geomorphology.

Two randomized 30-unit samples were developed to determine the average damage zone for lineaments with observed separation. Damage zones were measured to the nearest 5-foot increment for features with less than 100 feet of separation and again for those with more than 100 feet of observed separation. These results were averaged for each sample group then rounded to the nearest 5-foot increment (Table 4-9). A list of the sampled features and damage zone measurements is provided in Appendix C.

Geologic Atlas of Texas fault damage zones varied substantially in width, and in many cases were not observable along the thrust faults, fold belts, or where Quaternary cover deposits were present. A conservative (generally smaller than might be expected) 90-foot damage zone was assigned to Geologic Atlas of Texas faults to account for these structural features. Damage zone measurements were translated into a geographic information system polygon shapefile using the corresponding lineament polyline features and the ArcGIS buffer tool, which created a representative polygon feature for each mapped lineament based on the assigned damage zone widths.

Table 4-9. Mapped fracture and lineament categories by type with total feature count, feature damage zone, and weights.

Lineament	Damage Zone (feet)	Feature Weight
Fracture	NA	NA
Lineament with no observed displacement	15	0.25
Lineament with possible displacement		
Lineament with <100 feet of displacement	30	1.5
Lineament with 100–250 feet of displacement	60	3
Lineament with 251–500 feet of displacement		
Lineament with >500 feet of displacement		
Inferred offset based on unconformity		
Geologic Atlas of Texas fault	90	
Geologic Atlas of Texas fault replacement		
Geologic Atlas of Texas fault – Off	NA	NA

NA = Not applicable

It was assumed that lineaments with greater plan view separation provide more favorable areas for groundwater production. A feature weighting system that accounts for this assumption was developed (Table 4-9) and appended to the damage zone shapefile. The ArcGIS spatial join tool was used to translate the weighted damage zone features into a weighted grid. A "select by location" query was used to identify model grid cells with their centroids located within both the Marathon Aquifer and pre-Quaternary Geologic Atlas of Texas units. These selected cells correspond to the same general workspace used to identify lineaments. The ArcGIS spatial join tool was used to merge this selection with the weighted damage zone shapefile. This output included the selected grid cells and aggregated feature weights in cells where the two datasets coincided. Resulting cells with a value of 0 indicate that no overlapping features existed within the cells boundary, while values 0.25 through 9.25 provide context on the density and significance of the corresponding damage zone features (Figure 4-34).

Next, an interpolation methodology was developed to provide a weight for grid cells where Quaternary cover deposits were present. Model grid centroids were used to extrapolate aggregated feature weights from the spatial join model grid. These weights were converted into a raster surface using the ArcGIS Topo to Raster tool by defining the weighted centroid field as a point elevation type. The output extent was set to the Marathon Aquifer outline, drainage enforcement was not enforced, and the primary data type was set to "spot." A minimum and maximum data value was set based on the data range in the weighted model grid of 0 and 9.25. Output cell size was set to 50 for a smoother interpolation. The resulting raster provided a continuous surface for the aquifer area with interpolated values between grid centroids.

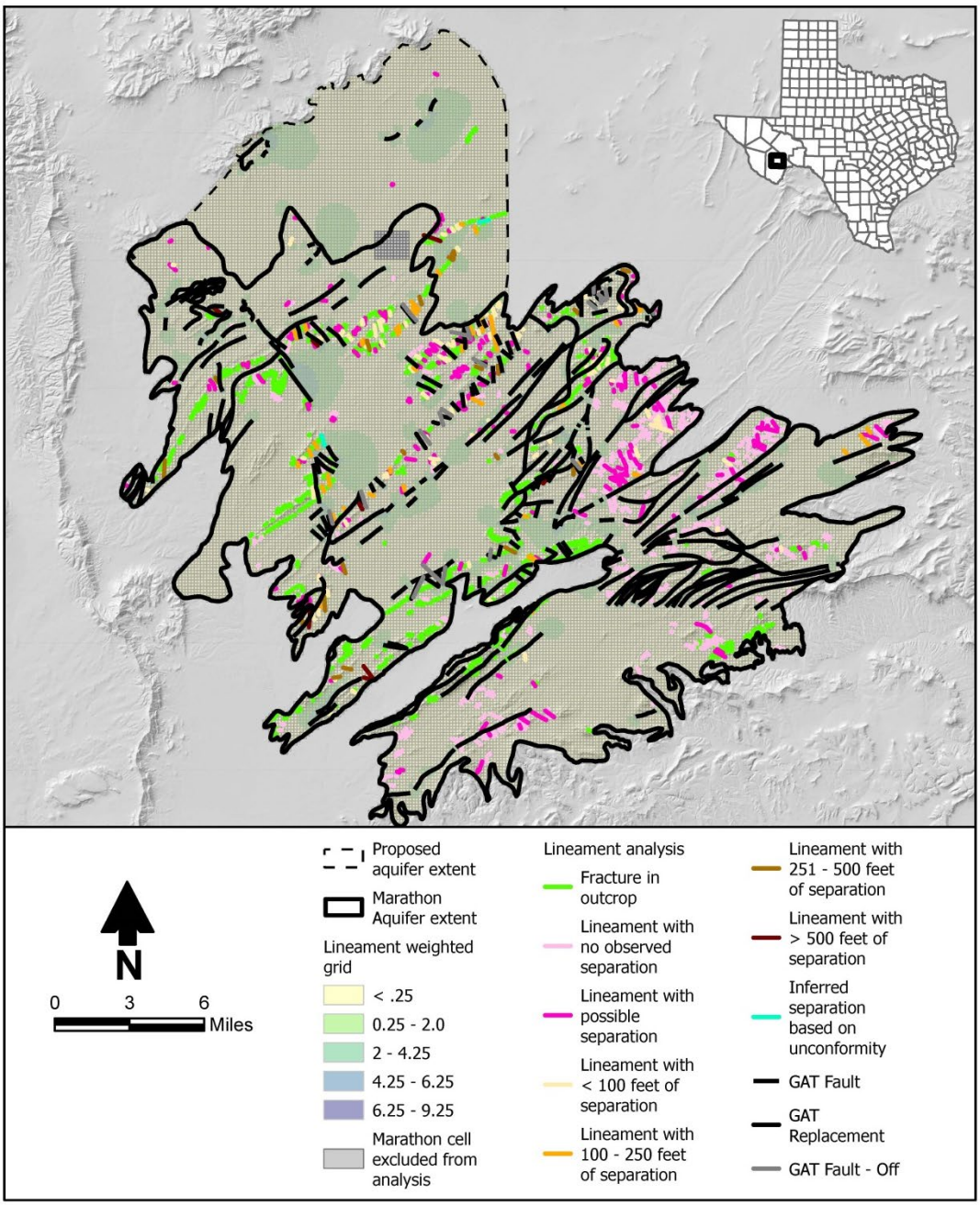

Figure 4-34. Weighted model grid for lineament analysis. GAT is Geologic Atlas of Texas.

Model grid centroids and the ArcGIS Extract Multi Values to Points tool were used to obtain interpolated values for the previously omitted Quaternary model grid cells. Centroid values less than 0.25 were set to 0 because that was the lower bound of the feature lineament weights. Interpolated values and spatial join weights were appended to the model grid shapefile for the Marathon Aquifer area.

The data were categorized into five classes using the natural breaks (Jenks) methodology, and the five classes were recategorized into a rank system of 0, 1, 2, 3, and 4. A rank of 0 conceptually represents no increased groundwater production potential, while a rank of 4 represents the highest potential for groundwater production (Figure 4-35). Note that this ranking does not account for alluvial water; production from this unit is not dependent on fractures and secondary porosity.

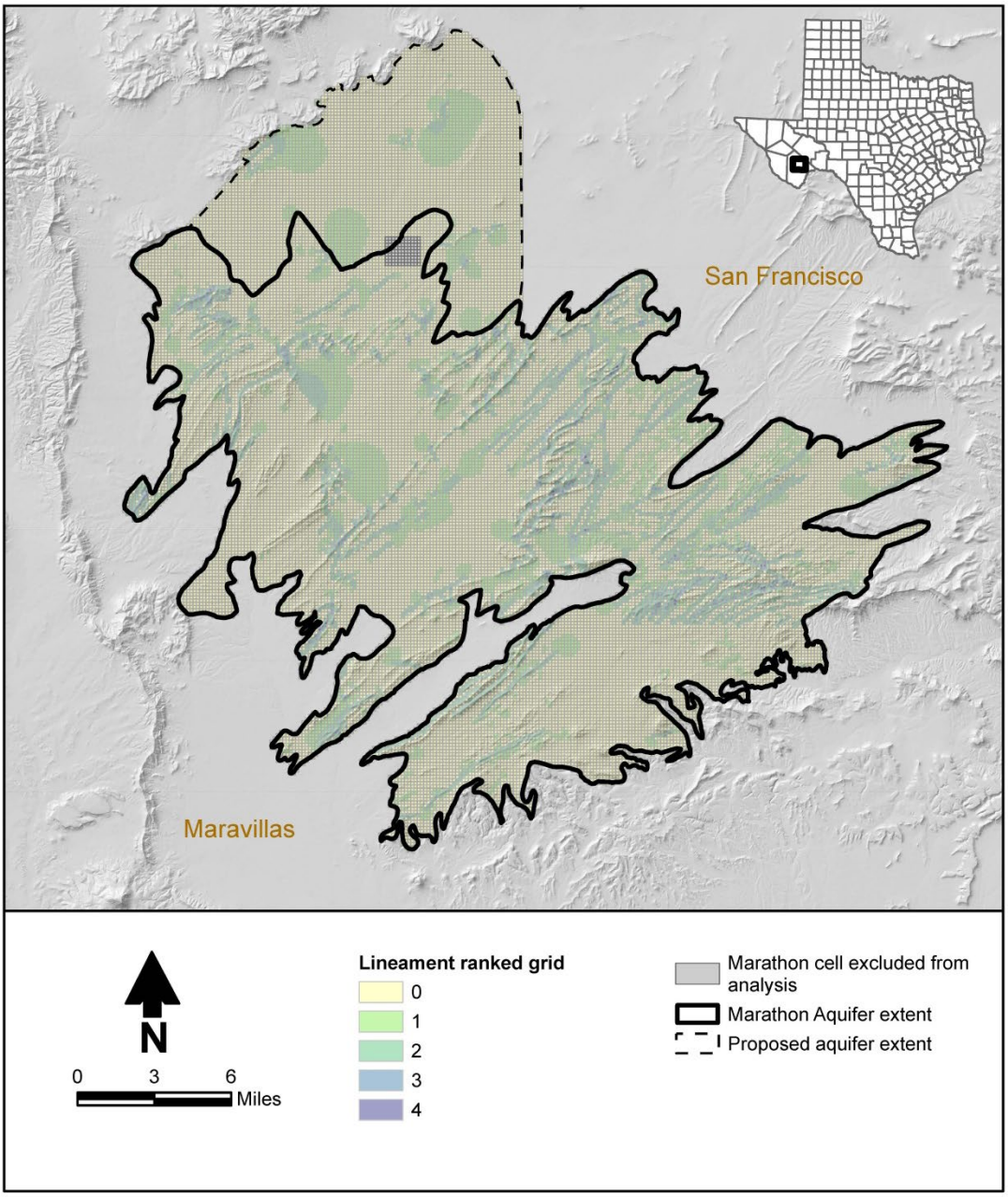

Figure 4-35. Ranked model grid for lineament analysis.

4.5.4.3 Results

Fractures overwhelmingly outpaced the number of observed lineaments (Table 4-10), but were almost exclusively located within the Caballos Novaculite in ridge lines above the basin floor. These were rarely visible in the hillshade model, likely because they are smaller features and/or, as their dark color would suggest, they have been infilled with sediment. Although this fracture volume indicates an intensely fractured formation, it is unlikely that these would penetrate through the shale interbeds located in the lower chert member, rendering these as mainly shallow surficial features (Section 4.1).

Table 4-10. Total mapped features by lineament type.

Lineament Type	Feature Count
Fracture	3,109
Lineament with no observed separation	480
Lineament with possible separation	242
Lineament with <100 feet of separation	103
Lineament with 100–250 feet of separation	48
Lineament with 251–500 feet of separation	20
Lineament with >500 feet of separation	8
Inferred separation based on unconformity	2
Geologic Atlas of Texas fault	229
Geologic Atlas of Texas fault replacement	20
Total	4,261

Lineaments without and with possible plan view separation accounted for nearly 80 percent of the mapped lineament features. These features most likely correspond to joints and faults. For the remaining 20 percent, plan view separation suggests that movement has occurred along the lineament plane, but does not necessarily reveal the amount of movement because of unknown variables such as possible rotation or angular bedding. Measured separation suggests that these lineaments are likely faults.

Mapped lineaments were primarily observed following a northwest to southeast trend following an average 132 degree angle measured clockwise from true north. This value is nearly a 90 degree departure from the northeast trending thrust faults, and is consistent with the same general orientation of Geologic Atlas of Texas mapped tear faults. Tear faults are summarized in greater detail below.

Faults compiled from the Geologic Atlas of Texas show two dominant, nearly orthogonal trends. The first trend group consists of northwest-trending, relatively straight and short faults, and the second trend group consists of dominantly northeast-trending, more curvilinear, and relatively longer faults (see the Geologic Atlas of Texas faults in Figure 4-34. The second trend group consists of mostly shallowly to steeply dipping thrust faults that carried rocks northwestward, while most of the first trend group consists of

steeply dipping oblique-slip or strike-slip tear faults (Muehlberger and Dickerson, 1989; Hickman and others, 2007).

Tear faults are relatively small-scale strike-slip faults that form in fold-thrust systems. They are characteristically steeply dipping (and thus have relatively straight map traces), and are oriented subparallel to the regional direction of thrust and folds transport, in this case northwestward. They occur in the hanging wall blocks of thrusts, terminating downward when reaching a thrust and the footwall block below (Figure 4-36). They form during thrusting and associated folding to accommodate differences in along-strike thrust displacements (B in Figure 4-36), or from differences in shorting within allied folds (A in Figure 4-36). Simply put, large bodies of rock lack the strength to move great lateral distances along thrust faults as single masses, and therefore break into smaller structural blocks bounded by thrust faults below and tear faults at their ends.

Many of the mapped lineaments are similar in orientation to known tear faults, and those with visible plan view separations are consistent with having strike-slip or oblique-slip offsets. Although similar in these respects, without field observation, a genetic relationship cannot be established. If the two are related, then the depths to which mapped lineaments might extend should follow the "rules" for tear faults; namely, they can penetrate to depths no farther than the thrust faults to which they are related.

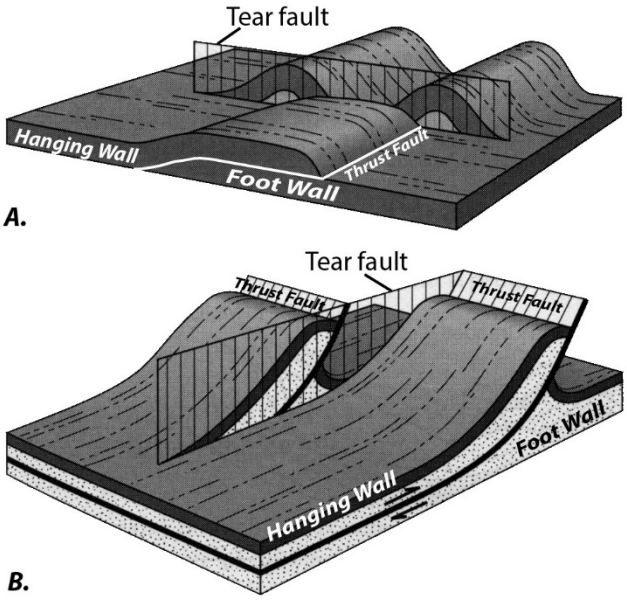

Figure 4-36. Thrust sheets segmented by tear faults (modified from Twiss and Moores, 1992). A: Shortening is accomodated by thrusting on one side of a tear fault and by folding on the other. B: Two noncoplanar imbricate thrusts are connected by a tear fault.

At one extreme, where thrust faults breach the surface along their mapped traces, intersecting tear fault-related lineaments would not be expected to penetrate any farther than the extant thickness of hanging wall strata along the thrust. At the other extreme, because Marathon thrust faults generally have some component of southward dip, tear fault-related lineament traces would be expected to penetrate to greater depths within

hanging wall strata with greater distances from thrust fault traces. However, because Marathon thrust fault surfaces are demonstrably not planar or of uniform dip, these relationships might hold only in a very general way.

4.6 Discharge

Groundwater discharge occurs through groundwater pumping from wells (pumpage). Very little pumping has occurred from the Marathon Aquifer to date. There are not many wells present in the study area. Figure 4-37 shows the types of wells present in the TWDB groundwater database and the Texas Department of Licensing and Regulation submitted driller's report database. As can be seen in this figure, the vast majority of wells are used for livestock purposes, with a smaller number of domestic wells. There are a very few public supply, irrigation, and industrial wells in the study area.

Figure 4-37 shows the TWDB estimated total pumpage for the period 1980 to 2019. This figure indicates that the total pumpage from the aquifer has increased from approximately 100 acre-feet per year in 1980 to approximately 250 acre-feet per year in 2019, with a maximum pumping of approximately 450 acre-feet per year in 2010. For most of the time period from 1980 to 2019, the majority of pumping from the Marathon Aquifer has been for municipal use. Municipal pumping from the aquifer is shown in Figure 4-38, and indicates that this pumping was slightly lower from 1980 to the mid-1990s, but overall has remained relatively stable at approximately 100 acre-feet per year. Municipal pumping from the Marathon Aquifer is mostly by the town of Marathon, as can be seen by comparing Figures 4-38 (total municipal pumping) and 4-39 (town of Marathon pumping only). There are also a number of domestic wells present in the study area, most of which are in the vicinity of the town of Marathon. Estimated pumping from the domestic wells in Marathon accounts for the difference between Figures 4-38 and 4-39.

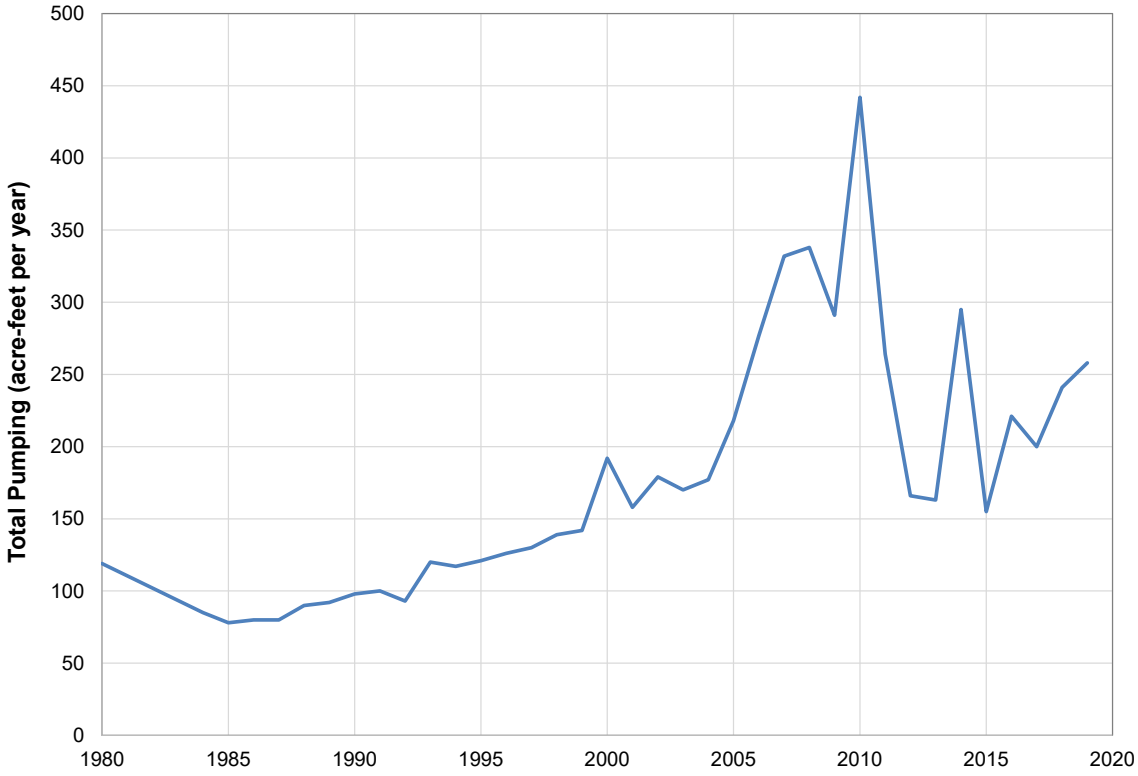

Figure 4-37. Total groundwater pumping from the Marathon Aquifer from 1980 to 2019.

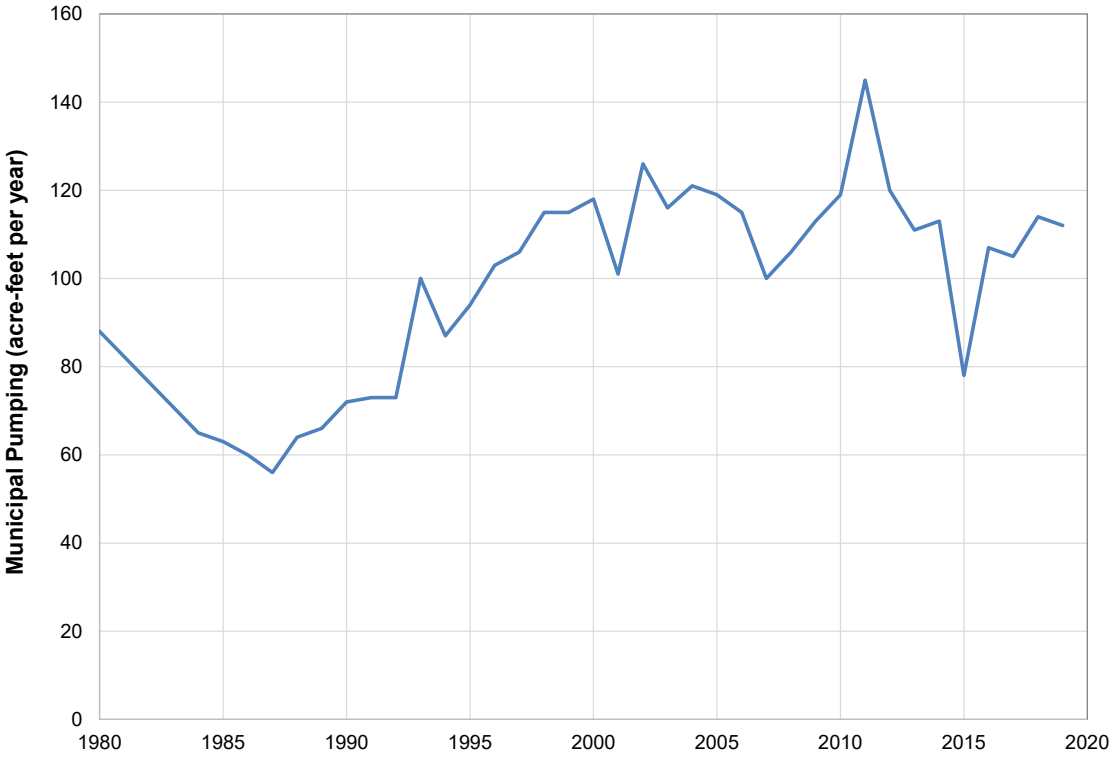

Figure 4-38. Estimated historical municipal pumping from the Marathon Aquifer, 1980 to 2019.

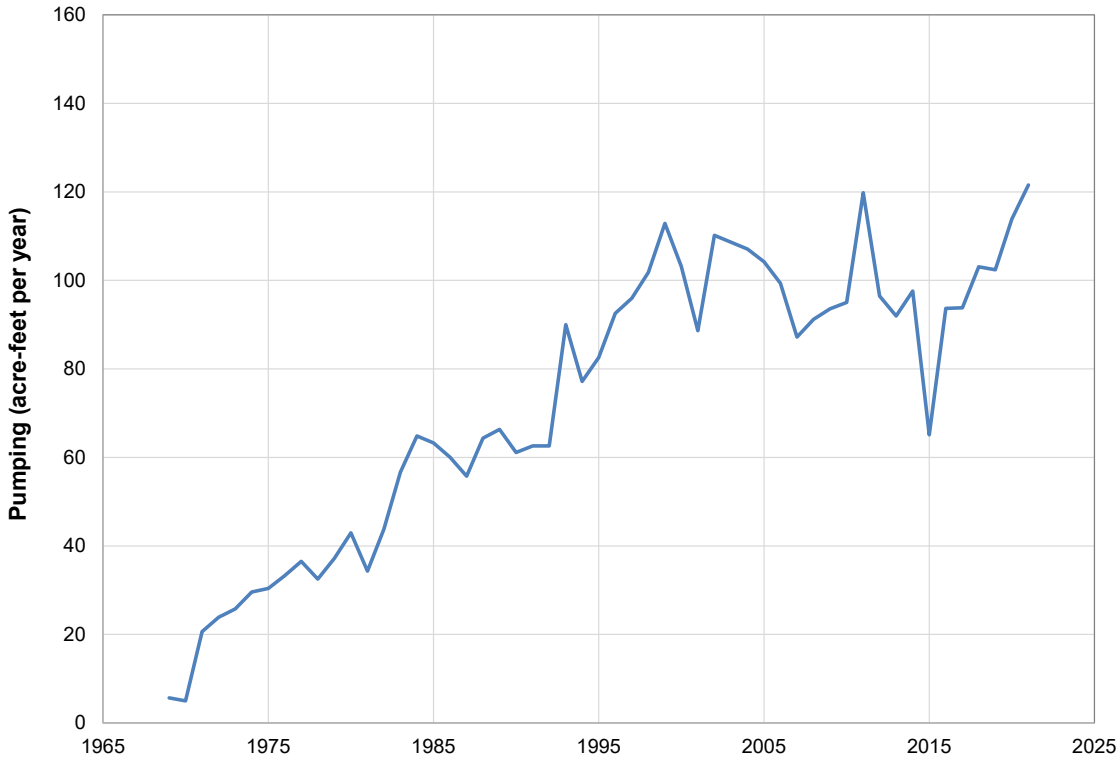

Figure 4-39. Reported historical pumping by the Town of Marathon, 1969 to 2021.

Reported irrigation pumpage from the Marathon Aquifer began to occur in the late 1990s. As shown in Figure 4-37, very few of the wells in the study area are for irrigation purposes, and irrigation wells listed are mostly located in or near the town of Marathon—specifically the town cemetery, "Post" county park, and Gage Gardens. At the end of the 1990s, the Blakemore Ranch began to irrigate a small area west of Marathon to grow alfalfa using an old oil test well. This irrigation likely accounts for much of the reported value as of the year 2000 in Figure 4-41. Use of this well reportedly affected the water levels in domestic wells on the southwest side of Marathon, and the ranch voluntarily ceased pumping for irrigation at that location around 2000 to 2001.

Irrigation pumping increased to over 300 acre-feet per year in 2010, but has since declined to approximately 100 acre-feet per year, as shown in Figure 4-41. Much of this reported irrigation pumping that peaked in 2010 appears to have occurred in conjunction with installation of the Gage Gardens in Marathon. Initial development of this 27-acre garden included the planting of large trees and turfgrass, which would have required a significant amount of water for establishment of vegetation. The Gage Gardens reportedly used old irrigation wells on the property to produce the water for their project, and irrigation water use has declined since the gardens were established.

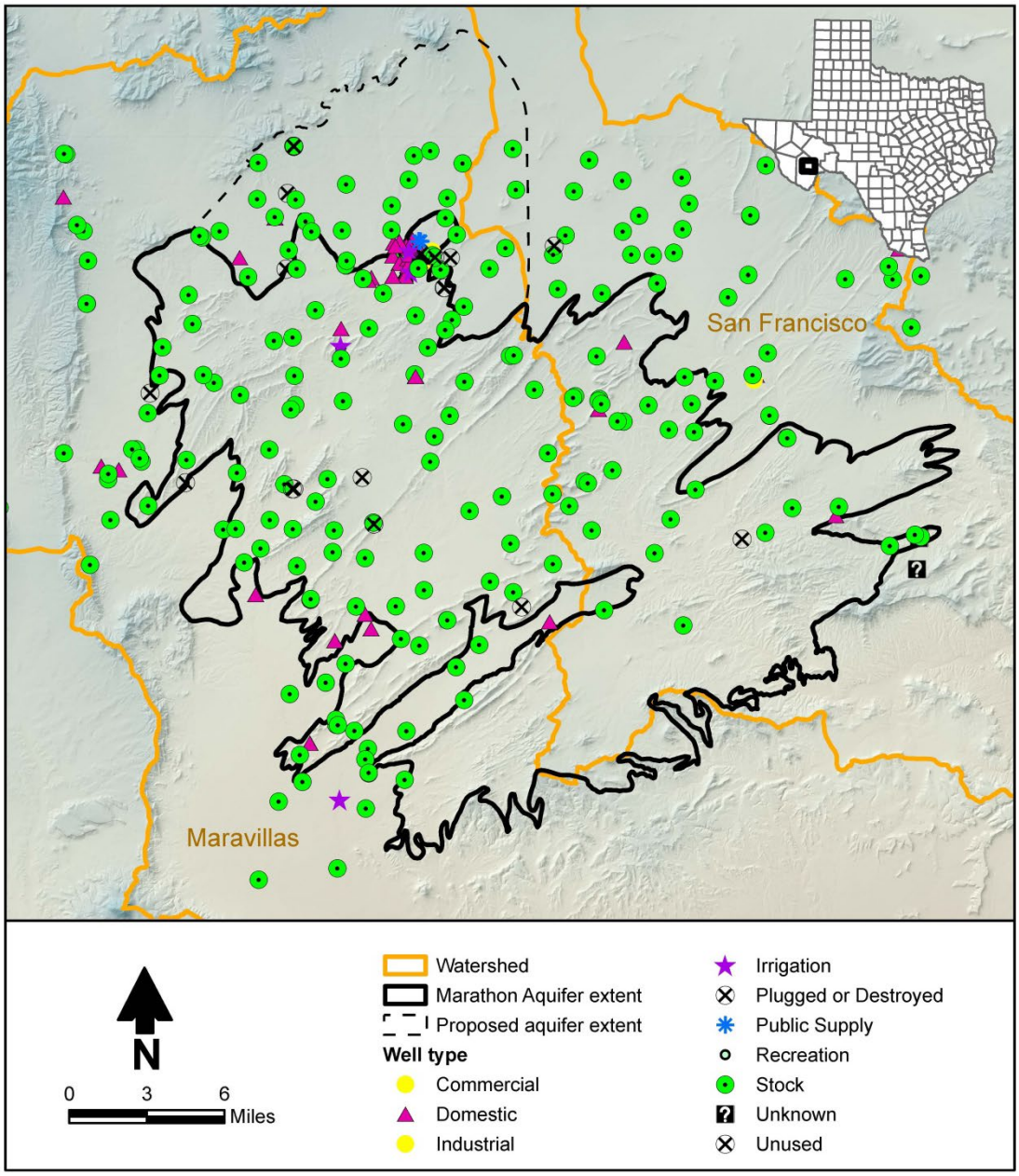

Figure 4-40. Types of wells present based on the TWDB groundwater database and the Texas Department of Licensing and Regulation submitted driller's report database.

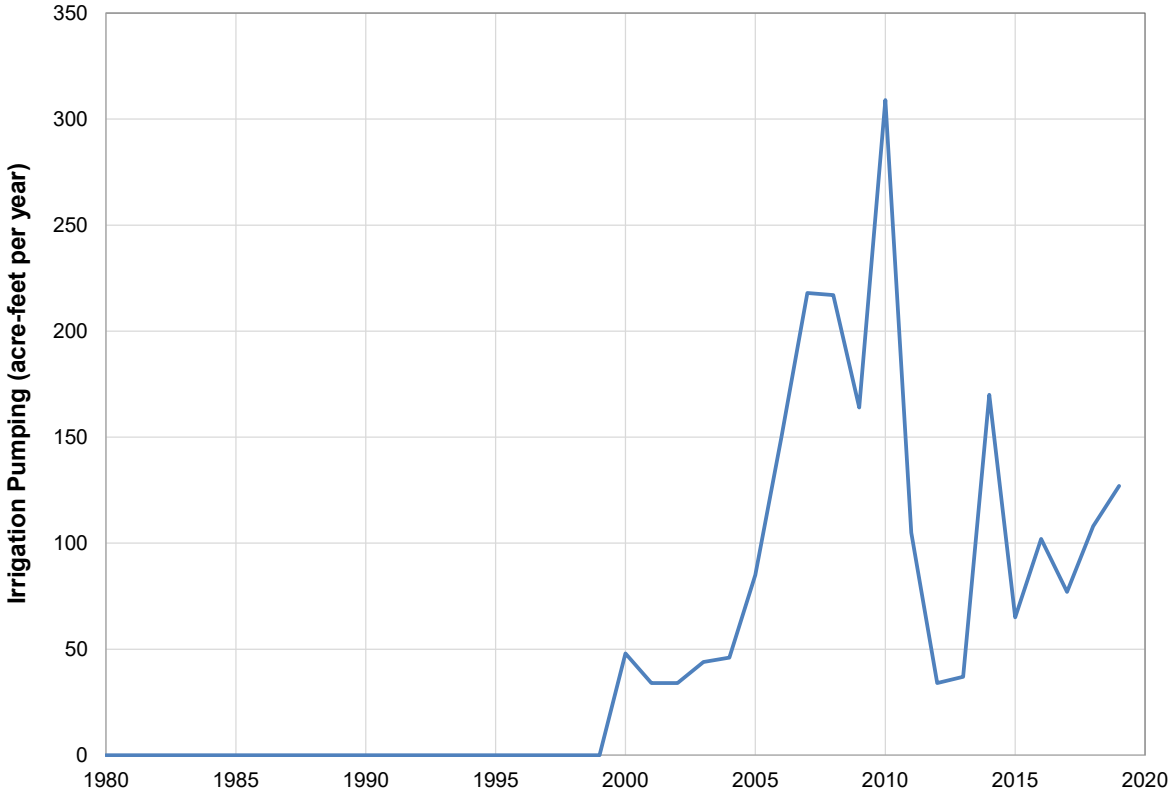

Figure 4-41. Estimated historical irrigation pumping from the Marathon Aquifer, 1980 to 2019.

According to the TWDB water use survey, the only other reported use of groundwater from the Marathon Aquifer is livestock pumping. As shown in Figure 4-37, the vast majority of wells present in the TWDB groundwater database and the Texas Department of Licensing and Registration submitted driller's report database are livestock wells. Although livestock wells make up most of the wells in the study area, total estimated historical pumpage for livestock use is small. Figure 4-42 shows the estimated historical pumping for livestock use, which is consistently less than 30 acre-feet per year, and for the past 15 years or so has been between 10 and 20 acre-feet per year.

There is no reported use of groundwater from the Marathon Aquifer for industrial, steam-electric power, or mining purposes.

In summary, there has been very little historical pumping from the Marathon Aquifer. Groundwater conditions are likely unaffected by pumping, with the possible exception of the area around the town of Marathon, where the majority of historical pumpage from the aquifer has occurred.

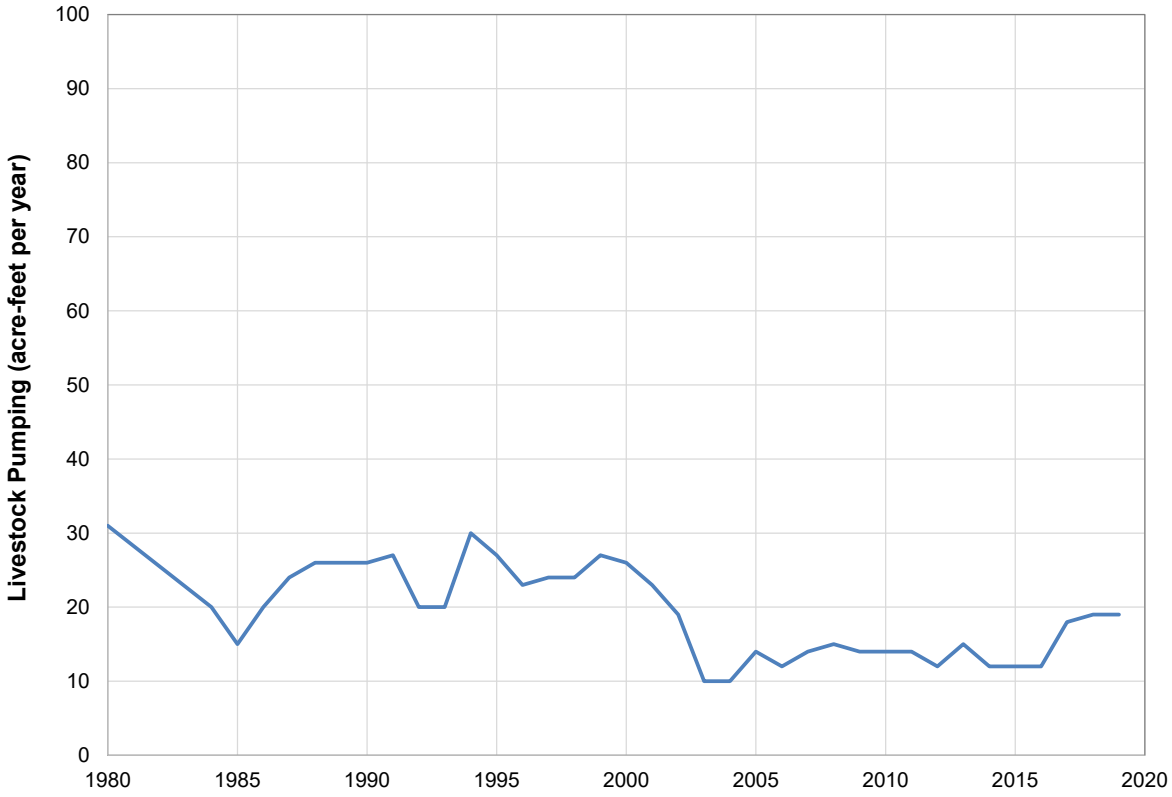

Figure 4-42. Estimated historical livestock pumping from the Marathon Aquifer, 1980 to 2019.

4.7 Water Quality

Water quality data available for the assessment of the Marathon Aquifer water quality were obtained from the TWDB groundwater database, downloaded on May 11, 2022. In nearly all cases, the most recent water quality data are the only values; time series of water quality data for Marathon Aquifer wells are virtually non-existent. However, due to the minimal development of groundwater from this aquifer, and the assessment that much of the aquifer remains in a quasi-steady-state condition, it is likely that water quality in the aquifer is not changing significantly over time. The one well with a long series of water quality data (well 5255104) indicates consistent water quality over the past 50 years.

In addition to the standard chemical analyses typically available for groundwater samples, a series of groundwater samples were collected for a regional study that used hydrogeochemical and isotopic analyses to help evaluate conceptual models of groundwater flow systems in many aquifers in the far western portion of Texas. Although the Marathon Aquifer was not one of the aquifers included in the study, 21 samples were collected in 2011 from the Marathon Aquifer to determine if it contributed groundwater to aquifers north of the Marathon Aquifer (Kreitler and others, 2013). These 21 samples were collected throughout the Marathon Aquifer, and provide significant detail on the overall water chemistry in the Marathon Aquifer. The following subsections discuss water quality in terms of the total dissolved solids, major ions, and isotope analyses.

4.7.1 Total Dissolved Solids

Because of the limited extent, remoteness, and limited development of the Marathon Aquifer, there is a limited amount of available water quality data. The groundwater salinity classification developed by Winslow and Kister (1956) for TWDB brackish aquifer studies (Table 4-11) was used to guide the total dissolved solids concentration plots for Marathon Aquifer wells.

Table 4-11. Groundwater salinity classification summary.

Groundwater Salinity Classification	Salinity Zone Code	Range in TDS Concentration (mg/L)
Fresh	FR	0 to 1,000
Slightly saline	SS	1,000 to 3,000
Moderately saline	MS	3,000 to 10,000
Very saline	VS	10,000 to 35,000
Brine	BR	Greater than 35,000

TDS = Total dissolved solids
mg/L = Milligrams per liter

The groundwater in the Marathon Aquifer is generally fresh. Figure 4-43 shows the distribution of total dissolved solids concentrations for available Marathon Aquifer wells and spring samples. As shown in this figure, the vast majority of samples indicate fresh water, with total dissolved solids concentrations less than 1,000 milligrams per liter. A few samples collected have total dissolved solids concentrations of just over 1,000 milligrams per liter—one livestock well located just outside of the Marathon Aquifer footprint has a total dissolved solids concentration of 1,632 milligrams per liter and one domestic well in the town of Marathon had a total dissolved solids concentration of 2,260 milligrams per liter. We are unsure of the reason for the higher total dissolved solids concentrations in Marathon, but the analysis is from 1957 and the well is located near many other wells producing fresh groundwater, and therefore does not appear to be indicative of a larger area lower quality groundwater. Regardless, even with the few slightly saline samples from wells and springs in the study area, these analyses are generally indicative of a good quality, fresh water aquifer.

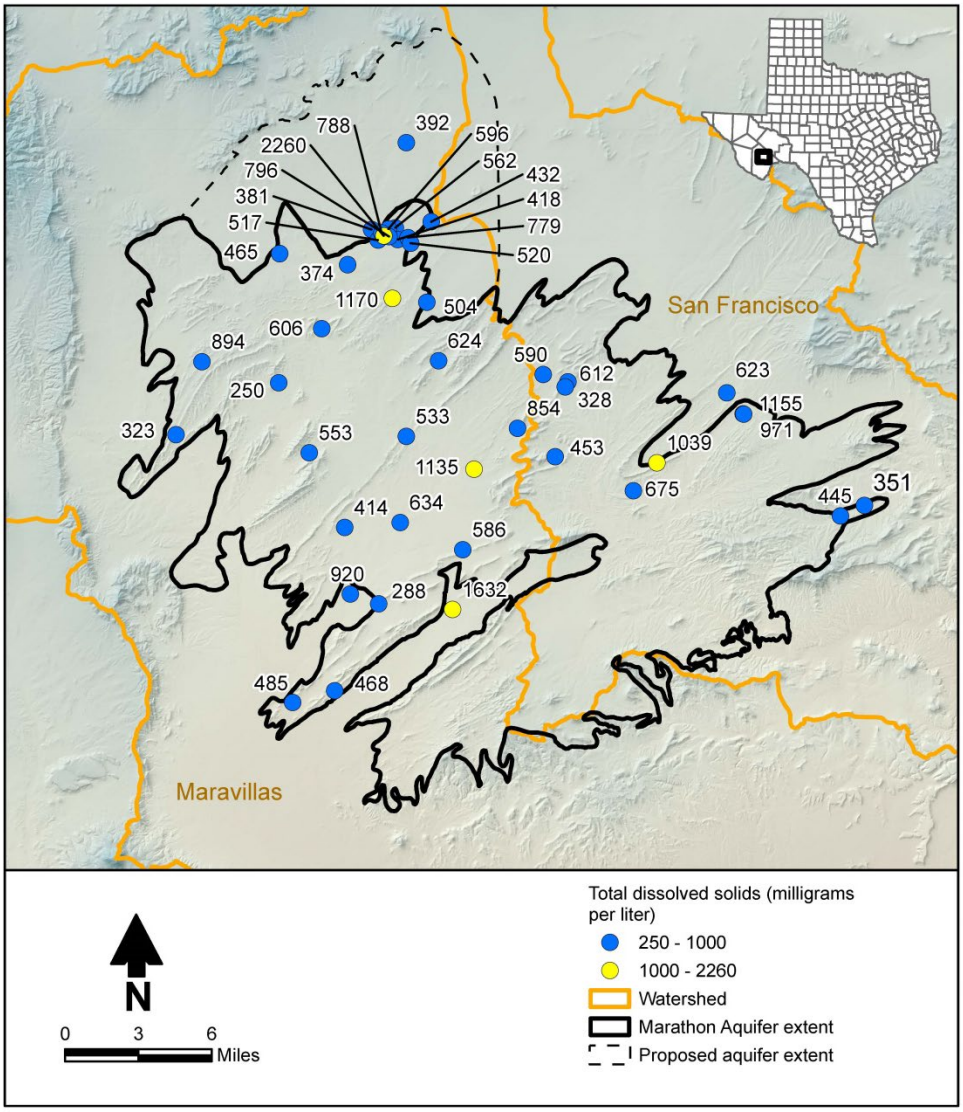

Figure 4-43. Total dissolved solids concentrations measured in the Marathon Aquifer area.

4.7.2 Major Ions

A Piper diagram, also referred to as a trilinear plot, for all samples from the 2011 study is provided in Figure 4-44. A Piper diagram for all the Marathon Aquifer system samples in the TWDB database is provided in Figure 4-45. As shown in this figure, cations are dominated by calcium and anions are dominated by alkalinity. Chloride is low throughout the aquifer, and sulfate varies from low to high. Water types include Ca-HCO_3, Ca-HCO_3 + SO_4, and mixed cation HCO_3 + SO_4. Different aquifer units within the Marathon Aquifer vary somewhat with respect to water types (Figure 4-45); the Marathon and Dagger Flat units are Ca-HCO_3 and mixed cation HCO_3 + SO_4, though still dominated by calcium, while the Dimple Formation tends to be mixed cation HCO_3 (Figure 4-46).

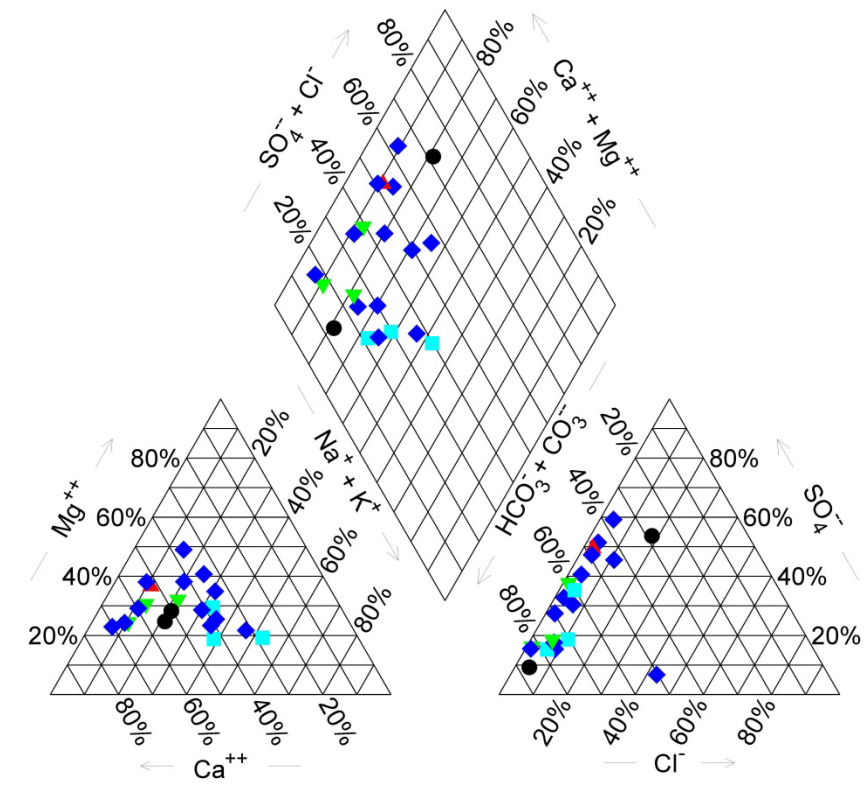

- Marathon-Dagger Flat Aquifer System
- Dimple-Tesnus Aquifer System
- Woods Hollow Shale Aquitard
- Caballos Novaculite Aquitard
- Unknown aquifer

Figure 4-44. Piper diagram for all samples from the 2011 study (Kreitler and others, 2013).

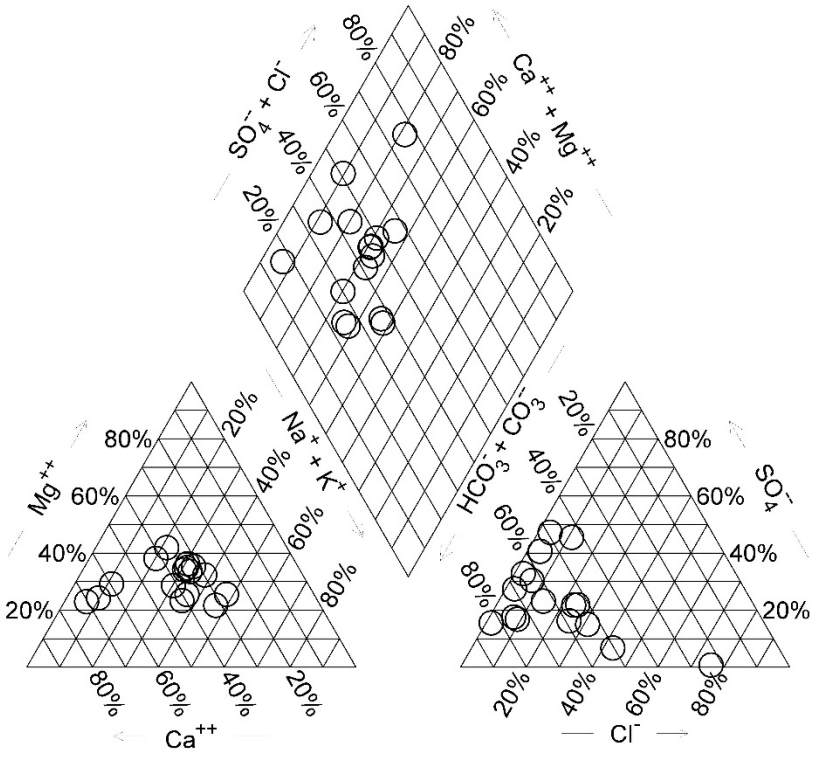

Figure 4-45. Piper diagram for wells in the Marathon Aquifer.

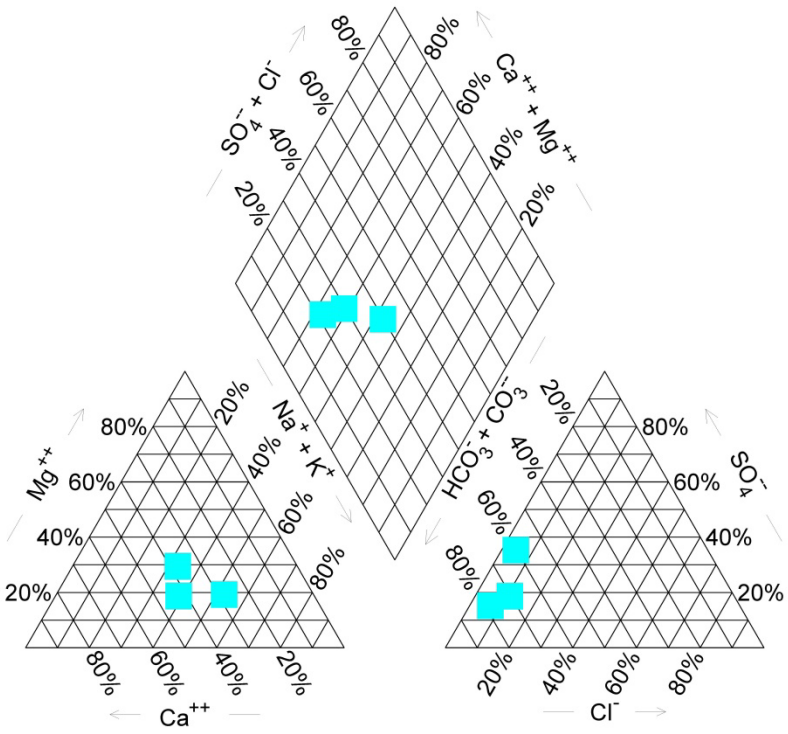

Figure 4-46. Piper diagram for Dimple Formation wells.

4.7.3 Isotope Analysis

In addition to basic inorganic suites of analyses, the samples collected in 2011 were also analyzed for a large suite of isotopes, including stable isotopes of deuterium and oxygen-18, and radioactive isotopes of tritium, carbon-14, and strontium. Evaluation of these data helps us understand the sources and ages of groundwater within the Marathon Aquifer.

4.7.3.1 Stable Isotopes

Stable isotopes of water help track the movement of water through the hydrologic cycle and the physical process of precipitation and evaporation. Groundwater is expected to reflect the stable isotope composition of the precipitation in the aquifer recharge area. As storms move from the Gulf of Mexico or the Pacific Ocean onto the continent, the stable isotope composition changes with each storm event. Because the isotopically "lighter" molecules tend to evaporate and remain in the atmosphere, the relatively "heavier" molecules tend to fall as precipitation. A particular storm will become "lighter" as it moves across the continent. This process is recognized across the globe and when global precipitation data for deuterium (δD) and oxygen ($\delta^{18}O$) are plotted, they fall along a Global Meteoric Water Line with the equation of $\delta D = 8(\delta^{18}O) + 10$ (Craig, 1961). Data are given as ratios of heavy to light isotopes relative to a standard laboratory value such as Vienna Standard Mean Ocean Water.

Stable isotope data from groundwater in the Marathon Aquifer from Kreitler and others (2013) are shown relative to the Global Meteoric Water Line in Figure 4-47. The data tend to plot parallel to the Global Meteoric Water Line in two groups. The group to the lower left plots parallel to the Global Meteoric Water Line and is considered lighter (more negative values). Some portion of this water may have been recharged during a cooler climate. The group to the right is considered heavier (more positive values) and tends to plot on a line with a different slope than the Global Meteoric Water Line, probably reflecting some amount of evaporation occurring before this water infiltrated into the subsurface.

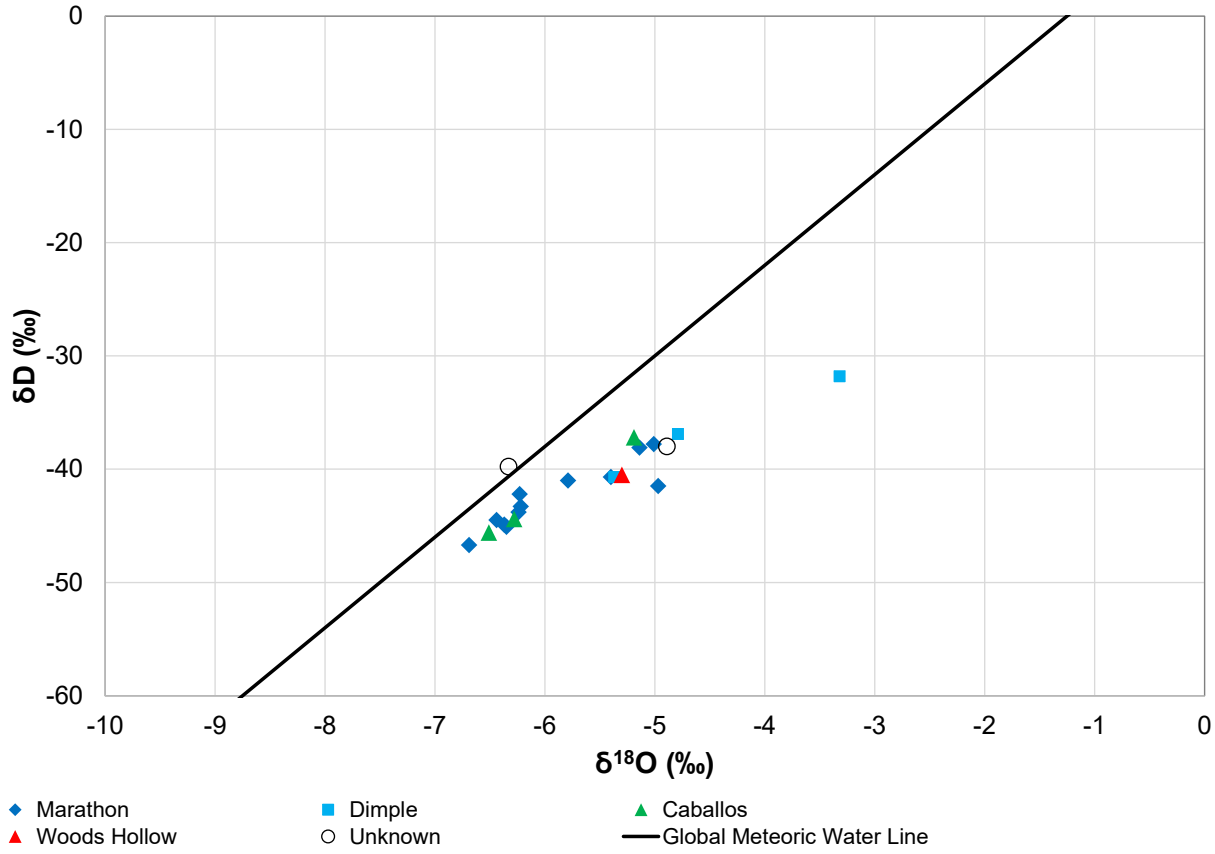

Figure 4-47. Plot of Marathon Aquifer stable isotopes data by geologic unit.

4.7.3.2 Radioactive Isotopes

Radioactive isotopes help determine groundwater age using tritium and carbon-14 and relative chemical differences between aquifer systems using strontium isotopes ratios (Sr^{87}/Sr^{86}).

Tritium is the radioactive isotope of hydrogen and is part of the water molecule. Tritium has a radioactive half-life of 12.3 years and is useful for dating relatively young groundwater that has been recharged in the last 50 to 60 years. For the 21 samples from Kreitler and others (2013) that were collected in 2011, tritium values range from 0.06 to 2.81 tritium units. Values less than 1 tritium unit are generally considered to have low tritium activity, and are considered to have been recharged greater than 60 years before the sample date (pre-1951 for these samples). Current tritium in the atmosphere is approximately 8 tritium units, so values near 8 tritium units would indicate very recent recharge. Values between 1 and 5 tritium units represent a mixture of pre-1951 water with groundwater recharged in the distant past. For these waters, carbon-14 data may help understand the groundwater age.

Carbon-14 data for the apparent groundwater age are also from Kreitler and others (2013). Apparent age calculations use the percentage of modern carbon in a water sample to calculate an age based only on radioactive decay. For the 21 samples from Kreitler and

others (2013) that were collected in 2011, carbon-14 values range from 20 to 9,860 years before present.

Figure 4-48 provides a plot of tritium versus carbon-14. This plot shows that the groundwater is represented by different age populations. Groundwater in the Dimple Formation tends to be younger, while samples from the Marathon Limestone and the Caballos Novaculite indicate a mixture of old and young water. The only sample from the Woods Hollow Shale (aquitard) is an older water. The distribution of groundwater age data is shown for tritium and carbon-14 in Figures 4-49 and 4-50, respectively. When considering groundwater flow paths for the Marathon Aquifer, particularly the western portion of the aquifer system, groundwater tends to become older along flow paths with increasing carbon-14 and decreasing tritium values. For example, well 5255110 has a carbon-14 age of 5,580 years before present and tritium of 2.45 tritium units, while downgradient well 5261301 has a carbon-14 age of 8,430 years before present and tritium of 0.31 tritium units (lower tritium units indicates older water).

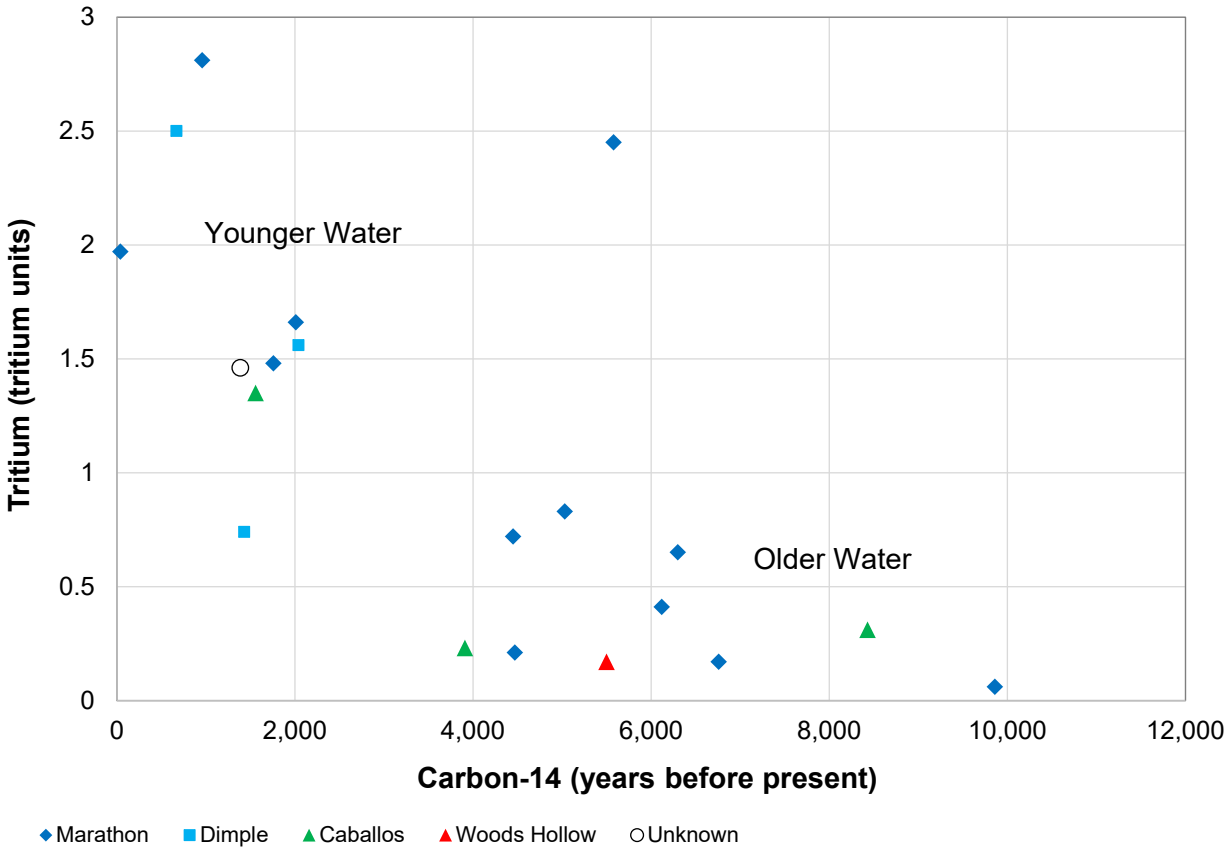

Figure 4-48. Plot of tritium versus carbon-14 for the Marathon Aquifer.

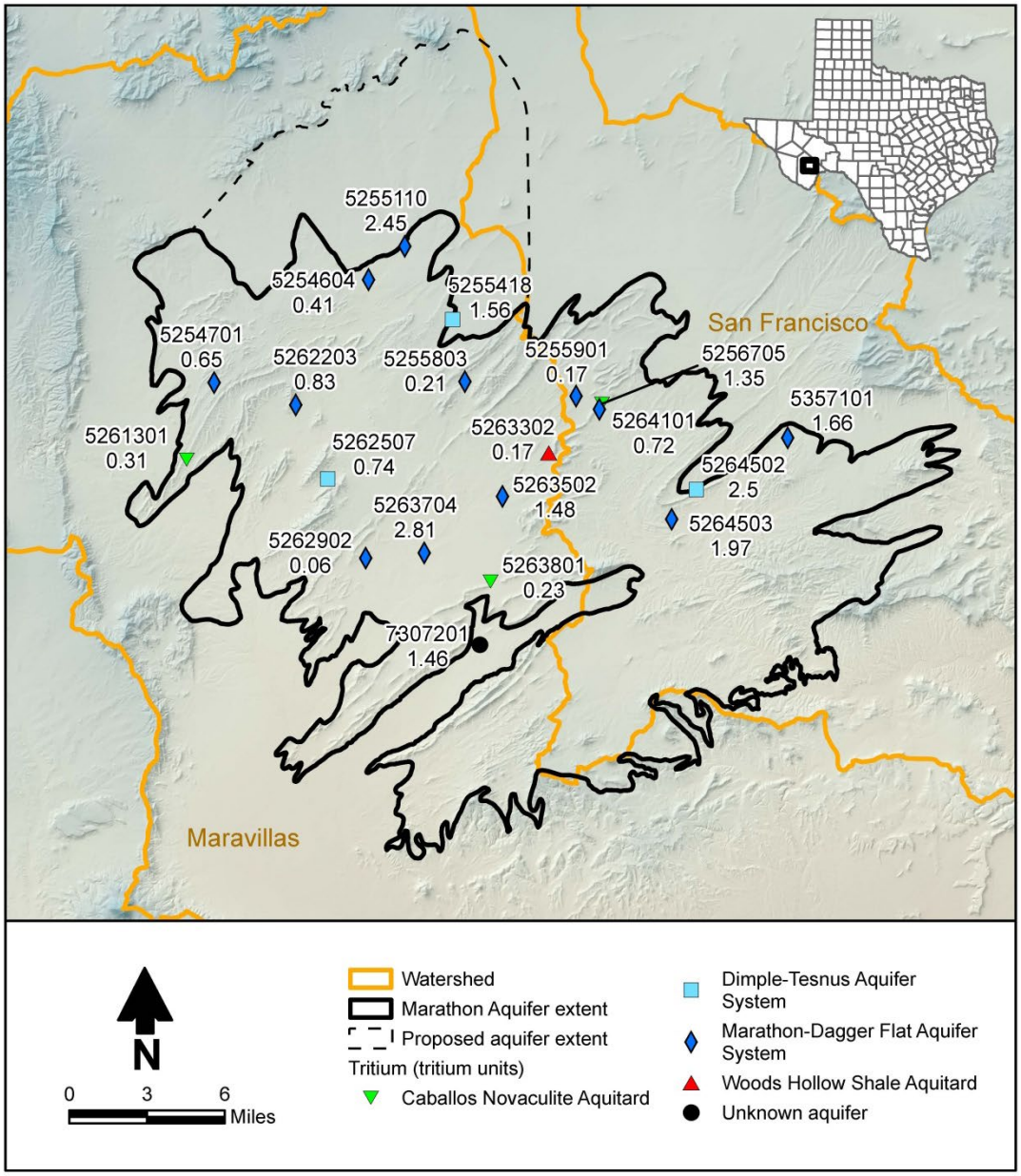

Figure 4-49. Tritium measured in the Marathon Aquifer area.

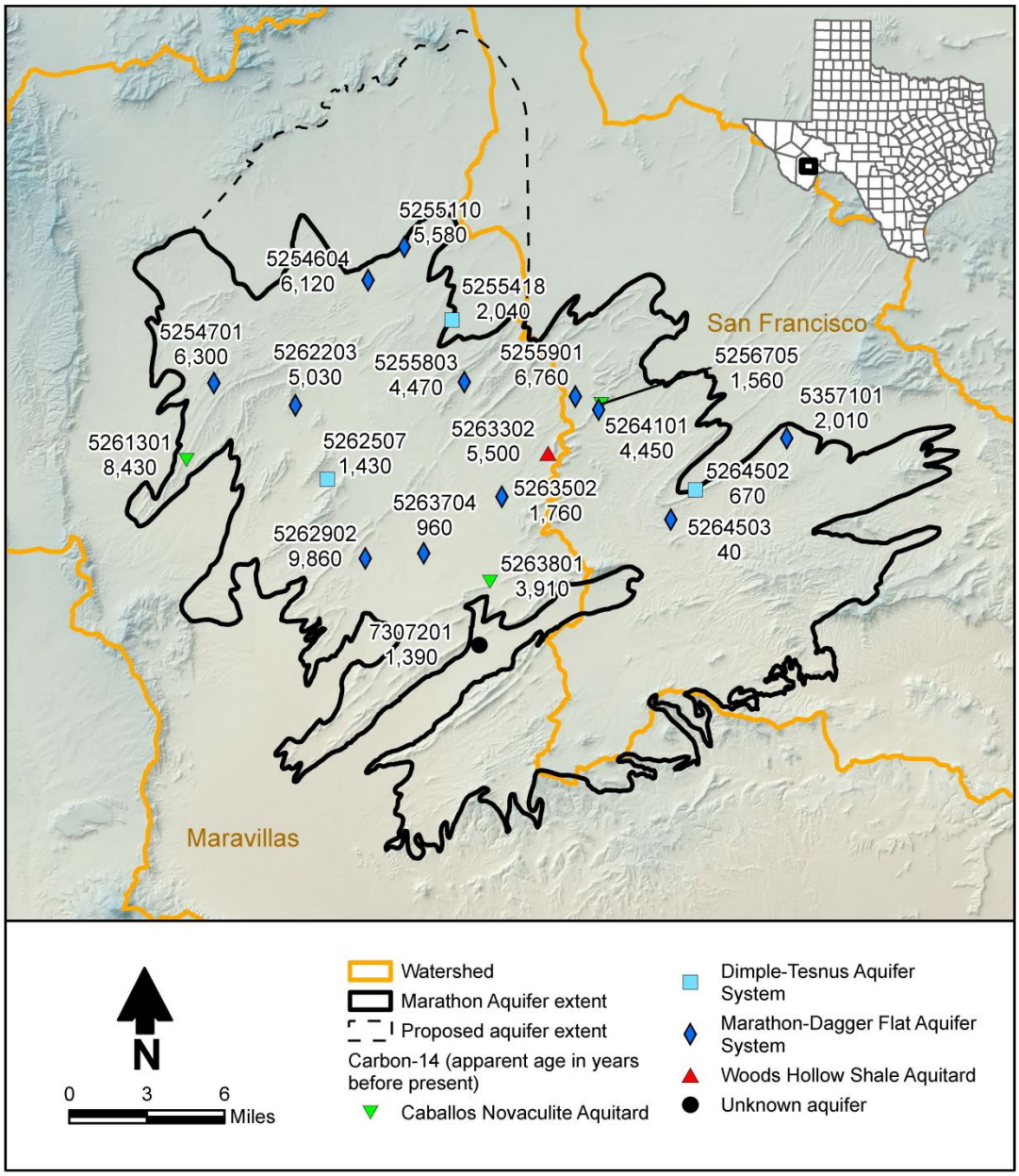

Figure 4-50. Carbon-14 measured in the Marathon Aquifer area.

Strontium isotopic ratios (Sr^{87}/Sr^{86}) may be used to help differentiate groundwater from different aquifer systems and may help identify communication between aquifer systems. Strontium in groundwater is derived from the aquifer matrix (Sr^{86}) and radioactive decay of rubidium (Sr^{87}).

Strontium ratios (Sr^{87}/Sr^{86}) range from 0.709438 to 0.713602 for the various aquifer systems (Figure 4-51). The ratios and concentrations show considerable variation that is likely related to variation of strontium ratios in the rock matrix of the Paleozoic rocks that

host the aquifer systems. Any hydrologic communication between aquifer systems is difficult to discern from the strontium isotope data.

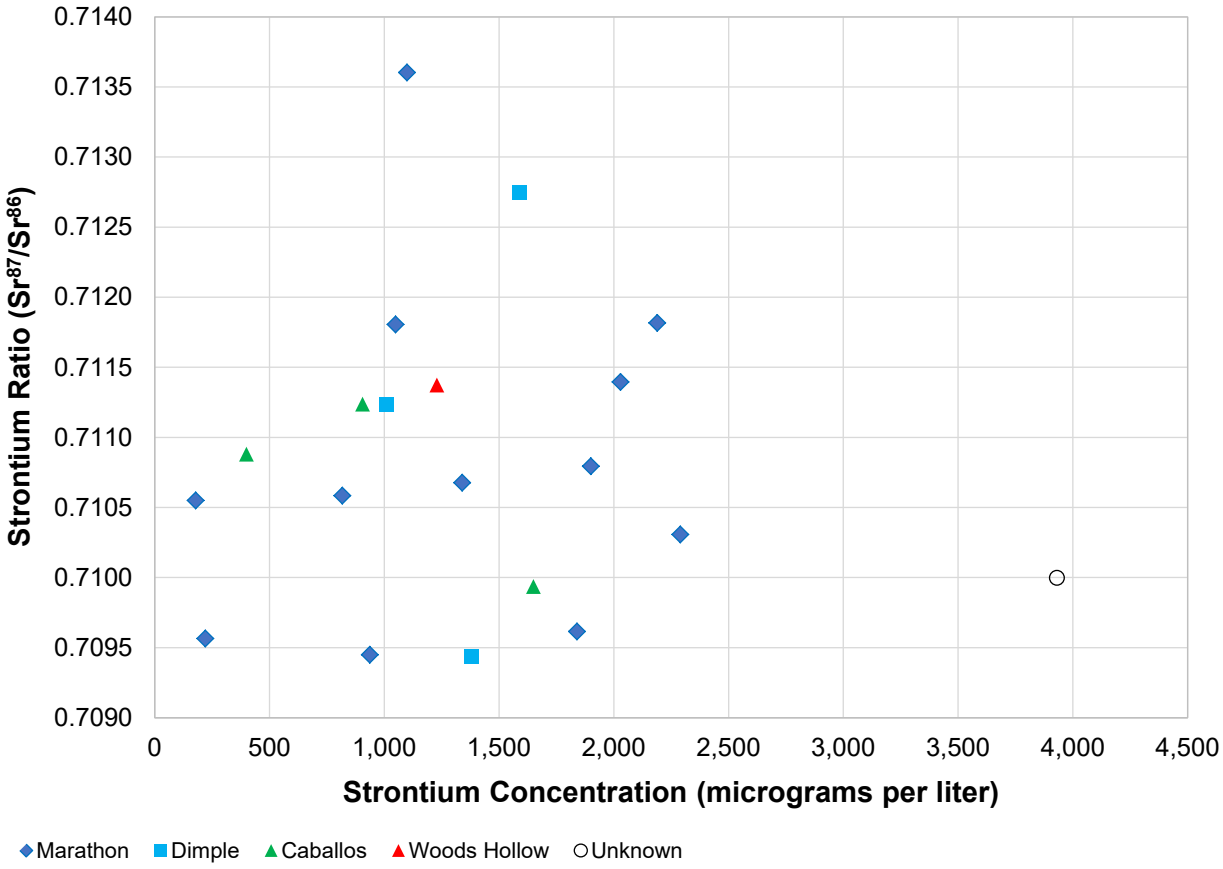

Figure 4-51. Strontium ratio versus strontium concentration.

5 Conceptual Model of Groundwater Flow in the Aquifer

Based on the data and analyses documented in the prior sections, the following conceptual model of groundwater flow is presented. The general conceptual model is illustrated schematically in Figure 5-1.

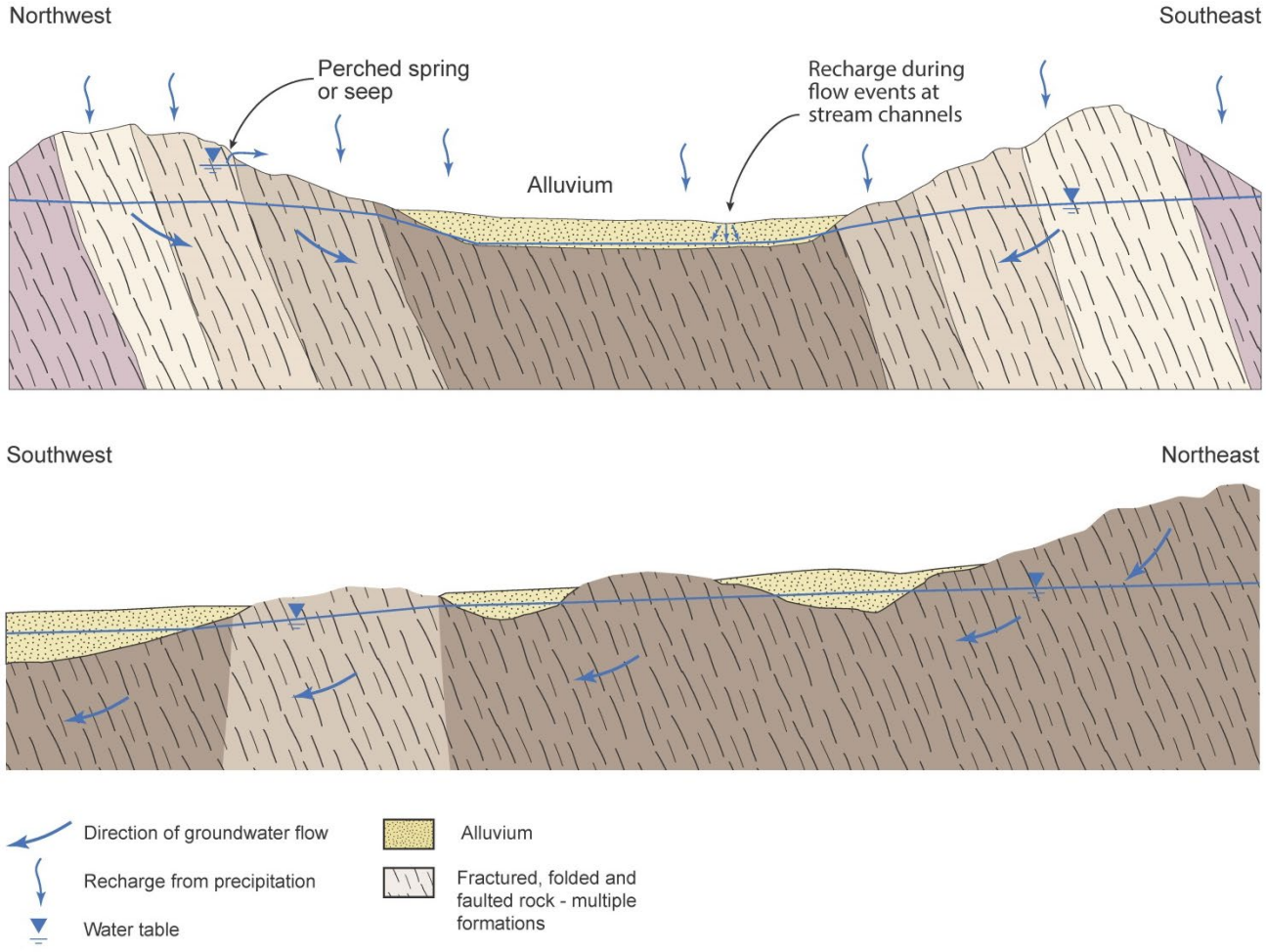

Figure 5-1. Schematic conceptual model of groundwater flow in the Marathon Aquifer. Top image is oriented northwest-southeast, approximately normal to the strike of major geologic features, and bottom image is oriented northeast-southwest, approximately along strike of major geologic features.

The Marathon Aquifer as envisioned and characterized in this report consists of primarily a shallow groundwater flow system; the majority of wells are less than 500 feet deep. Groundwater occurrence and flow is driven primarily by groundwater recharge and topography. Within the western portion of the aquifer, approximately coincident with the Maravillas Creek watershed, groundwater flow tends to be to the south-southwest. Groundwater tends to flow parallel to the distinct series of ridges and hills consisting most often of Caballos Novaculite, Maravillas Chert, and other rocks of hydrostratigraphic unit 5

(Table 4-1). However, it is believed that these formations are sufficiently fractured that groundwater can migrate through these features at depth. A portion of the observed southwestward flow component is likely attributable to the alluvium that overlies the fractured rocks between the topographic highs, which can act a higher-permeability aquifer unit where it is saturated.

Within the eastern portion of the aquifer, approximately coincident with the San Francisco Creek watershed, groundwater tends to flow south and east. In this area, Hell's Half Acre is a region of higher water levels, and groundwater flow is radially outward from this area.

Aquifer properties have been measured only for the Marathon Limestone and only in the vicinity of Marathon. The available data indicate that the hydraulic conductivity of the limestone can be high, and karst features have been observed by drillers. The hydraulic conductivity of the Marathon Limestone and other Paleozoic formations is also attributable to secondary porosity caused by fracturing of the rock. Fracture and joint systems in the rocks of the Marathon Aquifer are extremely complex based on the geologic history of folding and faulting, and the fact that different rock types respond differently to these events in terms of the degree of fracturing. The conceptual model illustrated in Figure 5-1 deals with this complexity by assuming that all rocks will be fractured to some degree and will have the ability to potentially produce at least small quantities of water to wells. There is, however, a hierarchy of expected permeability based on observed well yields and rock types, even if the absolute values of hydraulic conductivity are not known. The highest permeability is expected for the Marathon Limestone, followed by the alluvium, which has intrinsic (primary) permeability and is not fractured. These units are followed by the Gaptank, Haymond, Dimple and Tesnus formations, which are also expected to be fractured, but have a hydraulic conductivity significantly less than that of the Marathon Limestone. The Caballos Novaculite and Maravillas Chert would also be expected to have similar-magnitude hydraulic conductivity to the above formations based on reported well yields, although the Caballos Novaculite is noted to force water to the surface at several spring locations, implying low permeability in the subsurface. The Woods Hollow Shale and Fort Pena Formation are expected to have the lowest hydraulic conductivity based on existing information.

Groundwater in the Marathon area and likely other regions of the aquifer occurs primarily under unconfined conditions, but groundwater can be confined in places where permeable units are overlain by less permeable units. Groundwater is obtained for limited uses (mainly stock and domestic) from whatever formations yield water near surface at a given location. The Marathon Limestone can have high hydraulic conductivity and wells yields in excess of 300 gallons per minute have been reported. Where the Marathon Limestone occurs at greater depths, wells generally tap shallower formations for stock or domestic supply. It is possible that well yields on the order of several hundred gallons per minute may be obtained from the Marathon Limestone where it occurs at depth, but information on deeper portions of the groundwater flow system is virtually non-existent.

Groundwater pumping from the Marathon Aquifer is small, totaling only about 250 acre-feet per year. The highest value recorded was just under 450 acre-feet per year in 2010.

The majority of pumping is for municipal and irrigation uses in the town of Marathon. Natural groundwater discharge occurs as spring flow, base flow to some streams along the eastern and southern margins of the aquifer extent, evapotranspiration where the water table is shallow, and as groundwater underflow.

Groundwater recharge to the Marathon Aquifer (including the proposed extension) averages about 21,284 acre-feet per year based on simulations conducted for the period 1981 through 2021. During this period, the estimated annual values range from a high of 70,916 acre-feet in 1987 to a low of 2,035 acre-feet in 1998. An unknown portion of groundwater recharge is lost to seepage and spring flow from perched water tables that occur at higher elevation above the regional water table. A good example of this phenomena is Ridge Spring, which has the second highest reported spring flow in the region of 95 to 320 gallons per minute, but reportedly ceased to flow during the drought of the 1950s.

Groundwater inflow to the Marathon Aquifer is likely small. Groundwater inflow would occur from the north, where the subsurface is composed predominantly of Cretaceous rocks unlikely to transmit large quantities of groundwater. Some groundwater inflow from saturated alluvium could also occur, but the saturated thickness of alluvium is likely limited.

Based on the small amount of pumping from the aquifer and the amount of estimated recharge, the Marathon Aquifer exists primarily in a quasi-steady state condition, where changes in water levels and spring flow are primarily driven by changes in climatic conditions. The exception to this appears to be the town of Marathon, where moderate effects of groundwater pumping have been observed in the form of water levels that have declined through time.

6 Future Improvements

Future improvements to the Marathon Aquifer conceptual model and ultimately the groundwater availability model that will be constructed include the following items:

- Continued and more consistent water level monitoring across multiple aquifer units at dispersed locations
- Determination of aquifer properties through pump testing, particularly for formations other than the Marathon Limestone
- Seepage runs or measurements of base flow along portions of Maravillas and San Francisco creeks would assist with constraining and verifying groundwater recharge estimates and would assist with the quantification of groundwater discharge.

Finally, if more detailed analyses or studies are performed, it would make sense for these studies to be focused on the town of Marathon area in particular, as this is the location of

highest water use and will likely be the region of greatest Marathon Aquifer use in the future.

7 Acknowledgements

The project team would like to thank the community of Marathon for its participation in this study. In particular, Mr. Travis Roberts (deceased) shared his extensive knowledge of the groundwater conditions of the region. Mr. Tim Leary shared and assisted with the collection of critical water level data. Mr. Jim Roberts of Marathon Water and Sewer shared his knowledge and data regarding the Marathon public supply wells. We are also greatly appreciative of the Marathon Independent School District for allowing the use of school facilities for stakeholder meetings, community members who shared rain gauge data, local drillers who shared their knowledge of the region, the Brewster County Groundwater Conservation District for their support and input, and the many residents, businesses, and ranchers who allowed access to their properties for geological study and water level testing. We would also like to acknowledge those community members who participated in the study by sharing historical data, local histories of water use, and information about rainfall and historical flooding. This local participation improved the study significantly.

The input and critical review of our geologic and hydrostratigraphic interpretations by our subject matter experts Drs. Mark Helper and Patricia Dickerson is greatly appreciated, as are their contributions to the report regarding tear faults in the Marathon area (Dr. Helper) and aquifer and aquitard units (Dr. Dickerson). Any errors or omissions in this document are the responsibility of the project team and not these experts.

Two authors in particular deserve special recognition for their efforts on this project. Vince Clause, in addition to other contributions to the project, spent many hours conducting detailed lineament identification and related analyses, and his efforts are greatly appreciated. And finally, the assistance and persistence of Danielle Gallo contributed greatly to the successful completion of this project. Ms. Gallo's commitment to the project and invaluable assistance regarding local logistics and resources, stakeholder outreach, and data collection are gratefully acknowledged.

8 References

Adams, J.E. and H.N. Frenzel, 1952, Marathon Basin, Brewster and Pecos counties, Trans-Pecos Texas: West Texas Geological Society, 1952 spring field trip, 78 p.

Alexander, K.B., 1990, Correlation of structural lineaments and fracture traces to water-well yields in the Edwards Aquifer, Central Texas: University of Texas, Austin, dissertation.

Allen, R.G., L.S. Pereira, D. Raes, and M. Smith, 1998, Crop evapotranspiration guidelines for computing crop water requirements: FAO Irrigation and Drainage Paper 56, Rome, Italy.

Allen, R.G., L.S. Pereira, M. Smith, D. Raes, and J.L. Wright, 2005, FAO-56 dual crop coefficient method for estimating evaporation from soil and application extensions: *Journal of Irrigation and Drainage Engineering* 131(1): 2-13.

Anderson, J.E., J.B. Brown Jr., J.C. Gries, E.M.P. Lovejoy, D. McKalips, and V.E. Barnes, 1982, Fort Stockton sheet: Geologic Atlas of Texas, revised 1995.

Baker, C.L., 1928, The date of the major diastrophism and other problems of the Marathon Basin, Trans-Pecos, Texas: *American Association of Petroleum Geology Bulletin* 12: 1111–1117.

Barnes, V.E., 1979, Emory Peak-Presidio sheet: Texas Bureau of Economic Geology, Geologic Atlas of Texas, scale: 1:250,000.

Bjorklund, T.K., 1962, Structure of Horse Mountain Anticline (Southwest Extension), Brewster County, Texas: Master's thesis, University of Texas, Austin.

Brune, G., 1975, Major and historical springs of Texas: Texas Water Development Board, Report 189, March 1975.

Brune, G., 1981, Springs of Texas - Volume I: Branch-Smith, Inc.

Brune, G., 2002, Springs of Texas, second edition: Texas A&M University Press, College Station, Texas.

Byrd, W.M., 1958, The geology of a portion of the Combs Ranch, Brewster County, Texas: Master's thesis, University of Texas, Austin.

Carsel, R.F. and R.S. Parrish, 1988, Developing joint probability distributions of woil water retention characteristics: Water Resources Research 24(5): 755-769.

Chapman. J.B. and R.S. McCarty, 2013, Detachment levels in the Marathon fold and thrust belt, West Texas: *Journal of Structural Geology* XXX: 1–12.

Coley, K.L., 1987, Structural evolution of the Warwick Hills, Marathon Basin, West Texas: Master's thesis, University of Texas, Austin.

Cooper, H.H. Jr. and C.E. Jacob, 1946, A generalized graphical method for evaluating formation constants and summarizing well field history: *Transactions of the American Geophysical Union* 27: 526-534.

Craig, H., 1961, Isotopic variations in meteoric waters: *Science* 133: 1702-1703.

DeCook, K.J., 1961, A reconnaissance of the ground-water resources of the Marathon Area, Brewster County, Texas: Texas Board of Water Engineers, Bulletin 6111, December 1961.

DeMis, W.D., 1983, Geology of the Hell's Half Acre, Marathon Basin, Texas: Master's thesis, University of Texas, Austin.

Dickerson, P.W., 1987, Structural and depositional setting of southwestern U. S. and northern Mexico along a Paleozoic transform plate margin: p. 129-159 in Geological Society of Mexico, Chihuahua Section, Field Conference Guidebook.

Dickerson, P. W., 2012, The circum-Laurentian carbonate bank, the western Ouachita-Cuyania basin, and the prodigal Llanoria landmass: AAPG Memoir 98, chapter 38, p. 959–984.

Dickerson, P.W., 2013, Tascotal Mesa transfer zone: An element of the border corridor transform system, Rio Grande rift of West Texas and adjacent Mexico: p. 475-500 in Hudson, M.R. and V.J.S. Grauch, New perspectives on the Rio Grande rift: From Tectonics to groundwater, Geological Society of America Special Paper 494.

Dickerson, P.W. and W.R. Muehlberger (Eds.), 1985, Structure and tectonics of Trans-Pecos Texas: p. 185-194 in West Texas Geological Society, Publication 85-81.

Diggs, T.N., 1989, Sedimentology and structural geology of the Housetop Mountains/Castle Mountain area, the Marathon Basin, Trans-Pecos Texas: Unpublished master's thesis, University of Texas, Austin.

Domenico, P. A and F. W. Schwartz, 1998, Physical and chemical hydrogeology, 2 edition: John Wiley and Sons, New York.

Duncan, M.A., 1987, Geology of the West Bourland Mountain Area, Marathon Basin, West Texas: Master's thesis, University of Texas, Austin.

Ellison, S.P., E.F. McBride, and A. Thompson, 1964, The filling of the Marathon Geosyncline: Permian Basin Section, Society of Economic Paleontologists and Mineralogists, Publication 64-9.

Ewing, T.E., 2016, Texas through Time: Bureau of Economic Geology, Udden Series #6.

Flawn, P.T., 1956, Basement rocks of Texas and southwest New Mexico: Bureau of Economic Geology, Publication 5605.

Flawn, P.T., A. Goldstein Jr., P.B. King, and C.E. Weaver, 1961, The Ouachita System: Bureau of Economic Geology, Publication 6120.

Flint, A. and L. Flint, 2007, Application of the basin characterization model to estimate in-place recharge and runoff potential in the Basin and Range carbonate-rock aquifer system, White Pine County, Nevada, and adjacent areas in Nevada and Utah: U.S. Geological Survey Scientific Investigations Report 2007-5099.

George, P.G., R.E. Mace, and R. Petrossian, 2011, Aquifers of Texas: Texas Water Development Board, Report 380.

Heuscher, S.A, C.C. Brandt, and P.M. Jardine, 2005, Using Soil physical and chemical properties to estimate bulk density: *Soil Science Society of America Journal* 69.

Hevesi, J.A., A.L. Flint, and L.E. Flint, 2003, Simulation of net infiltration and potential recharge using a distributed-parameter watershed model of the Death Valley Region, Nevada and California: U.S. Geological Survey Water-Resources Investigations Report 03-4090.

Hickman, R.G., R.J. Varga, and R.M. Altany, 2009, Structural style of the Marathon thrust belt, West Texas: Journal of Structural Geology 31: 900–909.

Homer, C.H., J.A. Fry, and C.A. Barnes, 2012, The National Land Cover Database: U.S. Geological Survey Fact Sheet 2012-3020, 4 p.

Houser, J.F., 1967, Structural geology of Threemile Hill Area, Brewster County, Texas: Master's thesis, University of Texas, Austin.

King, P.B., 1937, Geology of the Marathon region, Texas: U. S. Geological Survey, Professional Paper 187.

King, P.B., 1980, Geology of the eastern part of the Marathon Basin, Texas: U.S. Geological Survey, Professional Paper 1157.

Kraft, J.L., 1984, Structural evolution of the Sunshine Springs Thrust Area, Marathon Basin, Texas: Master's thesis, University of Texas, Austin.

Kreitler, C.W., J.A. Beach, L. Symank, M.M. Uliana, R. Bassett, J.E. Ewing, and V.A. Kelley, 2013, Evaluation of hydrochemical and isotopic data in groundwater management areas 3 and 7: Contract report prepared for the Texas Water Development Board, LBG-Guyton, Austin, Texas.

LaRoche, M.T. and L. Higgins, 1990, Marathon Thrust Belt: Structure, stratigraphy and hydrocarbon potential: West Texas Geological Society, Permian Basin Society, and SEPM.

Lattman, L.H. and R.R. Parizek, 1964, Relationship between fracture traces and the occurrence of ground water in carbonate rocks: *Journal of Hydrology* 2(2): 73-91.

Leason, J.O., 1983, Structural geology of the Horse Mountain Area, Marathon Basin, Texas: Master's thesis, University of Texas, Austin.

Leavesley, G.H., R.W. Lichty, B.M. Troutman, and L.G. Saindon, 1983, Precipitation-runoff modeling system, User's manual: U.S. Geological Survey Water-Resources Investigations Report 83-4238, 207 p.

Lee, D.-H., 2005, Comparing the inverse parameter estimation approach with pedo-transfer function method for estimating soil hydraulic conductivity: Geosciences Journal 9(3): 269-276.

Lewis, F.R., and J.B. Barton, 1946, Glass Mountains-Marathon Basin: West Texas Geological Society, 1946 Fall Field Trip.

Liu, T, H. Yan, and L. Zhai, 2015, Extract relevant features from DEM for groundwater potential mapping: *The International Archives of Photogrammetry, Remote Sensing and Spatial Information Sciences* 40(7): 113.

Mace, R.E., 2001, Estimating transmissivity using specific-capacity data: Bureau of Economic Geology, Geological Circular 01-2.

Maxwell, R.A., J.T. Lonsdale, S.S. Goldich, and J.F. Smith Jr., 1949, Guidebook, Field Trip #1, Marathon Region, Big Bend Region, Green Valley-Paradise Valley, Sierra Blanca Region, Texas: West Texas Geological Society.

McBride, E.F.,1964a, Sedimentology of the Haymond Formation, Marathon Region, Texas: p. 35-40 in The filling of the Marathon Geosyncline, 1964 Field Trip, Society of Economic Paleontologists and Mineralogists, Publication 64-9.

McBride, E.F.,1964b, Stratigraphy and Sedimentology of the Gaptank Formation, Marathon Region, Texas: p. 41-44 in The filling of the Marathon Geosyncline, 1964 Field Trip, Society of Economic Paleontologists and Mineralogists, Publication 64-9.

McBride, E.F., 1988, Stratigraphy and structure of Marathon region, West Texas – 1. Geology of the Marathon Uplift, West Texas: Geological Society of America, Centennial Field Guide – South-Central Section.

McBride, E.F. and A. Thomson, 1964, Sedimentology of the Tesnus Formation, Marathon Region, Texas: p. 17-31 in The filling of the Marathon Geosyncline, 1964 Field Trip, Society of Economic Paleontologists and Mineralogists, Publication 64-9.

Mogaji, K.A., O.S. Aboyeji, and G.O. Omosuyi, 2011, Mapping of lineaments for groundwater targeting in the basement complex region of Ondo State, Nigeria, using remote sensing and geographic information system (GIS) techniques: *International Journal of Water Resources and Environmental Engineering* 3(7): 150-160.

Muehlberger, W.R., W.R. DeMis, and J.O. Leason, 1984, Geologic map and cross-sections, Marathon Region, Trans-Pecos, Texas: Geological Society of America Map and Chart Series MC-28T, scale 1:250,000.

Muehlberger, W.R. and P.W. Dickerson, 1989, A tectonic history: p. 35-54 in Structure and stratigraphy of Trans-Pecos Texas: 28th International Geological Congress, Field Trip Guidebook T-317.

Muse, R.W., 1966, Water-level data from observation wells in Culberson, Jeff Davis, Presidio and Brewster counties, Texas: Texas Water Development Board, Report 16.

Natural Resources Conservation Service, 2020, Soil Survey Geographic (SSURGO) Database: Accessed December 14, 2020 at <https://sdmdataaccess.sc.egov.usda.gov>, U.S. Department of Agriculture.

Neuman, S.P., 1975, Analysis of pumping test data from anisotropic unconfined aquifers considering delayed gravity response: *Water Resources Researc*h 11: 329-342.

PRISM Climate Group, 2004, <http://prism.oregonstate.edu>, Created February 4, 2004, Oregon State University.

Rawls, W.J. and D.L. Brakensiek, 1985, Prediction of soil water properties for hydrologic modeling: p. 293-299 in Proceedings of Symposium on Watershed Management, American Society of Civil Engineers.

Rawls, W.J., L.R. Ahuja, and D.L. Brakensiek. 1992. Estimating soil hydraulic properties from soils data: p. 329–340 in M.Th. van Genuchten and others (eds.), Proc. Int. Workshop on Indirect Methods for Estimating the Hydraulic Properties of Unsaturated Soils. Riverside, CA. 11–13 Oct. 1989, U.S. Department of Agriculture and University of California, Riverside.

Reed, T.A., 1990, Structural geology and petroleum exploration of the Marathon Thrust Belt, West Texas: p. 39-64 in Marathon Thrust Belt: Structure, stratigraphy and hydrocarbon potential, West Texas Geological Society, Permian Basin Society, and SEPM.

Ross, C.A., 1963, Standard Wolfcampian Series (Permian) Glass Mountains, Texas: Geological Society of America, Memoir 88.

Ross, C.A., 1986, Paleozoic evolution of southern margin of Permian Basin: Geological Society of America Bulletin 97: 536-554.

Ross, C.A. and J.R.P. Ross, 2003, Fusulinid Sequence evolution and sequence extinction in Wolfcampian and Lenardian Series (Lower Permian), Glass Mountains, Texas: Rivista Italiana di Paleontologia e Stratigrafia 9(2): 281-306.

Schaap, M.G., F.J. Leij, and M.Th. van Genuchten, 2001, ROSETTA: a computer program for estimating soil hydraulic parameters with hierarchical pedotransfer functions: *Journal of Hydrology* 251(3-4): 163-176..

Schroeder, P.R., T.S. Dozier, P.A. Zappi, B.M. McEnroe, J.W. Sjostrom, and R.L. Peyton, 1994, The hydrologic evaluation of landfill performance (HELP) model: Engineering documentation for version 3: U.S. Environmental Protection Agency Office of Research and Development, EPA/600/R-94/168b, September 1994.

Sellards, E.H., 1933, The pre-Paleozoic and Paleozoic systems in Texas, Part 1: p. 15-238 in Sellards, E.H, W.S. Adtkins, and F.B. Plummer, The geology of Texas: Volume 1, Stratigraphy: University of Texas, Bulletin No. 3232.

Smith, R., 2001, Hydrogeology of the Marathon Basin, Brewster County, Texas: p. 190-206 in Mace, R.E., W.F. Mullican III, and E.S. Angle (Eds.), Aquifers of West Texas: Texas Water Development Board Report 356.

Tauvers, P.R., 1988, Basement-influenced deformation in the Marathon fold-thrust belt, West Texas: Journal of Geology 96 (September).

Texas Bureau of Economic Geology, 2021, Physiography information: <beg.utexas.edu>, Accessed May 14, 2021.

Texas Water Development Board (TWDB), 2021, Water for Texas website: Accessed May 25, 2022.

Thomson, A. and M.R. Thomasson, 1964, Sedimentology and stratigraphy of the Dimple Limestone, Marathon Region, Texas: p. 22-30 in The filling of the Marathon Geosyncline,

1964 Field Trip, Society of Economic Paleontologists and Mineralogists, Publication 64-9.

Twiss, R.J. and E.M. Moores, 1992, *Structural geology*: Freeman and Company.

Udden, J.A., 1917, Notes of the geology of the Glass Mountains: p. 1-59 in University of Texas Bulletin 1753.

U.S. Department of Agriculture, 2020, Texas NAIP imagery, 2020-04-01: Downloaded on May 10, 2022.

U.S. Geological Survey, 2016, Moderate Resolution Imaging Spectroradiometer (MODIS) datasets. Accessed December 8, 2020 through the U.S. Geological Survey Global Visualization Viewer "MODIS Terra" collection and the "MOD15A2 LAI" images. <https://glovis.usgs.gov/>.

U.S. Geological Survey, 2019, West Texas Lidar, 2019-05-15: Downloaded on May 10, 2022.

Walton, W.C., 1970, Groundwater resource evaluation: McGraw-Hill, New York.

Wilde, G.L., 1990, Surface to subsurface structure and stratigraphy of the Marathon Fold Belt, Brewster, Pecos, and Terrell Counties: p. 65-82 in Marathon Thrust Belt: Structure, stratigraphy and hydrocarbon potential: West Texas Geological Society, Permian Basin Society, and SEPM.

Winslow, A.G. and L.R. Kister, 1956, Saline-water resources of Texas: U.S. Geological Survey Water Supply Paper 1365, 105 p.

Wuellner, D.E., L.R. Lehtonen, and W.C. James, 1986, Sedimentary-tectonic development of the Marathon and Val Verde Basins, West Texas, U.S.A., a Permo-Carboniferous migrating foredeep: p. 347-368 in Special Publication of the International Association of Sedimentologists, No. 8.

Xia, Y. and others, 2009, NCEP/EMC, NLDAS Primary Forcing Data L4 Hourly 0.125 x 0.125 degree V002, Edited by David Mocko, NASA/GSFC/HSL, Greenbelt, Maryland, Goddard Earth Sciences Data and Information Services Center (GES DISC): Accessed January 19, 2021.

Xia, Y., K. Mitchell, M. Ek, J. Sheffield, B. Cosgrove, E. Wood, L. Luo, C. Alonge, H. Wei, J. Meng, B. Livneh, D. Lettenmaier, V. Koren, Q. Duan, K. Mo, Y. Fan, and D. Mocko, 2012, Continental-scale water and energy flux analysis and validation for the North American Land Data Assimilation System project phase 2 (NLDAS-2): 1. Intercomparison and application of model products: J. Geophys. Res. 117: D03109.

Yenne, E.Y., Y.B. Anifowose, H. Dibal, and R.N. Nimchak, 2015, An assessment of the relationship between lineament and groundwater productivity in a part of the basement complex, Southwestern Nigeria: *IOSR Journal of Environmental Science, Toxicology and Food Technology* 9(6): 23-35.

Zhang, Y., 2017, Rosetta3 download: http://www.u.arizona.edu/~ygzhang/download.html, Accessed 5/23/2022.

Zhang, Y. and M.G. Schaap, 2017, Weighted recalibration of the Rosetta pedotransfer model with improved estimates of hydraulic parameter distributions and summary statistics (Rosetta3): *Journal of Hydrology* 547: 39-53.

Appendix A

Recent Water Level Data

Appendix A. Recent Water Level Data

Table A-1. Marathon Aquifer Water Levels Measured in 2021

Water Level Source	Tracking Number	State Well Number	Owner	Location (decimal degrees)		Depth to Water (feet)	Well Depth (feet)	Date
				Latitude	Longitude			
DBS&A	514518		David Mollard	30.203333	–103.245278	142	343	5/4/2021
DBS&A	82527	5255407	Alan Haley	30.202223	–103.237778	121	185	5/5/2021
DBS&A			Danielle Gallo	30.211376	–103.237017	173	Unknown	5/7/2021
DBS&A			Danielle Gallo	30.211376	–103.237017	173	Unknown	3/14/2022
DBS&A	100881	5255405	Jim Roberts	30.198056	–103.238334	134	205	5/4/2021
DBS&A	47422		Guilford Jones	30.200556	–103.250834	105	515	7/19/2021
DBS&A			Mike Bruce	30.194485	–102.89982	175	210	5/17/2021
DBS&A			Mike Bruce	30.17274	–102.918225		185	5/17/2021
DBS&A			Mike Bruce	30.115575	–102.574291	111	122	6/2/2021
DBS&A			Guy Combs	30.206173	–103.322665	57	Unknown	5/27/2021
DBS&A			Guy Combs	30.215513	–103.367394		Unknown	5/27/2021
DBS&A			Guy Combs	30.209002	–102.973979	29	Unknown	5/27/2021
DBS&A			Guy Combs	30.209002	-102.973979	13	Unknown	2/17/2022
DBS&A			Guy Combs	30.232909	–103.024561	47	Unknown	5/27/2021
DBS&A			Jp Bryan	30.048211	–103.411275	15	100	9/1/2020
DBS&A			JP Bryan	30.061256	–103.402495	41	146	9/3/2020
DBS&A			JP Bryan	30.019682	–103.364822	178	203	9/3/2020
DBS&A			Gage Gardens	30.202486	–103.239331	120	425	6/16/2021
DBS&A			Gage Gardens	30.204427	–103.24215	114	Unknown	6/16/2021
DBS&A			Phil Harvey	30.206905	–103.254886	69	Unknown	6/14/2021
DBS&A			Tim Leary	29.899722	–103.358056	190	Unknown	8/1/2021
DBS&A			Tim Leary	29.869167	–103.313611	111	Unknown	8/1/2021
DBS&A			Tim Leary	29.887778	–103.265	84	Unknown	8/1/2021
DBS&A			Tim Leary	29.861111	–103.278889	61	Unknown	8/1/2021
DBS&A			Tim Leary	29.995	–103.261944	36	Unknown	8/3/2021
DBS&A			Tim Leary	29.990833	–103.243056	12	Unknown	8/3/2021
DBS&A			Tim Leary	30.023056	–103.161944	103	Unknown	8/4/2021
DBS&A			Tim Leary	30.035	–103.145833	73	Unknown	8/4/2021
DBS&A			Tim Leary	30.01	–103.112778	87	Unknown	8/4/2021
DBS&A			Tim Leary	30.042222	–103.097222	96	Unknown	8/4/2021

Table A-1. Marathon Aquifer Water Levels Measured in 2021

Water Level Source	Tracking Number	State Well Number	Owner	Location (decimal degrees)		Depth to Water (feet)	Well Depth (feet)	Date
				Latitude	Longitude			
DBS&A			Tim Leary	30.045556	–103.172778	70	Unknown	8/7/2021
DBS&A			Tim Leary	30.088333	–103.109167	120	Unknown	8/7/2021
DBS&A			Tim Leary	30.051944	–103.024167	26	Unknown	8/7/2021
DBS&A			Tim Leary	30.0025	–103.146667	76	Unknown	8/8/2021
DBS&A			Tim Leary	29.931944	–103.350278	168	Unknown	8/8/2021
DBS&A			Tim Leary	29.955278	–103.376389	81	Unknown	8/8/2021
DBS&A			Tim Leary	29.902778	–103.392778	101	Unknown	8/8/2021
TWDB		5255104	Marathon Water Supply	30.213381	–103.238614	180.61	468	7/27/2021
TWDB		5264301	Hamilton Ranch	30.121424	–103.008567	29.51	183	7/28/2021
TWDB		5357101	Hamilton Ranch	30.109167	–102.996944	78.39	Unknown	7/28/2021
TWDB		5357102	Hamilton Ranch	30.109115	–102.996642	79.31	243	7/28/2021
TWDB		5357501	Martin Ranch	30.050353	–102.928589	13.37	142	7/27/2021
TWDB		7306601	Maravillas Gap Ranch	29.938467	–103.270803	128.07	225	7/29/2021
TWDB		7306603	Maravillas Gap Ranch	29.941389	–103.281667	89.46	603	7/29/2021
TWDB		7306604	Maravillas Gap Ranch	29.928694	–103.26175	96.26	163	7/29/2021
TWDB		7307101	Leary Ranch	29.990769	–103.242474	27.36	65	7/28/2021

DBS&A = Water level measurement by Daniel B. Stephens & Associates, Inc. staff or contractor.
TWDB = Water level collected by TWDB staff.

Table A-2. Marathon Aquifer Water Levels Measured in 2019-2021

Water Level Source	Tracking Number	State Well Number	Owner	Location (decimal degrees)		Depth to Water (feet)	Well Depth (feet)	Date
				Latitude	Longitude			
DBS&A	514518		David Mollard	30.203333	–103.245278	142	343	5/4/2021
DBS&A	82527	5255407	Alan Haley	30.202223	–103.237778	121	185	5/5/2021
DBS&A			Danielle Gallo	30.211376	–103.237017	173	Unknown	5/7/2021
DBS&A	100881	5255405	Jim Roberts	30.198056	–103.238334	134	205	5/4/2021
DBS&A	47422		Guilford Jones	30.200556	–103.250834	105	515	7/19/2021
DBS&A			Mike Bruce	30.194485	–102.89982	175	210	5/17/2021
DBS&A			Mike Bruce	30.17274	–102.918225		185	5/17/2021
DBS&A			Mike Bruce	30.115575	–102.574291	111	122	6/2/2021
DBS&A			Guy Combs	30.206173	–103.322665	57	Unknown	5/27/2021
DBS&A			Guy Combs	30.215513	–103.367394		Unknown	5/27/2021
DBS&A			Guy Combs	30.209002	–102.973979	29	Unknown	5/27/2021
DBS&A			Guy Combs	30.232909	–103.024561	47	Unknown	5/27/2021
DBS&A			Jp Bryan	30.048211	–103.411275	15	100	9/1/2020
DBS&A			JP Bryan	30.061256	–103.402495	41	146	9/3/2020
DBS&A			JP Bryan	30.019682	–103.364822	178	203	9/3/2020
DBS&A			Gage Gardens	30.202486	–103.239331	120	425	6/16/2021
DBS&A			Gage Gardens	30.204427	–103.24215	114	Unknown	6/16/2021
DBS&A			Phil Harvey	30.206905	–103.254886	69	Unknown	6/14/2021
DBS&A			Tim Leary	29.899722	–103.358056	190	Unknown	8/1/2021
DBS&A			Tim Leary	29.869167	–103.313611	111	Unknown	8/1/2021
DBS&A			Tim Leary	29.887778	–103.265	84	Unknown	8/1/2021
DBS&A			Tim Leary	29.861111	–103.278889	61	Unknown	8/1/2021
DBS&A			Tim Leary	29.995	–103.261944	36	Unknown	8/3/2021
DBS&A			Tim Leary	29.990833	–103.243056	12	Unknown	8/3/2021
DBS&A			Tim Leary	30.023056	–103.161944	103	Unknown	8/4/2021
DBS&A			Tim Leary	30.035	–103.145833	73	Unknown	8/4/2021
DBS&A			Tim Leary	30.01	–103.112778	87	Unknown	8/4/2021
DBS&A			Tim Leary	30.042222	–103.097222	96	Unknown	8/4/2021
DBS&A			Tim Leary	30.045556	–103.172778	70	Unknown	8/7/2021
DBS&A			Tim Leary	30.088333	–103.109167	120	Unknown	8/7/2021
DBS&A			Tim Leary	30.051944	–103.024167	26	Unknown	8/7/2021
DBS&A			Tim Leary	30.0025	–103.146667	76	Unknown	8/8/2021
DBS&A			Tim Leary	29.931944	–103.350278	168	Unknown	8/8/2021
DBS&A			Tim Leary	29.955278	–103.376389	81	Unknown	8/8/2021

Table A-2. Marathon Aquifer Water Levels Measured in 2019-2021

Water Level Source	Tracking Number	State Well Number	Owner	Location (decimal degrees)		Depth to Water (feet)	Well Depth (feet)	Date
				Latitude	Longitude			
DBS&A			Tim Leary	29.902778	–103.392778	101	Unknown	8/8/2021
DBS&A			Danny Self	30.21152	–103.23664	172	Unknown	3/16/2022
DBS&A			Tana Lee	30.20432	–103.2552	89	250	3/19/2022
DBS&A			Steven Jones	30.19491	–103.24732	147	195	3/19/2022
DBS&A			Kay Houston	30.21065	–103.24528	129	264	3/25/2022
DBS&A			Ike Roberts	30.20889	–103.2455		152	2/25/2022
DBS&A			Ike Roberts	30.20986	–103.24758	109	Unknown	2/25/2022
DBS&A			Melissa Watson	30.20055	–103.23778	146	Unknown	3/21/2021
DBS&A			Juan Gonzales	30.20154	–103.24403	117	225	4/3/2022
DBS&A			Russ Tidwell	30.2021	–103.24706	109	Unknown	4/3/20222
DBS&A			Mary Mitchell	30.21069	–103.24446	151	278	3/25/2022
DBS&A			Carol Townsend	30.20438	–103.25516	83	230	3/19/2022
DBS&A			Charlie Sansom	30.21016	–103.2411		160	3/19/2022
TWDB		5255104	Marathon Water Supply	30.213381	–103.238614	180.61	468	7/27/2021
TWDB		5264301	Hamilton Ranch	30.121424	–103.008567	29.51	183	7/28/2021
TWDB		5357101	Hamilton Ranch	30.109167	–102.996944	78.39	Unknown	7/28/2021
TWDB		5357102	Hamilton Ranch	30.109115	–102.996642	79.31	243	7/28/2021
TWDB		5357501	Martin Ranch	30.050353	–102.928589	13.37	142	7/27/2021
TWDB		7306601	Maravillas Gap Ranch	29.938467	–103.270803	128.07	225	7/29/2021
TWDB		7306603	Maravillas Gap Ranch	29.941389	–103.281667	89.46	603	7/29/2021
TWDB		7306604	Maravillas Gap Ranch	29.928694	–103.26175	96.26	163	7/29/2021
TWDB		7307101	Leary Ranch	29.990769	–103.242474	27.36	65	7/28/2021
TDLR	558072		Hamilton Real Estate	30.143933	–103.020233	20	183	8/12/2020
TDLR	534809		Agripina Carrasco	30.1993	–103.245133	120	303	11/18/2019
TDLR	568365		Brent & Leslea Charlesworth	30.193333	–103.254722	137	400	2/8/2021
TDLR	568477		Carolyn Labait	30.115915	–103.106635	127	379	2/10/2021

Table A-2. Marathon Aquifer Water Levels Measured in 2019-2021

Water Level Source	Tracking Number	State Well Number	Owner	Location (decimal degrees)		Depth to Water (feet)	Well Depth (feet)	Date
				Latitude	Longitude			
TDLR	565034		A.S. Gage Ranches Partnership, Ltd.	29.915278	–103.260833	145	380	1/12/2021
TDLR	568362		Susan Combs	30.195833	–103.316944	26	180	2/4/2021
TDLR	565032		A.S. Gage Ranches Partnership, Ltd.	30.00185	–103.213	220	460	1/7/2021
TDLR	568363		Susan Combs	29.988611	–103.285278	32	220	2/3/2021
TDLR	517597		Susan Combs 2012 Exemption	29.9759	–103.27781	49	258	7/9/2019
TDLR	549074		A.S. Gage Ranches Partnership, Ltd.	30.104567	–103.224755	106	382	6/5/2020
TDLR	565033		A.S. Gage Ranches Partnership, Ltd.	30.001867	–103.213017	145	360	1/10/2021

DBS&A = Water level measurement by Daniel B. Stephens & Associates, Inc. staff or contractor.
TWDB = Water level collected by TWDB staff.
TDLR = Water level reported in Texas Department of Licensing and Regulation database

Photographic log of field-tested wells

Combs, Lennox Ranch 1

Combs, Lennox Ranch 2 (no test, steel tape too short)

Combs, Lennox Ranch 3 (dry well)

Combs, Spradley Ranch 1

Combs, Spradley Ranch 2

Gage Gardens, Greenhouse

Gage Gardens, Back 18 1

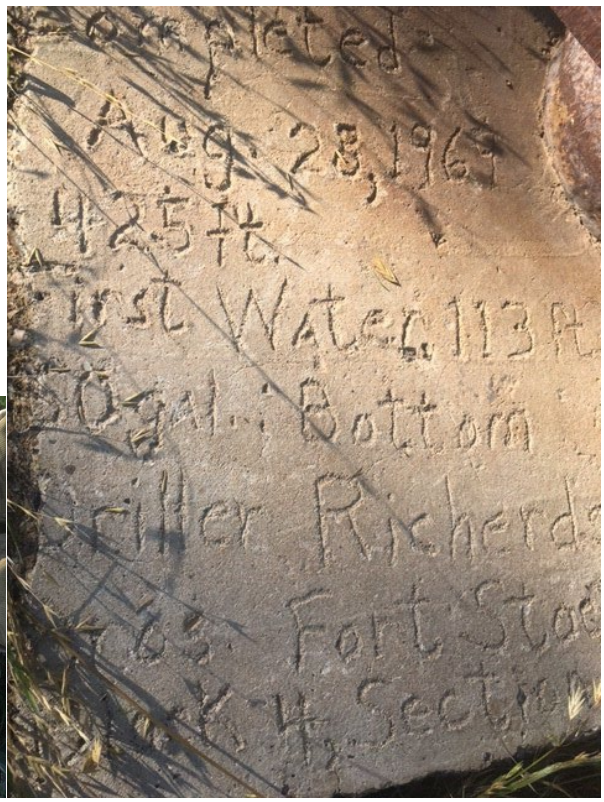

Gage Gardens, Back 18 slab

Housetop Mountain Test 1

Housetop Mountain Ranch Dry Well

Jones, Hostel Well

Mollard, Post Road House Well

Appendix B

Distributed Parameter Watershed Model Inputs

Table B-1. General distributed parameter watershed model input values.

Parameter	Variable	Units	Value	Comment
Field capacity	head_fc	centimeters	341	3/10 bar
Wilting point	head_wp	centimeters	15,353	15 bar
Average elevation for basin	elevavg	meters	1211	Average of model grid cells in the sub-basin
Average latitude for basin	Latavg	degrees	30.10	Approximate basin midpoint
Adjustment coefficient in Hargreaves' radiation formula	Krs	$°C^{-0.5}$	0.16	0.16 is recommended for "interior" (non-coastal) locations where land mass dominates and air masses are not strongly influenced by a large water body (Allen and others, 1998, p. 60)
Depletion factor	p	—	0.5	Varies 0 to 1 but typically ranges from 0.30 for shallow rooted plants at high values of ET_c (>8 mm/d) to 0.70 for deep rooted plants at low values of ET_c (<3 mm/d) with 0.5 in common use.
Dew point offset	Kdew_Yoff	°C	2	Assumes dew point is 2ºC less than the daily minimum temperature
Evaporation layer depth	Ze	meters	0.15	Depth of the surface soil layer that is subject to drying by way of evaporation. Upper end of range in Allen and others (1998), p. 144 (ranges 0.10 to 0.15 meters)
Readily evaporable water	REW	millimeters	8	Upper end of range for loamy sand (Allen and others, 1998, Table 19)
Initial capillary head node 1	IC1	centimeters	15,353	Set to wilting point (15 bar)
Initial capillary head node 2	IC2	centimeters	15,353	Set to wilting point (15 bar)
Initial capillary head node 3	IC3	centimeters	15,353	Set to wilting point (15 bar)
Initial capillary head node 4	IC4	centimeters	341	Set to field capacity (3/10 bar)
Minimum air temperature for transpiration	TETMIN	°C	5	There is no transpiration when the average daily temperature is below 5°C
Maximum air temperature for transpiration	TETMAX	°C	40	There is no transpiration when the average daily temperature is above 40°C
Fraction of reference evapotranspiration for sublimation above freezing	SUBPAR1	—	1	1 assumes sublimation is equal to reference evapotranspiration

°C = Degrees Celsius mm/d = Millimeters per day
mm/d/°C = Millimeters per day per degree Celsius

Table B-1. General distributed parameter watershed model input values.

Parameter	Variable	Units	Value	Comment
Fraction of reference evapotranspiration for sublimation below freezing	SUBPAR2	—	1	1 assumes sublimation is equal to reference evapotranspiration
Minimum snowmelt factor	MFMIN	mm/d/°C	2.0	Minimum expected to occur on December 21 (Schroeder and others, 1994)
Maximum snowmelt factor	MFMAX	mm/d/°C	5.2	Maximum expected to occur on June 21 (Schroeder and others, 1994)
Turbidity coefficient for solar radiation	Kcln	—	0.59	Average annual value published for Midland, TX (https://www.homerenergy.com/products/pro/docs/latest/_hm_print_window.htm?published_solar_data.html)
Minimum transpiration coefficient (Kc) for dry surface soil (upper 0.10 to 0.15 meter) with no vegetation cover	Kc_min	—	0.15	Lower end of 0.15–0.20 range recommended by Allen and others (1998).

°C = Degrees Celsius mm/d = Millimeters per day
mm/d/°C = Millimeters per day per degree Celsius

Table B-2. Vegetation input values for Distributed Parameter Watershed Model

Vegetation Name	National Land Cover Database Code	Mean Maximum Rooting Depth (meters)	Mean Maximum Plant Height (meters)	% of Model Domain
Open Water	11	0.15	0.15	0.001%
Developed, Open Space	21	2.60	0.15	0.1%
Developed, Low Intensity	22	2.60	0.15	0.031%
Developed, Medium Intensity	23	2.60	0.15	0.005%
Barren Land	31	0.30	0.15	0.001%
Deciduous Forest	41	5.00	4.00	0.1%
Evergreen Forest	42	5.00	10.00	1.2%
Mixed Forest	43	5.00	4.00	0.001%
Shrub/Scrub	52	1.10	2.23	88.5%
Herbaceous	71	0.91	1.27	9.8%
Woody Wetlands	90	1.40	2.00	0.031%
Emergent Herbaceous Wetlands	95	0.91	1.27	0.2%

Table B-3. Soil input values for Distributed Parameter Watershed Model.

SSURGO Map Unit Key	Saturated Hydraulic Conductivity (feet per day)	van Genuchten α (1/cm)	van Genuchten N (unitless)	Saturated Water Content (unitless)	Residual Water Content (unitless)	Soil Depth (meters)
58822	0.806	1.51×10^{-2}	1.244	0.471	0.099	0.380
58701	0.537	2.80×10^{-2}	1.352	0.423	0.068	0.150
58710	1.10	5.38×10^{-2}	1.278	0.487	0.100	0.200
58821	0.806	1.51×10^{-2}	1.244	0.471	0.099	0.380
58824	1.03	1.83×10^{-2}	1.261	0.449	0.095	10.000
58825	0.836	2.00×10^{-2}	1.257	0.449	0.097	10.000
58826	0.871	3.96×10^{-2}	1.303	0.442	0.090	0.440
58827	1.43	1.82×10^{-2}	1.263	0.370	0.092	0.230
58828	0.645	3.25×10^{-2}	1.325	0.417	0.082	0.230
58829	0.892	3.61×10^{-2}	1.294	0.436	0.092	0.460
58830	2.26	3.43×10^{-2}	1.318	0.404	0.085	10.000
58832	1.52	2.14×10^{-2}	1.269	0.423	0.093	0.270
58833	1.52	2.14×10^{-2}	1.269	0.423	0.093	0.270
58834	1.30	6.14×10^{-2}	1.336	0.370	0.089	0.180
58835	1.30	6.14×10^{-2}	1.336	0.370	0.089	0.180
58836	1.84	2.84×10^{-2}	1.236	0.370	0.099	10.000
58837	1.30	2.38×10^{-2}	1.197	0.385	0.103	0.180
58838	2.55	4.38×10^{-2}	1.381	0.398	0.069	10.000
58842	1.30	9.36×10^{-2}	1.367	0.392	0.082	0.180
58843	2.20	3.87×10^{-2}	1.372	0.376	0.074	10.000
58844	2.26	8.43×10^{-2}	1.325	0.480	0.084	10.000
58846	1.43	2.94×10^{-2}	1.288	0.480	0.093	0.380
58847	1.43	2.94×10^{-2}	1.288	0.480	0.093	0.380
58853	0.627	7.89×10^{-3}	1.121	0.385	0.093	10.000
58854	1.00	6.37×10^{-3}	1.099	0.401	0.090	0.710
58855	1.57	2.74×10^{-2}	1.283	0.417	0.092	0.230
58857	0.720	3.16×10^{-2}	1.294	0.458	0.091	0.300
58859	0.720	3.16×10^{-2}	1.294	0.458	0.091	0.300
58862	0.698	2.71×10^{-2}	1.348	0.398	0.073	0.410
58863	0.537	3.19×10^{-2}	1.339	0.398	0.079	0.150
58865	2.55	2.14×10^{-2}	1.292	0.408	0.087	10.000
58866	1.92	1.56×10^{-2}	1.167	0.423	0.105	10.000
58867	7.33	8.66×10^{-2}	1.426	0.442	0.049	10.000
58868	7.33	8.66×10^{-2}	1.426	0.442	0.049	10.000
58870	0.370	1.04×10^{-2}	1.153	0.430	0.102	10.000
58871	0.765	1.06×10^{-2}	1.140	0.423	0.102	10.000

Table B-3. Soil input values for Distributed Parameter Watershed Model.

SSURGO Map Unit Key	Saturated Hydraulic Conductivity (feet per day)	van Genuchten α (1/cm)	van Genuchten N (unitless)	Saturated Water Content (unitless)	Residual Water Content (unitless)	Soil Depth (meters)
58872	1.66	1.52×10^{-2}	1.210	0.408	0.099	10.000
58873	26.1	5.39×10^{-2}	1.476	1.000	0.014	10.000
58876	2.55	2.35×10^{-2}	1.271	0.401	0.093	10.000
58882	2.55	7.41×10^{-3}	1.147	0.442	0.098	10.000
58888	0.0595	6.89×10^{-3}	1.130	0.433	0.096	10.000
58890	1.79	2.39×10^{-2}	1.269	0.417	0.094	0.460
1910082	0.666	2.62×10^{-2}	1.325	0.458	0.075	0.250
1910084	0.666	2.62×10^{-2}	1.325	0.458	0.075	0.250
1910088	1.83	6.03×10^{-2}	1.234	0.423	0.107	0.200
1910090	1.83	6.03×10^{-2}	1.234	0.423	0.107	0.200
1910198	2.55	2.02×10^{-2}	1.282	0.449	0.090	10.000
NA	23.4	0.145	2.680	0.430	0.045	10.000

Table B-4. Bedrock input values for Distributed Parameter Watershed Model.

Distributed Parameter Watershed Model Name	Description	Rock Type	Vertical Saturated Hydraulic Conductivity (feet per day)
Cd	Dagger Flat Sandstone	Sandstone	0.850
IPd	Dimple Limestone	Limestone	0.851
IPgt	Gaptank Formation	Limestone/Sandstone	0.851
IPh	Haymond Formation	Shale/Sandstone	5.67×10^{-4}
IPMt	Tesnus Formation	Shale/Sandstone	5.67×10^{-4}
IPt	Tesnus Formation	Shale/Sandstone	5.67×10^{-4}
Kbd	Denton Clay Member	Shale	5.67×10^{-4}
Kbo	Boquillas Flags	Shale/Limestone	5.67×10^{-4}
Kbse	Boquillas Formation	Limestone	0.851
Kdt	Del Canyon Limestone and Telephone Canyon Formations undivided	Limestone	0.851
Kfr	Edwards Limestone, Comanche Peak Limestone, and Walnut Formation undivided	Limestone	0.851
Kft	Fort Terrett Member of Edwards Limestone	Limestone	0.851
Kgr	Glen Rose Formation	Limestone	8.51×10^{-2}
Kmx	Maxon Sandstone	Sandstone	0.850
Ks	Segovia Member of Edwards Limestone	Limestone	0.851
Kse	Santa Elena Limestone	Limestone	0.851
Ks-t	Santa Elena Limestone, Sue Peaks Formation, Del Carmen Limestone, and Telephone Canyon Formation undivided	Limestone	0.851
Ksu	Sue Peaks Formation	Shale/Limestone	5.67×10^{-4}
Kt	Trinity Sand	Limestone/Sandstone	0.851
Kw	Washita Group undivided	Clay	0.157
MDc	Caballos Novaculite	Chert	1.00×10^{-2}
MDO	Caballos Novaculite and Maravillas Chert	Chert	1.00×10^{-2}
O	Ordovician undivided	Sandstone	0.850
OC	Marathon Limestone and Dagger Flat Sandstone	Limestone/Sandstone	0.851
Ofa	Fort Pena Formation and Alsate Shale	Shale	5.67×10^{-4}
Oml	Marathon Limestone	Limestone	0.851
Omv	Maravillas Formation	Limestone	1.00×10^{-2}
Ow	Woods Hollow Shale	Shale	5.67×10^{-4}
Owf	Woods Hollow Shale, Fort Pena Formation, and Alsate Shale	Shale	5.67×10^{-4}

Table B-4. Bedrock input values for Distributed Parameter Watershed Model.

Distributed Parameter Watershed Model Name	Description	Rock Type	Vertical Saturated Hydraulic Conductivity (feet per day)
Owh	Woods Hollow Shale	Shale	5.67×10^{-4}
Pc	Cloud Chief Formation	Shale/Limestone	5.67×10^{-4}
Pcm	Cathedral Mountain Formation	Shale/Limestone	5.67×10^{-4}
Plh	Lenox Hills Formation	Conglomerate	8.50×10^{-2}
Pn	Nacona Formation	Sandstone	0.850
Psh	Skinner Ranch Formation and Hess Limestone	Limestone	8.51×10^{-2}
Pw	Word Formation	Shale	5.67×10^{-4}
Qal	Alluvium	Alluvium	23.4
Qao	Quaternary deposits	Alluvium	23.4
Qf	Young Quaternary deposits	Alluvium	23.4
Ql	Lissie Formation undivided	Alluvium	23.4
Qu	Quaternary deposits undivided	Alluvium	23.4
Tdp	Duff Tuff and Pruett Formations undivided in Cuesto del Burro area	Intrusive	5.67×10^{-5}
Ti	Diabase Dike	Intrusive	5.67×10^{-5}
Tpct	Crossen Trachyte	Intrusive	5.67×10^{-5}
Tpr	Pruett Formation	Intrusive	5.67×10^{-5}
Tps	Sheep Canyon Basalt	Intrusive	5.67×10^{-5}

Appendix C

Lineaments with <100 feet of Separation

Appendix C. Lineaments with <100 feet of Separation: Sample Group

ID	Lineament	Damage Zone Width (feet)
6	Lineament with <100 of displacement	60
47	Lineament with <100 of displacement	15
65	Lineament with <100 of displacement	40
85	Lineament with <100 of displacement	45
97	Lineament with <100 of displacement	20
102	Lineament with <100 of displacement	140
129	Lineament with <100 of displacement	50
147	Lineament with <100 of displacement	15
161	Lineament with <100 of displacement	30
169	Lineament with <100 of displacement	15
180	Lineament with <100 of displacement	40
183	Lineament with <100 of displacement	15
187	Lineament with <100 of displacement	15
204	Lineament with <100 of displacement	15
215	Lineament with <100 of displacement	30
216	Lineament with <100 of displacement	20
247	Lineament with <100 of displacement	15
256	Lineament with <100 of displacement	20
278	Lineament with <100 of displacement	25
300	Lineament with <100 of displacement	20
304	Lineament with <100 of displacement	25
347	Lineament with <100 of displacement	20
350	Lineament with <100 of displacement	15
370	Lineament with <100 of displacement	15
402	Lineament with <100 of displacement	20
416	Lineament with <100 of displacement	30
420	Lineament with <100 of displacement	40
441	Lineament with <100 of displacement	50
448	Lineament with <100 of displacement	30
467	Lineament with <100 of displacement	70
	Average	28.28

Appendix D

Photographs of Study Area

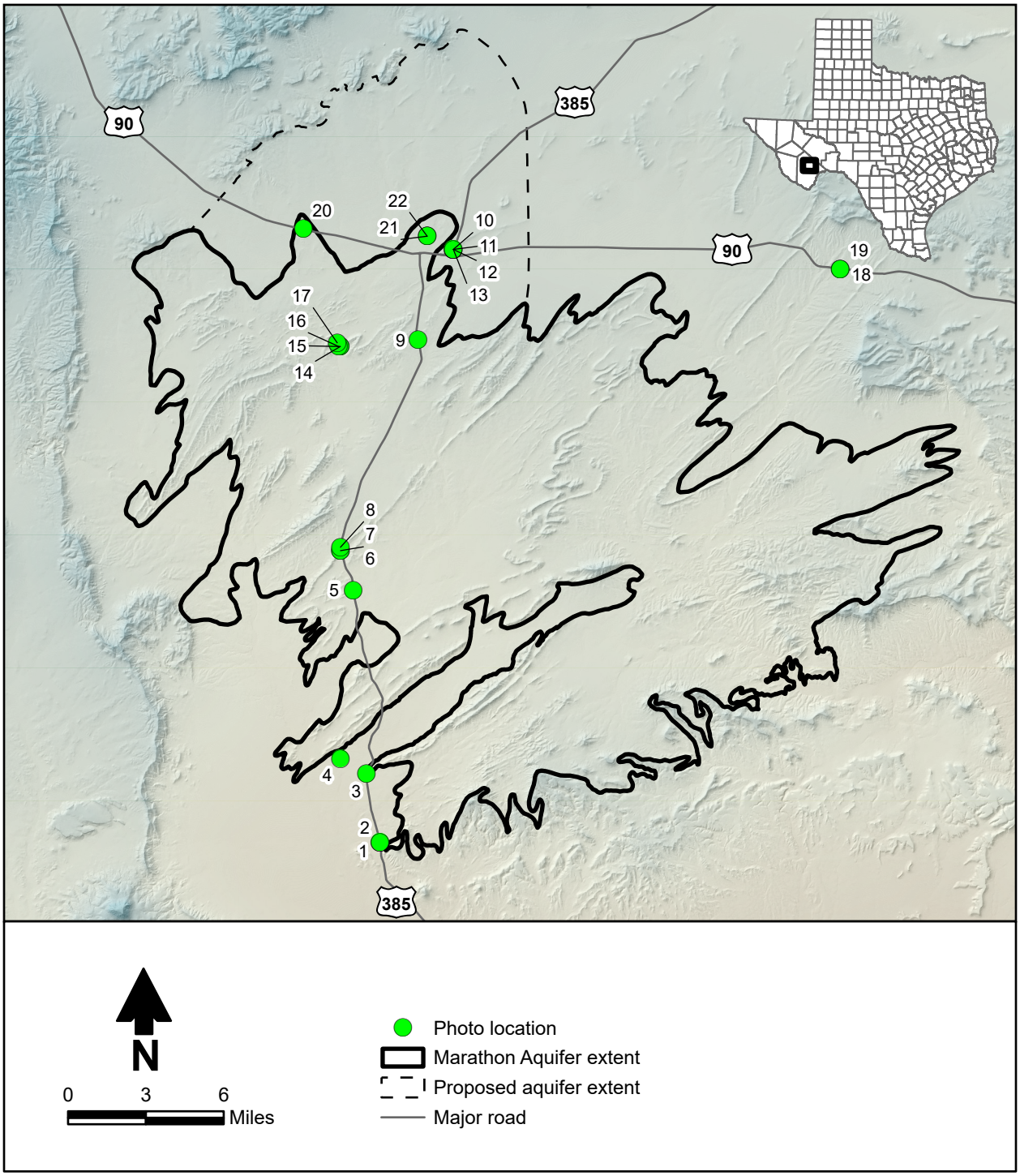
90
385
90
385
1
2
3
4
5
6
7
8
9
10
11
12
13
14
15
16
17
18
19
20
21
22
N
0
3
6
Miles
Photo location
Marathon Aquifer extent
Proposed aquifer extent
Major road

1. Bedded Cretaceous rocks with volcanic dome, southeast edge of Marathon Aquifer, South Highway 385, looking south-southeast (29.877, -103.252)

2. Santiago Peak, distant center of photograph, volcanic, South Highway 385, looking west (29.877, -103.252)

3. Undifferentiated Mississippian, Devonian, and Ordovician formations, South Highway 385, looking northeast (29.915, -103.262)

4. Alternating near-vertical ridges of Ordovician Maravillas Formation, South Highway 395, looking northwest (29.923, -103.259)

5. Outcrop of Ordovician Fort Pena and Alsate Formation, South Highway 395, looking east (30.017, -103.274)

6. Ordovician Woods Hollow, South Highway 385, looking east (30.039, -103.283)

7. Localized small-scale deformation, South Highway 395, looking east (30.039, -103.283 vicinity)

8. Simpson Spring Mountains, Ordovician Marathon Limestone and Cambrian Dagger Flat Sandstone forming ridges, South Highway 395, looking northwest (30.041, -103.283)

9. Lower Pennsylvanian Tesnus Formation outcrop, South Highway 395, looking west (30.158, -103.237)

10. Marathon Limestone outcrop, North Highway 385, looking west (30.209, -103.216)

11. Alternating colors of Marathon Limestone beds, North Highway 385, looking southwest (30.209, -103.216)

12. Evidence of karst development, Marathon Limestone, North Highway 385, looking west (30.209, -103.216)

13. Alluvial deposits overlying Marathon Limestone, North Highway 385, looking west (30.209, -103.216)

14. Fort Pena Colorada Park pond, Ordovician sequence, Maravillas Formation cap, possibly Marathon Limestone at base, looking northeast (30.153, -103.287)

15. Fort Pena Colorada Park, possibly Ordovician Marathon Limestone outcrop at base, east side of pond, looking north (30.153, -103.287)

16. Fort Pena Colorada Park, Devonian Caballos Novaculite outcrop, by road to park, looking west (30.153, -103.288)

17. North of Fort Pena Colorada Park, Ordovician sequence Maravillas Formation cap through Marathon Limestone at base, looking north (30.155, -103.289)

18. Lower Pennsylvanian Tesnus Formation sandstone and shale, East Highway 90, looking north (30.204, -102.966)

19. Lower Pennsylvanian Tesnus Formation sandstone and shale with alluvial cap, East Highway 90, east of Marathon, looking north (30.204, -102.966)

20. Upper Pennsylvanian Gaptank Formation, west of Marathon on Highway 90, looking south (30.218, -103.313)

21. Glass Mountains, dirt road northeast of Town of Marathon, looking west-northwest (30.216, -103.233)

22. Iron Mountain (center), volcanic intrusion, dirt road northeast of Town of Marathon, looking north (30.216, -103.233)